Flexible podand and metal-based hosts for anion binding and sensing

Dickson, Sara-Jane

Flexible Podand and Metal-Based Hosts for Anion Binding and Sensing

A thesis submitted for the fulfillment of the requirements for the degree of

Doctor of Philosophy

In the faculty of Science of Durham University

by

Sara-Jane Dickson

Department of Chemistry

Durham University

South Road

Durham

2008

Abstract

A series of amino-pyridyl and aminomethyl-pyridyl ligands, all with both pyridyl and secondary amine functionalities have been synthesised. A new series of organic and metal-based derivatives of these ligands have been prepared, along with the preparation of an organic viologen host, with previously reported urea arms,[1] and the properties of these new compounds, and in particular their anion binding behaviour have been studied.

The 3-aminomethyl-pyridyl ligands interact with transition metals and anions, in both solution and the solid state. They showed a particular affinity for copper(II) salts, and a nitrate sensing system has been prepared using the ligands fluorescence, through the addition of copper to a solution of the photo-active aminomethyl-pyridyl ligand. However, the active species has proved difficult to characterise.

Ruthenium-based derivatives have been shown to form both 1:1 and 2:1 host:guest complexes with a variety of anions. These compounds have also shown an equilibrium in which anion binding promotes time-averaging of diastereotopic methylene protons. The addition of anions to the fluorescent sensing analogues has shown quenching of the fluorescence.

Organic systems involving amino-pyridyl ligands around a di- and tri-substituted aryl core bind anions in solution. The fluorescent pyrene-derived host shows 2:1 host:guest binding in NMR spectroscopic studies, which is in contrast to work on aryl derivatives and previous work on anthracene containing hosts,[2] which has shown 1:1 host:guest binding.

Organic viologen compounds with urea arms and a control compound with pyridyl arms, show a colourimetric response to carboxylates, although in the presence of oxygen, decomposition occurs. These hosts also show an affinity for halide anions, which do not bring about this colourimetric response.

For my parents.

'Nothing can come of nothing'

William Shakespeare

Acknowledgements

I would like to start by thanking my supervisor for this project, Jon Steed, for providing me with an interesting project over the last three years. My thanks also for all his support, suggestions, ideas and encouragement during my time working in his group.

I must also thank the technical staff at Durham, who have helped with this work. Big thanks must go to the NMR staff, Dr Alan Kenwright, Catherine Heffernan, and Ian McKeag, without their help and understanding, it would not have been possible to complete the binding studies, or to have the stacked plots. Thanks also to Mike Jones, Jackie Moseley and Lara Turner, for mass spectroscopy, Judith Mcgee and Jaroka Dostal for the CHN analysis of compounds, and Doug Carswell for running DSC analysis. Dr Andrew Beeby for the use of his UV-Vis spectrometer, and Prof. Todd Marder for the use of his fluorometer, and their groups for making me welcome into their labs.

During this work there have been several collaborations. Thanks to Prof. Luca Prodi and his group, University of Bologna, for the extensive photophysical studies on the di- and tripodal studies, and explainations of the results they obtained. Dr Martin Paterson, Herriot-Watt University, has been extremely helpful, in running numerous DFT studies, on a range of compounds. Drs Mike Probert, and Andres Goeta for the X-ray crystal analysis, and Dr Kirsty Anderson and Gareth Lloyd for their crystal analysis and helping me with all things crystal, I wouldn't have the structures without their help. My thanks goes to Emma Wallace for all her work on the viologen compounds, and the gossip during the endless hours doing NMR titration on these compounds, and thanks Adam Swinburne, for growing the viologen crystal structure. Thanks also to Dr Charlotte Willans, for all her help, particularily with the ruthenium work, and for growing the crystal of her derivative, and proving the ideas about my complex to be correct.

My thanks must go to the Steed group, past and present, my great thanks must go to Joe and Maria, who welcomed me into the group, and helped me with my research in the early days, and also those not mentioned by name, for making the lab an enjoyable place. Thanks must also go to friends made during this time at Durham, to mention a few, Emma, Helen, Matt and Jamie (CDM has been wonderful), Simon, Dave, and my housemate Victoria, for looking after me over the last 2 years.

Lastly, I would like to thank my friends, those who live a little further away, but have been endlessly supportive, you know who you are, and most importantly my parents, whose support, encouragement and understanding has been amazing during my time at university, and my sister, for being a fantastic sister.

Table of Contents

List of Figures

Chapter One

Chapter Two

Chapter Three

Chapter Four

Chapter Five

Chapter Six

Appendix

List of Schemes

List of Tables

Chapter One

Chapter Two

Chapter Three

Chapter Four

Abbreviations

A (crystallography)	Acceptor
ADP	Adenosine Diphosphate
AMP	Adenosine Monophosphate
Ar (NMR)	Aromatic
ASU	Asymmetric Unit
ATP	Adenosine Triphosphate
br (NMR)	Broad
C_i	Coefficient of the Single Particle-hole State
CSD	Cambridge Structural Database
CT	Charge Transfer
D (crystallography)	Donor
d (NMR)	Doublet
dd (NMR)	Doublet of doublets
ddd (NMR)	Doublet of doublet of doublets
dt (NMR)	Doublet of triplets
DCM	Dichloromethane
DFT	Density Functional Theory
DMSO	Dimethylsulfoxide
DSC	Differential Scanning Calorimetry
ESI	Electro-Spray Ionisation
EtOH	Ethanol
HOMO	Highest Occupied Molecular Orbital
Hz	Hertz
IR	Infra Red
$K_{1:1}$	1:1 Host:Guest Binding Constant
$K_{1:2}$	1:2 Host:Guest Binding Constant
$K_{2:1}$	2:1 Host:Guest Binding Constant
K_a	Association constant
LUMO	Lowest Unoccupied Molecular Orbital
ILCT	Intra-Ligand Charge Transfer

m (NMR)	Multiplet
MeCN	Acetonitrile
MeOD	Deuterated Methanol
MeOH	Methanol
MS	Mass Spectroscopy
MHz	Mega-Hertz
NMR	Nuclear Magnetic Resonance
OMe	Methoxy
PET	Photo-Electron Transfer
ppm	Parts Per Million
q (NMR)	Quintet
RT	Room Temperature
s (NMR)	Singlet
SCE	Saturated Calomel Electrode
t (NMR)	Triplet
TBA	Tetrabutylammonium

Chapter One

Introduction

1.1 Anion Supramolecular Chemistry

'Beyond molecular chemistry based on the covalent bond, supramolecular chemistry aims at developing highly complex chemical systems from components interacting through non-covalent intermolecular forces' [17]

The supramolecular coordination chemistry of anions has provided an area of great interest over recent years, despite the intrinsic challenges of anion binding, compared to cationic and neutral guest binding.[1] This interest is due to the realization of the many roles of anions in biology, medicine, catalysis and the environment.[1, 18-21] Anions are involved in many key functions, including acting as cofactors, substrates or signalling devices, in which each anion is being selectively recognized by its receptors,[22] and their potential applications in ion sensing and extraction.[23] The interest in studying the binding of anions is due to the many potential applications in biological systems[24-26] and industry,[27] as well as the lethal effects of anions that have been observed on the environment.[28]

Anions have several features that must be catered for when designing an effective receptor, to which the anion will bind strongly,[29, 30]

- ***Charge:*** Anions have a negative charge, and therefore electrostatic interactions can play an important role in strengthening the binding between the anion and the receptor.[29] However electrostatic charges are non-directional so all anions are attracted to the host on an electrostatic basis, forming a solvated ion pair in solution. It would be expected that anions with a higher charge density would show greater affinity for the host.[31] Due to the size of anions their charge density is lower than their isoelectric cations, thus the electrostatic forces will be weaker than those with cations.[30]

- ***Size:*** Anions are larger than their isoelectric cations, and thus the cavities within the receptors must be large enough to successfully bind the desired anion.[29]

- ***pH dependence:*** Many anions only exist over a small pH range (e.g. carboxylates, phosphates, or sulphate), unlike simple metal cations. At low pH, anions become protonated and consequently lose their negative charge. This is especially important if the anion recognition is to take place in water.[29]

- ***Solvation:*** The solvation of an anion depends on the three factors; i.e. charge, size and basicity and plays and important role in controlling anion binding selectivity. The *Hofmeister series*[29] reflects the degree of aqueous solvation of an anion and ranks anions in order of increasing hydrophobicity, i.e. low aqueous solvation. In a hydrophobic binding site, the less hydrated anions are bound more strongly. Conversely, in a binding site which is accessible to polar solvents, the more hydrated anions are often more strongly bound.[29]

- ***Geometry:*** Anions can form a range of geometries, which can make it difficult to design a binding site which will complement this geometry.[29] This can bring about the opportunity for selectivity because anions are different from one another.

- ***Lewis Basicity:*** Most anions are Lewis bases, although some of them do not have a lone pair (e.g. AlH_4^-, $B(C_6H_5)_4^-$, *closo*-$B_{12}H_{12}^{2-}$) or are only very weak bases (e.g. $B(C_6F_5)_4^-$). This suggests that as anions have the ability to donate an electron pair to a certain extent, it is possible that Lewis acids can be used as anion receptors.[29,31]

- ***High Polarisability:*** Anions are highly polarisable, and thus van der Waals interactions will be significant. These forces are non-directional but are related to the surface area of the host and anion, and so three-dimensional encapsulation of the anion should enhance the binding of all anions capable of fitting into the host cavity.[31]

It is possible to synthesize receptor molecules which bind inorganic anions strongly with high selectivity, from the combination and preorganisation of different anion binding groups, for example, amides, urea moieties or Lewis acidic metal centres.[32] A receptor must provide a cavity, in which to encapsulate the envisaged guest, and this cavity should contain groups which are capable of interacting with the desired guest.[33] The selectivity of the receptor depends on energy terms related to the strength of the receptor-substrate interaction, and on geometric factors, size and shape matching between the receptor and substrate. As anions tend to interact with the host by either electrostatic or hydrogen bond interactions, the receptor must with either contain positively charged groups, for example, ammonium, or neutral hydrogen bond donor groups, for example, amides.[33]

1.2 Anion Binding

The design of anion binding and sensing systems have been an area of active research since 1968, when Park and Simmons reported the encapsulation of halide anions in a charged molecular frame work.[34, 35]

Many groups have researched chloride ion transport, due to its biological importance in the management of cystic fibrosis. Cystic fibrosis is the most common life-shortening autosomal recessive disorder in Europe.[36] The disease results in a mutation in the cystic fibrosis transmembrane conductance regulator which controls chloride channels *in vivo*,[37] and those who suffer from it have higher than normal concentrations of chloride ions in their blood. Gale *et al.* reported the synthesis of a synthetic prodigiosin mimic which co-transports H^+/Cl^- across vesicle membranes.[38] The compound was shown to have potential in combating cystic fibrosis, by helping to restore the normal chloride ion concentration balance.

Anion sensing has many environmental applications.[28, 39] The early detection of elevated levels of the anions of nitric and sulphuric acids would be beneficial, as it could help prevent the effects of acid rain becoming more serious in a particular area. The detection of nitrates and phosphates from fertilisers would prevent the build-up of high concentrations of these

anions in freshwater systems, which greatly alters the ecosystem.[28] Receptors which could selectively bind anions present in radioactive waste,[27] or are radioactive themselves,[40] could play an appreciable role in radioactive waste disposal and detection. All of these examples illustrate the great importance of the continued research into anion recognition and binding.

1.3 Ammonium-Based Anion Receptors

Amines and ammonium groups have been used as effective hosts for the binding of anions. Amine NH protons are acidic and capable of forming strong non-covalent contacts. The production of a quaternary ammonium group, by protonation of an amine, leads to enhanced hydrogen bonding compared to amines, as well as the resulting positive charge being able to attract anionic guests.

Hutson and co-workers, synthesised two polyamine receptors containing fluorescent reporter groups, **1.1** and **1.2**, in 1989. They synthesised hosts based on anthrylpolyamines, and the interactions with oxo-anions, carboxylate, phosphate and sulphate were investigated.[41, 42] Garcia-España *et al*, extended this work to focus on a variety of linear amines, of varying chain lengths, and containing one or two terminal anthracenyl groups, **1.3a-b**. These compounds were found to be fluorescence-signalling receptors for ATP, ADP and AMP. They found that ATP was bound significantly stronger than the other nucleotides, log K = 8.1-9.9, measured in a 0.15 M NaCl solultion.[43] They also synthesised a dibenzylated host molecule, **1.4**, and measured the binding ability of **1.4**, with $Co(CN)_6^{3-}$. The binding constants of **1.4** were measured by quenching of the steady-state fluorescence emission, and indicated a range of log K = 2.41 for the shortest chain to 2.60 for the longest chain.[44]

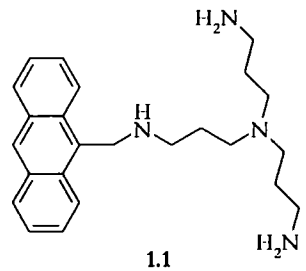

1.1

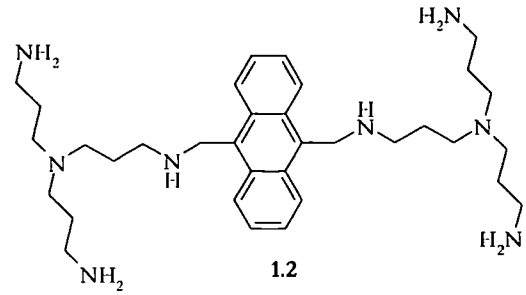

1.2

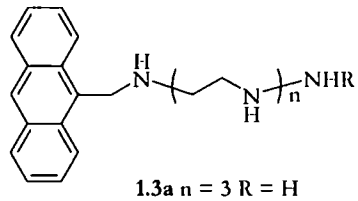

1.3a n = 3 R = H
1.3b n = 3, 4 R = H, CH_2

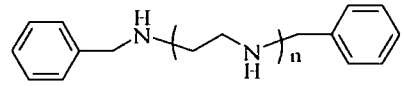

1.4 n = 1 - 4

Protonated or alkylated polyammonium macropolycycles were some of the earliest examples of synthetic anion receptors. Hossain and Schneider measured the stability constants of the complexes formed between open-chained α,ω-dications and α,ω-dianions, **1.5** and **1.6**, by NMR titration techniques in water. They found that as the number of flexible single bonds ranged from 6-13, the strength of the complexes formed does not vary to a great extent (ΔG values range from -12.6 to 16.3 kJ mol^{-1}). The authors thus concluded that the importance of conformationally preorganised receptors for molecular recognition has been over estimated.[4, 45]

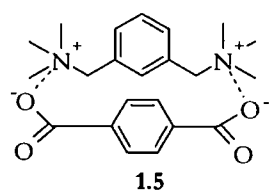

1.5

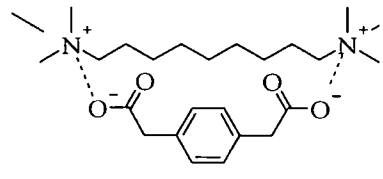

1.6

However, the major drawback of polyammonium based receptors is the limited pH range over which they remain protonated. This is particularly a problem when binding basic anions, such as phosphates or carboxylates. Sessler *et al*, in addressing this problem, used sapphyrin, an expanded polyphrin macrocycle, **1.7**, to bind nucleotides. They showed that this receptor binds anions using a combination of electrostatic, hydrogen bonding and π-stacking interactions.[22]

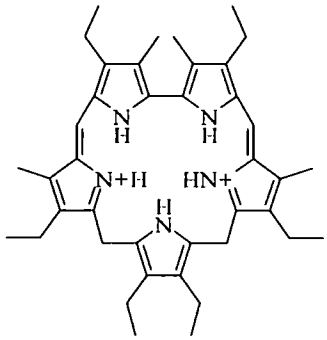

1.7

Garcia-España, Celda, Bianchi and co-workers have used pH-metric titration, cyclic voltammetry and NMR to study the interactions between 1,2,3,10,13,16,19-heptaazacyclohenicosane, **1.8**, and NAD^+, **1.9** and $NADP^+$, **1.10**, in aqueous solution. They found that both NAD^+, **1.9**, and $NADP^+$, **1.10**, bind strongly to the polyammonium macrocycle (with varying degrees of protonation of the macrocycle). They have found that $NADP^+$, **1.10**, is selectively bound to the receptor over NAD^+, **1.9**. This increased selectivity is due to the extra phosphate moiety strongly interacting with two adjacent ammonium groups present in the receptor.[4, 45, 46]

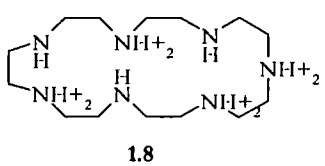

1.8

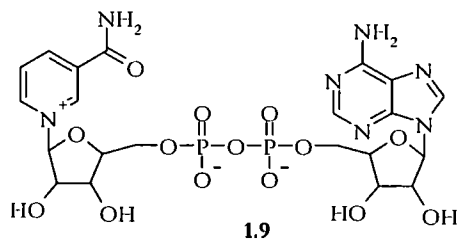

1.9

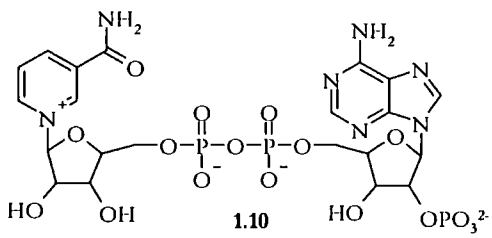

1.10

Lincoln and co-workers have shown that the charge and the hydrophobicity of the receptor and the guest are significant factors in controlling the stability of the complex formed. They studied this using the formation of complexes between 6^-(ω-aminoalkylamino)-6^-deoxy-β-cyclodextrins, **1.11**, and carboxylic acids and carboxylates in aqueous solutions. They

concluded that as the pH increased the host charge and hydration decreased, while the hydrophobicity increases. At the same time, the guest charge and hydration increased and the hydrophobicity decreased. This said, with a less hydrophobic host, having a dipositive charge and either a neutral or a negatively charged guest, a stronger complex stabilization was observed. It was concluded by Lincoln and co-workers that the complex stability was affected by the significant secondary interactions generated by the charge and the hydrophobicity of the host and the guest.[4, 47, 48]

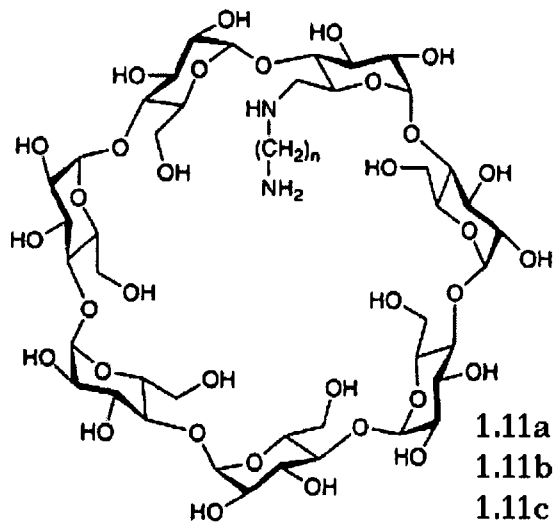

1.11a n = 2
1.11b n = 3
1.11c n = 4
1.11d n = 6

Bianchi and co-workers, have studied[49] the synthesis and characterization of two new bis([9]aneN$_3$) ligands, which contain two [9]aneN$_3$ macrocyclics separated by a 2,6-dimethylenepyridine unit, **1.12** and **1.13**.[50, 51] The coordination of the hosts to both cations and anions was measured, the coordination properties to Cu(II), Zn(II), Cd(II) and Pb(II) were studies by potentiometric and UV spectrophotometric measurements. The coordination to halides was measured using potentiometric and ^{1}H-NMR spectroscopic experiments, and it was found that **1.12** was selective for bromide while **1.13**[49] is selective for chloride.

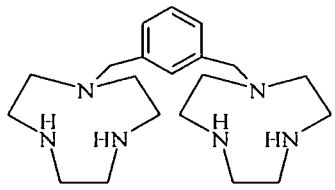

1.12

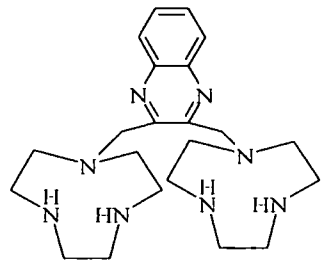

1.13

Bowman-James *et al* have synthesised a substituted tris(aminomethyl)amine based amine.[52] They did not expect the host to be selective to anions due to the repulsion of protected primary amine groups by each other, hence making the formation of a C_3-symmetric cavity unlikely. As well as crystallographic studies, they undertook NMR titration experiments, with various anions as their tetrabutylammonium salts. Upon addition of $H_2PO_4^-$, HSO_4^-, NO_3^-, Br^- and Cl^- to the protonated ligand H_3**1.14**$^{3+}$ in chloroform-*d*, they observed a downfield shift of the NH resonances suggesting the amine protons are involved in the binding of anions via hydrogen bonding interactions. The titration data implied a 1:1 host:guest binding model, and associations constants were calculated from the data. They found the oxo acid anions were bound more strongly than halide anions, with log K = 3.25 for $H_2PO_4^-$, 3.20 for HSO_4^-, 1.55 for NO_3^-, 1.70 for Br^- and 1.80 M^{-1} for Cl^-. They suggest that from the data they have obtained that the host is not actually selective for the oxo acid anions but it is more due to anion charge and basicity than true selectivity of the host.

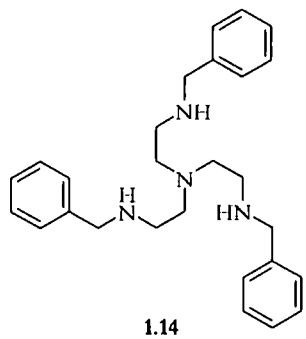

1.14

1.4 Guanidinium Based Anion Receptors

Guanidinium hosts contain both a positive charge and two hydrogen bond donor groups. The combination of hydrogen bonding and electrostatic interactions leads to the formation of strong complexes, even in very competitive hydrogen bond accepting and donating solvents, for example, water.[19]

Anion sensing also has practical uses in the beverage industry, in the detection of citrate in energy and soft drinks, Anslyn *et al* have synthesised a molecule, **1.15** for such purposes.[53-55] They have also developed a series of molecules which can sense the age of whisky,[56] which have the potential to be used in quality control and prevention of imitation of trade-mark brands. This receptor, **1.15**, is a tris-guanidinium host based around an aryl core, which has shown recognition of tri-carboxylate and tri-phosphate polyanions. Because the host contains three guanidinium groups it is complementary to the guests containing three carboxylates or phosphates, and results have shown that guests which contain three anionic moieties, e.g. citrate (K = 6.9 x 10^3 M^{-1}) are bound more strongly than those with fewer anionic moieties, e.g. acetate (K < 10 M^{-1}).[55]

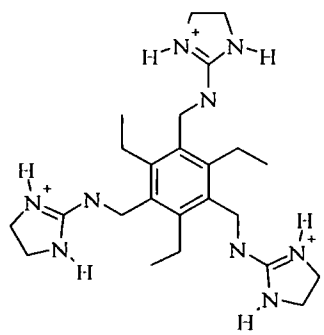

1.15

Jadhav and Schmidtchen have studied the interactions of hosts **1.16** and **1.17** with guests **1.18** – **1.23**, as tetrabutylammonium salts using isothermal calorimetry in acetonitrile.[51, 57] They found a large difference in entropy between the two hosts and the set of guests, which they attributed to variations in the 'stiffness' and the number of mutual binding modes, as opposed to desolvation processes. Binding studies showed that **1.16** has a higher affinity for anions than **1.17**, which is explained by a lower degree of 'structural definition' present in

complexes with **1.17** which results in more favourable entropic component to binding rather than being due to the presence of extra hydrogen bonding groups. [51, 57]

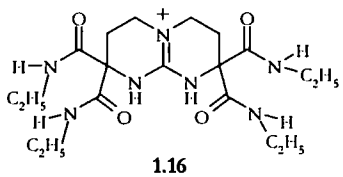

1.16

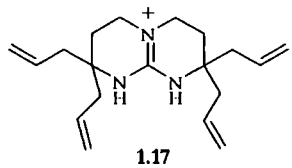

1.17

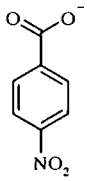

1.18

1.19

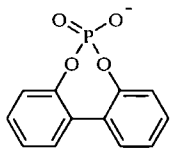

1.20

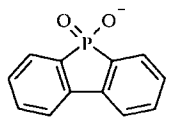

1.21

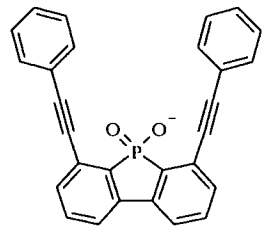

1.22

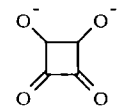

1.23

Kato and co-workers have synthesised the pyrene functionalized monoguanidinium species, **1.24**, and shown that it forms a 2:1 receptor-anion complex with pyrophosphate.[58, 59] The sensing of this anion results in dramatic changes in the fluorescence of the pyrene moiety. The addition of other anions, such as HPO_4^{2-}, $H_2PO_4^-$, CH_3COO^-, SCN^-, Cl^- or Br^-, do not result in the formation of the self-assembled array and hence show a much weaker change in the fluorescence of the pyrene moiety.

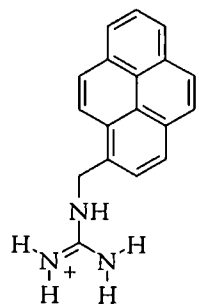

1.24

1.5 Amide Based Anion Receptors

Amide groups have been used to produce a wide range of receptors, which are capable of coordinating anions. These can either have a completely organic scaffold, which usually utilize either completely hydrogen-bonding or a combination of hydrogen-bonding and electrostatic forces.[20]

Crabtree *et al*, have shown that very simple amides, for example isophthalic acid derivatives **1.25**, can bind anions.[19, 60] NMR spectroscopic titration experiments were undertaken with both hosts and **1.25b** was found to bind chloride more strongly than both bromide and iodide in dichloromethane-d_2. Stability constants were calculated for the addition of halides and with values of K = 6.1 x 10^4, 7.1 x 10^3 and 4.6 x 10^2 M^{-1} for chloride, bromide and iodide respectively being obtained. Jobs plot analysis showed the formation of 1:1 host:anion stoichiometry exclusively for **1.25b** and halides.

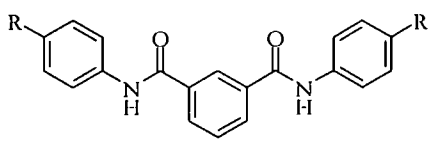

1.25a R=H
1.25b R = n-Bu

Tripodal tris-2-aminoethylamine (tren) based receptors containing amide functionalities have been shown to be effective anion binding hosts.[19, 61, 62] Stilbor has shown that amide groups have been shown to be activated, to enhance their binding with anions, by synthesizing receptors to contain electron withdrawing fluoro substituents, and electron poor pyridine rings, **1.26** and **1.27**.[19] They observed the anion binding ability of these tripodal molecules by NMR spectroscopic titration experiments in a variety of solvents, and in all cases found 1:1 host:guest complexes were formed. Receptor **1.26** was found to be selective for $H_2PO_4^-$ over other recognised anions, Cl^-, Br^-, I^-, HSO_4^-, and NO_3^-, in all of the solvent systems studied, with a binding constant of 7550 M^{-1} for $H_2PO_4^-$ and 1350 for Cl^-, which was the next most strongly bound anion, in acetonitrile solution. Receptor **1.27** is selective for HSO_4^- over $H_2PO_4^-$, with binding constants of 5120 M^{-1} for HSO_4^-, and 154 M^{-1} for $H_2PO_4^-$, in chloroform-*d* solution.

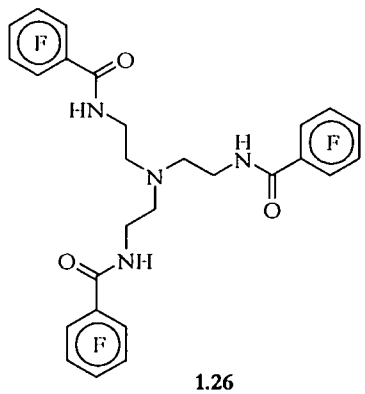

1.26

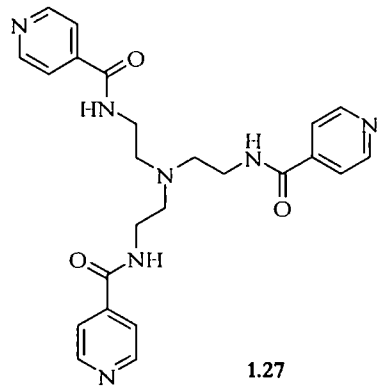

1.27

Bowman-James *et al.* have used amine linkers to join together two isophthalic acid derived amide clefts, to give a receptor **1.28**, which forms strong complexes with phosphate and sulfate, when they are added as dihydrogen phosphate and hydrogen sulphate.[18, 63] It is presumed that this is due to the anion being deprotonated by the amine groups present in the receptor, providing an electrostatic component to binding, as well as the complementarity between the receptor and oxo-anion.[18]

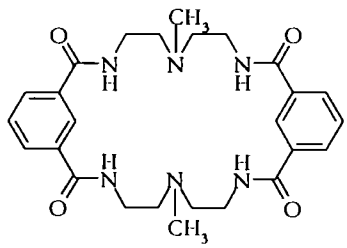

1.28

Choi and Hamilton have described the synthesis and anion binding properties of cyclic tri-amide based receptors **1.29**. NMR spectroscopic evidence has suggested that this receptor binds I^-, and at low I^- concentration binds in a sandwich fashion. But at higher concentrations of I^-, binding switches to a 1:1 binding mode, which has been confirmed by an initial up-field of the NH resonances in the ^{1}H-NMR spectrum of the receptor upon addition of I^- followed by a chemical shift change after about 0.5 equivalents of I^-.[18, 64]

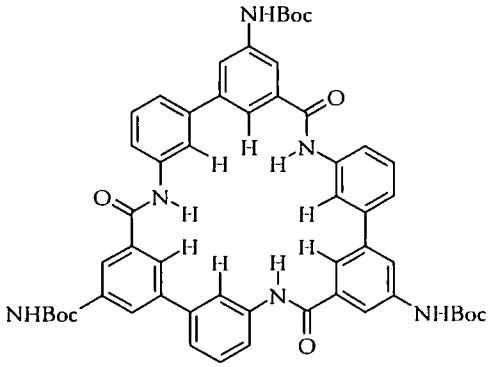

1.29

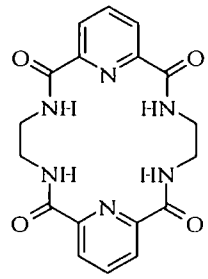

1.30

Szumna and Jurczak have prepared an acetate selective macrocyclic receptor by linking together two pyridine clefts **1.30**.[18, 65] They found that in solution, it was predominately 1:1 receptor : anion complexes are formed, but in the solid state, the crystal structure of the tetrabutylammonium acetate complex, showed a 2:1 receptor : anion ratio.[18, 65]

Anslyn and co-workers have extended their displacement assay paradigm, to include a molecular ensemble, consisting of a trigonal molecular box **1.33**[19, 65]and a colorimetric dye, such as resorufin **1.32** or Methyl Red **1.31**.[3-5, 66] The addition of the colorimetric dye, allows the determination of the binding constant between the receptor and the anion. The changes in the absorbance of Methyl Red **1.31** and resorufin **1.32** were measured upon addition of the receptor, by UV/Vis spectrometry. To sense nitrate, an aliquot of **1.33** was mixed with the indicator, **1.32** in 50% MeOH-50% CH_2Cl_2. The competition of nitrate and the indicator were monitored for binding to the receptor as a function of different concentrations of the receptor, **1.33**. The indicator, **1.32**, is increasingly bound as the receptor, **1.33** is added, but the amount of nitrate in the solution modulates the extent to which the indicator is bound. **Figure 1.1** shows the results of six experiments, each with a different concentration of nitrate and the same concentration of **1.32**.[3] In the presence of 40 mM nitrate, the absorbance spectrum of **1.32** was not affected by the addition of **1.33** because the nitrate prohibited binding between **1.32** and **1.33**[3] The addition of nitrate anions to the receptor, and indicator complex, either resorufin **1.32** or methyl red **1.31**, show large changes in the absorbance due to the equilibrium between the complex and its component parts being

perturbed.[3-5, 66] The competition inhibition given by the anions against the formation of the **1.32** – **1.33** complex can be used to measure the association constants for the anions.[3]

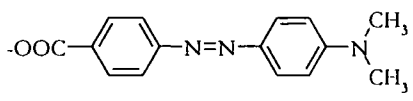

1.31

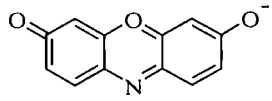

1.32

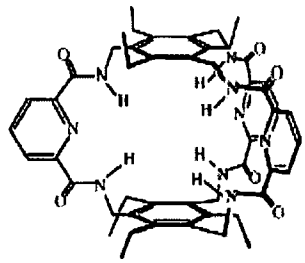

1.33 – Reproduced from reference [3].

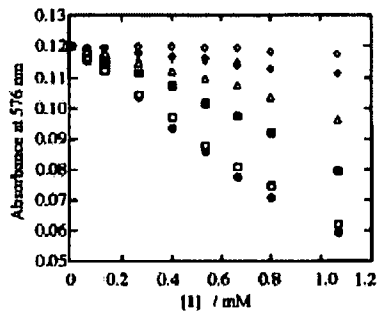

Figure 1.1 – Change in the intensity of absorption of Resorufin **1.32** upon addition of **1.33** in the presence of sodium nitrate in 50% methanol-50% CH_2Cl_2 (*v*/*v*). Concentration of sodium nitrate = 0 (●); 1 (■); 4 (□); 10 (Δ); 20 (◆); 40 (◇) mM. Reproduced from reference [3].

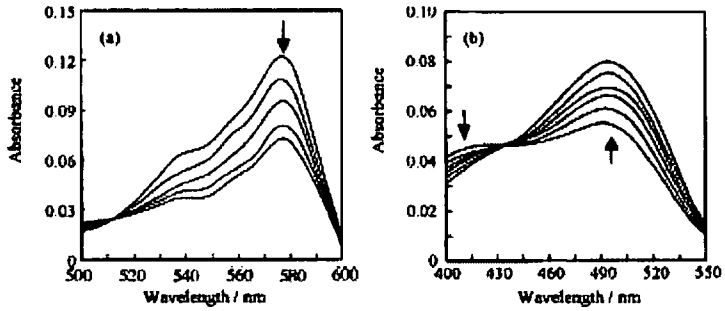

Figure 1.2 - UV/VIS absorption spectra of (a) Resorufin, **1.32** and (b) Methyl Red, **1.31** upon addition of **1.33** in 50% methanol-50% CH_2Cl_2 (v/v). Reproduced from references [3-5].

Costa and co-workers have reported using a receptor **1.34**, in a fluorescent ensemble to monitor sulphate concentration in water.[6, 18] The squaramide binds to SO_4^{2-}, with an association constant K_a of (4.6 ± 1.0) x 10^6 M^{-1} in methanol at 294K. The receptor **1.34** also quenches the fluorescence of fluorescein **1.35**, and so the receptor-fluorescein ensemble maybe used as a displacement assay with sulphate competing for the squaramide binding site with the quenched bound fluorophore and so displacing it and restoring the macrocycle's fluorescence.

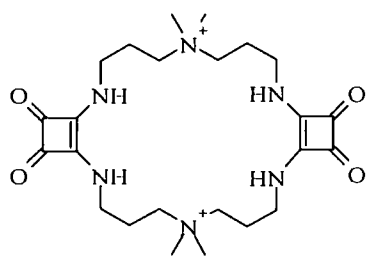

1.34

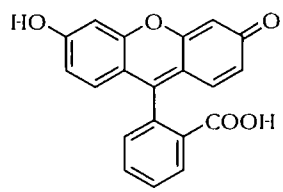

1.35

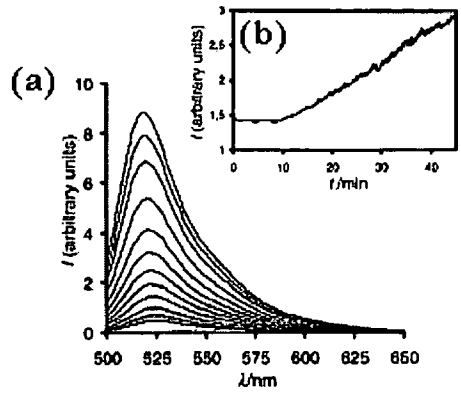

Figure 1.3 - (a) Fluorescence emission band ($\lambda_{exc.}$ 490 nm) of fluorescein, concentration of **1.35** = 1.4 x 10^{-5} M before (upper band) and after addition of receptor, concentration of **1.34** = 2.0 x 10^{-4} M (lower band). Fluorogenic emission response with several concentrations of sulphate = 4.6, 6.5, 8.4, 10.0, 11.7, 13.3, 14.8, 15.9 x 10^{-5} M. (b) In this experiment, after approximately 10 min period, the sulphate concentrate of a water solution was continuously increased from 0 to 200 ppm and mixed at 0.10 mL min^{-1} together with a stream of receptor, concentration of receptor = 2.6 x 10^{-4} M and concentration of **1.34** = 7.4 x 10^{-4} M in MeOH-H_2O (90:10 v/v) at a flow rate 0.90 mL min^{-1}. Reproduced from reference [6].

1.6 Pyrrole Based Anion Receptors

Applications of pyrrole based anion receptors have been seen in areas as diverse as anion sensing and transport, as well as allowing the stabilization of supramolecular structures, with species ranging from fluorine, to the complex structure of DNA. Part of its attraction is that pyrrole does not have a built-in hydrogen bond acceptor, unlike many other anion receptors which often self-associate via C=O···HN interactions (e.g. amides and urea).[67, 68] Because pyrrole is neither acidic nor basic, it can be used to support NH-anion hydrogen bond interactions under a variety of different conditions.[67, 68] Pyrroles can be relatively easy to functionalize and incorporate into cyclic and acyclic systems, whether they are structures as venerable as porphyrins, or new structures such as pyrrole amides. These pyrrole-based anion receptors display a richness in size, shape, structure and electronic characteristics.[67]

Sessler *et al.*, have synthesized a number of macrocyclic systems containing more isolated pyrrolic subunits. One of these compounds is *ansa*-ferrocene,[67, 69] which contains two

pyrrolic NH and two amidic NH groups that can combine to make it and its analogues efficient anion receptors.[67, 70] In **1.36**, the binding stoichiometry has been found to be dependant on the size of the anion guest. Job plots revealed that a 2:1 (anion to host) binding stoichiometry for the complexation of fluoride anion, and a 1:1 ratio for the other anions (chloride, bromide, hydrogen sulfate and dihydrogen phosphate).[67]

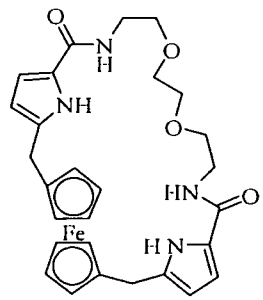

1.36

Gale *et al*, have produced an oxo-anion selective receptor, by attaching amide groups to the 2,5-positions of the pyrrole ring. These systems can be regarded as pyrrolic analogues of the isophthalic amide anion receptors produced by Crabtree *et al*.[60] The compounds both proved to be selective for oxo-anions in polar organic solvents **1.37** and **1.38** (CD_3CN or DMSO-d_6 (0.5% water)). Differences in the binding characteristics of **1.37** and **1.38**, were observed.[71, 72] Association constants were measured for **1.38** with dihydrogen phosphate and benzoate, in acetonitrile-d_3, where K = 357 and 2500 M^{-1} respectively. Association constants were also measured for **1.37** with dihydrogen phosphate and benzoate, in DMSO-d_3/H_2O 0.5 %, where K = 1450 and 560 M^{-1} respectively, suggesting **1.38** has a greater affinity for benzoate, and **1.37** dihydrogen phosphate.[71] 2-Amido-5-methylpyrrole compounds were synthesized to gain insight into the binding mode adopted by these compounds in solution. It was seen that both of the compounds showed significantly reduced affinities for oxo-anions compared to the 2,5-diamido anologues, **1.37** and **1.38**. That said, **1.39** binds benzoate anions with an association constant of 202 M^{-1} in acetonitrile-d_6. On the basis of these findings it was suggested that in the 2,5-diamido systems, all three NH hydrogen bond donors are involved in hydrogen bond donation to the oxo-anions.[67]

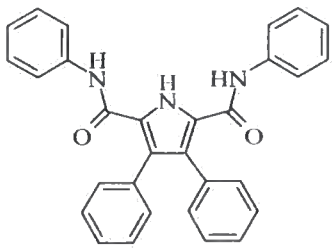

1.37

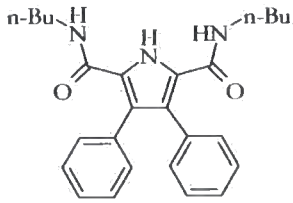

1.38

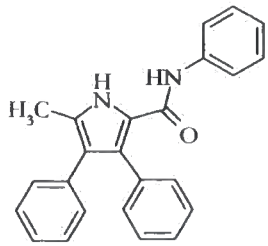

1.39

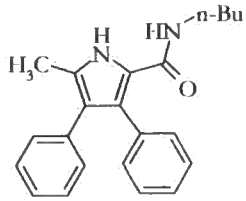

1.40

The x-ray structure of **1.38** binding with benzoate shows that all three hydrogen bonds are indeed involved in hydrogen bonding to the anionic guest. The benzoate anion was found to be coordinated within the cleft formed by the amide and pyrrole moieties by the three NH-O hydrogen bonds in the range 2.771(3) – 2.864(3) Å. As can be seen in **figure 1.4**, one of the oxygen atoms of the benzoate is in the plane of the pyrrole ring and one of the amide groups. The other amide group is twisted out of the plane by 38.03(10)° to accommodate a hydrogen bond to the other benzoate oxygen atom.[67]

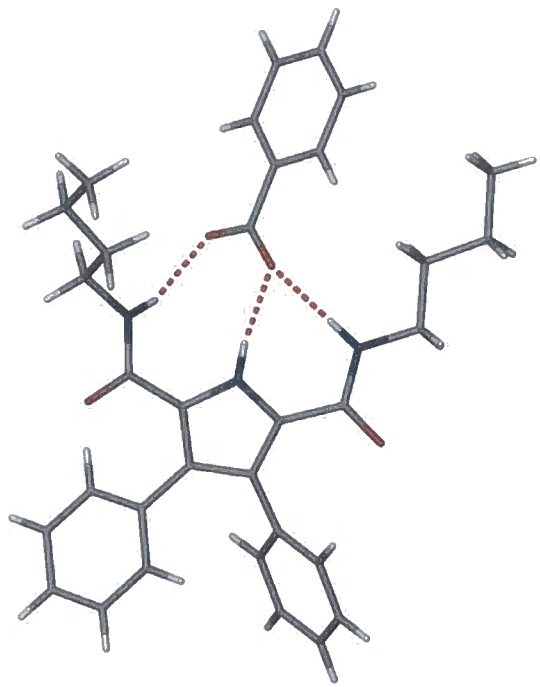

Figure 1.4 – Molecular structure of benzoate anion complex of **1.38**.[72]

The addition of ferrocene groups to the 2,5-diamido ligand has shown that these compounds maybe used as electrochemical sensors for anions. Gale *et al*, have added the ferrocene groups directly to the amide group as in **1.41** or via a methylene spacer, **1.42**. The

electrochemistry of these compounds was investigated by cyclic voltammetry, and significant shifts of the ferrocene-ferrocenium redox couple were observed upon addition of a variety of anions to solutions of the receptors. However, in a number of cases the shape of the voltammetric wave was found to be seriously distorted as the product of the electrochemical reaction passivates the electrode.[67]

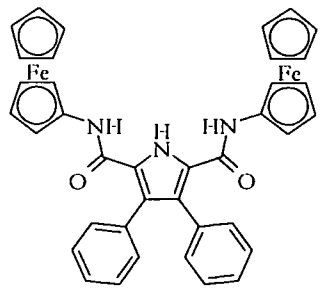

1.41

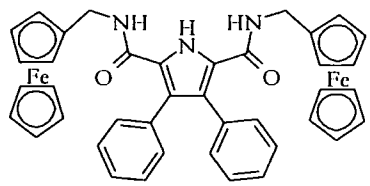

1.42

1.7 Urea Based Anion Receptors

Urea and thiourea binding groups have been widely used as they are excellent hydrogen bond donors, and have been found to form particularly strong complexes with carboxylates.[15]

Hoffmann and co-workers have synthesised a series of tripodal urea hosts, containing a triazine-trione core, elaborated by three urea arms.[73] The complexation of these hosts with anions was measured using NMR spectroscopic titration experiments. Anions were added to a chloroform-*d* solution of the host as their tetrabutylammonium salts, and the chemical shifts of the urea NH resonances were monitored. Job Plot experiments confirmed a 1:1 host:guest stoichiometry suggested by the NMR spectroscopic titration data. They observed the highest affinity for chloride for all hosts, followed by bromide, and the least affinity for nitrate, with stronger binding seen with hosts **1.43** and **1.44**. Association constants for addition of chloride were, K = 18300 for **1.43**, 19500 for **1.44** and 7400 M^{-1} for **1.45**. As self association is quite common in urea containing hosts, they undertook some self association NMR experiments, and from these were able to calculate self association constants, K = 16 M^{-1} for **1.44**, and 17 M^{-1} for **1.45**. As the self association constants are at least an order of magnitude smaller than the anion binding constants, the authors concluded that self-

association was not a matter of concern for the anion binding affinities. They also found that the preorganisation in the hosts has an effect on anion binding, for example, in **1.45** were there is no preorganisation in the host, less affinity was seen for chloride than for the more preorganised hosts **1.43** and **1.44**, but in the case of nitrate a greater affinity was observed for the non-preorganised host **1.45**, and there was little difference in the binding affinities seen in all hosts with respect to bromide. This suggests that conformational preorganisation may lead to an increase in binding (chloride), no change in binding (bromide) or a decrease in the binding (nitrate), and leads to the conclusion that conformational preorganisation can have a strong influence on binding selectivities.

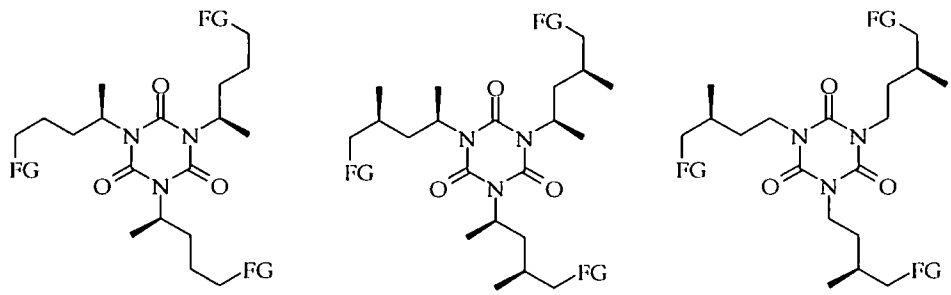

1.43 **1.44** **1.45**

FG = urea = NH-CO-NH-*p*C_6H_4-*n*C_4H_9

Yoon *et al* have reported a new series of colourimetric and fluorescent sensors, in which two *p*-nitrophenylurea groups or two phenylurea groups are attached to the first and eight-positions of anthracene, **1.46a** and **1.46b**.[15, 74] The host have shown affinity for fluoride and pyrophosphate, and binding constants for **1.46b** were measured using fluorescent titration techniques on DMSO, and were found to be 108,000, 9700 and 6000 M^{-1} for fluoride, bromide and pyrophosphate respectively. Host **1.46b**, showed a higher affinity for anions than host **1.47b**, and it is suggested that this is due to cooperative effect of the two thiourea groups. It was also observed than anion complexation to fluoride and pyrophosphate was enhanced by the formation of a hydrogen bond from the 9-H of anthracene (between the two urea groups).

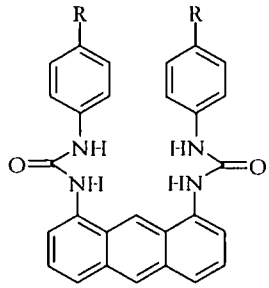

1.46a R = NO_2
1.46b R = H

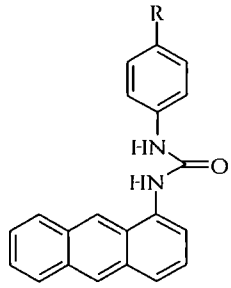

1.47a R = NO_2
1.47b R = H

Das *et al* have synthesised a urea, **1.48a**, and thiourea receptor, **1.48b**, which experience a visible colour change upon addition of $H_2PO_4^-$, OH^-, CH_3COO^-, $PhCOO^-$, in DMSO/Acetonitrile solution.[75] In acetonitrile solution, they saw that $H_2PO_4^-$ was selectively recognized over the other oxo-anions studied. They observed no colour change for the urea host, **1.48a**, at room temperature, but when the same experiments were carried out at 60°C, a pale red colour results. In contrast, at room temperature, upon additions of anions to the thiourea host, **1.48b**, an immediate colour change from pale yellow to violet resulted. They observed a red-shift in the UV-Vis spectrum upon addition of anions to both hosts, and this was explained by the charge-transfer interaction from the electron-rich urea/thiourea to the electron-poor anthraquinone moiety. NMR spectroscopic titration experiments and Job plots, showed the formation of 1:1 host:guest complexes in the case of both hosts, suggesting the two arms on the host are exhibiting cooperative binding. Significantly stronger binding was observed for the thiourea host, **1.48b**, compared to the urea host, **1.48a**, by 100 fold, for example K = 7.9 x 10^3 and 1.5 x 10^5 M^{-1} for the urea and thiourea host upon addition of chloride.

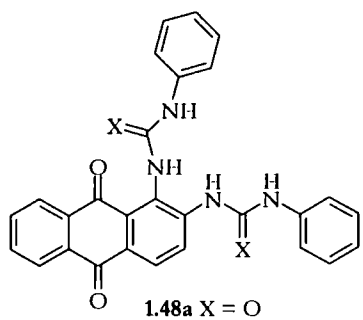

1.48a X = O
1.48b X = S

Jiang and co-workers have designed a series of neutral *N*-(substituted-benzamido)-*N'*-phenylthioureas[14, 15] **1.49a-h** which show large red-shifts in their absorption spectra upon anion binding and substantially enhanced anion affinities (13-590 times) compared with their *N'*-phenylthiourea derivatives. They measured binding constants towards different anions by measuring the absorption spectra of the host in acetonitrile, **Table 1.1**. The authors found that *N*-(*p*-ethoxybenzamido)-*N'*-(*p*-nitrophenyl)thiourea showed sensitive and selective binding to acetate in acetonitrile containing 10 % water by volume with a binding constant of 1.74 x 10^5 M^{-1} (which is higher than that of *N*-(*p*-ethoxybenzamido)-*N'*-(*p*-nitrophenyl)thiourea for binding acetate in pure acetonitrile). They also observed consistently stronger binding of all the tested anions for host **1.49c** with binding constants, K = 11.5 x 10^6 for F^-; 12.6 x 10^6 for AcO^- and 32.4 x 10^6 M^{-1} for $H_2PO_4^-$, compared to K = 0.157 x 10^6 for F^-; 1.84 x 10^6 for AcO^- and 0.0169 x 10^6 M^{-1} for $H_2PO_4^-$, for **1.49b**, and the difference between the hosts being the position of the R group, which is a methyl group in both cases.

Compound	F^-	AcO^-	$H_2PO_4^-$
1.49a	0.188 x 10^6	1.71 x 10^6	0.0123 x 10^6
1.49b	0.157 x 10^6	1.84 x 10^6	0.0169 x 10^6
1.49c	11.5 x 10^6	12.6 x 10^6	32.4 x 10^6
1.49d	0.0694 x 10^6	0.297 x 10^6	0.0053 x 10^6
1.49e	0.510 x 10^6	5.58 x 10^6	0.0399 x 10^6
1.49f	0.158 x 10^6	1.47 x 10^6	0.509 x 10^6
1.49g	0.0562 x 10^6	4.05 x 10^6	0.090 x 10^6
1.49h	0.685 x 10^6	2.48 x 10^6	0.138 x 10^6

Table 1.1: Binding constants K_a (M^{-1}) of receptor **1.49** with different anions (as their tetrabutylammonium salts) in acetonitrile.[14, 15]

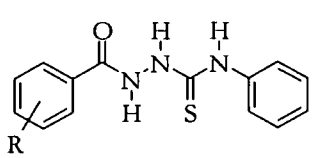

1.49a R=*p*-OC_2H_5 **1.49e** R=*p*-Cl
1.49b R=*p*-CH_3 **1.49f** R=*p*-Br
1.49c R=*m*-CH_3 **1.49g** R=*m*-Cl
1.49d R=H **1.49h** R=*p*-NO_2

Fabbrizzi and co-workers have synthesised the *S,S* and *R,R* chiral urea based hosts, **1.50**, which form a hydrogen-bonded complexes with the biologically important D-2,3-diphosphoglycerate anion.[51, 76] They found that the *S,S* enantiomer, **1.50**, has a stability constant that is twice that formed with the *R,R* isomer.

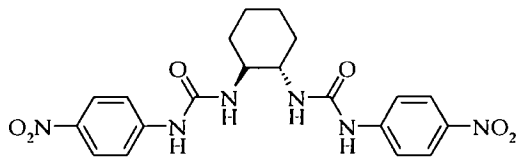

1.50

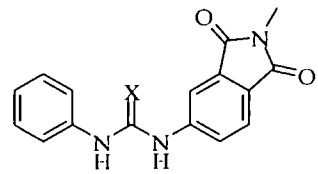

1.51a X = O
1.51b X = S

Fabbrizzi and co-workers have also studied anion triggered deprotonation in ureas and thioureas. Using a series of neutral hydrogen bond donor receptor systems they found the addition of basic anions such as fluoride and acetate brought about deprotonation of the host.[51, 77-79] Fabbrizzi observed that the deprotonation was often driven by the formation of stable species such as HF_2^-. Fabbrizzi *et al* compared the anion complexation of the urea, **1.51a**, and thiourea, **1.51b**, and they found that the more acidic thiourea, deprotonates in the presence of anions including fluoride, carboxylates and dihydrogen phosphate, but the less acidic urea is only deprotonated by the most basic anions studied.[80]

Fabbrizzi and co-workers have also synthesised a chemosensor, **1.52**, as deprotonation processes can be used to colourimetrically sense anions.[51, 81, 82] This colourimetric sensor consists of a thiourea group substituted with two chromophoric electron-withdrawing napthalnimide subunits.[7, 83] Somewhat basic anions such as acetate and dihydrogen phosphate were found to induce single deprotonation of the receptor, **1.52**, while more basic anions, fluoride and hydroxide, have been shown to induce a double deprotonation. The deprotonated species were shown to be red (LH^-) and blue (L^{2-}) respectively, **figure 1.5**.

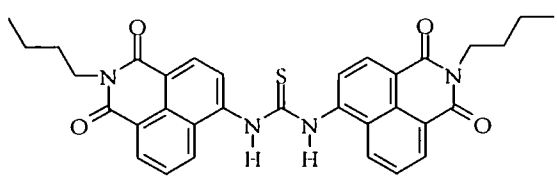

1.52

Figure 1.5: Colour changes observed upon addition of TBA-F to a DMSO solution of **1.52** (= LH_2). Left to right: free receptor (dominant species LH_2); plus 5 equiv. TBA-F (dominant species LH^-); plus 40 equiv. TBA-F (dominant species L^{2-}). Reproduced from reference [7].

1.8 Lewis Acid Based Anion Receptors

Anions can donate an electron pair to some extent, which allows the use of hydrogen bonds to bind these guests. Lewis acids, can accept an electron pair, which makes them very versatile as anion receptors and this has led to much research into a rich variety of Lewis acid based anion receptors based on heteroatom element chemistry.[4]

Many Lewis acid based anion receptors have metal atoms contained within them. These metal atoms play several different roles within the receptor:

- Metals or Lewis acids as binding sites in anion receptors
- Metals or Lewis acids as organizational elements in anion receptors
- Metals or Lewis acids as anion sensors,[4] a non-coordinating reporter group which signals the presence of the anion by a perturbation of its physical change, i.e. by changes in redox or spectroscopic properties.[18]
- An element in the receptor designed to withdraw electron density from a π-electron system and so increase the affinity of a hydrophobic anion receptor.[4, 18]

Peringer and co-workers have prepared subvalent mercury clusters, $Hg_3(\mu\text{-dppm})_3(SiF_6)_2$, and $Hg_3(\mu\text{-dppm})_3(PF_6)_2$ **1.53**, and showed that the mercury containing cations coordinate with anions. From the determination of the crystal structures of $Hg_3(\mu\text{-dppm})_3(O_3SCF_3)_4$, $Hg_3(\mu\text{-dppm})_3(O_3SCF_3)_4.MeOH$, $Hg_3(\mu\text{-dppm})_3(O_3SCH_3)_4$ and $Hg_3(\mu\text{-dppm})_3(O_3SCH_3)_4.4H_2O$,

Peringer and co-workers found in all cases that there were two anions inside the cavities formed by the twelve phenyl groups.[4, 84] It is possible to distinguish between different anions using the ^{31}P NMR spectroscopy as a shift in ^{31}P resonance was seen with different counter anions.[4, 84]

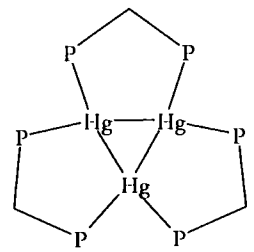

Anions either SiF_6^{2-} or PF_6^-

1.53

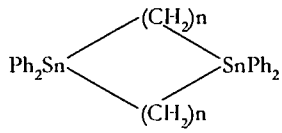

n = 4, 5, 6, 8, 10, 12

1.54

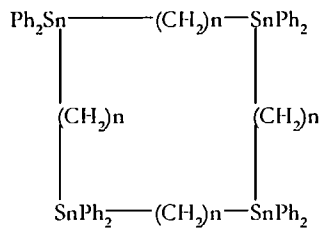

1.55

Another example is that of tin based receptors, which have been used as neutral carriers for selected anions in membrane electrodes, since the late 1960's.[85] Generally the compounds used were mononuclear tin species, such as trioctyl tin chloride. A more recent example in which a multiple number of Lewis acid tin centres are present, to create a receptor which is designed specifically to bind anions, were synthesized by Newcomb and co-workers. In 1984 they reported several tin based macrocycles, **1.54** and **1.55**. Receptors **1.54** and **1.55**, were reported, in 1987, to form 1:1 and 1:2 stoichiometric complexes with chloride ions in acetonitrile. They found that stability constants ranged between 400 – 850 M^{-1} with little difference between the first and second anion coordination, though it has been suggested that there may be some uncertainty over the reliability of these values.[85] This in turn casts some doubt as to whether the tin atoms act independently or cooperatively within this receptor, **1.54**. Newcomb and co-workers also observed a small size effect (n = 8, binding more strongly than n = 10) and a small macrocyclic effect was observed on comparison with an acyclic analogue.[85]

Beer and co-workers have synthesized a series of nickel(II) and cobalt(III) complexes of *S*-substituted isothiosemicarbazides, for example **1.56**. They used ^1H NMR spectroscopy to study the complexation of the host molecules with a variety of anionic guest species in DMSO-d_6.[4, 86] Significant downfield shifts of the terminal NH resonances were found upon addition of tetrabutylammonium chloride in DMSO-d_6. The addition of 1 equivalent of

TBA-Cl to the host led the imine proton resonance to shift downfield by 0.6 ppm. They concluded from these results that favourable NH ··· Cl^- hydrogen bonding interactions play a key role in the anion complexation process, proposed structure, **1.57**, shown in **figure 1.6(b)**. Titration experiments clearly indicated a 1:1 host:anion complex stoichiometry. [4, 86]

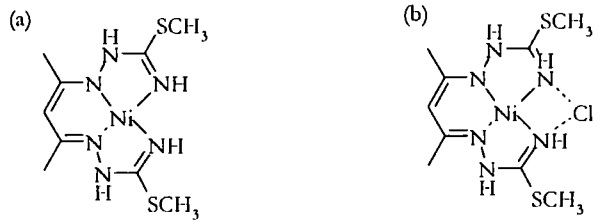

1.56 **1.57**

Figure 1.6: (a)An example of a nickel(II) complex of *S*-substituted isothiosemicarbazides, **1.56**. (b) Proposed structure for a nickel(II) complex of *S*-substituted isothiosemicarbazides chloride complex in DMSO, **1.57**.

Beer and co-workers synthesized a series of acyclic and macrocyclic ferrocene amine ligands, which can selectively bind and electrochemically detect phosphate anions in water. They found that at pH 7, their host **1.58**, senses phosphate via a cathodic response, i.e. ΔE° of 50 mV whereas sulphate does not induce a redox response. But a different host, **1.59**, in aqueous THF solutions electrochemically discriminates for sulphate over phosphate at pH 4 with a cathodic shift of 54 mV. Calibration curves of the change in the half-wave potential ΔE versus [A]/[L] ratio at a certain pH were used to quantitatively determine phosphate and sulphate concentrations in the presence of competing anions.[4, 87]

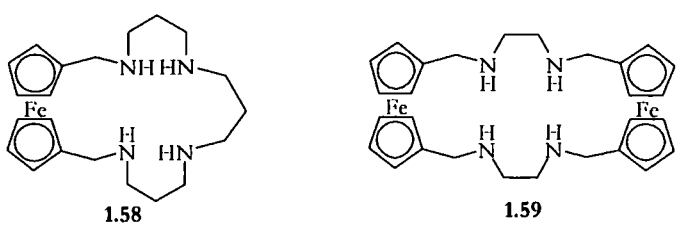

1.58 **1.59**

New derivatives of carborane cages have been developed which contain mercury(II) centres, for example, [12]mercuracarborand-4 host, **1.60**.[88, 89] These derivatives form cyclic structures, which bind halide ions, as well as other anions and electron rich molecules. The example of the unsubstituted [12]mercuracarborand-4 chloride ion complex was first published by

Hawthorne and co workers in 1991.[88, 89] Since then they have reported other mono-chloride,[88, 90, 91] mono-[88, 92] and di-bromo,[88, 93] and mono-[88, 90, 92, 94, 95] and di-iodide[88, 91-93, 95-97] complexes of the substituted and unsubstituted [12]mercuracarborand-4 hosts, **1.60**. On comparison of the monohalide ion complexes of [12]mercuracarborand-4 cycles, it was observed that only Cl^- was small enough to fit within the plane formed by the four mercury centres. In the corresponding monobromide complex saw the Br^- ion partially displaced from the plane formed by the four mercury centres. While the I^- ion was displaced a long way from the mercury plane, causing the structure to adopt a saddle-like shape.[88]

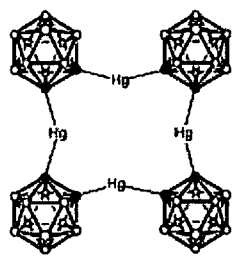

1.60

[12]mercuracarborand-4 host (adapted from references 88, 89)

The 4,4'-bipyridinium di-cation is an electron-deficient compound (Lewis acid) which can readily form coloured charge-transfer complexes with electron-rich donor species (Lewis base), e.g. chloride. Monk *et al* have investigated how the rate of electron transfer to methyl viologen, **1.61**, varies as a function of complexation of various anions.[98] The tendency of the methyl viologen (MV^{2+}) to form an association with an anion was so great that it behaved as a weak electrolyte. If the ionisation energy of the donor anion is compatible with methyl viologen's electron affinity, a charge-transfer interaction occurs. If there is insufficient orbital overlap, the interaction is purely electrostatic and an ion pair results. Nine anions were investigated, fluoride, perchlorate and sulfate formed association pairs, and iodide, hydroquinone, bromide, ethylamine, hexacyanoferrate(II) and chloride formed charge-transfer complexes.[98] The rate of electron transfer depends strongly on the anion e.g. chloride is six times faster than iodide. The rate of dissociation is proportional to the rate of electron transfer. This implies that dissociation is the rate-determining step in the two electron transfer mechanism.[98]

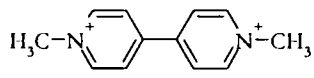

1.61

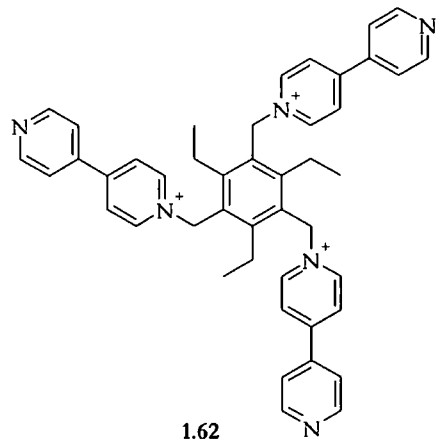

1.62

Steed and co-workers have synthesised **1.62** which incorporates the 4,4'-bipyridinium monocation group as its binding arms around an aryl core.[8, 9] A salt of host **1.62,** with bromide, was crystallised which had two forms in the same crystal. In **figure 1.7(a)**,[9] the host acted as a second sphere ligand for solvated bromide whereas in **figure 1.7(b)** (non-solvated)[9] the host acted as a first sphere ligand for bromide, **figure 1.7**. In the non-solvated form, the two bipyridinium arms were co-planar, facilitating CH···Br interactions and mutually-interpenetrating π-stacking between pairs of cations in the solid state. These two structures provide an insight into how the anion is gradually desolvated and co-ordinated to the host.[9] They also undertook NMR solution studies with this compound and found the resonance assigned to the *ortho*-pyridinium protons were most affected by the addition of anion, thus suggesting that the X-ray structure of the bromide complex may be retained in solution.

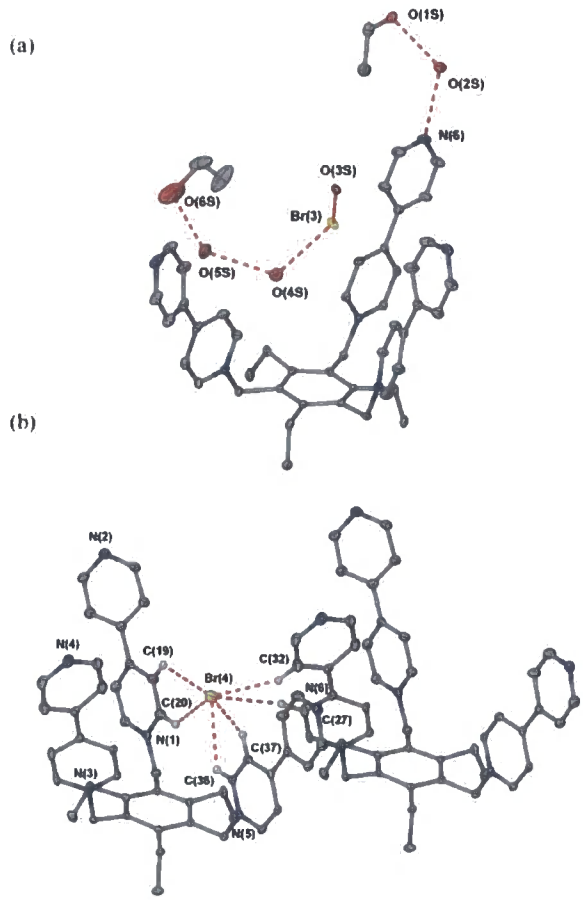

Figure 1.7: Crystal structure of **1.62**(a) with solvated bromide. (b) and solvent-free bromide.[8, 9]

1.9 Calix-[*n*]-arene Based Anion Receptors

Gale and co-workers have synthesised two calix-[*4*]-arenes, **1.63** and **1.64**, and have shown their ability to bind a variety of bis-carboxylates. During NMR spectroscopic titration experiments the data suggested the formation of lower-rim bridged complexes upon addition of tetrabutylammonium di-carboxylate salts to the receptors. The crystal structure of **1.64** – malonate complex showed three different binding modes for malonate in the solid state; bridging, end-on and side on, **figure 1.8**.[10, 99] They also isolated a crystal of the difluorophosphinate salt of **1.63**, which revealed the ability of the guest molecule to accept hydrogen bonds from the amidinium through both oxygen and fluorine.[99, 100]

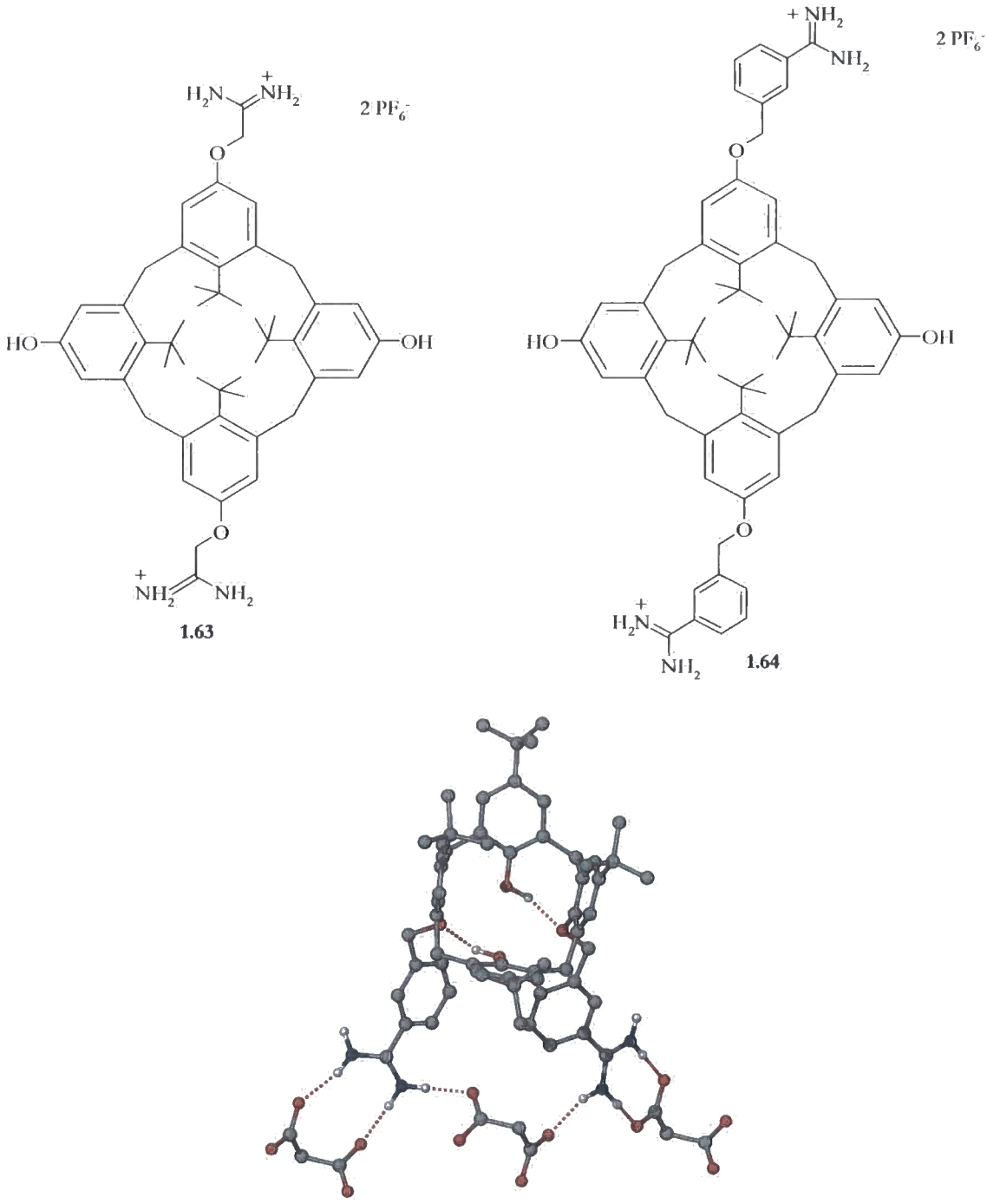

Figure 1.8: Crystal Structure of malonate complex of **1.64** showing three carboxylate binding modes (left to right: side-on, bridging and end-on binding). (Hydrogen atoms not involved in hydrogen bonding have been removed for clarity).[10]

1.10 Organic Podand Anion Receptors

Steed and co-workers have synthesised a series of tripodal compounds around a hexa-substitued aryl core alternating between 3-aminopyridinium and alkyl arms which introduces pre-organization into the hosts.[15, 101] The aminopyridinium moieties have been functionalized with redox active (ferrocene) and fluorescent (anthracene) sensor groups. Binding constants for these compounds were determined by ^{1}H-NMR spectroscopic titration experiments in MeCN-d_3, with a variety of anions as their tetrabutylammonium salts. Compound **1.68** was found to have a high affinity for chloride over other anions, with a binding constant for chloride, $K>10^6$ M^{-1}, an affinity over 25 times stronger than for any other anions tested. Compound **1.70**, is selective for acetate over spherical anions with K_a values of 49,000 M^{-1} for acetate and 5270 M^{-1} for chloride.[15, 101]

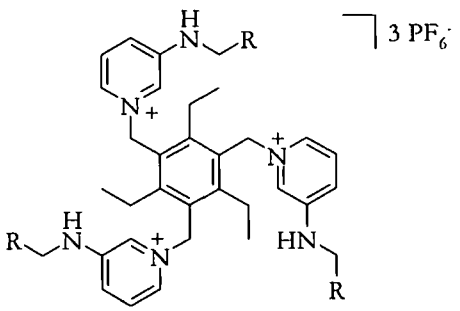

1.65 R=H
1.66 R=ferrocene
1.67 R=CH_3
1.68 R=C_6H_5
1.69 R= $C_6H_4CH_2CH_2CH_2CH_2CH_3$
1.70 R= 9-anthracenyl

Bencini and co-workers have synthesised two tren-based macrocycles which contain three [12]aneN$_4$, **1.71**, or [14]aneN$_4$, **1.72**.[51, 102] The binding of these macrocyclic receptors with benzene tricarboxylate isomers have been studied by photophysical measurements, and calculation of association consants. The receptors have large bowl-shaped cavities, in which it is possible to control the degree of protonation of the cyclic amines. It was shown that both hosts bind 1,3,5-benzene tricarboxylate selectively over the pH range studied.

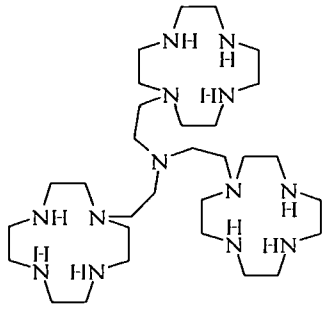

1.71

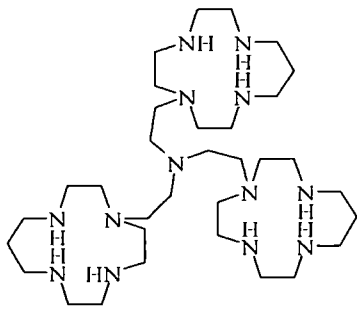

1.72

Cheng *et al* have synthesised the neutral tripodal host molecule, **1.73**, which shows selective binding to F^- and $H_2PO_4^-$ anions.[103] NMR spectroscopic titration experiments were carried out in DMSO-d_6, and only one signal was observed for the pyrrole NH moieties, suggesting the host molecule is symmetrical. Upon addition of tetrabutylammonium salts of F^-, Cl^-, $H_2PO_4^-$ and HSO_4^-, to a solution of the host molecule, **1.73**, downfield shift of the pyrrole NH proton was observed, suggesting the NH is involved in the binding of anion to the host molecule. They saw the largest chemical shift change upon addition of F^-, which was coupled with a broadening of the NH resonance. A large chemical shift of this resonance was also observed upon addition of $H_2PO_4^-$, compared to that seen upon addition of Cl^- and HSO_4^-, which showed much smaller shifts. They suggest that the large shifts seen upon addition of F^- and $H_2PO_4^-$ can be explained by their higher negative charge and better hydrogen bond acceptor properties compared to Cl^- and HSO_4^-. Association constants were calculated for a 1:1 host : guest binding model, which confirmed the stronger binding to F^- and $H_2PO_4^-$, where K_a = 187 and 240 M^{-1}, respectively and Cl^- and HSO_4^-, K_a = 29 and <10 respectively.

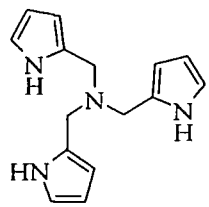

1.73

Kaifer *et al* have synthesised three new dendrimers based around a 4,4'-bipyridinium ('viologen') core, covalently attached to two identical Fréchet dendrons,[104] **1.74 – 1.76**.[105] They undertook voltammetric studies on these compounds and found the first one-electron reduction of the viologen core is reversible (fast) and rather insensitive to the size of the

dendrimers throughout the series, which from previous work on dendrimers was unexpected.[106-114] Typically viologen derivative exhibit two reversible reduction waves that correspond to the formation of a cation radical ($V^{2+} \rightarrow V^{+\cdot}$) and a neutral species ($V^{+\cdot} \rightarrow V$). The first reduction is generally very fast and the second is often coupled to precipitation process due to the uncharged nature of the fully reduced species, which is insoluble in solvents of intermediate to high polarity. For compounds, **1.74** – **1.76**, they found the half–wave potentials, $E_{1/2}$, for the first reduction process shift to less negative values as the dendrimer generation increases. From analysis of the peak to peak potential splittings, ΔE_p, they found this electrochemical process to be reversible at moderate scan rates for all dendrimers, but some distortions associated with precipitation of the one-electron reduced species at the electrode surface were evident in the voltammograms of **1.76**. When the scans rates were increased they discovered that the first reduction was quite fast, with the largest ΔE_p measured was 78 mV. They found the half-wave potentials corresponding to the second electron uptake followed the same trend with the less negative values with increasing dendrimer size. Overall, they found the trend in $E_{1/2}$ values reveals that the reduction process is thermodynamically more favoured as the dendritic structure grows, and they attribute this to increasing hydrophobic character of the dendrimer core, thus making it more difficult to solvate the two positive charges of the viologen core. The authors concluded that reduction (partial or total elimination of the core charges) becomes more favourable with increasing dendrimer generation.

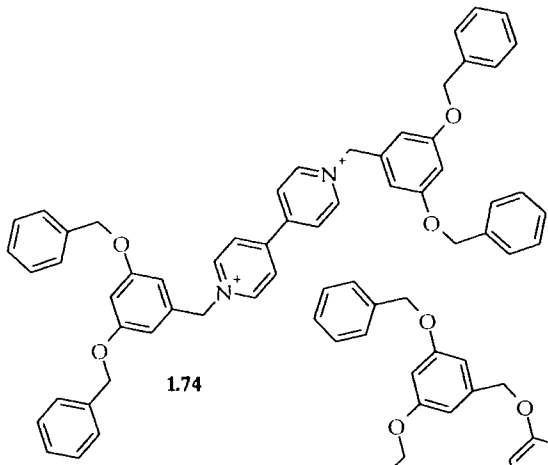

1.74

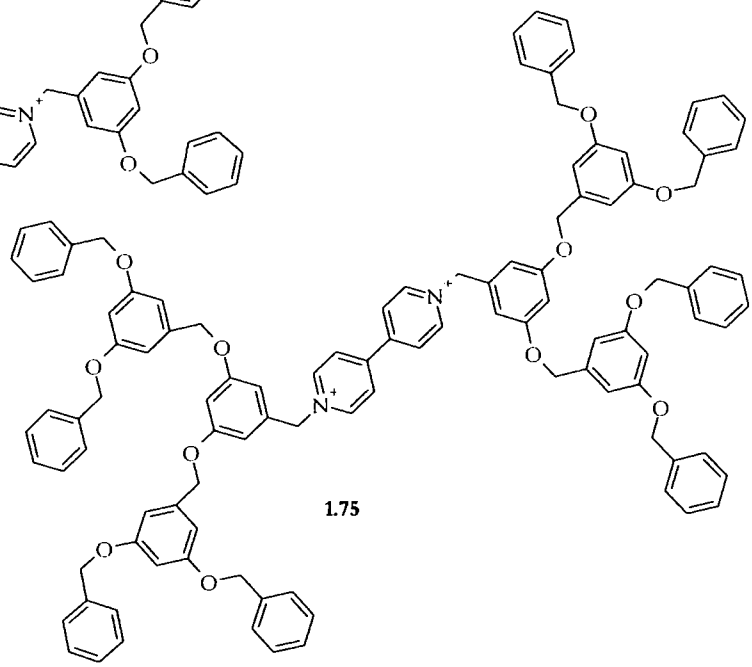

1.75

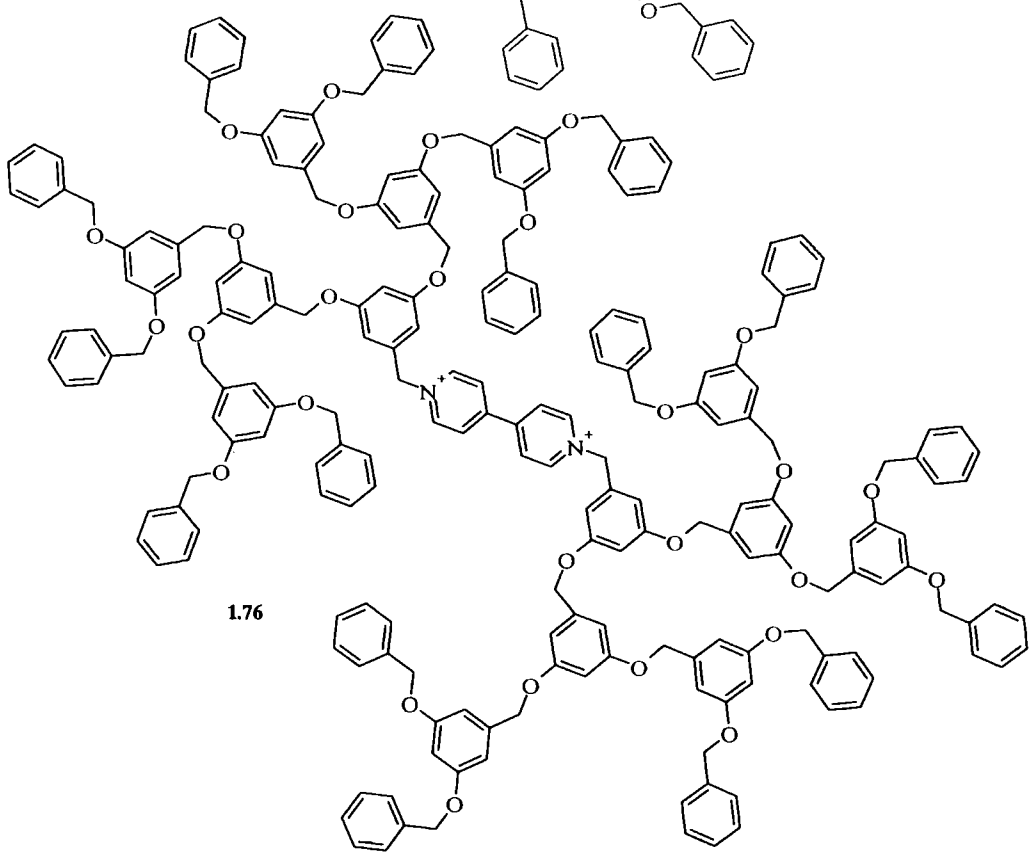

1.76

1.11 Metal/Inorganic Based Anion Receptors

Anion receptors containing transition metal and organometallic hosts are designed so that they can selectively bind and sense the anion recognition via a macroscopic physical response from the inorganic redox or photo-active moiety. One of the most researched systems is tris(2,2'-bipyridyl)ruthenium(II) ($[Ru(bpy)_3]^{2+}$), which is chemically stable, has redox properties, excited-state reactivity and luminescent emission.[115-117] Beer and co-workers have incorporated this moiety into a variety of structural frameworks, including acyclic, macrocyclic, and calix[4]arene to produce a new class of optical and electrochemical sensing.[117-119] They saw strong complexes with the acyclic receptors **1.77** and **1.78** and both chloride and dihydrogen phosphate, the receptors **1.79** – **1.81** also formed complexes with dihydrogen phosphate which were highly selective and thermodynamically stable. The electrochemical studies on these receptors showed substantial anion-induced cathodic perturbation of the ligand centred amide substituted 2,2'-bipyridine reduction redox couple. They found that these shifts correlated with the stability constant values with **1.81**, sensing $H_2PO_4^-$ ions in the presence of a ten-fold excess of HSO_4^- and Cl^- ions. Upon addition of $H_2PO_4^-$ and Cl^- ions, all receptors showed a significant blue shift in the MLCT emission band λ_{max} during luminescent emission measurements. Receptor **1.81** showed the largest shift of 16 nm. These perturbations were not seen in the unfunctionalised $[Ru(bpy)_3]^{2+}$. All shifts were accompanied by a large increase in the emission intensity, and they proposed this might be due to the bound anion making the receptor more rigid and inhibiting the vibrational and rotational relaxation modes of nonradiative decay.[117-120]

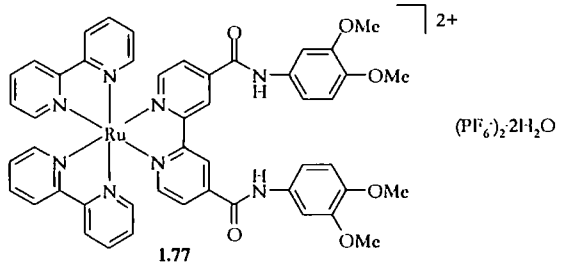

1.77

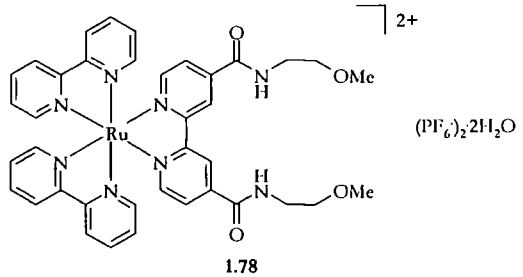

1.78

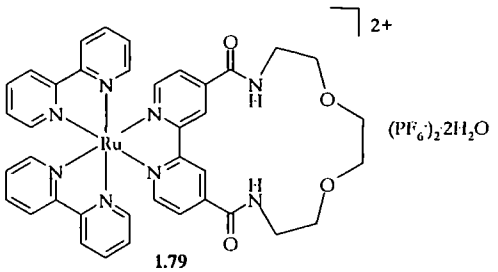

1.79

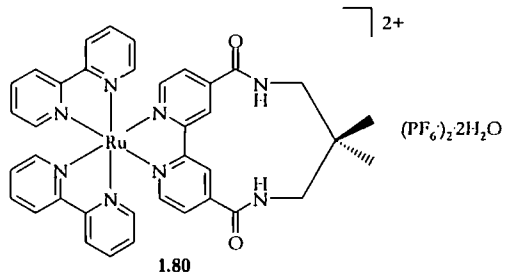

1.80

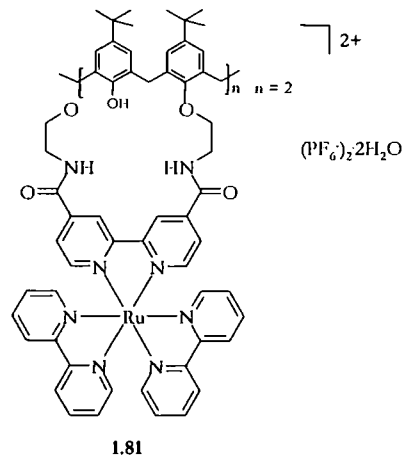

1.81

Gale and co-workers have attached $Cr(CO)_3$ groups to a Crabtree- type amide cleft,[18, 60, 121] producing a receptor which is highly selective for chloride.[18, 121] The aim of the addition of the two electron withdrawing $Cr(CO)_3$ groups, was to increase the acidity of the NH protons. However, it was observed that as well as binding anions, hydrogen bonds were formed in the solid state between the amide NH and the chromium carbonyl moieties leading to the formation of a three-dimensional coordination array.[121-123] This said, the presence of the carbonyl and amide groups provides additional hydrogen bond acceptors and donors, with each molecule **1.82** donating six hydrogen bonds. It is this that facilitates the formation of a supramolecular assembly.[121, 124, 125] The association constants of the receptor were determined by ^1H NMR spectroscopic titration in acetonitrile, which revealed its selectivity for chloride.

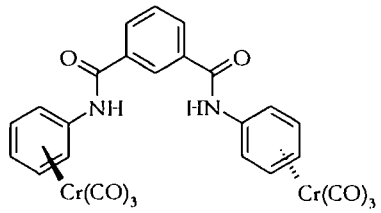

1.82

1.12 Receptors containing signaling moieties

1.12.1 Receptors containing redox-active groups

Electrochemical techniques can be used to determine the redox potentials of a supramolecular system and then to correlate them with the intrinsic molecular properties of the system.[126]

It is possible to alter the structure and the thermodynamic stability of supramolecular assemblies using electrochemical (redox) conversions. Thus, electron-transfer reactions can be utilized to exert some degree of control on supramolecular aggregates. Considering a host-guest complexation at equilibrium, and assuming that the host (H) is redox active and the guest (G) is not, redox or electrochemical reactions on the host will introduce pronounced changes in electric charge and hydrophobic character. These changes usually translate into considerable changes in the structure of the corresponding host-guest complex. Thus, changes in the oxidation state of the host, will lead to changes in the equilibrium constant for the formation of the complex.

To take an example of the electrochemical sensing of anions by a porphyrin receptor, **1.83**. Compound **1.83** has a particular affinity for halides, $H_2PO_4^-$ and HSO_4^- over NO_3^-. The anion binding properties were monitored by NMR, UV/Vis spectroscopy and electrochemistry. When anions were added to solutions containing this porphyrin host, shifts in only the oxidation potentials of the porphyrin rings, and reduction potentials of the cobaltocenium ligands were detected. No influence was detected on the reduction potential of the porphyrin ring, from anion binding.

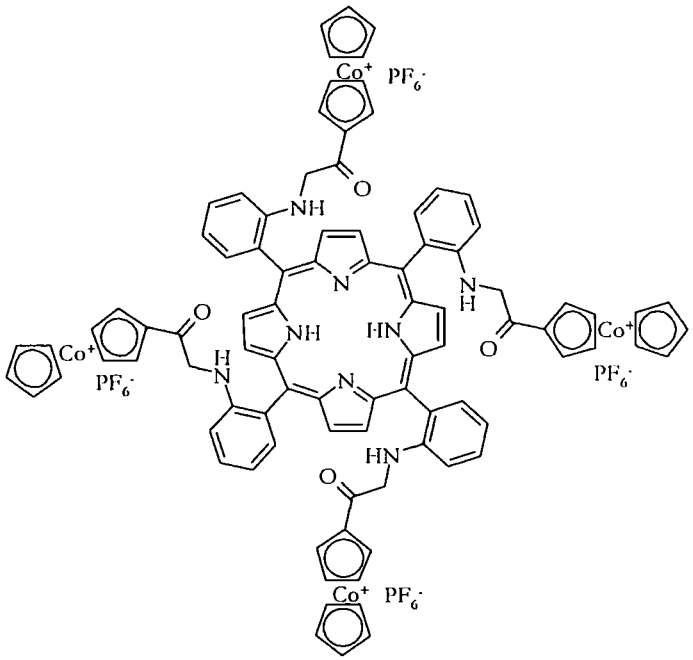

1.83

1.12.2 Receptors containing fluorescence-active groups

Fluorescent techniques have been used in the sensing of anions due to the high selectivity in the sensing of guest species. As such there has been a great deal of work in the covalent attachment of organic and inorganic luminophores to guest recognition sites.[127] These include the anthracene fluorophore combined with polyammonium,[128] guanidinium,[129] zinc(II) amine,[130] and calixpyrrole binding sites.[131]

Fabbrizzi and co-workers have designed a series of tripodal amino receptors, **1.84** and **1.85** which contain one or two vacant coordination sites on the metal ion for anion coordination and some sort of functionality can be introduced which can affect selectivity or impart signalling capability. They found the zinc complex of **1.85** binds aromatic anions such as 4-*N*,*N*-dimethylaminobenzoate in ethanol, with progressive quenching of the fluorescence of the anthracenyl moiety, and saw complete quenching with a 1:1 sensor:analyte ratio.[117, 132] The log *K* value for the complex is 5.45. The zinc complex of **1.85** gives stable adducts with carboxylate anions in methanol with log *K* values between 4 and 5. The emission of the ligand was only quenched by carboxylates containing an aromatic substituent.[117, 133]

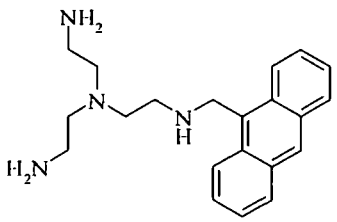

1.84

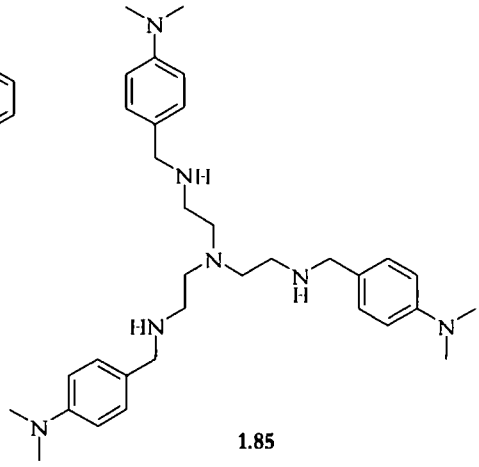

1.85

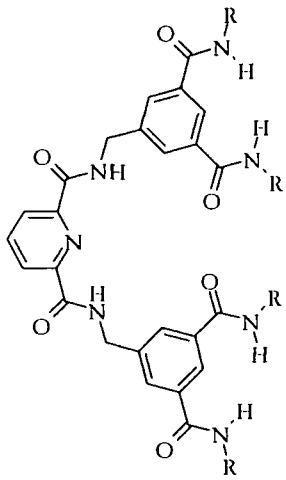

1.86a R=cyclohexyl
1.86b R=(1-pyrenyl)methyl

Fang and co workers have designed a neutral host in a 'pseudotetrahedral' cleft arrangement containing six amide groups, **1.86**. This host has shown a particular affinity for phosphates. The host was subsequently functionalised with pyrene groups, thus introducing a fluorescent probe into the host. Binding constants were calculated by ^{1}H-NMR titration experiments in DMSO-d_6 and were found to be 1374 and 549 M^{-1} for **1.86a** and **1.86b** respectively. [15, 134] Upon addition of anions, namely F^-, Cl^-, Br^-, SCN^-, AcO^-, NO_3^-, ClO_4^-, HSO_4^-, $H_2PO_4^-$, PO_4^{3-}, to **1.86b**, there was no observed change in the emission, except upon the addition of phosphate ions. Upon addition of phosphate ions there was a decrease in the excimer and the monomer emission, and an isoemissive point occurs, suggesting that only one type of complexation is involved. The association constants calculated for the fluorescence studies were 186300 ± 16200 and 328400 ± 19200 M^{-1} for $H_2PO_4^-$ and PO_4^{3-} respectively.[134]

Project Aims

The aims of this project are to design and develop a series of molecular receptors for anion sensing in the shape of dipodal, tripodal and tetrapodal species. These receptors will either contain an organic spacer, in the form of an aryl substituent, **1.87**, **1.88** and **1.89**, or an inorganic spacer in the form of a transition metal ion, **1.90** and **1.91**. Both types of receptor will contain hydrogen bonding sites on the pendant arms, and a positive charge, either from the pyridinium groups, or from the metal centre. The host – guest complexes will be stabilized by both hydrogen bonding and electrostatic interactions. Some of the systems also contain a photo-active moiety to act as a sensor on the receptor, these will be either carbazole, or pyrene moieties. The pendant arms mainly focus on the use of secondary amine groups as hydrogen bond donor groups, with some receptors using a urea group for hydrogen bond interactions.

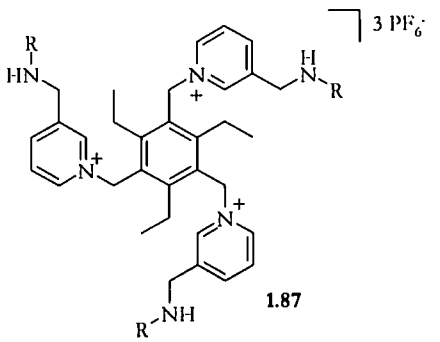

1.87

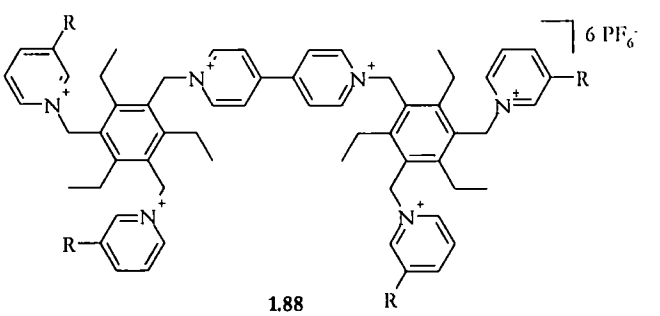

1.88

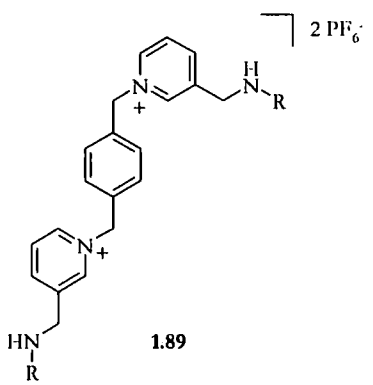

1.89

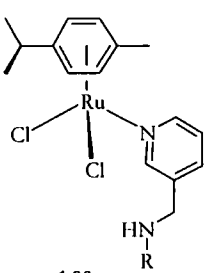

1.90

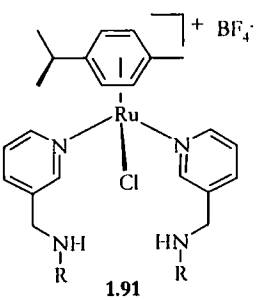

1.91

The basic design of the tripodal receptor, **1.87** is built around an aromatic core, which is elaborated by three pendant arms, in the 1, 3, 5 positions of the aromatic ring. Preorganisation is introduced into the receptor by the addition of ethyl groups in the 2,4,6 position of the core for a '3-up and 3-down' conformation. The tetrapodal receptor, **1.88** is built around a 4,4'-bipyridinum core with two of the tripodal style receptors added so the pyridinium moiety replaces one of the pendant arms of both tripodal systems, thus enabling the host to act as two dipodal receptors or all the arms to bind cooperatively to bind in a 1:1 host:guest stoichiometry. The dipodal receptors are less preorganised and have either an organic, **1.89** or inorganic spacer, **1.91** between the two arms.

The behaviour of the new hosts towards simple inorganic and organic (carboxylates) anions will be studied by various techniques such as ^{1}H-NMR spectroscopy, mass spectrometry, UV-Vis spectrophotometry, fluorimetry, and X-ray crystallography.

Chapter Two

Ligand Synthesis and Properties

Amine containing ligands have been shown to be good anion binding groups, due to their ability to form hydrogen bonds with anions. Examples of amine containing ligands are discussed in **section 1.3**. In this chapter the synthesis and properties of amine containing pyridyl ligands will be discussed. Their chemistry as ligands for metal ions is discussed in chapter three, their role in ruthenium containing anion hosts is covered in chapter four and their role in podand anion hosts is covered in chapter five.

2.1 Synthesis and Characterization

The ligands were readily prepared by reacting together *o*, *m* or *p*-pyridine carboxaldehyde with the relevant amine, which are relatively cheap and readily available. The simple synthetic procedure involves a condensation step followed by the reduction of the imine, using $NaBH_4$, to produce a secondary amine. Reactions were carried out in 1,2-dichloroethane at reflux for 6 hours. All products were recrystallised from dichloromethane and hexane, and were collected by filtration.

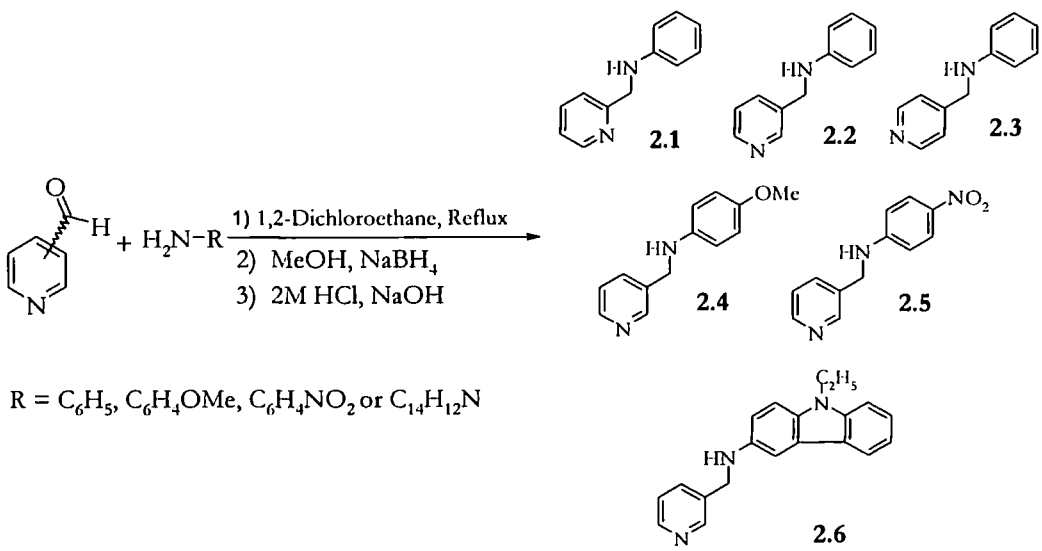

Scheme 2.1: Preparation of ligands **2.1** – **2.6**

Some of the intermediate imine products, **2.1**, **2.2**, **2.5** and **2.6**, were impure sticky oils so not possible to fully characterize, while others were obtained as solid products and as such have been fully characterized. The experimental data obtained agreed with the proposed structures. For example, the reduction of the imine to the secondary amine resulted in the appearance of a broad singlet assigned to the NH resonance in the ^{1}H-NMR spectrum occurring at 4.66 ppm for **2.1**, 4.19 ppm for **2.2**, 4.36 ppm for **2.3**, 3.75 ppm for **2.4**, 4.92 ppm for **2.5** and 4.44 for **2.6**. The ES+ mass spectrum shows a peak at m/z = 184 for **2.1** – **2.3**, a peak observed at m/z = 215 for **2.4**, a peak observed at m/z = 230 for **2.5**, and a peak observed at m/z = 302 for **2.6** all of which represent the relevant $[M]^+$ ions. The fragmentation is also consistent with the proposed structure in each case. Full characterization data is given at the end of this chapter, **section 2.5**.

2.2 Ligand Crystal Structures

Crystals were grown of ligands, **2.2** – **2.6**, from a solution of dichloromethane and hexane by slow evaporation, and characterized by Gareth Lloyd, Drs Kirsty Anderson and Mike Probert, using x-ray crystallographic methods.

Compound **2.2** exists as two polymorphs. The first is a Z' = 2 structure,[135] in which there are two molecules in the asymmetric unit, **figure 2.1**. Hydrogen bonding is seen between the pyridyl nitrogen (N1) of one molecule and the amine proton (H2N) of a symmetry related molecules, and is in an A--A--A pattern, forming helical hydrogen bonded chains. Intramolecular hydrogen bonding is also observed between the pyridyl proton, CH, H3 and amine nitrogen, N2, and, H15A and N4. The length of this hydrogen bond is approximately 0.3 Å longer than the intermolecular hydrogen bonding observed between H2N and N3, and similarly between, H4N and N3. The second polymorph of **2.2** is a Z' = 1 structure, so there is only one molecule in the asymmetric unit, **figure 2.2**. Both crystals were grown from dichloromethane and hexane, but in this case the crystals were grown more slowly, and from a more concentrated solution of ligand. The two sets of crystals were grown from different batches of the ligand, but the same synthetic procedure was followed, and experimental data obtained agreed with both structures. As with the other polymorph, hydrogen bonding is seen between pyridyl nitrogen (N3) and the amine proton (H2), but no intramolecular

hydrogen bonding is observed in this polymorph. DSC measurements were carried out on samples of these two crystals, to see if the polymorphs interconvert, as a change was observed upon cooling of the Z' = 2 polymorph. However, no phase changes were observed with the DSC measurements, contrary to the observation of crystal suggested.

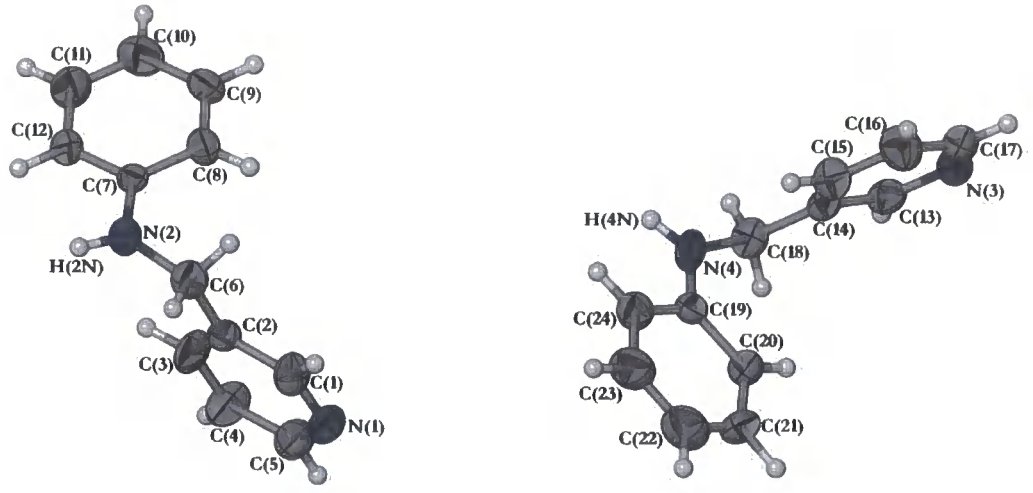

(a)

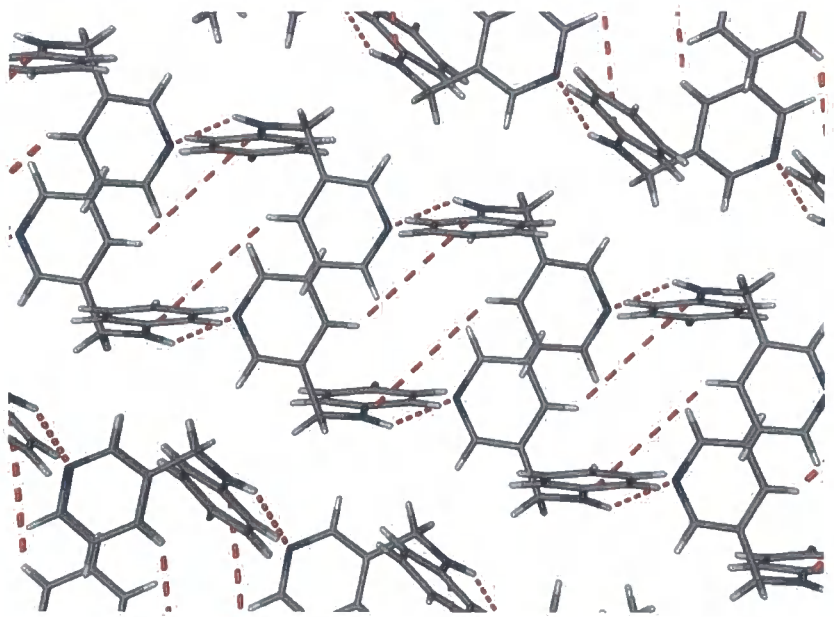

(b)

Figure 2.1: X-ray crystal structure of **2.2**, Z' = 2 polymorph (a) Asymmetric unit (ASU) of the crystal structure **2.2** Atoms shown in thermal ellipsoid representation at 50 % with labels. (b) Packing diagram of the crystal structure, viewed along b-axis.

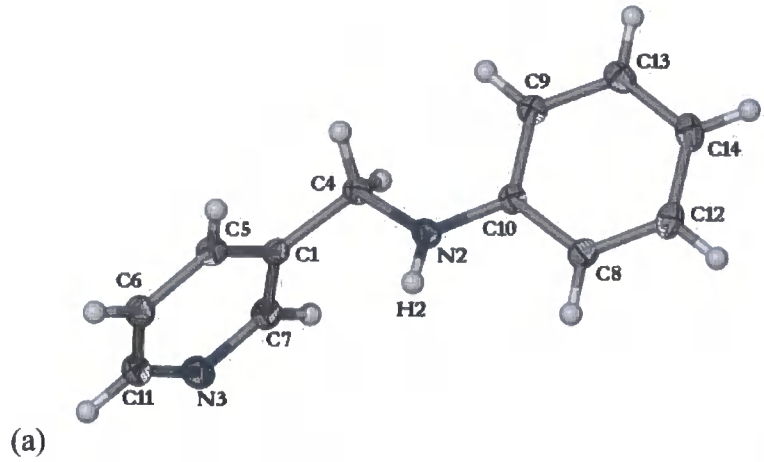

(a)

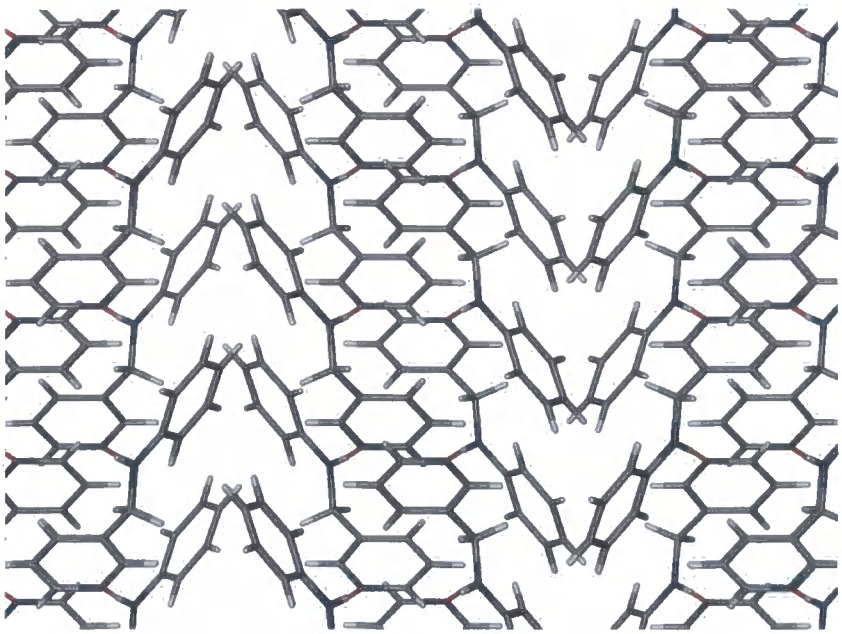

(b)

Figure 2.2: X-ray crystal structure of **2.2** (a) Asymmetric unit (ASU) of the crystal structure **2.2** Atoms shown in thermal ellipsoid representation at 50 % with labels. (b) Packing diagram of the crystal structure, viewed along a-axis.

In the case of the X-ray crystal structure of **2.3**, intermolecular hydrogen bonding is seen between the pyridyl nitrogen (N3) and the amine proton (H2N), as well as hydrogen bonding between N1 and H3N, of the two molecules in the asymmetric unit, **figure 2.3**. This structure is also a Z' = 2 structure.[135] Intramolecular hydrogen bonding is observed

between H4 and N2, and H14 and N4, and the lengths of these hydrogen bond is approximately 0.5 Å longer than is observed for the intermolecular hydrogen bonding.

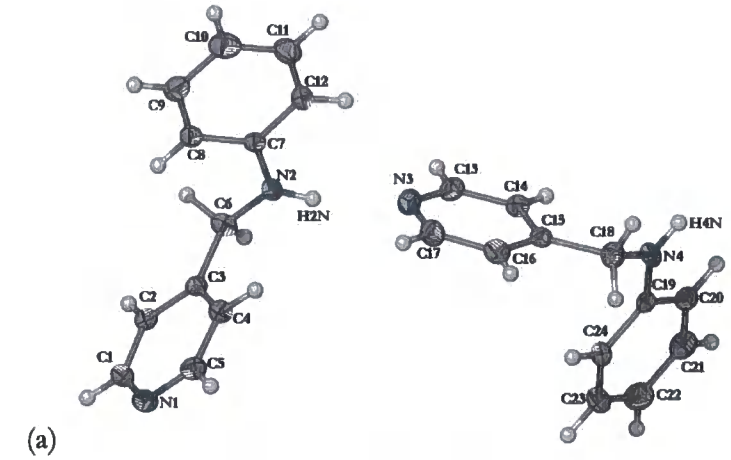

(a)

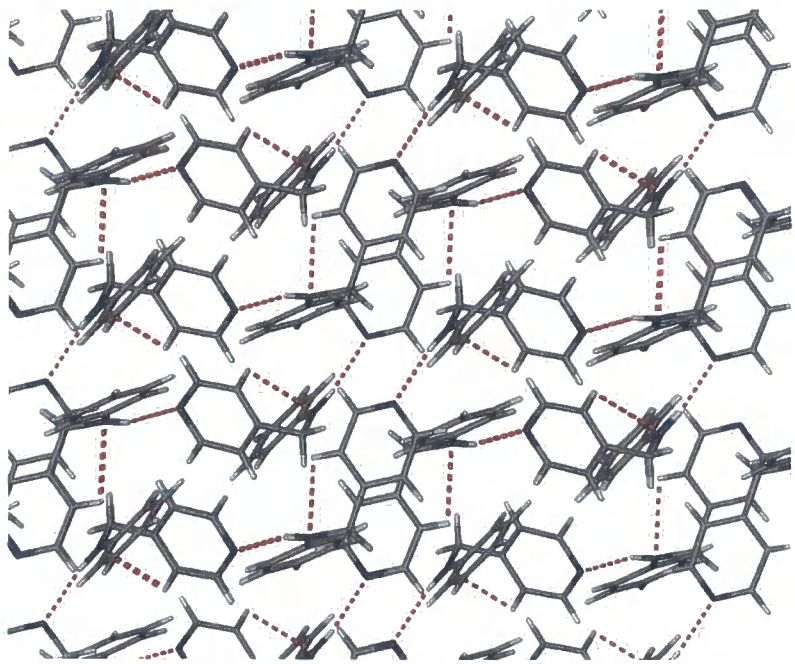

(b)

Figure 2.3: X-ray crystal structure of **2.3** (b-axis) (a) Asymmetric unit (ASU) of the crystal structure **2.3** Atoms shown in thermal ellipsoid representation at 50 % with labels. (b) Packing diagram of the crystal structure, viewed along b-axis.

In the crystal structure of **2.4,** hydrogen bonding is seen between the pyridyl nitrogen (N1) and the amine proton, (H2N) on an adjacent molecule, in the crystal structure, **figure 2.4**.

Intermolecular hydrogen bonding is also observed between the oxygen (O1) on the methoxy group, and the hydrogen (H5) at C5 on the pyridyl ring. The length of the hydrogen bonds of type O1 – H5 are approximately 0.3 Å longer than those observed between N1 and H2N. The combination of hydrogen bonding forms chains in which two rows of ligands are bound, end to end by O1 – H5 bonding and face to face by N1 – H2N bonding.

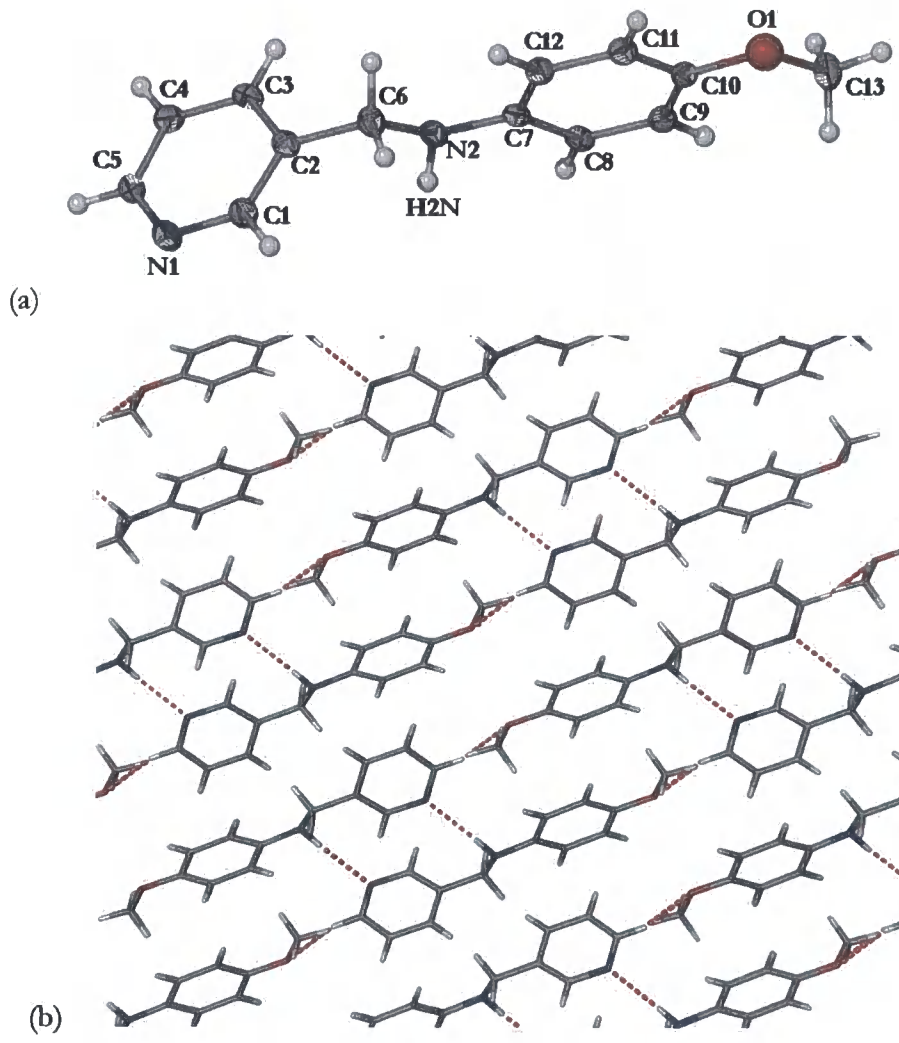

Figure 2.4: X-ray crystal structure of **2.4** (a) Asymmetric unit (ASU) of the crystal structure **2.4** Atoms shown in thermal ellipsoid representation at 50 % with labels. (b) Packing diagram of the crystal structure, viewed along b-axis.

In the asymmetric unit of **2.5** there are two molecules, so it is described as being a $Z' = 2^{135}$ structure, **figure 2.5**. Hydrogen bonding is seen between the two molecules in the

asymmetric unit, between pyridyl nitrogen (N4) and amine proton (H2N), and between the pyridyl nitrogen (N1) and amine proton (H5N), the hydrogen bond length between these two types of hydrogen bond, is different, being longer between N1 and H5, which could be explained by the difference in bond angle between N2—H2N....N4 being closer to 180°, than that of N5—H5N....N1. Hydrogen bonding is also seen between the oxygen atoms (O1, O3 and O4) and the pyridyl and methylene protons (H13, H1 and H18A, respectively), **figure 2.5(b)**. The hydrogen bond lengths between the oxygen and protons are approximately 0.3 Å longer than those between the nitrogen atoms and protons, suggesting the nitrogen to hydrogen bonding, NH---N, is stronger than the oxygen to hydrogen bonding, CH---O.

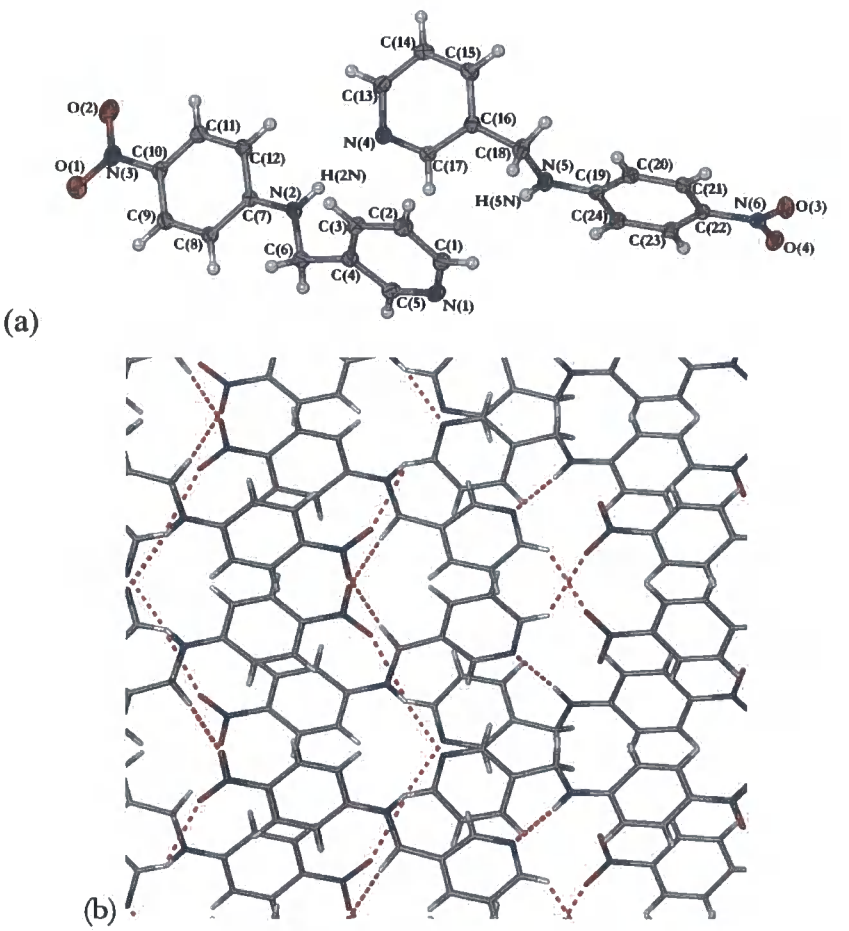

Figure 2.5: X-ray crystal structure of **2.5** (a) Asymmetric unit (ASU) of the crystal structure **2.5** Atoms shown in thermal ellipsoid representation at 50 % with labels. (b) Packing diagram of the crystal structure, view along c-axis.

The crystal structure of **2.6** shows intermolecular hydrogen bonding between the pyridyl nitrogen (N1) and the amine nitrogen (H2N), **figure 2.6**, but no intramolecular hydrogen bonding is observed in this structure. The pyridyl ring is in one plane, and the carbazole rings are in a plane nearly perpendicular to that of the pyridyl ring at an angle of 86.43°.

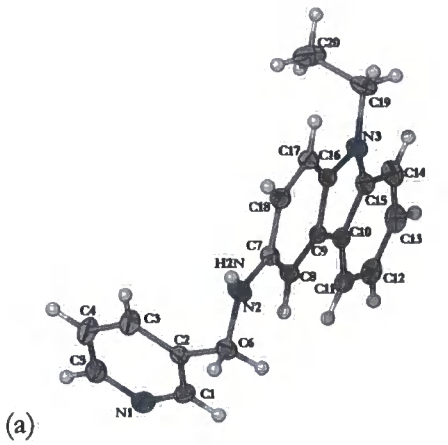

(a)

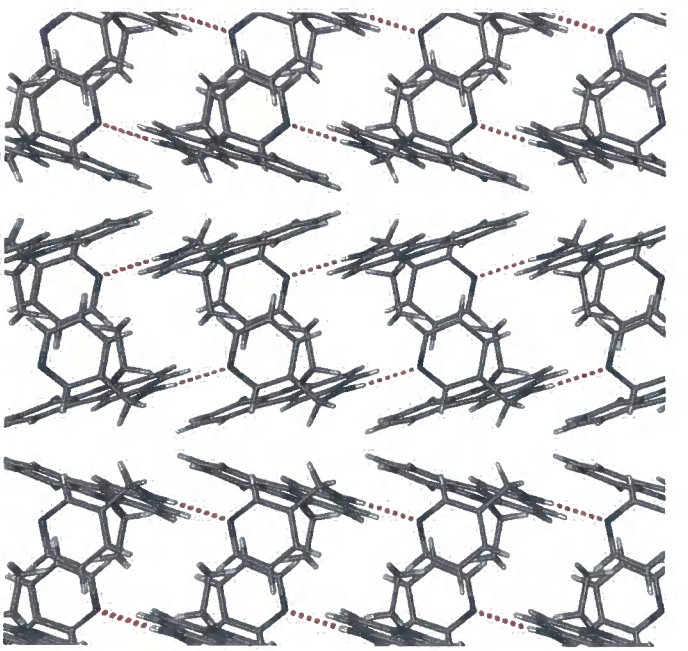

(b)

Figure 2.6: X-ray crystal structure of **2.6** (a) Asymmetric unit (ASU) of the crystal structure **2.6** Atoms shown in thermal ellipsoid representation at 50 % with labels. (b) Packing diagram of the crystal structure, viewed along c-axis.

Compound	D--H	H - - - - - A	D - - - - - A	D--H - - - A
2.2 (Z' = 2)	0.870	2.258	3.007(7)	144
	(N2-H2N)	(H2N-N1)	(N2-N1)	(N2-H2N-N1)
	0.870	2.210	2.990(6)	149
	(N4-H4N)	(H4N-N3)	(N4-N3)	(N4-H4N-N3)
	0.940	2.560	2.879(7)	100
	(C3-H3A)	(H3A-N2)	(C3-N2)	(C3-H3A-N2)
	0.94	2.580	2.897(7)	100
	(C15-H15A)	(H15A-N4)	(C15-N4)	(C15-H15A-N4)
2.2 (Z' = 1)	0.880	2.21	3.038(2)	157
	(N2-H2)	(H2-N3)	(N2-N3)	(N2-H2-N3)
2.3	0.880	2.100	2.955(2)	164
	(N2-H2N)	(H2N-N3)	(N2-N3)	(N2-H2N-N3)
	0.880	2.080	2.956(2)	171
	(N4-H4N)	(H4N-N1)	(N4-N1)	(N4-H4N-N1)
	0.950	2.580	2.906(3)	100
	(C4-H4)	(H4-N2)	(C4-N2)	(C4-H4-N2)
	0.950	2.600	2.914(3)	100
	(C14-H14)	(H14-N4)	(C14-N4)	(C14-H14-N4)
2.4	0.874(17)	2.217(17)	3.088(2)	175(2)
	(N2-H2N)	(H2N-N1)	(N2-N1)	(N2-H2N-N1)
	0,950	2.520	3.284(2)	137
	(C5-H5A)	(H5A-O1)	(C5-O1)	(C5-H5A-O1)
2.5	0.860	2.170	3.021(2)	174
	(N2-H2N)	(H2N-N4)	(N2-N4)	(N2-H2N-N4)
	0.860	2.230	3.044(2)	159
	(N5-H5N)	(H5N-N1)	(N5-N1)	(N5-H5N-N1)
	0.930	2.520	3.189(2)	129
	(C1-H1)	(H1-O3)	(C1-O3)	(C1-H1-O3)
	0.930	2.500	3.154(2)	128
	(C13-H13)	(H13-O1)	(C13-O1)	(C13-H13-O1)
	0.970	2.470	3.172(2)	129
	(C18-H18A)	(H18A-O4)	(C18-O4)	(C18-H18A-O4)
2.6	0.89(2)	2.25(2)	3.133(2)	168(2)
	(N2-H2N)	(H2N-N1)	(N2-N1)	(N2-H2N-H1)

Table 2.1: Crystal data for ligands **2.1 – 2.6**.

In the *meta* substituted ligands, **2.2**, **2.4**, **2.5** and **2.6**, the addition of a group to the aryl ring, seems to increase the distance between the donor (D) and acceptor (A) atoms, where D = amine nitrogen and A = pyridyl nitrogen. There appears to be no trend in the results obtained linking hydrogen bond length and the addition of an electron-withdrawing or –donating group to the aryl ring. A search on the CSD was undertaken, this was searching for the D----A distance in compounds containing a secondary amine, and a pyridyl group, the average distance was 3.11 Å, and the range was between 2.75 and 3.59 Å, **figure 2.7**, and as is seen in **table 2.1**, all the D----A distances measured in the crystal structures of ligands **2.2** – **2.6** fall between this range, are all close to the modal average, which falls at 3.02 Å. The D----A distances were also compared with ligands previously synthesised in the group, and they were observed to be similar to those obtained for ligands **2.2** – **2.6**, which were 3.108(5) Å for ferrocenyl and 3.135(3) Å for anthracenyl derivatives.[136] The hydrogen bond lengths are also similar to the previous values of 2.38(3) Å for a ferrocenyl derivative, and 2.23(3) Å for an anthracenyl derivative.[136]

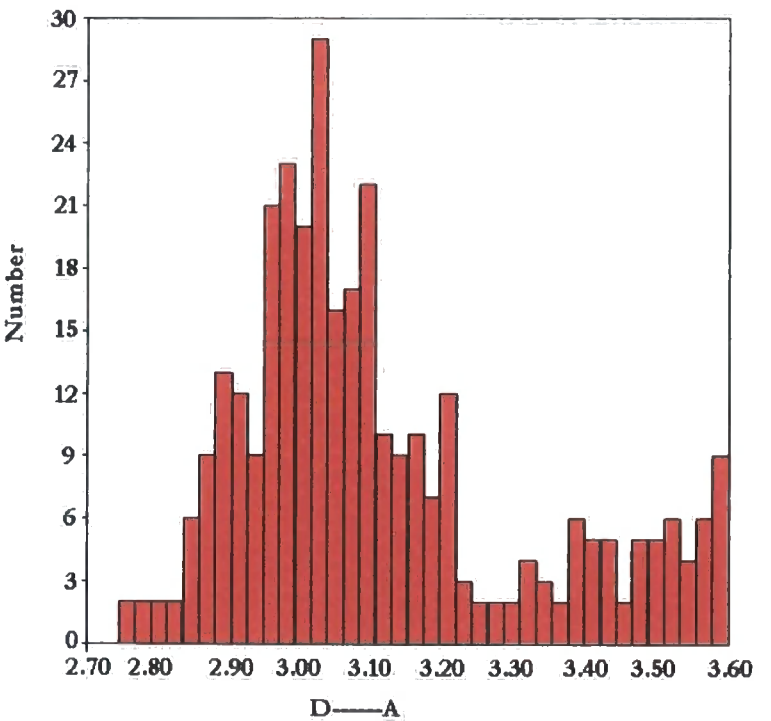

Figure 2.7: Distribution of D----A distance from a secondary amine (N), to a pyridyl nitrogen (N), data obtained from a search of the CSD.

2.3 DFT calculations

In collaboration with Martin Paterson, Herriot-Watt University, the geometry of **2.6** was optimized using density functional theory, with B3LYP functional and the 6-31G* basis set on all atoms. Once this had found the minimum energy conformation, it was verified as a minimum by computing the Hessian matrix, and observing all the eigenvalues were positive. With this geometry, time-dependant DFT calculations with the same functional, B3LYP, to determine the electronic absorption spectrum, were completed. The three lowest-lying singlet excited states were observed to be 347.3 nm (3.57 eV), 344.6 nm (3.60 eV), and 325.8 nm (3.80 eV). The oscillator strengths for transitions to these states are f=0.0318, f=0.0121, and f=0.0213. Therefore these transitions give rise to intense absorption bands. In assigning the nature of these states, the single particle-hole configurations of the response eigenvectors were examined. The larger the coefficient of one of these configurations the more it contributes to the excited state. For each of the 3 calculated transitions there is a large dominant configuration corresponding to an intramolecular charge-transfer from an orbital localised on the carbazole to one localised on the pyridyl group. For example, in the lowest excited state (S1), the HOMO → LUMO single particle-hole configuration has a coefficient of 0.48, **figure 2.8**. In each of the other two states there are dominant CT configurations. Therefore we assign the calculated band between 320 nm and 340 nm as an intramolecular CT band.[137, 138] Experimental data is in agreement with the calculated data, and the ILCT appears at 375 nm.

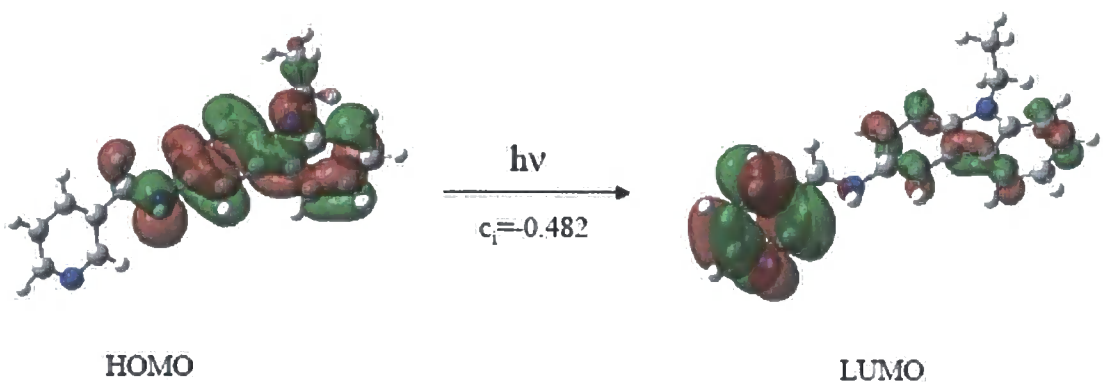

Figure 2.8: Dominant configuration of the first excited state.

DFT calculations were only completed for **2.6**, but from this, it is suggested that the band centred on, 377 nm for **2.4**, 378 nm for **2.5** are assigned as the ILCT bands for these ligands, but there is no evidence of an ILCT for **2.2**, **figure 2.9**. It would be expected that the host with the electron donating, OMe group attached to the aryl ring, would result in a shift of the ILCT to lower wavelength. Hence the energy transition would be higher than for **2.5**, which has an electron withdrawing NO_2 group attached. The intensity of the absorbance of the nitro-substituted ligand, **2.5** is approximately double that observed for **2.4** and **2.6**, at the same concentration. The experimental data has shown however that this was not the case, and that the ILCT bands occur at practically the same wavelength. It is therefore suggested that there is a difference in the energy at which the HOMO and LUMO occur, rather than the transition between the two, but without further studies, it is not possible to explain this fully.

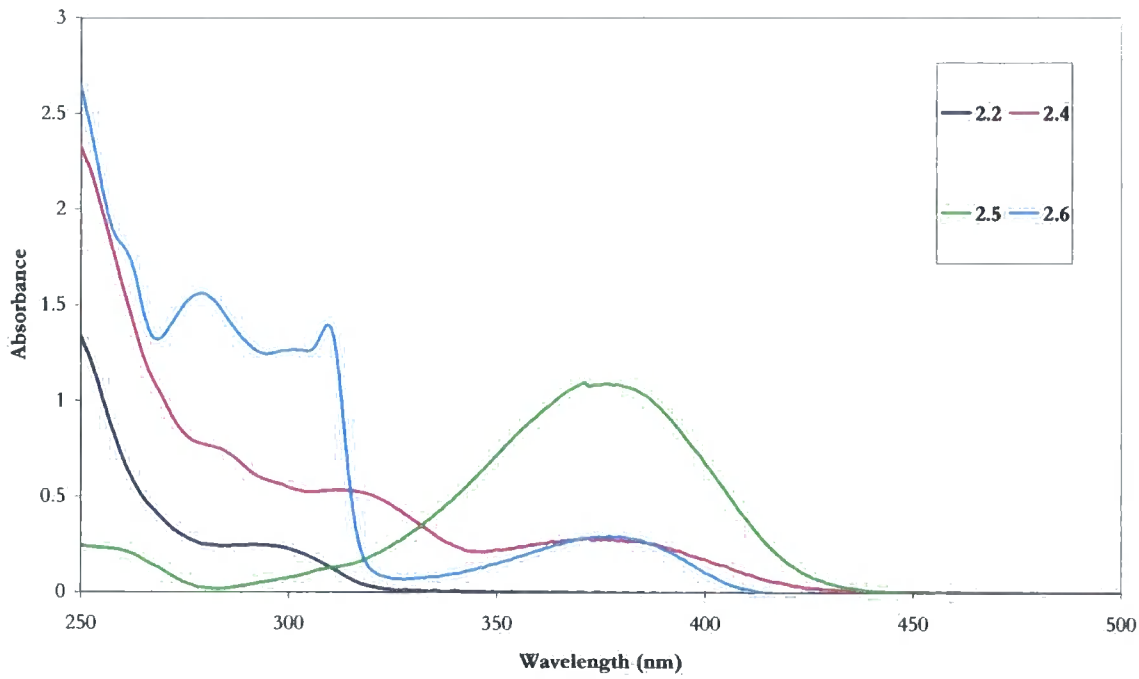

Figure 2.9: Comparison of the wavelength at which the ILCT occurs in ligands **2.2**, **2.4** – **2.6**.

2.4 Summary

Ligands **2.1** - **2.6** have been synthesised using straight-forward synthetic procedures, and in all cases clean samples of each molecule were synthesised, and have been fully characterized using NMR spectroscopy, mass spectrometry, infra-red spectroscopy, and elemental analysis, and structural data obtained using X-ray crystallography on those for which it was possible to grow crystals, **2.2** – **2.6**. The crystal structures show intramolecular hydrogen bonding between amine protons, and pyridyl nitrogen atoms on adjacent molecules for ligands **2.2** – **2.6**. Ligand **2.3** exists as two polymorphs, one which is a $Z'=2$[135] structure, and a $Z'=1$ structure, and ligands **2.2** and **2.5** exist in a single $Z'=2$[135], while **2.4** and **2.6** exist as $Z'=1$ structures. DFT calculations have shown the dominant configuration corresponds to an intramolecular charge transfer (ILCT) from the electron rich carbazole moiety to the electron poor pyridyl group, in **2.6**. The calculated and the experimental wavelength at which this band occurs are in close agreement. The ILCT band is observed for ligands **2.4** – **2.6**, and occurs at a similar wavelength for the substituted ligands, **2.4** – **2.6**, compared to that of the aryl ligand, **2.2**, which does not appear to have an ILCT, in the measured wavelength.

2.5 Experimental

2.5.1 General

NMR experiments were performed on a Bruker Avance 400 spectrometer, Varian Mercury 400 MHz, Varian Inova 500 MHz or Varian D 700 MHz at the frequency of 400 MHz, 500 MHz or 700 MHz for proton spectra and 100 MHz or 125 MHz, for carbon spectra. Chemical shifts are reported in parts per million (δ) and coupling constants (J) are recorded in Hertz (Hz). The multiplicities in the ^{1}H-NMR are reported as broad (*br*), singlet (*s*), doublet (*d*), doublet of doublets (*dd*), triplet (*t*), quintet (*q*). All spectra were recorded at ambient temperature unless otherwise stated. Microanalyses were recorded on an Excitor Analytical Inc CE440 elemental analyser and are reported as the calculated and experimentally measured values for each given formula and corrected for the inclusion of solvents, as indicated. IR spectra were recorded on Perkin Elmer Precisely Spectrum 100 FT-IR spectrometer as nujol mulls and the peaks of interest are reported as wavenumbers (cm^{-1}) and described as weak (*w*), medium (*m*) and strong (*s*). Mass spectra were obtained on a Thermo Finnigan LTQ mass spectrometer in ES+ mode.

2.5.2 Synthesis

All reagents were of commercial quality and the solvents were dried, where necessary, using standard procedures (1,2-dichloroethane over calcium hydride). All other solvents were used as obtained. The starting materials were brought from Aldrich, Alfa Aesar or Fluorochem and were used without further purification. All reactions were carried out under nitrogen, but no products showed oxygen or moisture sensitivity.

2.5.3 General Procedure for the Preparation of Imines

Pyridine carboxaldehyde and the relevant amine were dissolved in 1,2-dichloroethane and refluxed for 6 hours. The solvent was then removed under reduced pressure and the residue washed with ether, to remove unreacted starting materials. The crude product was further reacted without further purification. Any differences from this procedure are stated where necessary.

2.5.4 General Procedure for the Preparation of Amines

The appropriate imine was dissolved in methanol, and 10 molar equivalents of sodium borohydride was slowly added. The resulting solution was stirred for a further 2 hours, then 2 M HCl was added to destroy unreacted sodium borohydride. Hydrochloric acid was added until the solution reached pH 3. Sodium hydroxide solution (2 M) was then added until the solution became basic (approximately pH 9). The mixture was extracted into CH_2Cl_2, washed with water and dried over $MgSO_4$. The solution was then filtered to remove $MgSO_4$, and solvent removed under reduced pressure. The product was recrystallised from CH_2Cl_2 and hexane to give the desired product as a pure solid. Any differences from this procedure are stated where necessary.

(*E*)-*N*-((pyridine-2-yl)methylene)benzenamine

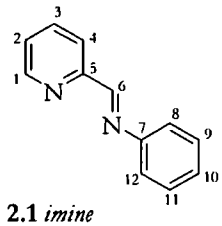

2.1 *imine*

Aniline (10.7 g, 0.11 mol) and 2-pyridine carboxaldehyde (12.3 g, 0.11 mol) were dissolved in dry 1,2-dichloroethane (500 mL), and magnesium sulfate (13.2 g) was added. The solution was refluxed for 6 hours whilst stirring. After this time the solution was filtered to remove the magnesium sulfate, and the solution concentrated under reduced pressure to yield the product as a yellow oil.

^{1}H-NMR ($CDCl_3$, 500 MHz, δ / ppm, J / Hz): 8.99 (1H, d, J=7.5, Pyridyl-H(H4)); 8.49 (1H, d, J=7.5, Pyridyl-H(H1)); 8.46 (1H, s, CH(H6)); 7.48 (1H, dt, J=7.5, 1.0, Pyridyl-H(H3)); 7.22 (1H, t, J=7.5, Pyridyl-H(H2)); 7.14 (2H, d, J=7.0, Ar-H(H8&12)); 7.04 – 7.09 (3H, m, Ar-H(H9 - 11)).

^{13}C{^{1}H}-NMR ($CDCl_3$, 100 MHz, δ / ppm): 160.7(C5); 154.7(C7); 151.1(C1); 149.8(C3); 136.6(C4); 129.4(C2); 126.9(C9&11); 125.2(C10); 121.9(C8&12); 121.3(C6).

ES+ MS: m/z = 183 [M^+]

***N*-((pyridin-2-yl)methyl)benzenamine**

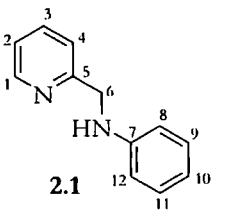

2.1

2.1 *imine* was dissolved in methanol, and whilst stirring $NaBH_4$ (12.2 g, 0.33 mol) was added until the solution ceased to effervesce. The solution was stirred for a further 2 hours. 50:50 HCl:H_2O (10 mL) was added until the solution was pH 3, and then 2 M NaOH (50 mL) was added until the solution was pH 9. The product was extracted using dichloromethane. The organic layer was dried over $MgSO_4$, and then filtered. The solvent was evaporated under reduced pressure, and the product extracted, as a white crystalline solid and recrystallised with dichloromethane and diethylether (6.5 g, 35 mmol, 32 %).

^{1}H-NMR ($CDCl_3$, 400 MHz, δ / ppm, J / Hz): 8.61 (1H, d, J=7.6, Pyridyl-H(H1)); 7.62 (1H, dt, J=7.6, 1.5, Pyridyl-H(H3)); 7.34 (1H, d, J=7.6, Pyridyl-H(H4)); 7.17 – 7.23 (3H, m, Pyridyl-H(1H)(H2) & Ar-H(2H)(H9&11)); 6.76 (1H, t, J=7.5, Ar-H(H10)); 7.69 (2H, d, J=7.5, Ar-H(H8&12)); 4.66 (1H, bs, NH); 4.47 (2H, s, CH_2(H6)).

^{13}C{^{1}H}-NMR ($CDCl_3$, 125 MHz, δ / ppm): 159.0(C5); 158.9(C1); 148.2(C7); 137.0(C4); 129.6(C3); 122.4(C9&11); 121.9(C10); 117.8(C2); 113.3(C8&12); 49.5(C6).

ES+ MS: m/z = 185 [M^+]

Anal: Calculated for $C_{12}H_{12}N_2$: C, 78.23; H., 6.52; N, 15.20 %
Found: C, 77.99; H, 6.52; N, 15.21 %

IR: 3393 ν (NH)

(*E*)-*N*-((pyridine-3-yl)methylene)benzenamine

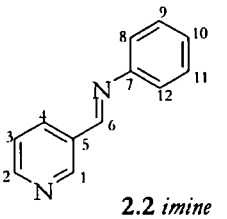

2.2 *imine*

Aniline (2.05 g, 21 mmol) and 3-pyridine carboxaldehyde (2.35 g, 22 mmol) were dissolved in dry 1,2-dichloroethane (250 mL), and magnesium sulfate (3.0 g) was added. The solution was refluxed for 6 hours whilst stirring. After this time the solution was filtered to remove the magnesium sulfate, and the solution concentrated under reduced pressure to yield the product as an orange oil.

^{1}H-NMR ($CDCl_3$, 400 MHz, δ / ppm, J / Hz): 8.88 (1H, d, J = 1.9, Pyridyl-H(H1)); 8.56 (1H, dd, J = 7.6, 1.9, Pyridyl-H(H4)); 8.34 (1H, s, CH(H6)); 8.14 (1H, dt, J = 7.8; 1.9, Pyridyl-H(H3)); 7.32-7.08 (6H, m, Pyridyl-H (H2), Ar-H (H8-12)).

^{13}C{^{1}H}-NMR ($CDCl_3$, 100 MHz, δ / ppm): 157.1; 152.0; 151.4; 150.9; 134.8; 131.8; 129.2; 126.5; 123.7; 120.8; 43.5. (*^{13}C spectrum not assigned as correlation spectrum not obtained, due to insolubility*).

***N*-((pyridin-3-yl)methyl)benzenamine**

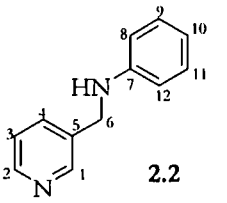

2.2

2.2 *imine* was dissolved in methanol, and whilst stirring $NaBH_4$ (5.03 g, 13 mmol) was added until the solution ceased to effervesce. The solution was stirred for a further 2 hours. 50:50 HCl:H_2O (5 mL) was added until the solution was pH 3, and then 2 M NaOH (25 mL) was added until the solution was pH 9. The product was extracted using dichloromethane. The organic layer was dried over $MgSO_4$, and then filtered. The solvent was evaporated under reduced pressure, and the product extracted, as a white crystalline solid and recrystallised with dichloromethane and hexane (3.15 g, 17 mmol, 77 %).

^{1}H-NMR ($CDCl_3$, 400 MHz, δ / ppm, J / Hz): 8.53 (1H, dd, J=7.5, 1.5, Pyridyl-H(H2)), 8.39 (1H, d, J=1.5, Pyridyl-H(H1)), 7.71 (1H, d, J=7.5, Pyridyl-H(H4)), 7.64 (2H, d, J=8.0, Ar-H(H8&12)), 7.27 (1H, m, Ar-H(H10)), 7.20 (2H, t, J=8.0, Ar-H(H9&11)), 6.76 (1H, t, J=7.5, Pyridyl-H(H3)), 4.36 (2H, s, CH_2(H6)), 4.19 (1H, bs, NH).

^{13}C{^{1}H}-NMR ($CDCl_3$, 125 MHz, δ / ppm): 149.4(C1); 148.9(C4); 148.0(C7); 135.4(C3); 135.2(C5); 129.6(C9&11); 123.8(C10); 118.3(C2); 113.2(C8&12); 46.0(C6).

ES+ MS: m/z = 185 [M^+]

Anal: Calculated for $C_{12}H_{12}N_2$: C, 78.23; H, 6.57; N, 15.21 %
Found: C, 78.15; H, 6.56; N, 15.20 %

IR: 3258 ν (NH)

(*E*)-*N*-((pyridine-4-yl)methylene)benzenamine

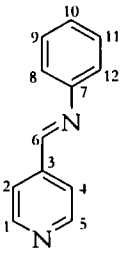

2.3 *imine*

Aniline (5.35 g, 57 mmol) and 4-pyridinecarboxaldehyde (6.2 g, 57 mmol) were dissolved in dry 1,2-dichloroethane, and magnesium sulfate (6.84 g) was added. The solution was refluxed for 6 hours whilst stirring. After this time the solution was filtered to remove magnesium sulfate, and then concentrated under reduced pressure to yield a yellow oil. The product was washed with ether, and the yellow solid impurities removed by filtration. Some of the ether was removed under reduced pressure, and the product was collected by filtration and yielded the imine as white powder (6.58 g, 36 mmol, 63 %).

^{1}H-NMR ($CDCl_3$, 500 MHz, δ / ppm, J / Hz): 8.76 (2H, dd, J=4.5, 2.0, Pyridyl-H(H1&5)); 8.46 (1H, s, CH(H6)); 7.76 (2H, dd, J=4.5, 2.0, Pyridyl-H(H2&4)); 7.43 (2H, t, J=7.5, Ar-H(H9&11)); 7.32-7.23 (3H, m, Ar-H(H8,10&12)

^{13}C{^{1}H}-NMR ($CDCl_3$, 125 MHz, δ / ppm): 158.2(C6); 151.2(C3); 150.84(C1&5); 143.0(C7); 129.5(C2&4); 127.3(C9&11); 122.5(C10); 121.2(C8&12).

ES+ MS: m/z = 183 [M^+]

Anal: Calculated for $C_{12}H_{10}N_2$: C, 79.10; H, 5.53; N, 15.37 %
Found: C, 78.51; H, 5.53; N, 15.14 %

***N*-((pyridin-4-yl)methyl)benzenamine**

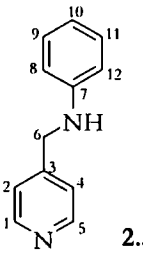

2.3

2.3 *imine* (6.0 g, 33 mmol) was dissolved in methanol, and whilst stirring $NaBH_4$ (6.1 g, 165 mmol) was added until the solution ceased to effervesce. The solution was stirred for a further 2 hours. 50:50 HCl:H_2O (10 mL) was added until the solution was pH 3, and then 2 M NaOH (50 mL) was added until the solution was pH 9. The product was extracted using dichloromethane. The organic layer was dried over $MgSO_4$, and then filtered. The solvent was evaporated under reduced pressure, and the product, re-crystallized from dichloromethane and hexane (4.9 g, 26.6 mmol, 81 %).

^{1}H-NMR ($CDCl_3$, 500 MHz, δ / ppm, J / Hz): 8.54 (2H, dd, J=4.5, 1.5, Pyridyl-H(H1&5)); 7.29 (2H, dd, J=4.5, 1.5, Pyridyl-H(H2&4)); 7.17 (2H, dd, J=7.0, 1.5, Ar-H(H8&12)); 6.75 (1H, tt, J=7.0, 1.5, Ar-H(H10)); 6.58 (2H, dd, J=7.0, 1.5, Ar-H(H9&11)); 4.37 (2H, s, CH_2(C6)), 4.36 (1H, bs, NH).

^{13}C{^{1}H}-NMR ($CDCl_3$, 125 MHz, δ / ppm): 150.2(C1&5); 149.1(C7); 147.8(C3); 129.6(C8&12); 122.3(C2&4); 118.2(C10); 113.1(C9&11); 47.3(C6).

ES+ MS: m/z = 185 [M^+]

Anal: Calculated for $C_{12}H_{10}N_2$: C, 78.23; H, 6.57; N, 15.21 %
Found: C, 78.00; H, 6.57; N, 15.20 %

IR: 3255 ν (NH)

(*E*)-4-methoxy-*N*-((pyridin-3-yl)methylene)benzamine

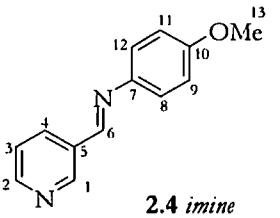

2.4 *imine*

4-methoxyaniline (4.90 g, 40 mmol) and 3-pyridinecarboxaldehyde (4.26 g, 40 mmol) were dissolved in dry 1,2-dichloroethane, and magnesium sulfate (5.00 g) was added. The solution was refluxed for 6 hours whilst stirring. After this time the solution was filtered to remove magnesium sulfate, and then concentrated under reduced pressure. The product was washed with ether, and the solution filtered to yield the imine, which was used in its crude state for the synthesis of **2.4** (1.07 g, 5.0 mmol, 13 %).

^{1}H-NMR ($CDCl_3$, J/Hz, δ/ppm): δ 8.92 (1H, d, J=1.6, Pyridyl-H(H1)); 8.60 (1H, dd, J=8.0, 1.6, Pyridyl-H(H2)); 8.45 (1H, s, CH(H6)); 8.20 (1H, dt, J=8.0, 1.6, Pyridyl-H(H3)); 7.32 (1H, dd, J=8.0, 1.6, Pyridyl-H(H4)); 7.19 (2H, m, 7.21-7.17, Ar-H(H8&12)); 6.87 (2H, m, 6.89-6.85, Ar-H(H9&11)); 3.79 (3H, s, CH_3(H13)).

ES+ MS: m/z = 213 $[M+H]^+$

4-methoxy-*N*-((pyridine-3-yl)methyl)benzenamine

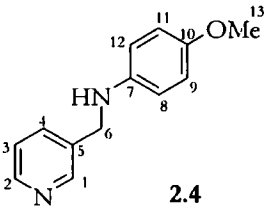

2.4

2.4 *imine* (1.00 g, 4.7 mmol) was dissolved in methanol, and whilst stirring $NaBH_4$ (1.61 g, 43.5 mmol) was added until the solution ceased to effervesce. The solution was stirred for a further 2 hours. 50:50 HCl:H_2O (5 mL) was added until the solution was pH 3, and then 2 M NaOH (50mL) was added until the solution was pH 9. The product was extracted using dichloromethane. The organic layer was dried over $MgSO_4$, and then filtered. The solvent was evaporated under reduced pressure, and the product, (0.72 g, 3.3 mmol, 71 %) re-crystallized from dichloromethane and hexane.

^{1}H-NMR ($CDCl_3$, J/Hz, δ/ppm): δ 8.55 (1H, d, J=2.0, Pyridyl-H(H1)); 8.44 (1H, dd, J=8.0, 2.0, Pyridyl-H(H2)); 7.62 (1H, dt, J=8.0, 2.0, Pyridyl-H(H3)); 7.18 (1H, m, 7.20-7.17, Pyridyl-H(H4)); 6.70 (2H, m, 6.72-6.68, Ar-H(H8&12)); 6.52 (2H, m, 6.54-6.50, Ar-H(H9&11)); 4.24 (2H, s, CH_2(H6)); 3.75 (1H, s, NH); 3.67 (3H, s, CH_3(H13))

ES+ MS: m/z = 215 $[M+H]^+$

Anal: Calculated for $C_{13}H_{14}N_2O$: C, 72.87; H, 6.59; N, 13.07 %
Found: C, 72.57; H, 6.54; N, 12.81 %

IR: 3244 ν (NH)

(*E*)-4-nitro-*N*-((pyridin-3-yl)methylene)benzamine

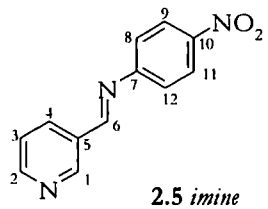

2.5 *imine*

4-nitroaniline (13.60 g, 65 mmol) and 3-pyridinecarboxaldehyde (6.93 g, 65 mmol) were dissolved in dry 1,2-dichloroethane, and magnesium sulfate (5.00 g) was added. The solution was refluxed for 6 hours whilst stirring. After this time the solution was filtered to remove magnesium sulfate, and then concentrated under reduced pressure. The product was washed with ether, to yield the impure imine as dark yellow solid, which was used in its crude state for the synthesis of **2.4**.

^{1}H-NMR (MeOD, 400 MHz, δ / ppm, J / Hz): 8.78 (1H, d, J=5.6, Pyridyl-H(H4)); 8.58 (1H, dd, J=8.0, 5.6, Pyridyl-H(H2)); 8.08 (2H, dd, J=6.8, 2.0, ArH(H9&11)); 7.53 (1H, dd, J=8.0, 5.6, Pyridyl-H(H3)); 7.45 (1H, s, Pyridyl-H(H1)); 6.77 (2H, dd, J=6.8, 2.0, ArH(H8&12)); 6.29 (1H, s, CH(H6)).

ES+ MS: m/z = 228 [M^+]

4-nitro-*N*-((pyridine-3-yl)methyl)benzenamine

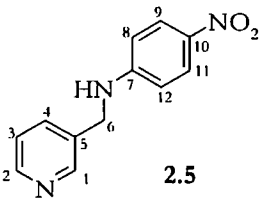

2.5

2.5 *imine* (7.0 g, 30.0 mmol) was dissolved in methanol, and whilst stirring $NaBH_4$ (6.0 g, 162.0 mmol) was added until the solution ceased to effervesce. The solution was stirred for a further 2 hours. 50:50 HCl:H_2O (15 mL) was added until the solution was pH 3, and then 2 M NaOH (50 mL) was added until the solution was pH 9. The product was extracted using dichloromethane. The organic layer was dried over $MgSO_4$, and then filtered. The solvent was evaporated under reduced pressure, and the product, (4.4 g, 19.1 mmol, 62 %) re-crystallized from dichloromethane and hexane.

^{1}H-NMR ($CDCl_3$, 500 MHz, δ / ppm, J / Hz): 8.63 (1H, s, Pyridyl-H(H1)); 8.57 (1H, d, J=5.0, Pyridyl-H(H4)); 8.09 (2H, dd, J=7.0, 2.0, Ar-H(H9&11)); 7.67 (1H, dd, J=8.0, 2.0, Pyridyl-H(H2)); 7.30 (1H, dd, J=8.0, 5.0, Pyridyl-H(H3)); 6.59 (2H, dd, J=7.0; 2.0, Ar-H(H8&12)); 4.92 (1H, bs, NH); 4.47 (2H, d, J=6.0, CH_2(H6)).

^{13}C{^{1}H}-NMR (CDCl3, 125 MHz, δ / ppm): 207.3(C10); 152.8(C7); 149.6(C1); 149.3(C4); 135.2(C2); 133.2(C5); 126.6(C9&11); 124.0(C3); 111.72(C8&12); 45.4(C6).

ES+ MS: m/z = 230 [M^+]

Anal: Calculated for $C_{12}H_{12}N_3O_2$: C, 62.60; H, 5.25; N, 18.25 %
Found: C, 62.40; H, 4.80; N, 18.38 %

IR: 3239 ν (NH)

(*E*)-9-ethyl-*N*-((pyridine-3-yl)methylene)-9*H*-carbazole-3-amine

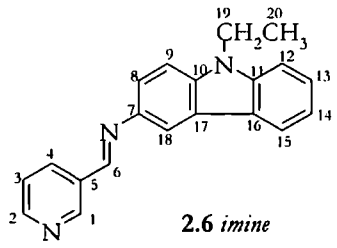

2.6 *imine*

3-amino-9-ethylcarbazole (9.60 g, 46 mmol) and 3-pyridinecarboxaldehyde (5.00 g, 47 mmol) were dissolved in dry 1,2-dichloroethane, and magnesium sulfate (5.00 g, 42 mmol) was added. The solution was placed under reflux for 6 hours whilst stirring. After this time the solution was filtered to remove magnesium sulfate, and then concentrated under reduced pressure to yield a brown oil. The product was washed with ether, and the brown solid impurities removed by filtration, and the product collected as a dark yellow oil.

^{1}H-NMR ($CDCl_3$, 400 MHz, δ / ppm, J / Hz): 8.92 (1H, s, Pyridyl-H(H1)), 8.53 (1H, d, J=3.2, Pyridyl-H(H2)), 8.49 (1H, s, CH(H6)), 8.15 (1H, dt, J=7.6, 1.6, Pyridyl-H(H3)), 7.97 (1H, ddd, J=8.0, 0.4, 1.2, Ar-H(H9)), 7.91 (1H, d, J=1.6, Pyridyl-H(H4)), 7.33 (2H, m, Ar-H(H12, 13, 15, 18)), 7.11 (1H, dt, J=7.2, 1.2, Ar-H(H14)), 4.15 (2H, q, J=7.2, CH_2(H19)), 1.26 (3H, t, J=7.2, CH_3(H20)).

^{13}C{^{1}H}-NMR ($CDCl_3$, 125 MHz, δ / ppm): 154.2(C2); 152.0(C1); 150.7(C5); 143.0(C7); 140.6(C10); 134.6(C9); 132.4(C17); 126.1(13); 124.0(C14); 123.8(C11); 123.5(C16); 123.1(C8); 120.4(C18); 120.0(C3); 119.1(C15); 112.9(C4); 108.9(C12); 53.5(C6); 37.7(C19); 13.9(C20).

9-ethyl-*N*-((pyridine-3-yl)methyl)-9*H*-carbazol-3-amine

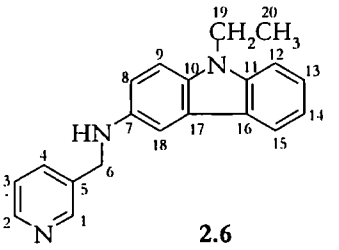

2.6

2.6 *imine* (2.15 g, 7.18 mmol) was dissolved in methanol, and whilst stirring $NaBH_4$ (2.69 g, 71.8 mmol) was added until the solution ceased to effervesce. The solution was stirred for a further 2 hours. 50:50 HCl:H_2O (30 mL) was added until the solution was pH 3, and then 2 M NaOH (100 mL) was added until the solution was pH 9. The product was extracted using dichloromethane. The organic layer was dried over $MgSO_4$, and then filtered. The solvent was evaporated under reduced pressure, and the product, re-crystallized from dichloromethane and hexane (1.26 g, 4.18 mmol, 58 %).

^{1}H-NMR ($CDCl_3$, 400 MHz, δ / ppm, J / Hz): 8.72 (1H, d, J=2.0, Pyridyl-H(H1)), 8.56 (1H, dd, J=7.5, 2.0, Pyridyl-H(H2)), 8.02 (1H, d, J= 7.5, Ar-H(H8)), 7.60 (1H, d, J=7.5, Pyridyl-H(H4)), 7.46 (1H, t, J=7.5, Pyridyl-H(H3)), 7.37 (2H, m, Ar-H(H18&15)), 7.27 (2H, m, Ar-H(H12&13)), 7.20 (1H, t, J=7.5, Ar-H(H14)), 6.90 (1H, dd, J= 8.5, 2.0, Ar-H(H9)), 4.44 (2H, s, CH_2(H6)), 4.30 (2H, q, J=7.5 CH_2(H19)), 4.05 (1H, bs, NH), 1.40 (3H, t, J=7.5, CH_3(H20)).

^{13}C{^{1}H}-NMR ($CDCl_3$, 125 MHz, δ / ppm): 149.3(C2); 148.6(C1); 140.7(C5); 140.4(C7); 135.5(C10); 135.3(C9); 134.4(C17); 125.5(C13); 123.7(C14); 123.6(C11); 122.5(C16); 120.4(C8); 118.1(C18); 114.6(3); 109.3(15); 108.4(C4); 104.0(C9); 47.51(C6); 37.5(C19); 13.8(C20).

ES+ MS: m/z = 302 [M^+]

Anal: Calculated for: C, 79.70; H, 6.35; N, 13.94 %
Found: C, 79.76; H, 6.38; N, 14.03 %

IR: 3303 ν(NH)

2.6 Crystal Data

2.6.1 General Procedure for X-ray Crystallographic Studies

Suitable single crystals were mounted using silicon grease on a thin glass fibre. Crystallographic measurements were carried out using Bruker SMART 1K or 6K (Durham University). The instrument was equipped with graphite monochromatic Mo-Kα radiation (λ= 0.71073 Å). The standard data collection temperature was 120 K, maintained using an open flow N_2 Oxford Cryostream device. Integration was carried out using SAINT software. Data sets were corrected for Lorentz and polarization effects and for the effects of absorption. Structures were solved using direct methods in SHELXS-97[139] and developed using conventional alternating cycles of least-squares refinement with SHELX-97[139] and difference Fourier synthesis with the aid of the graphical interface program XSeed.[140] In all cases non-hydrogen atoms were fixed in idealised positions and allowed to ride on the atom to which they were attached. Hydrogen atom thermal parameters were tied to those of the atom to which they were attached. Where possible O-H hydrogen atoms were located experimentally and their position and displacement parameters refined. Molecular graphics were produced using the program POV-Ray.

Crystal data for 2.2 (Z' = 2 polymorph): $C_{12}H_{12}N_2$, M = 184.24, colourless block, 0.20 x 0.20 x 0.20 mm^3, monoclinic, space group $P2_1/c$ (No. 14), a = 19.859(3), b = 8.3393(14), c = 12.950(2) Å, β = 107.061(3)°, V = 2050.3(6) Å^3, Z = 8, D_c = 1.194 g/cm^3, F_{000} = 784, MoKα radiation, λ = 0.71073 Å, T = 220(2)K, $2\theta_{max}$ = 60.8°, 19657 reflections collected, 5638 unique (R_{int} = 0.2243). Final *GooF* = 1.021, *R1* = 0.1203, *wR2* = 0.2568, R indices based on 1898 reflections with I >2sigma(I) (refinement on F^2), 254 parameters, 0 restraints. Lp and absorption corrections applied, μ = 0.072 mm^{-1}.

Crystal data for 2.2 (Z' = 1 polymorph): $C_{12}H_{12}N_2$, M = 184.24, colourless prism, 0.31 x 0.24 x 0.11 mm^3, orthorhombic, space group *Pbca* (No. 61), a = 11.2980(7), b = 8.3784(5), c = 20.5888(13) Å, V = 1948.9(2) Å^3, Z = 8, D_c = 1.256 g/cm^3, F_{000} = 784, Smart 1K, MoKα radiation, λ = 0.71073 Å, T = 120(2)K, $2\theta_{max}$ = 58.3°, 16049 reflections collected, 2632 unique (R_{int} = 0.0398). Final *GooF* = 1.022, *R1* = 0.0423, *wR2* = 0.1141, R indices based on 2015 reflections with I >2sigma(I) (refinement on F^2), 127 parameters, 0 restraints. Lp and absorption corrections applied, μ = 0.076 mm^{-1}.

Crystal data for 2.3: $C_{12}H_{12}N_2$, M = 184.24, 0.34 x 0.31 x 0.18 mm^3, triclinic, space group *P*-1 (No. 2), a = 8.1148(7), b = 12.0865(10), c = 12.5931(10) Å, α = 62.144(3), β = 78.526(3), γ = 71.670(3)°, V = 1034.61(15) Å^3, Z = 4, D_c = 1.183 g/cm^3, F_{000} = 392, Smart 1K, MoKα radiation, λ = 0.71073 Å, T = 120(2)K, $2\theta_{max}$ = 56.3°, 13808 reflections collected, 5019 unique (R_{int} = 0.0769). Final *GooF* = 1.008, *R1* = 0.0608, *wR2* = 0.1151, R indices based on 3189 reflections with I >2sigma(I) (refinement on F^2), 253 parameters, 0 restraints. Lp and absorption corrections applied, μ = 0.071 mm^{-1}.

Crystal data for 2.4: $C_{13}H_{14}N_2O$, M = 214.26, colourless block, 0.20 x 0.20 x 0.20 mm^3, monoclinic, space group $P2_1/c$ (No. 14), a = 13.1451(8), b = 5.7545(3), c = 16.2583(9) Å, β = 113.139(2)°, V = 1130.90(11) Å^3, Z = 4, D_c = 1.258 g/cm^3, F_{000} = 456, MoKα radiation, λ = 0.71073 Å, T = 120(2)K, $2\theta_{max}$ = 60.8°, 13405 reflections collected, 3391 unique (R_{int} = 0.1475). Final *GooF* = 0.906, *R1* = 0.0503, *wR2* = 0.1253, *R* indices based on 2088 reflections with I >2sigma(I) (refinement on F^2), 149 parameters, 0 restraints. Lp and absorption corrections applied, μ = 0.081 mm^{-1}.

Crystal data for 2.5: $C_{12}H_{11}N_3O_2$, M = 229.24, yellow plate, 0.38 x 0.34 x 0.24 mm^3, monoclinic, space group $P2_1/c$ (No. 14), a = 25.7333(17), b = 11.0475(7), c = 7.4793(5) Å, β = 93.271(3)°, V = 2122.8(2) $Å^3$, Z = 8, D_c = 1.435 g/cm^3, F_{000} = 960, Smart 6K, MoKα radiation, λ = 0.71073 Å, T = 393(2)K, $2\theta_{max}$ = 69.9°, 23936 reflections collected, 8749 unique (R_{int} = 0.0549). Final *GooF* = 0.924, *R1* = 0.0531, *wR2* = 0.1263, *R* indices based on 5279 reflections with I >2sigma(I) (refinement on F^2), 307 parameters, 0 restraints. Lp and absorption corrections applied, μ = 0.101 mm^{-1}.

Crystal data for 2.6: $C_{20}H_{19}N_3$, M = 301.38, colourless block, 0.20 x 0.20 x 0.20 mm^3, monoclinic, space group $P2_1/c$ (No. 14), a = 7.5121(2), b = 18.9330(5), c = 11.6372(3) Å, β = 103.6790(10)°, V = 1608.17(7) $Å^3$, Z = 4, D_c = 1.245 g/cm^3, F_{000} = 640, MoKα radiation, λ = 0.71073 Å, T = 120(2)K, $2\theta_{max}$ = 61.0°, 15204 reflections collected, 4895 unique (R_{int} = 0.0287). Final *GooF* = 0.982, *R1* = 0.0537, *wR2* = 0.1417, *R* indices based on 3775 reflections with I >2sigma(I) (refinement on F^2), 212 parameters, 0 restraints. Lp and absorption corrections applied, μ = 0.075 mm^{-1}.

Chapter Three

Preliminary Study on Co-ordination and Anion Binding Chemistry

There has recently been a lot of work in the use of transition metals as sensing and structural elements in hosts for anion binding, and of course the use of organic ligands to bind metal atoms both in solution and solid complexes.[12, 117, 119, 141-144] Steed *et al.* have previously reported the preparation of complex in which a silver atom is bridging between two pyridyl nitrogen atoms from pyridyl urea ligands and the nitrate anion is bound by the four urea NH protons.[1, 144] Gale and co-workers have synthesised a new series of compounds based around a 2,6-dicarboxamindopyridine core, which has shown a particular affinity for chloride.[145] In the solid state, they saw the chloride anion was hydrogen bonded to the amide NH protons.[145] As ligand **2.6** was designed as a photo-active anion binding sensor, its binding ability was monitored by UV-Vis titration experiments with ligand and metal salts, and those interactions where measured with **2.2** as a control compound, and due to the fluorescent properties of **2.6**, the effect of adding metal salts to solutions of **2.6** was monitored by fluorescent titration experiments. The effect of adding metal salts to solutions of control compounds **2.2**, **2.4** and **2.5**, was monitored by UV-Vis titration experiments.

3.1 Synthesis and Characterisation

Solid complexes, of ligand **2.6** and $Cu(CF_3SO_3)_2$ were obtained by mixing solutions of the ligand with solutions of differing concentrations of $Cu(CF_3SO_3)_2$. Three solutions were prepared, the first contained a 2:1 mixture of **2.6** and $Cu(CF_3SO_3)_2$, the second a 1:1 mixture, and the third a 1:2 mixture of **2.6** and $Cu(CF_3SO_3)_2$. The solid products were obtained from the concentrated solutions by filtration. These solid products obtained were analysed by elemental analysis which indicates the formation of 2:1, 1:1 and 1:2 **2.6**:$Cu(CF_3SO_3)_2$ species, and possible structures are shown in **figure 3.1**, although no crystallographic data could be obtained and the structures of the complexes are therefore unclear.

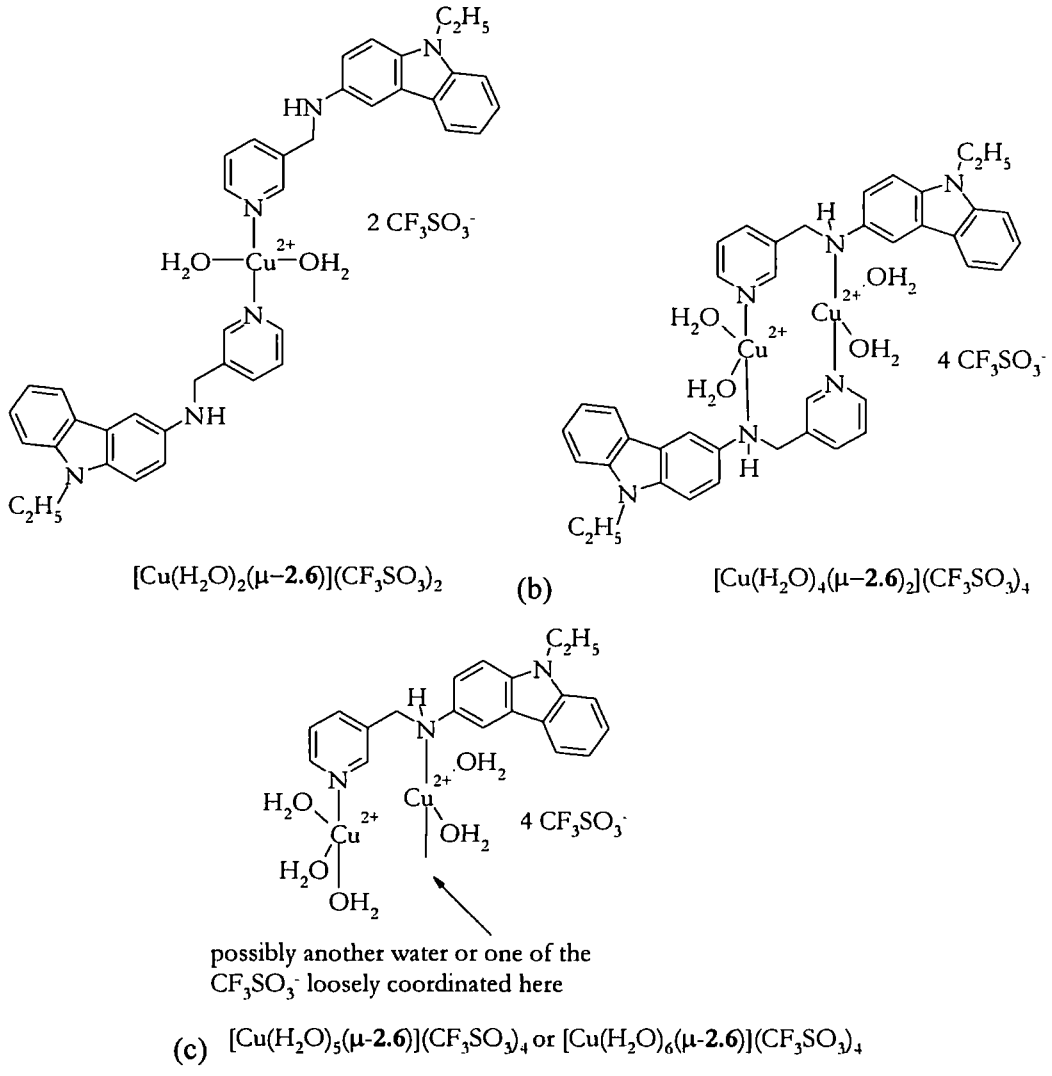

(a) $[Cu(H_2O)_2(\mu\text{–}\mathbf{2.6})](CF_3SO_3)_2$ (b) $[Cu(H_2O)_4(\mu\text{–}\mathbf{2.6})_2](CF_3SO_3)_4$

(c) $[Cu(H_2O)_5(\mu\text{-}\mathbf{2.6})](CF_3SO_3)_4$ or $[Cu(H_2O)_6(\mu\text{-}\mathbf{2.6})](CF_3SO_3)_4$

Figure 3.1: Possible structures of $\mathbf{2.6}(Cu(CF_3SO_3)_2$ complexes. (a) $[Cu(H_2O)_2(\mu\text{-}\mathbf{2.6})_2](CF_3SO_3)_2$; (b) $[Cu_2(H_2O)_4(\mu\text{-}\mathbf{2.6})_2](CF_3SO_3)_4$; (c) $[Cu_2(H_2O)_5(\mu\text{-}\mathbf{2.6})](CF_3SO_3)_4$ or $[Cu_2(H_2O)_6(\mu\text{-}\mathbf{2.6})](CF_3SO_3)_4$

The suggested structure of $[Cu(H_2O)_2(\mu\text{-}\mathbf{2.6})_2](CF_3SO_3)_2$, shown in **figure 3.1(a)**, is analogous to a structure previously observed in the Steed group, in which a copper (II) ion is bound between the pyridyl-N atoms of two ligands, and to the oxygen in coordinated water ligands,[11] **figure 3.2**. The suggested structure of the $[Cu_2(H_2O)_4(\mu.\mathbf{2.6})_2](CF_3SO_3)_4$, shown in **figure 3.1(b)** is analogous to a structure of a known palladium complex, in which the

palladium is bridged between a pyridyl nitrogen and an amine nitrogen atom on the adjacent ligand, **figure 3.3**.[12]

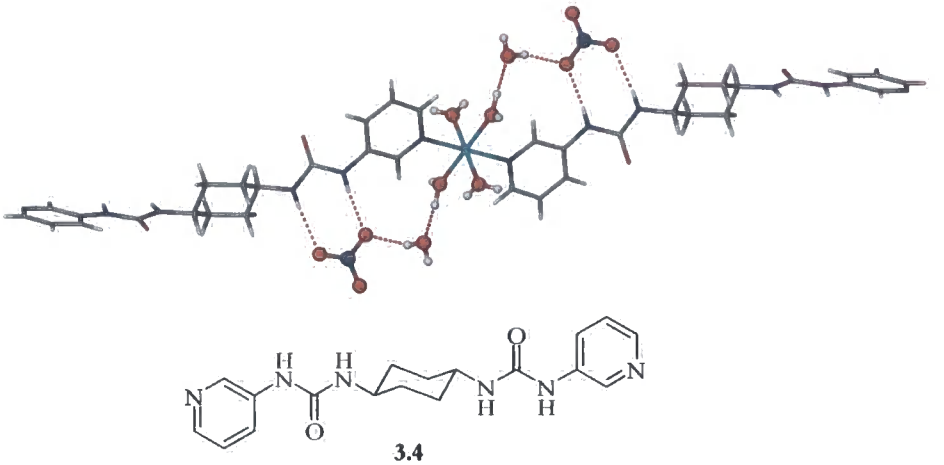

3.4

Figure 3.2: X-ray crystal structure of $[Cu(H_2O)_6(\mu\text{-}\mathbf{3.4})_2](NO_3)_2$ and a diagram of ligand **3.4**.[11]

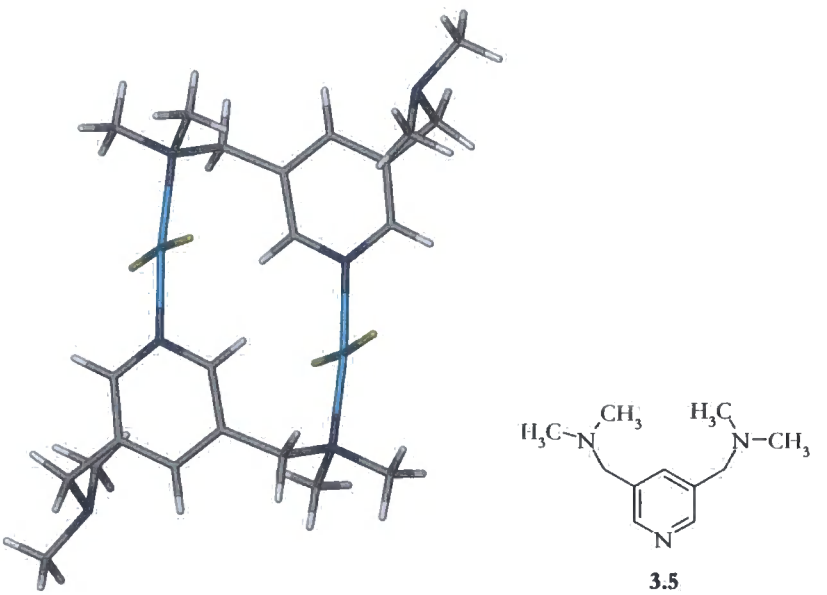

3.5

Figure 3.3: X-ray crystal structure of $[Cu_2Cl_4\ (\mu\text{-}\mathbf{3.5})_2]$ and a diagram of ligand **3.5**.[12]

Further attempts to synthesise solid complexes were made, in which solutions of ligands, **2.2 – 2.6**, were mixed with solutions of metal salts in the desired stoichiometry. The solvent in which the compounds were mixed was varied, and a series of solutions were prepared, and attempts were made to grow crystals, showing interactions between the ligands and both metal atoms and their anions. Several crystals which were analysed by X-ray diffraction

methods, were grown, but in the majority of cases the ligands had been protonated, and hydrogen bonding interactions were seen between the protonated ligands and anions from the metal salts, **figures 3.6** and **3.7**. To try and promote interactions between the metal centre and ligand, rather than the protonation of the ligand, a small amount of organic base, Et_3N was added to solutions, to increase the pH of the solutions, but this did not result in the formation of any solid products. However in the case of $Cu(CH_3COO)_2$, crystals were grown with ligands, **2.2** and **2.5**, and the structures analysed by X-ray diffraction studies.

In the crystal structure of $[Cu_2(\mu\text{-}O_2CMe)_4(\mathbf{2.2})_2]$, the ligand, **2.2**, is coordinated to the copper atoms via the pyridyl nitrogen atom. The acetate counter ions are not interacting with the ligand but are part of the coordination sphere of the transition metal, which results in the paddle wheel motif for the complex made up of two ligands, two copper atoms and four acetate ligands, **figure 3.4**. The complex exhibits intermolecular hydrogen bonding between amine protons and oxygen atoms in the acetate group, as well as hydrogen bonding between pyridyl CH protons and acetate oxygen atoms. There is also some intramolecular hydrogen bonding within the acetate group observed. The robust lantern structure means this structure is not representative of those shown in **figure 3.1**. This paddle wheel structure with copper(II)acetate and pyridyl ligands has been previously observed in the literature,[146, 147] and comparison of bond lengths and bond angles with those obtained by Barquin *et al*, showed that they are similar, for example, Cu(1)—O(1) = 1.975(2) and 1.983(2)[146]; Cu(1)—N(1) = 2.179(3) and 2.233(2)[146]; Cu(1)—Cu(1) = 2.647 and 2.719(1)[146]; and O(3)-Cu(1)-O(2) = 91.11(10) and 89.32(2) ; O(3)-Cu(1)-N(1) = 94.29(9) and 98.22(9)[146]; N(1)-Cu(1)-Cu(1) = 173 and 178.92(6)[146]. Similarly, in the crystal structure of $[Cu_2(\mu\text{-}O_2CMe)_4(\mathbf{2.5})_2]$, the ligand, **2.5**, is coordinated to the copper atoms via the pyridyl nitrogen atom. The acetate counter ions are not interacting with the ligand but are part of the coordination sphere of the transition metal, which results in the paddle wheel motif for the complex made up of two ligands, two copper atoms and four acetates, **figure 3.5**, analogous to the crystal structure of $[Cu_2(\mu\text{-}O_2CMe)_4(\mathbf{2.2})_2]$, **figure 3.4**. In the crystal structure of $[Cu_2(\mu\text{-}O_2CMe)_4(\mathbf{2.5})_2]$, hydrogen bonding is observed between the amine NH and the one oxygen from the NO_2 group, and not between the amine proton and acetate groups as is seen in the **2.2** analogue. The distance between the hydrogen bonding O and H-N in $[Cu_2(\mu\text{-}O_2CMe)_4(\mathbf{2.5})_2]$, is 2.245 Å, but the distance between the same atoms in the ligand structure, **2.5**, is 3.840 Å. So in this structure

the ligands are in a different orientation, and form hydrogen bonded chains, in which two dimers are linked via the oxygen atom from a nitro-group, to the hydrogen atom of the amine group on an adjacent ligand, forming hydrogen bonded chains along the b-axis. The copper-copper distance in both complexes are similar, as are the pyridyl nitrogen and copper distances, and the nitrogen-copper-copper angles, as detailed in **table 3.1**.

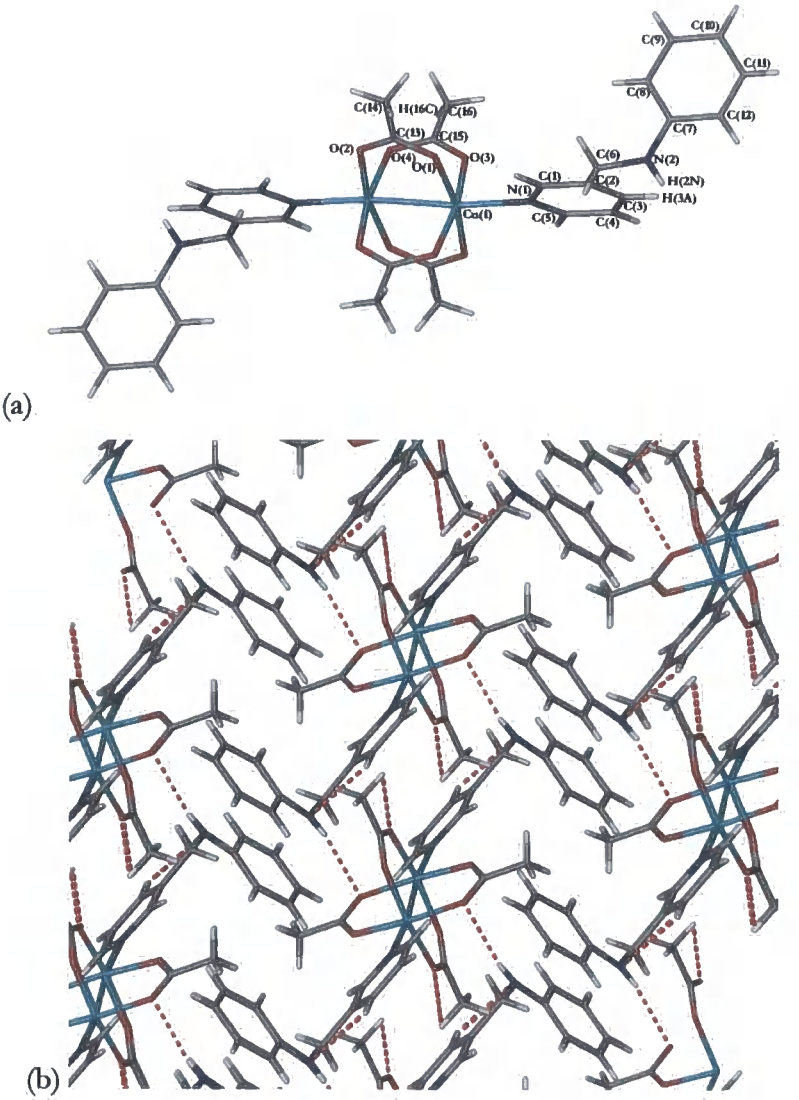

Figure 3.4: X-ray crystal structure of $[Cu_2(\mu\text{-}O_2CMe)_4(\mathbf{2.2})_2]$ (a) Molecular structure (b) Packing diagram viewed along c-axis.

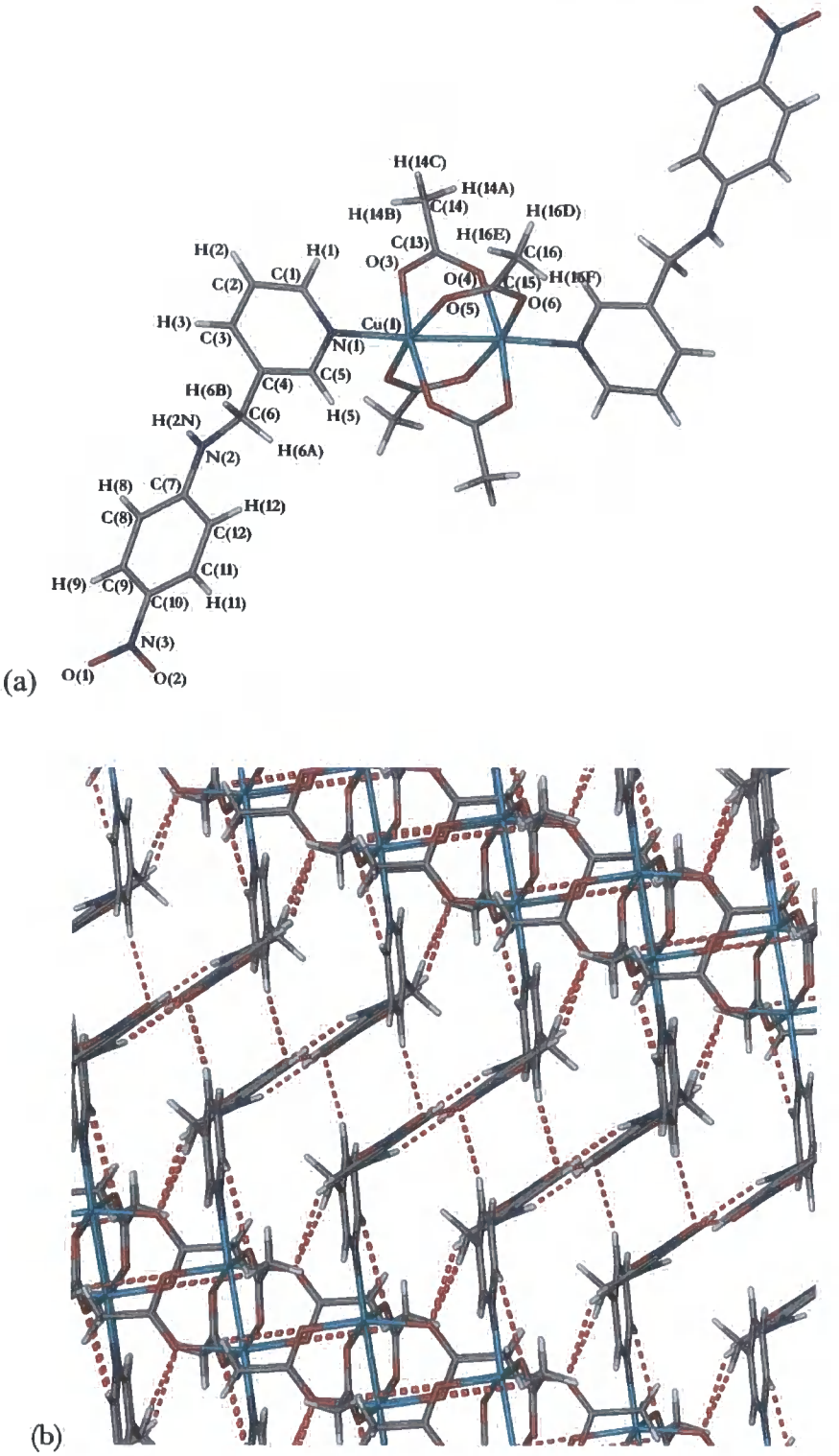

Figure 3.5: X-ray crystal structure of $[Cu_2(\mu\text{-}O_2CMe)_4(\mathbf{2.5})_2]$ (a) Molecular structure (b) Packing diagram viewed along b-axis.

	$[Cu_2(\mu\text{-}O_2CMe)_4(\mathbf{2.2})_2]$	$[Cu_2(\mu\text{-}O_2CMe)_4(\mathbf{2.5})_2]$
Cu-----Cu	2.647	2.615
N------Cu	2.179(3)	2.1825(15)
N^Cu^Cu	173.3	176.0
D--H	0.83(4) (N2-H2N) 0.98 (C16-H16C)	0.860 (N2-H2N) 0.930 (C3-H3) 0.970 (C6-H6A) 0.930 (C8-H8) 0.930 (C12-H12) 0.96 (C16-H16E)
H - - - - - -A	2.41(5) (H2N-O2) 2.48 (H16C-O4)	2.25 (H2N-O1) 2.48 (H3-O1) 2.42 (H6A-O6) 2.44 (H8-O1) 2.44(H12-O6) 2.54(H16E-O5)
D - - - - - - A	3.220(4) (N2-O2) 3.416(4) (C16-O4)	3.044(2) (N2-O1) 3.373(2) (C3-O1) 3.386(2) (C6-O6) 3.235(2) (C8-O1) 3.248(2) (C12-O6) 3.440(2) (C16-O5)
D--H - - - A	167(4) (N2-H2N..O2) 160 (C16-H16C..O4)	155 (N2-H2N..O1) 162 (C3-H3..O1) 172 (C6-H6A..O6) 143 (C8-H8..O1) 145 (C12-H12..O6) 156 (C16-H16E..O5)

Table 3.1: Crystal data for $[Cu_2(\mu\text{-}O_2CMe)_4(\mathbf{2.2})_2]$ and $[Cu_2(\mu\text{-}O_2CMe)_4(\mathbf{2.5})_2]$

Figures 3.6 and **3.7** show the failed metal/ligand crystalisations of ligand **2.6** and **2.2** with copper(II) nitrate, and chromium(III) nitrate respectively. The ligands have formed protonated nitrate salts. This protonation presumably occurs because of the polar nature of the solvent from which they were grown with protons arising from coordinated water on the Lewis acidic metal salt, as the presence of a metal cation can dramatically lower the pKa of water.[148] In the crystal structure of (**2.6**-H_2)$(NO_3)_2$, the ligand **2.6** has been protonated at both the pyridyl-nitrogen and also the amine nitrogen atoms, **figure 3.6**. This crystal structure is a Z' = 2 structure in which there are two molecules in the asymmetric unit.[135] There is one nitrate bound between the amine protons, H2N, of two adjacent ligand molecules, and a second to the other amine proton, and each ligand is hydrogen bonded to a third nitrate via the protonated pyridyl nitrogen, N1, and a fourth nitrate anion is bound via the pyridinium CH proton, H22. Hydrogen bonding is not seen between the ligand molecules, in this structure. In the crystal structure of (**2.2**-H)(NO_3), the ligand is protonated on the pyridyl nitrogen only. Nitrate anions are hydrogen bonded via both the protonated pyridyl nitrogen, H1N, and also the amine proton, H2N, of ligand **2.2, figure 3.7**. This forms hydrogen bonded chains of ligands, bound via nitrate anions, in which each anion is bound to two ligands. The nitrate anions are also hydrogen bonded to the methylene protons, and pyridyl protons, to give cross-linked hydrogen bonded chains.

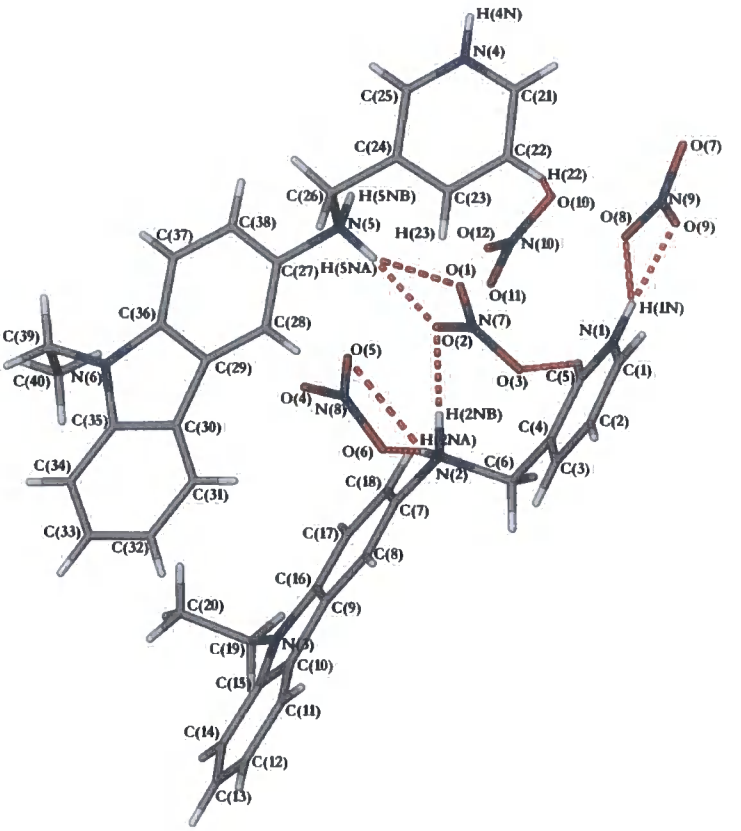

Figure 3.6: X-ray crystal structure of (**2.6**-H_2)$_2$(NO_3)$_2$

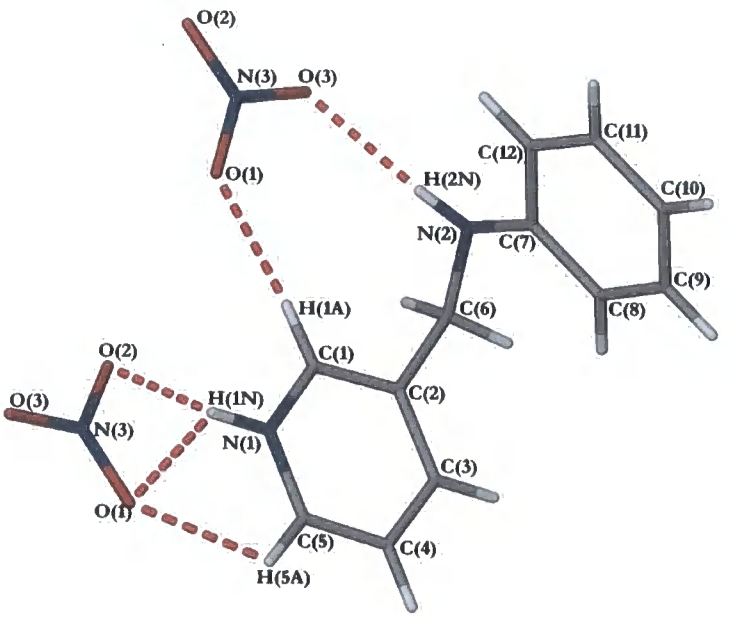

Figure 3.7: X-ray crystal structure of (**2.2**-H)(NO_3)

Compound	D--H	H - - - - - -A	D - - - - - - A	D--H - - - A
(**2.6**-H_2)(NO_3)$_2$	0.90	2.46	3.042(2)	123
(More hydrogen bonding is observed	(N2-H2NA)	(H2NA-O5)	(N2-O5)	(N2-H2NA..O5)
but only the most relevant	0.90	1.84	2.739(2)	174
interactions are included here)	(N2-H2NA)	(H2NA-O6)	(N2-O6)	(N2-H2NA..O6)
	0.86	2.42	3.074(2)	133
	(N1-H1N)	(H1N-O8)	(N1-O8)	(N1-H1N..O8)
	0.86	1.82	2.665(2)	167
	(N1-H1N)	(H1N-O9)	(N1-O9)	(N1-H1N..O9)
	0.90	1.92	2.820(2)	179
	(N2-H2NB)	(H2NB-O2)	(N2-O2)	(N2-H2NB..O2)
	0.90	2.44	3.094(2)	130
	(N5-H5NA)	(H5NA-O1)	(N5-O1)	(N5-H5NA..O1)
	0.90	1.87	2.768(2)	171
	(N5-H5NA)	(H5NA-O2)	(N5-O2)	(N5-H5NA..O2)
	0.93	2.52	3.343(2)	147
	(C5-H5)	(H5-O3)	(C5-O3)	(C5-H5..O3)
	0.93	2.50	3.154(3)	128
	(C22-H22)	(H22-O10)	(C22-O10)	(C22-H22..O10)
(**2.2**-H)(NO_3)	0.934(18)	2.475(17)	3.1192(14)	126.2(13)
	(N1-H1N)	(H1N-O1)	(N1-O1)	(N1-H1N..O1)
	0.934(18)	1.802(18)	2.7332(14)	173.8(17)
	(N1-H1N)	(H1N-O2)	(N1-O2)	(N1-H1N..O2)
	0.864(17)	2.150(17)	3.0110(15)	174.6(15)
	(N2-H2N)	(H2N-O3)	(N2-O3)	(N2-H2N..O3)
	0.95	2.36	3.1945(16)	146
	(C1-H1A)	(H1A-O1)	(C1-O1)	(C1-H1A..O1)
	0.95	2.57	3.1547(16)	120
	(C5-H5A)	(H5A-O1)	(C5-O1)	(C5-H5A..O1)
	0.95	2.44	3.2144(16)	139
	(C5-H5A)	(H5A-O2)	(C5-O2)	(C5-H5A..O2)
	0.99	2.51	3.4659	162
	(C6-H6B)	(H6B-O3)	(C6-O3)	(C6-H6B..O3)

Table 3.2: Crystal data for (**2.6**-H_2)(NO_3)$_2$ and (**2.2**-H)(NO_3).

3.2 Photophysical Studies

Even though it was not possible to characterize the solid products, we decided to look at the solution complexation of metals and anions by the ligands **2.2** – **2.6**, by photophysical methods.

3.2.1 Effect of different metal salts

An acetonitrile solution of $Co(NO_3)_2.6H_2O$ was added to an acetonitrile solution of **2.6**, in aliquots of 0.5 equivalents, and an absorbance spectrum was measured after each addition. **Figure 3.9**(a), shows that there is little change in the UV-Vis spectrum, upon addition of $Co(NO_3)_2.6H_2O$, with a small increase in absorbance centred around 525 nm, which could be explained by Co^{2+} *d-d* transitions. The increase in the broad band centred on 525 nm does not occur until after the addition of 3 equivalents of salt, suggesting no metal interaction with the ligand until this point, which could be due to ligand – anion interactions or possibly the protonation of ligand from the water added in the form of the hydrated salt. After the addition of 3 equivalents of $Co(NO_3)_2.6H_2O$, there is a linear increase in the absorbance as a function of increasing concentration of added salt. Upon addition of $Co(NO_3)_2.6H_2O$ to an acetonitrile solution of ligand **2.2**, **figure 3.9**(b) there is a slight increase in the absorbance at 300 nm and as is observed in the titration with **2.6** there is the appearance of a broad band centred on 525 nm, but contrary to the titration of $Co(NO_3)_2.6H_2O$ with **2.6**, the absorbance centred on 525 nm increases linearly after the addition of 1 equivalent of salt. This suggests that the metal – ligand interaction occurs after the addition of 1 equivalent of metal compared to 3 equivalents for **2.6**.

Upon addition of $Ni(NO_3)_2.6H_2O$, **figure 3.10**(a) to **2.6**, there is a small increase in the ILCT band centred on 325 nm, and after the addition of 5 equivalents of $Ni(NO_3)_2.6H_2O$, there is the appearance of a broad band which is centred on 630 nm, and is assigned to a Ni^{2+} *d-d* transition, suggesting metal – ligand interaction after the addition of 5 equivalents, but the intensity is less than that observed with Co^{2+}. Upon addition of $Ni(NO_3)_2.6H_2O$, **figure 3.10**(b) to **2.2**, there is a small increase in the band centred on 300 nm, and after the addition of 1 equivalent of salt, there is the appearance of a broad band which is centred on 630 nm, and a second band centred on 380 nm and are assigned to a Ni^{2+} *d-d* transitions, suggesting

metal – ligand interaction after the addition of 1 equivalents, but the intensity is less than that observed with Co^{2+}. The multiple *d-d* transitions observed upon addition of $Ni(NO_3)_2.6H_2O$ to **2.2** suggests the interaction of multiple metal atoms to one ligand, or that the metal is interacting with the counterion, or possibly water present in solution, something which is not observed upon addition of $Co(NO_3)_2.6H_2O$. Upon addition of $Zn(CF_3SO_3)_2$, **figure 3.11**, there is a small increase in the absorbance around 325 nm for **2.6** and 300 nm for **2.2**, which could indicate binding. In the cases of both ligands the largest increase in absorbance is observed upon addition of 0.5 equivalent of $Zn(CF_3SO_3)_2$ to ligand solutions. No *d-d* transitions are observed upon addition of $Zn(CF_3SO_3)_2$, as Zn^{2+} has a filled *d*-orbital so there is no where to promote an electron within the *d*-orbital. The addition of $Zn(CF_3SO_3)_2$, to an NMR solution sample of ligand **2.6** resulted in a shift of the two resonances assigned to the protons closest to the pyridyl nitrogen, and also the amine NH proton, suggesting binding at both the pyridyl nitrogen, and the amine group. The shape of the titration isotherm, **figure 3.8**, suggested multiple host:guest species, but due to precipitation a binding constant could not be calculated, and the same chemical shift changes were not observed at a lower concentration, suggesting that binding to $Zn(CF_3SO_3)_2$, is concentration dependant. The concentration used in the NMR spectroscopic titration experiment was greater than that used in the UV-Vis titration, due to limitations of equipment.

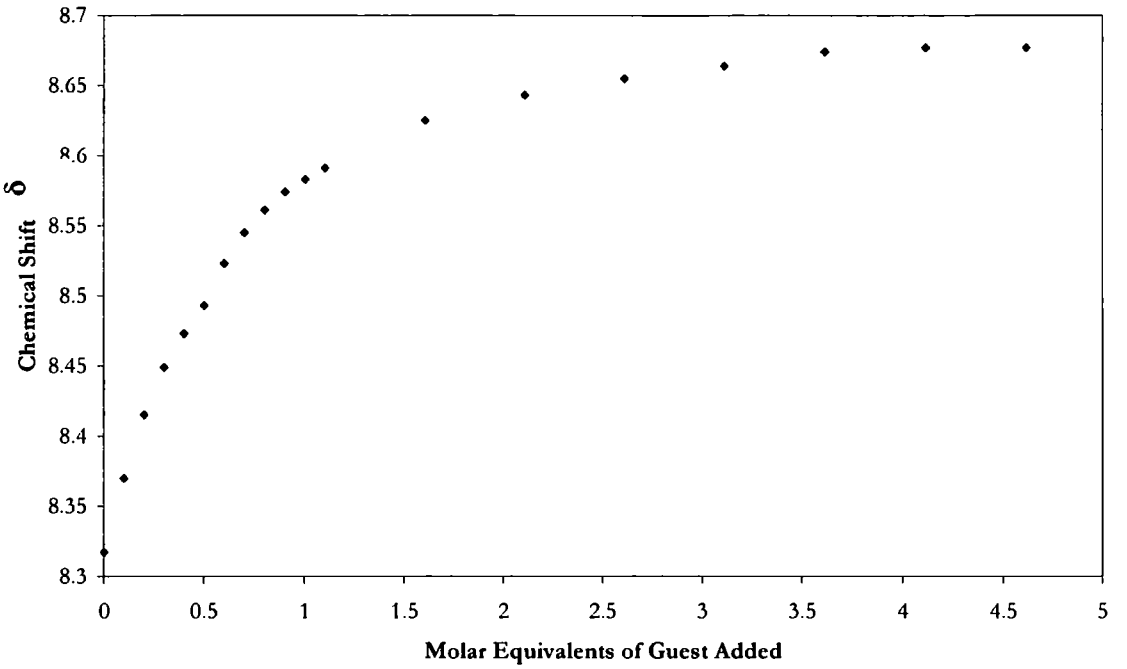

Figure 3.8: ^{1}H-NMR titration data showing chemical shift of the pyridyl proton resonance for **2.6** upon addition of $Zn(CF_3SO_3)_2$.

(a)

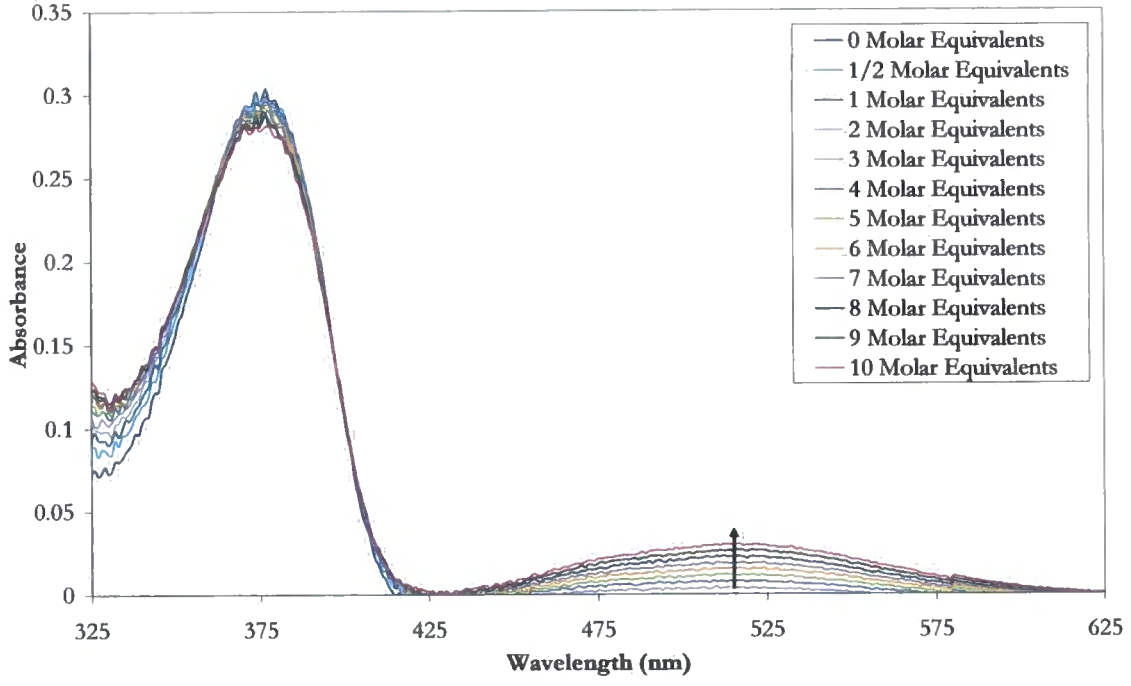

(b)

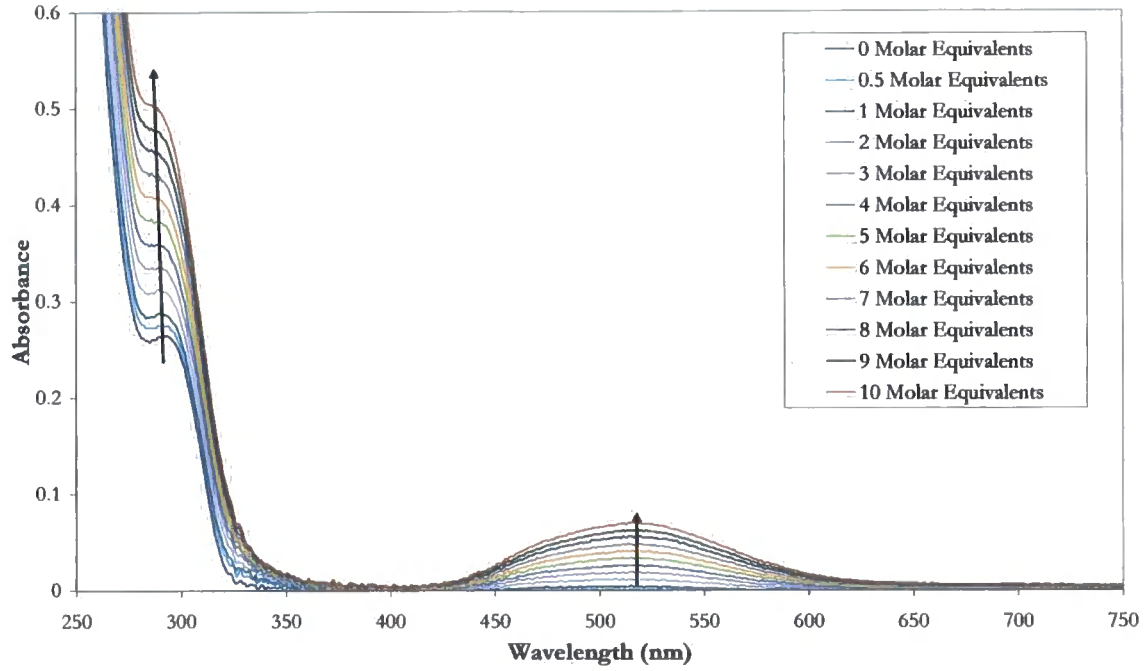

Figure 3.9: Absorption spectrum of (a) **2.6** and (b) **2.2** (1.03×10^{-4} M) in CH_3CN, and upon addition of increasing amounts of $Co(NO_3)_2.6H_2O$ upto 10 equivalents.

(a)

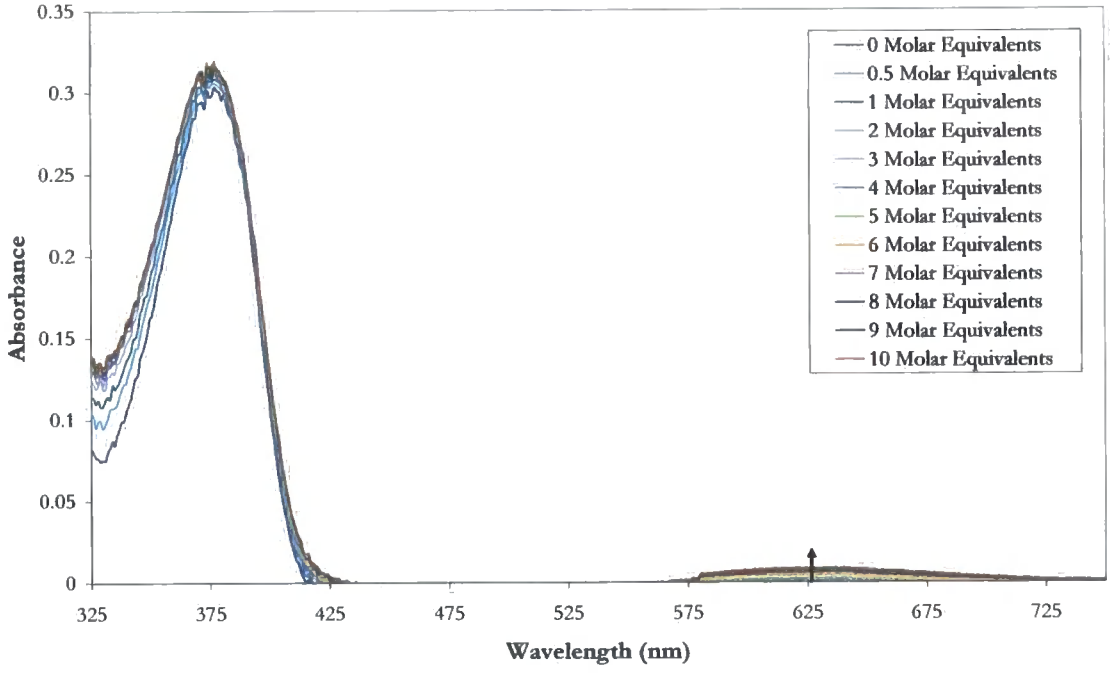

(b)

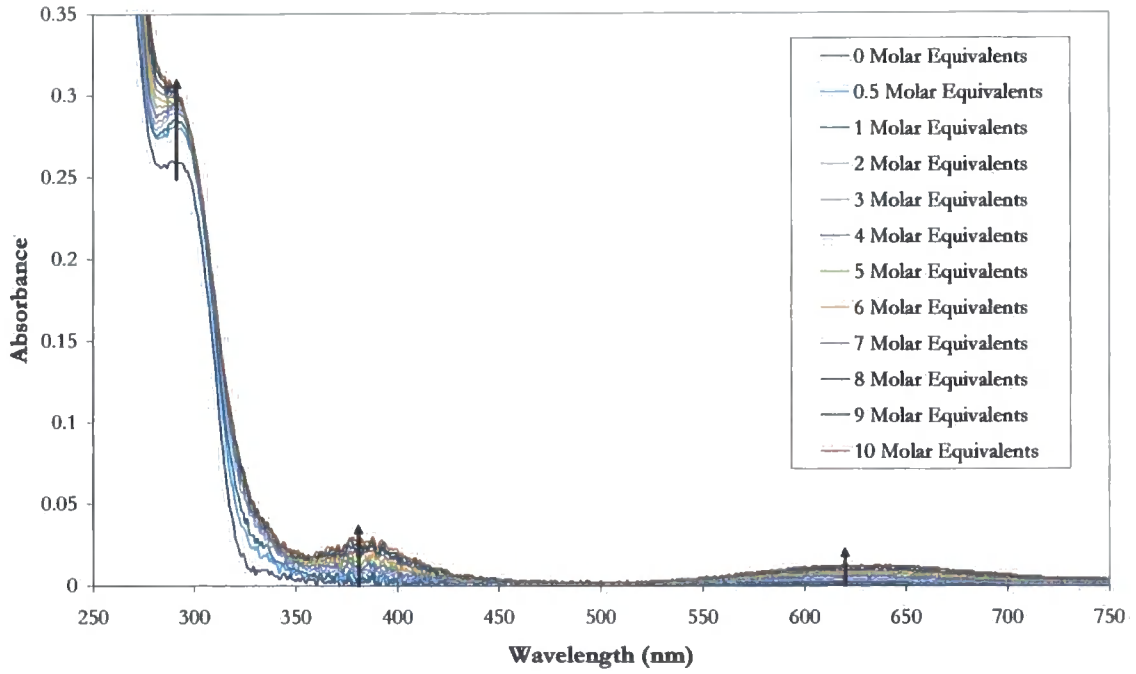

Figure 3.10: Absorption spectrum of (a) **2.6** and (b) **2.2** (1.03×10^{-4} M) in CH_3CN, and upon addition of increasing amounts of $Ni(NO_3)_2.6H_2O$ upto 10 equivalents.

(a)

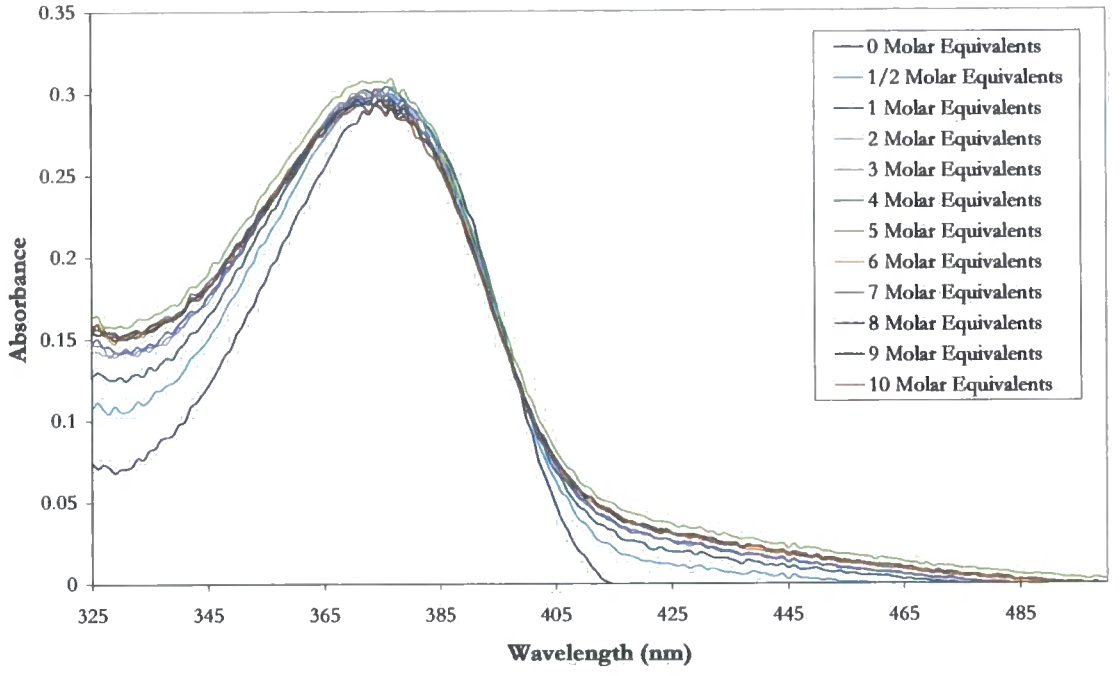

(b)

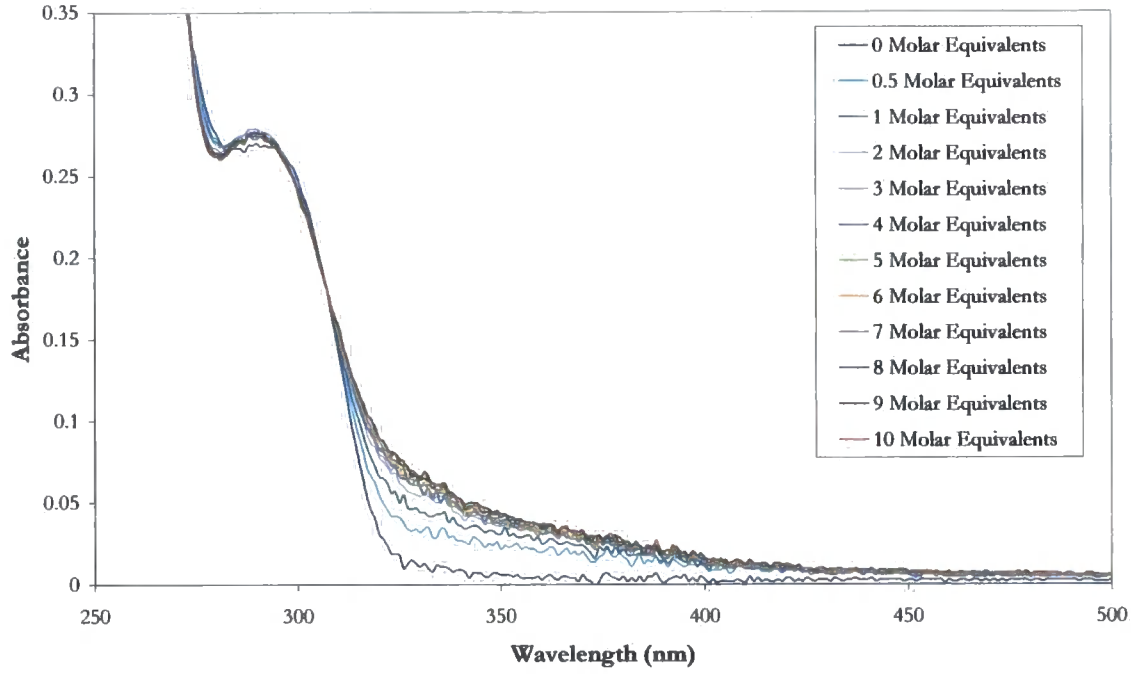

Figure 3.11: Absorption spectrum of (a) **2.6** and (b) **2.2** (1.03×10^{-4} M) in CH_3CN, and upon addition of increasing amounts of $Zn(CF_3SO_3)_2$ upto 10 equivalents.

Upon addition of $Cu(CH_3CO_2)_2.H_2O$, an increase in absorbance is seen upon addition of 0.5 equivalent to a solution of **2.6**, centred on 370 nm, which is followed by a very small shift upon addition of a further half equivalent, and a larger shift upon addition of the second equivalent **figure 3.12**(a). This peak continues to increase and blue shifts slightly, until 10 equivalents of $Cu(CH_3CO_2)_2.H_2O$ have been added. There is also a broad band centred on 675 nm, which is assigned to Cu^{2+} *d-d* transitions, and increases linearly after the addition of two equivalents of $Cu(CH_3CO_2)_2.H_2O$ to **2.6**. This peak appears immediately upon addition of metal to ligand, suggesting immediate metal – ligand interaction, which is not observed upon addition of the previously mentioned $Co(NO_3)_2.6H_2O$, $Ni(NO_3)_2.2H_2O$ and $Zn(CF_3SO_3)_2$. Upon addition of $Cu(CH_3CO_2)_2.H_2O$ to **2.4** an increase in the absorbance of the band centred on 375 nm is observed, **figure 3.12**(b), and upon addition of further equivalents of $Cu(CH_3CO_2)_2.H_2O$ to **2.4**, there is a linear increase in the absorbance at this wavelength. There is also the appearance of a broad peak centred around 675 nm, after the addition of one equivalent of $Cu(CH_3CO_2)_2.H_2O$, to **2.4** which is assigned to the copper *d-d* transitions, and again reaches a maximum upon addition of upto ten equivalents, and after the addition of one equivalent of $Cu(CH_3CO_2)_2.H_2O$, sees a linear increase in the absorbance at this wavelength.

(a)

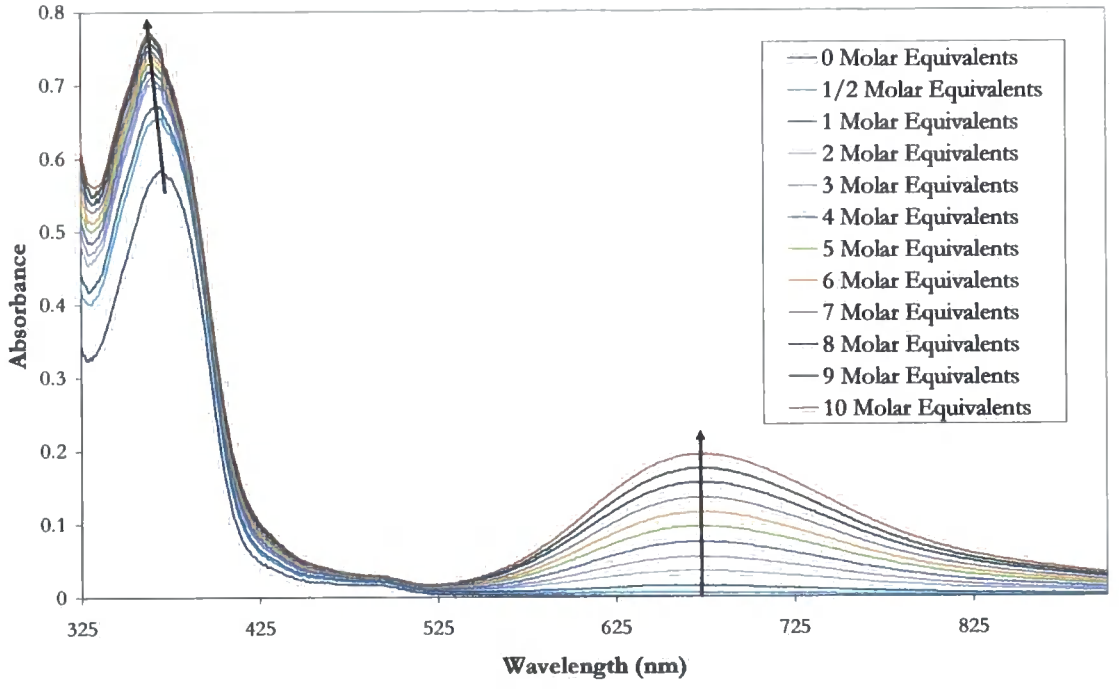

(b)

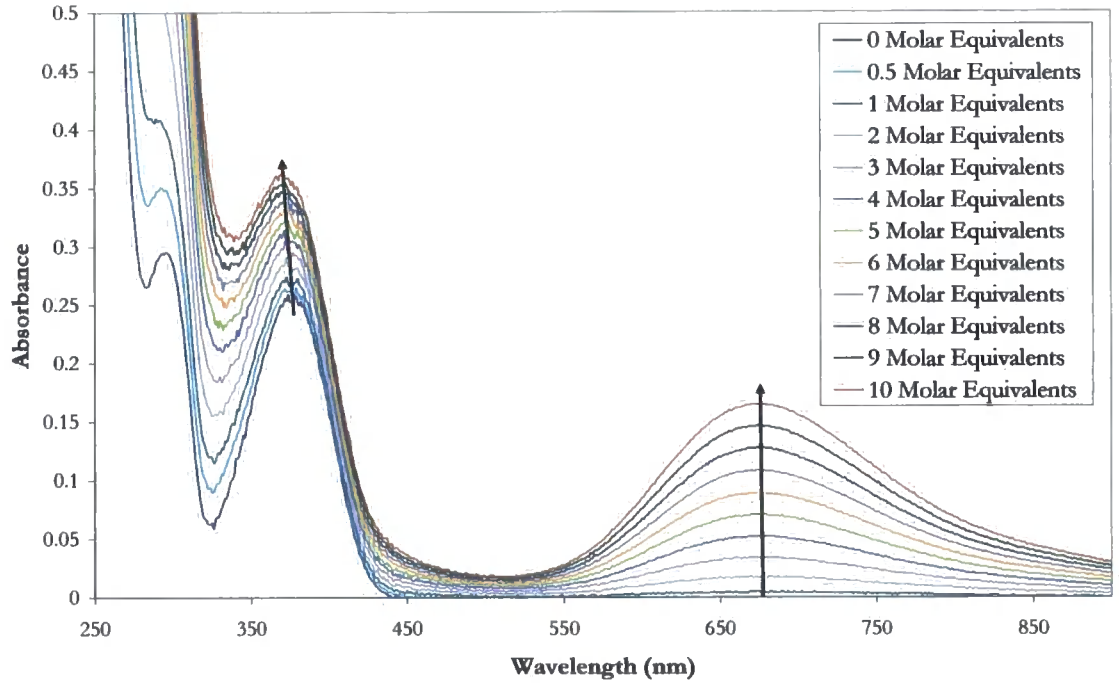

Figure 3.12: Absorption spectrum of (a) **2.6** and (b) **2.4** (1.03 x 10^{-4} M) in CH_3CN, and upon addition of increasing amounts of $Cu(CH_3CO_2)_2.H_2O$ upto 10 equivalents.

Upon addition of $CuCl_2.2H_2O$ to **2.6**, there is first an increase in the ILCT (intra ligand charge transfer) band, centered on 370 nm, **figure 3.13**(a). This increases and is slightly red-shifted until 2 equivalents of salt have been added. This could be the formation of a 1:2 ligand:metal species, as there is no increase in the absorbance of at this wavelength, 370 nm, upon addition of further equivalents of $CuCl_2.2H_2O$. There is also the appearance of a peak at 470 nm, which increases after the addition of 2 equivalents, up to the addition of 10 equivalents; this peak may be assigned to the copper *d-d* transitions. However, the appearance of the band centred around 470 nm, suggested that there is unbound copper, due to the excess copper in solution, as is observed upon addition of copper(II) chloride to an acetonitrile solution. It could be a 1:1 ligand:metal complex being formed, or a combination of the species being formed as is suggested by the binding constants measured, **table 3.3**. Upon addition of $CuCl_2.2H_2O$ to **2.2**, an increase in the band centred on 300 nm, **figure 3.13**(b) and as with **2.6** there is the appearance of a new peak centred on 470 nm, after the addition of 2 equivalents of copper(II) chloride has been added. Conversely to **2.6** in this case only 1:1 species appears to exist as measured with the calculated binding constant. Upon addition of $Cu(CF_3SO_3)_2$ to **2.6** an increase in the intensity of ILCT band, up to the addition of one equivalent of $Cu(CF_3SO_3)_2$, is observed, **figure 3.14**(a), as was seen upon addition of $CuCl_2.2H_2O$.

(a)

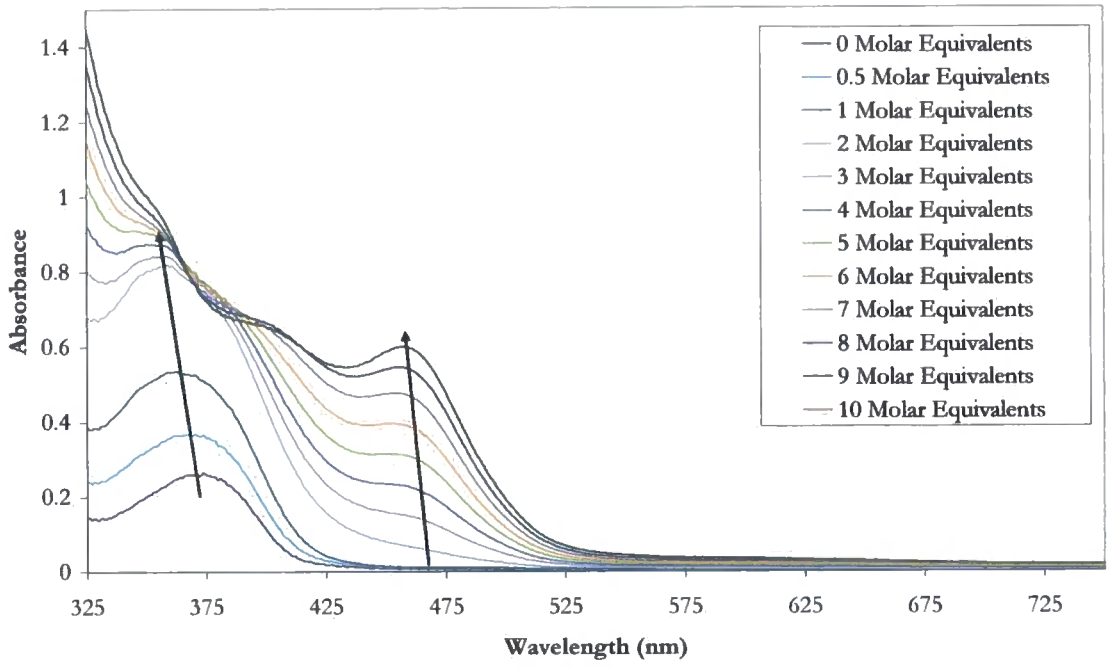

(b)

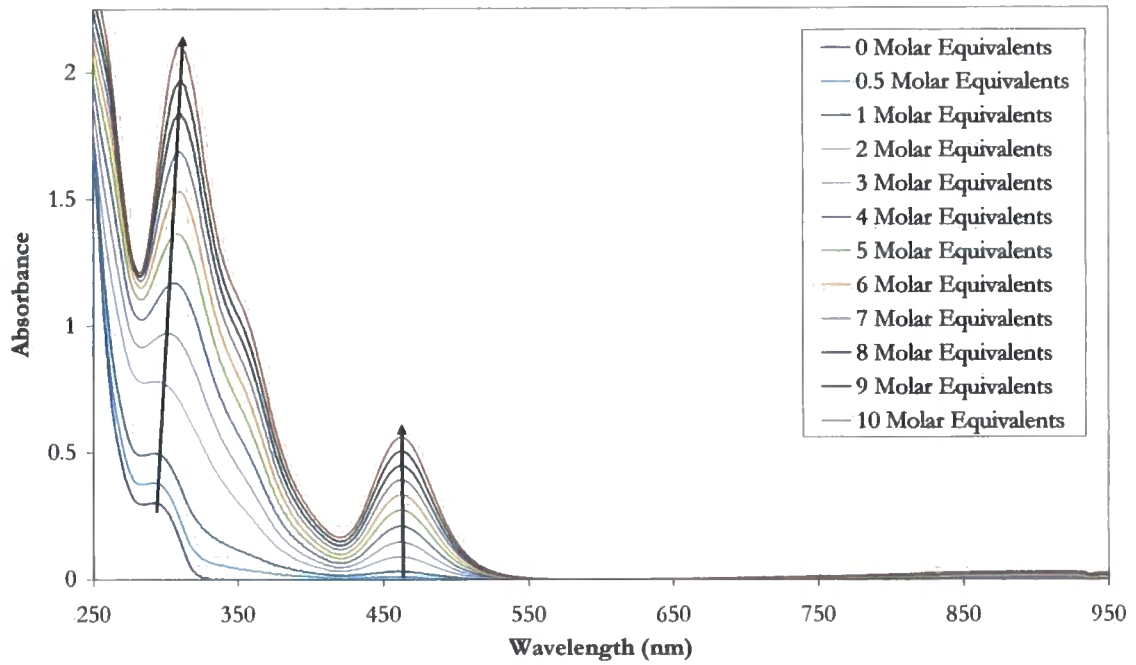

Figure 3.13: Absorption spectrum of (a) **2.6** and (b) **2.2** (5.15 x 10^{-5} M) in CH_3CN, and upon addition of increasing amounts of $CuCl_2.2H_2O$ upto 10 equivalents.

In contrast to the addition of $CuCl_2.2H_2O$, there is a red-shift and a broadening of the ILCT band, upon addition of 2 equivalents of $Cu(CF_3SO_3)_2$, there is a red-shift of this band. A decrease in the absorbance of this band, centred on 370 nm is seen, and the appearance of a broad band centred on 525 nm, which is assigned to the copper *d-d* transitions. After the addition of 5 equivalents, there is no change in the absorbance, suggesting, that there is no further species being formed. The increase in the ILCT band after the addition of 0.5 and 1 equivalents of $Cu(CF_3SO_3)_2$, suggested the formation of 2:1 and 1:1 ligand:metal complexes. The shift in the ILCT between the addition of 1 and 2 equivalents suggests the formation of a new species of 1:2 ligand:$Cu(CF_3SO_3)_2$, after the initial formation of a 1:1 species. The proposed structures of the solid species in **figure 3.1,** would agree with this data, suggesting the formation of 2:1, 1:1 and 1:2 complexes, and the complex nature of the binding was confirmed as it was not possible to calculate a binding constant from the data measured. **Figure 3.14**(b) shows the change in absorbance at 517 nm, which is the centre point of the band assigned to the copper *d-d* transition upon addition of increasing amounts of $Cu(CF_3SO_3)_2$ to ligand **2.6**. Upto the addition of 1.5 equivalents of $Cu(CF_3SO_3)_2$, there is no absorbance at this point, and after 1.5 equivalents there is a small increase in the absorbance, which is followed by a much sharper increase in the absorbance. After the addition of 5 equivalents, the graph reaches a plateau and there is no further increase in absorbance, suggesting that after the addition of 5 equivalents of copper(II) triflate, there is no further copper – ligand interactions. However, upon addition of $Cu(CF_3SO_3)_2$ to **2.2,** there is an increase in the band centred on 300 nm, **figure 3.14**(c) and after the addition of 0.5 equivalent there is the appearance of a broad band centred on 375 nm, which is red shifted upon addition of 3 equivalents to 446 nm. A broad band assigned to the copper *d-d* transition is observed at 714nm. **Figure 3.14**(d) shows the change in absorbance at 714 nm, which is the centre point of the band assigned to the copper *d-d* transition upon addition of increasing amounts of $Cu(CF_3SO_3)_2$ to ligand **2.2**. There is no change in absorbance upon addition of the first half equivalent of $Cu(CF_3SO_3)_2$ to ligand **2.2**, and a small change is observed upto the addition of 2 equivalents. After the addition of two equivalents of $Cu(CF_3SO_3)_2$ to ligand **2.2** there is a sharp increase in the absorbance, until the addition of three equivalents, when there is a slight decrease in the rate of increase in absorbance until the addition of 6 equivalents of $Cu(CF_3SO_3)_2$ to ligand **2.2**, after which point a plateau in the graph is reached, and no further change in the absorbance occurs.

(a)

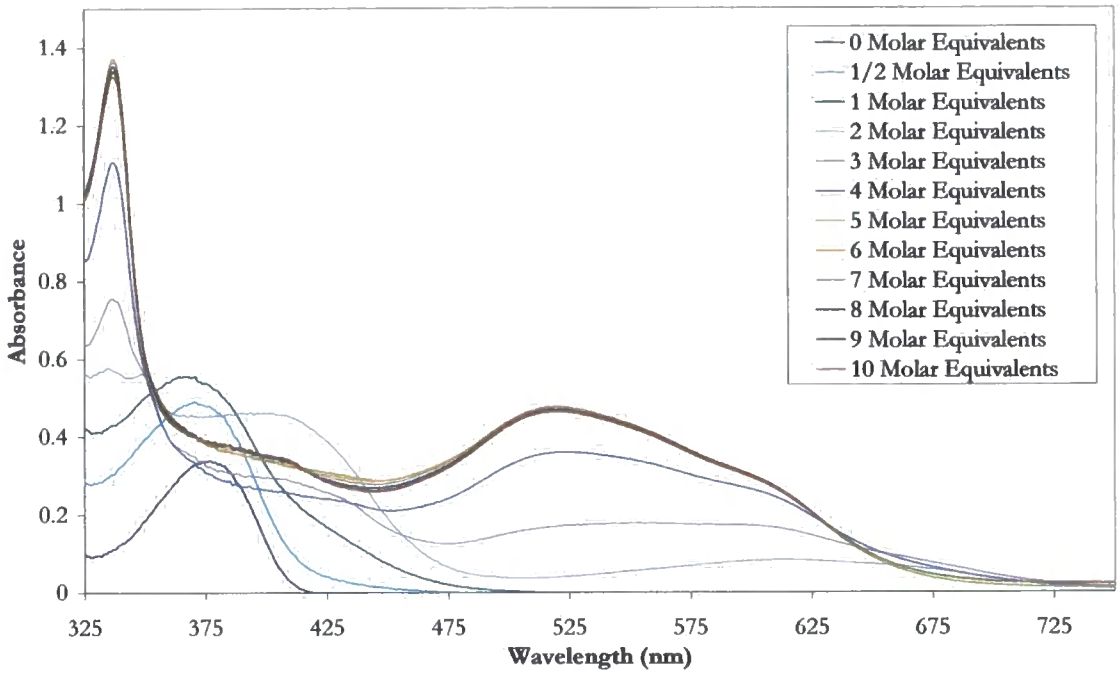
0 Molar Equivalents
1/2 Molar Equivalents
1 Molar Equivalents
2 Molar Equivalents
3 Molar Equivalents
4 Molar Equivalents
5 Molar Equivalents
6 Molar Equivalents
7 Molar Equivalents
8 Molar Equivalents
9 Molar Equivalents
10 Molar Equivalents
Absorbance
Wavelength (nm)

(b)

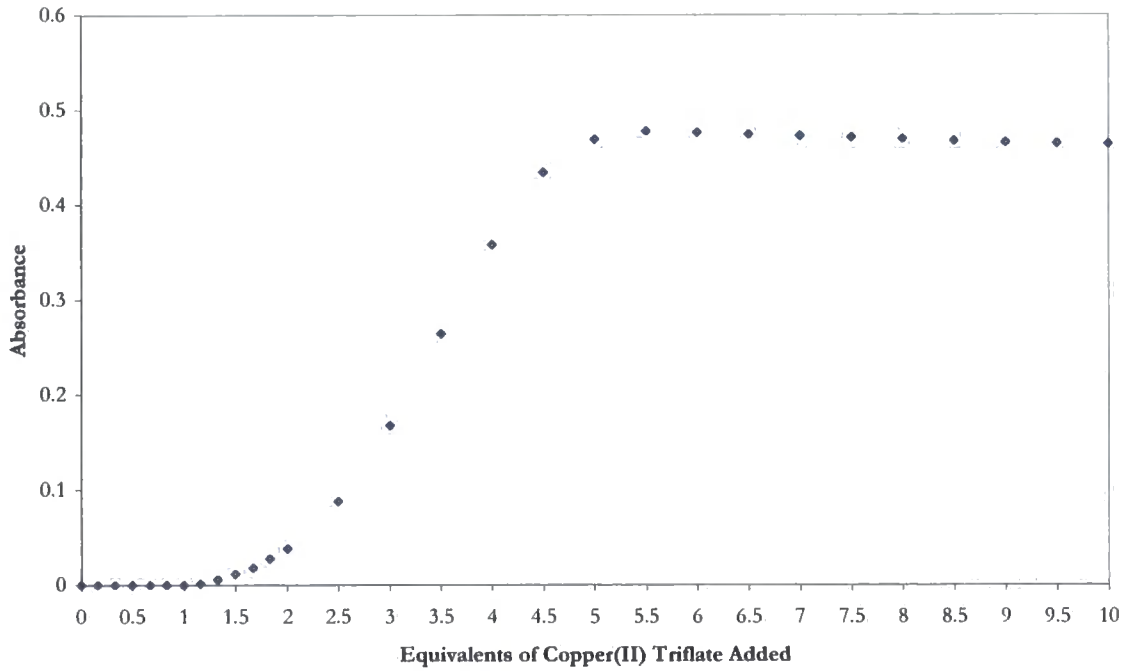
Absorbance
Equivalents of Copper(II) Triflate Added

(c)

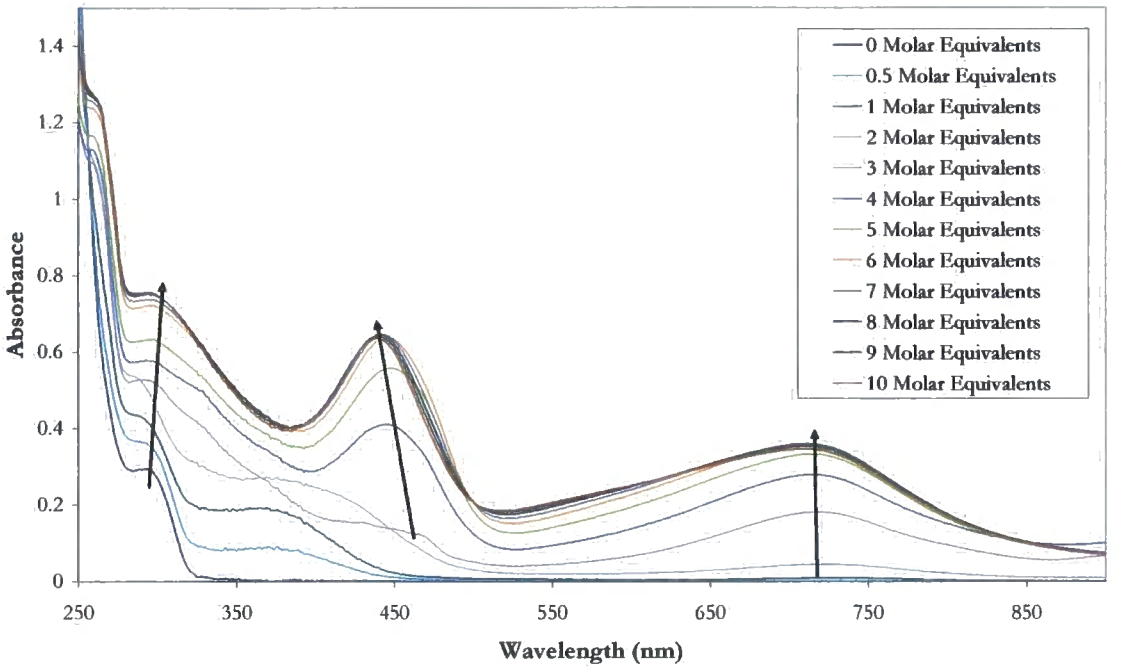

(d)

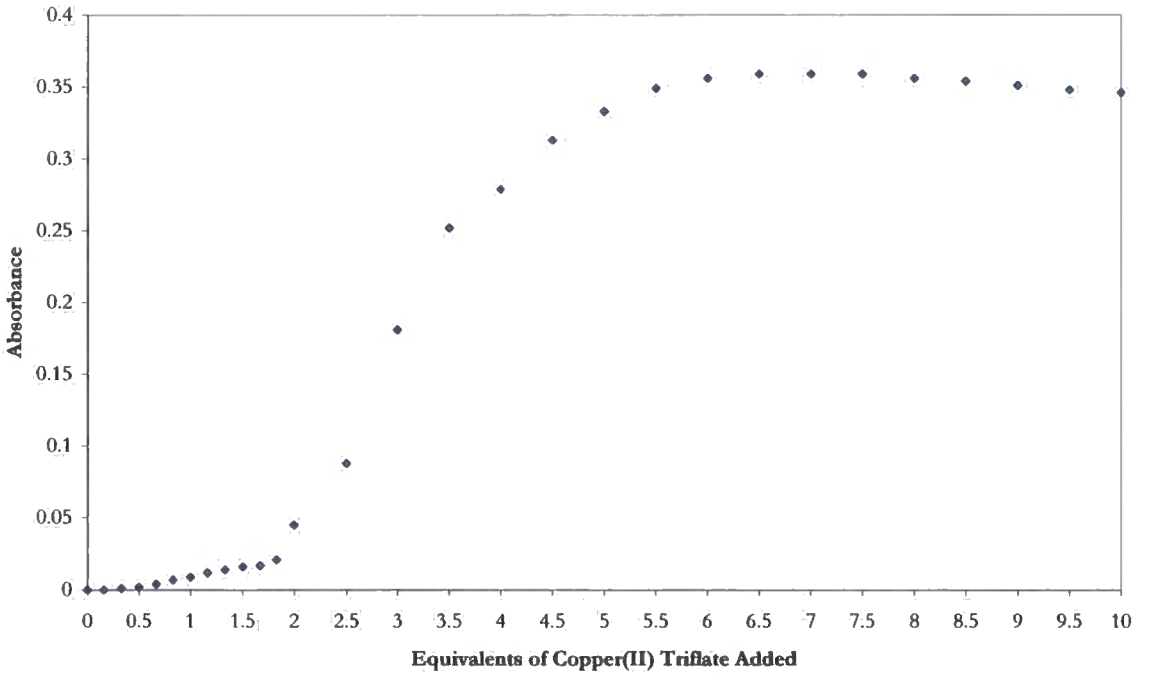

Figure 3.14: Absorption spectrum of (a) **2.6** (1.03 x 10^{-4} M) (b) change in absorbance of **2.6** at 517 nm, (c) **2.2** (1.03 x 10^{-4} M) and (d) change in absorbance of **2.2** at 714 nm, in CH_3CN, and upon addition of increasing amounts of $Cu(CF_3SO_3)_2$ upto 10 equivalents.

Addition of $Cu(NO_3)_2.2.5H_2O$ to a solution of **2.6**, sees an increase in the ILCT band centred on 370 nm, upto the addition of one equivalent, **figure 3.15**(a). The addition of a further equivalent of $Cu(NO_3)_2.2.5H_2O$, sees a further increase in the absorbance of the ILCT band, which is accompanied by a red-shift of the band, so it is centred on 415 nm, which has a shoulder at a lower wavelength of higher absorbance, and a second shoulder at higher wavelength, with a much lower extinction coefficient. **Figure 3.15**(b) shows the change in the absorbance at 496 nm, which is the band assigned to the copper *d-d* transitions, upon addition of copper(II) nitrate to ligand **2.6**. It shows an initial slow increase in the absorbance, until the addition of one equivalent of copper(II) nitrate, and then a much shaper increase in the absorbance between the addition of 1.5 and 2.5 equivalents, and the increase then slows down, until it reaches a plateau after the addition of approximately six equivalents of copper(II) nitrate to ligand **2.6**. This suggests the formation of multiple species, which was also suggested when calculating binding constants, as the data was too complicated to give a single binding mode. Upon addition of $Cu(NO_3)_2.2.5H_2O$ to **2.2**, there is an increase in the band centred on 300 nm, **figure 3.15**(c) and after the addition of the first equivalent a red shift of this band to 312 nm, which increases in intensity until the addition of 10 equivalents. Also after the addition of 1 equivalent there is the appearance of a new band centred on 273 nm, and a broad band centred on 575 nm which is assigned to the copper *d-d* transitions.

(a)

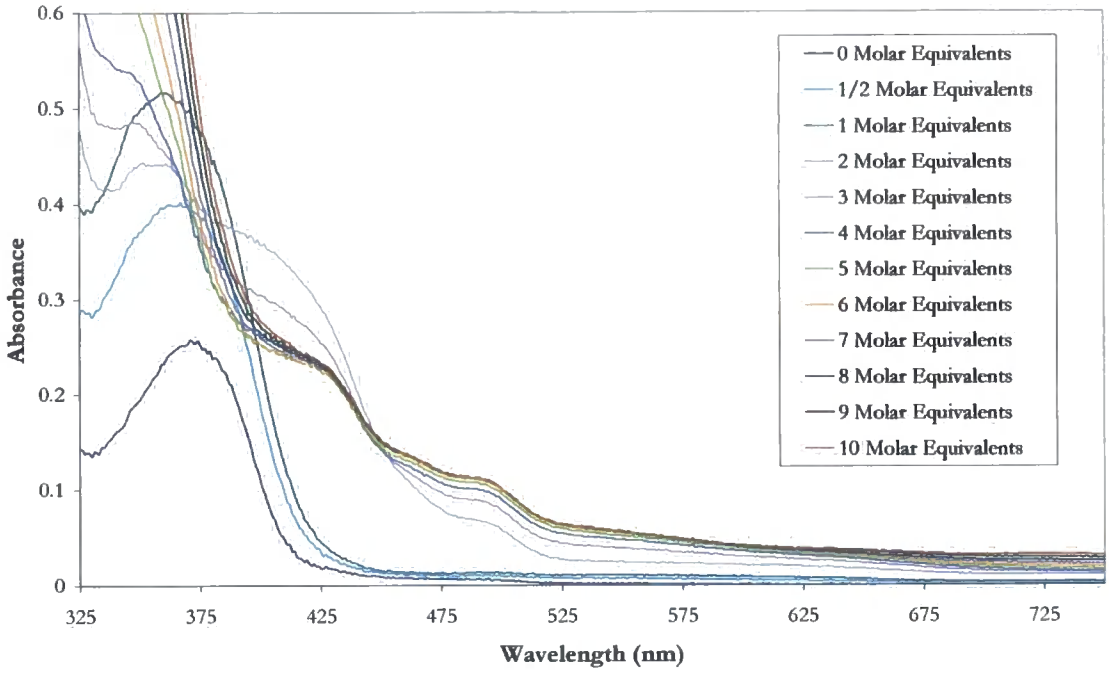
0.6
0.5
0.4
0.3
0.2
0.1
0
Absorbance
325
375
425
475
525
575
625
675
725
Wavelength (nm)
0 Molar Equivalents
1/2 Molar Equivalents
1 Molar Equivalents
2 Molar Equivalents
3 Molar Equivalents
4 Molar Equivalents
5 Molar Equivalents
6 Molar Equivalents
7 Molar Equivalents
8 Molar Equivalents
9 Molar Equivalents
10 Molar Equivalents

(b)

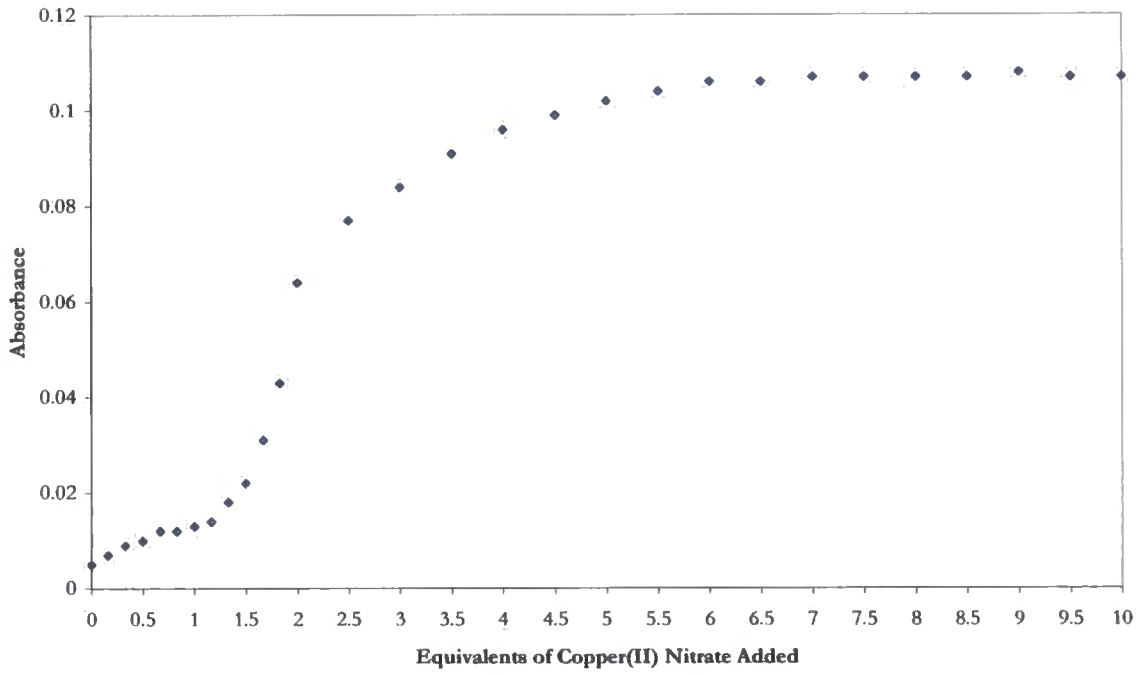
0.12
0.1
0.08
0.06
0.04
0.02
0
Absorbance
0
0.5
1
1.5
2
2.5
3
3.5
4
4.5
5
5.5
6
6.5
7
7.5
8
8.5
9
9.5
10
Equivalents of Copper(II) Nitrate Added

(c)

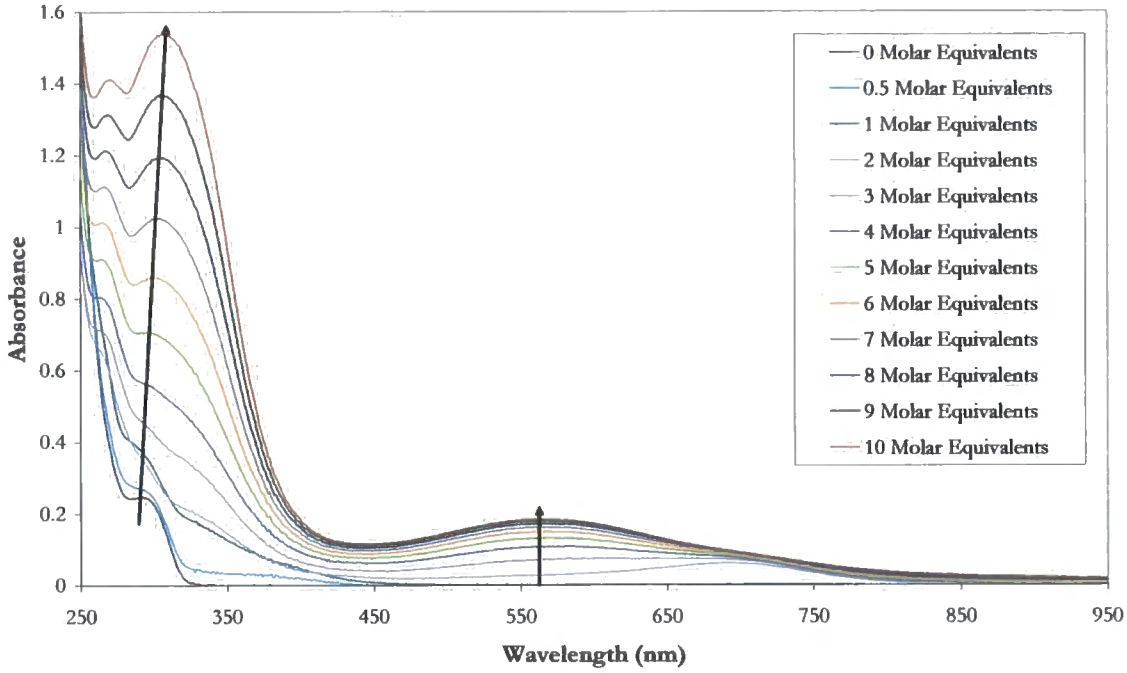

(d)

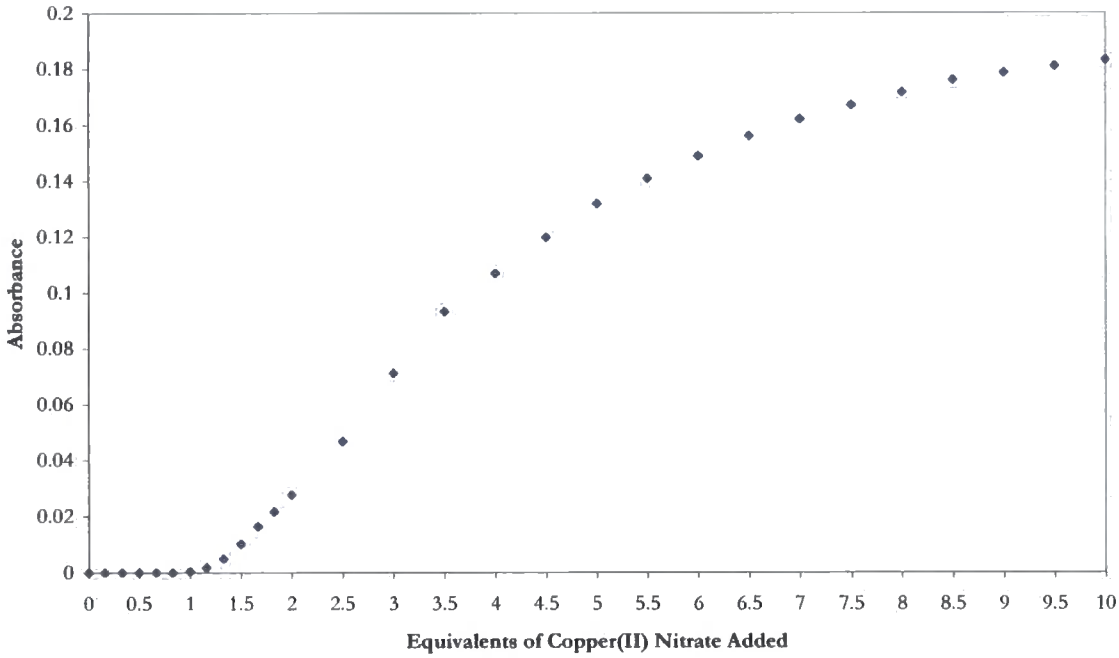

Figure 3.15: Absorption spectrum of (a) **2.6** (5.15×10^{-5} M) (b) change in absorbance of **2.6** at 496 nm (c) **2.2** (5.15×10^{-5} M) and (d) change in absorbance of **2.2** at 560 nm, in CH_3CN, and upon addition of increasing amounts of $Cu(NO_3)_2.2.5H_2O$ upto 10 equivalents.

Approximate binding constants were calculated from the absorbance data measured upon addition of the mentioned metal salts to ligand solutions. Surprisingly relatively strong binding was observed with the addition of $Co(NO_3)_2.6H_2O$, $Ni(NO_3)_2.6H_2O$ and $Zn(CF_3SO_3)_2$, which showed less changes in the absorbance than was observed upon addition of copper(II) salts. It seems that with the exception of $Co(NO_3)_2.6H_2O$, which is bound more strongly by ligand **2.2**, ligand **2.6** binds the metals more strongly. In the cases of both ligands **2.2** and **2.6** and $Cu(CH_3CO_2)_2.H_2O$, the errors were smaller for a 2:2 metal:ligand stoichiometry, which is consistent with the x-ray crystal structure of **2.2** and **2.5**, **figures 3.4** and **3.5**. Upon addition of $CuCl_2.2H_2O$ to ligand **2.6** binding in a 1:1 and 2:1 metal:ligand stoichiometry is observed, but with ligand **2.2**, only 1:1 binding is observed. Binding to $Cu(NO_3)_2.2.5H_2O$, appears to be more complicated than has been observed in the case of the others measured, and it has not been possible to calculate binding constants suggesting that binding is to both metal and anion, but for the case of the other salts, only binding to the metal being observed. The addition of $Cu(CF_3SO_3)_2$ to ligand **2.6** results in data which is too complicated for binding constants to be measured, this could be due to the formation of several species as is suggested in **figure 3.1**.

	log K_{11}	
Metal Salt	**2.2**	**2.6**
$Co(NO_3)_2.6H_2O$	4.22(7)	3.98(11)
$Ni(NO_3)_2.6H_2O$	3.99(13)[a]	4.47(11)
$Zn(CF_3SO_3)_2$	4.13(15)	4.50(9)
$Cu(CH_3CO_2)_2.H_2O$	2.55(16) log β_{22} 10.26(8)	3.06(6) log β_{22} 10.69(7)
$CuCl_2.2H_2O$	3.22(5)	log β_{11} 4.36(9) log β_{21} 7.21(15)
$Cu(CF_3SO_3)_2$	3.11(11)	[b]
$Cu(NO_3)_2.2.5H_2O$	[b]	[b]

Table 3.3: Binding constants (log *K*) for $M(X)_2.yH_2O(L)$ complexes in CH_3CN determined using specfit 32.[16] Errors are shown in brackets, ligand concentration 1.03 x 10^{-4} M.

a) very little change in absorbance observed

b) binding constant not calculated due to complicated binding mode

3.2.2 Effect of Adding $Cu(BF_4)_2$ to Different Ligands

As a change in the absorbance of ligands had been observed upon addition of a variety of metal(II) salts had been observed, a comparison study between ligand **2.2** – **2.6**, and as a control pyridine, were undertaken upon the addition of copper(II) tetrafluoroborate.

As with the addition of $CuCl_2.2H_2O$, $Cu(CF_3SO_3)_2$ and $Cu(NO_3)_2.2.5H_2O$, an increase in the absorbance and a red-shift of the ILCT is observed, upon addition of $Cu(BF_4)_2.6H_2O$ to ligand **2.6, figure 3.16**. The effect is most obvious upon addition of $Cu(BF_4)_2.6H_2O$, where an increase in the ILCT is observed upto the addition of one equivalent, with no shift in the ILCT, but the addition of a further addition of $Cu(BF_4)_2.6H_2O$, a further increase in the ILCT is observed, and this is the largest increase observed, as well as a red-shift of the peak to 409 nm. It is suggested that there is the formation of a 1:2 host:guest complex, as the maximum absorbance is seen after the addition of two equivalents of guest, the increases in absorbance after the addition of the first two half equivalents, suggests the formation of a complex, which may be a 2:1 and/or a 1:1 host:guest complex. There appears to be no significant change in the absorbance after the addition of 4 equivalents of $Cu(BF_4)_2.6H_2O$. The broad peak centred on 515 nm, is explained as copper *d-d* transitions, which appears after the addition of two equivalents of $Cu(BF_4)_2.6H_2O$, and reaches a maximum after the addition of 5 equivalents, as has been previously observed upon addition of other copper salts, **figures 3.9 – 3.13**, and suggests that there is not an immediate interaction between the ligands and metal cations, which maybe explained by the high water content of the salt, but as the trend is the same as upon addition of $Cu(CF_3SO_3)_2$, which is anhydrous, this is not likely, but it could indicate that firstly there is a ligand - anion interaction, and it is the formation of this species which promotes the formation of the copper complex. $Cu(BF_4)_2.6H_2O$ was also added to solutions of **2.2**, which has a band assigned to the band centred on 300 nm, and this band increases and gradually red-shifts, upon addition of $Cu(BF_4)_2.6H_2O$, **figure 3.17**. A new band appears at 375 nm, after the addition of the first half equivalent of $Cu(BF_4)_2.6H_2O$, and the absorbance of this band continues to increase until six equivalents have been added. Upon addition of 4 equivalents of $Cu(BF_4)_2.6H_2O$, a

shoulder grows on this band at a higher wavelength and this band reaches a maximum absorbance after the addition of seven equivalents of $Cu(BF_4)_2.6H_2O$. A broad band appears at 570 nm, upon addition of two equivalents of $Cu(BF_4)_2.6H_2O$, which reaches a maximum after the addition of six equivalents of guest has been added. This broad band centred around 570 nm, has been assigned as the copper *d-d* transitions, suggesting that the energy of the *d-d* transition is affected by the ligand and/or complexes present. The ILCT band is centred on 379 nm for **2.4**, and upon addition of $Cu(BF_4)_2.6H_2O$, there is an increase in the absorbance, and a blue-shift of this band, **figure 3.17**. The largest increase in this band is upon addition of one equivalent of $Cu(BF_4)_2.6H_2O$, suggesting the formation of a 1:1 host:guest complex, and upon addition of further increase, there is smaller increases in absorbance of this peak until a maximum of ten equivalents have been added. There is a broad band which appears after the addition of two equivalents, and reaches it maximum at the same point, this band is assigned to the copper *d-d* transitions, and is centred on 527 nm. Ligand **2.5** has an ILCT which is centred on 375 nm, **figure 3.18**, and upon addition of $Cu(BF_4)_2.6H_2O$, a decrease in this band is observed, suggesting that no complex is being formed and that the decrease is due to dilution factors. There is also a broad peak at 800 nm, which has been assigned to the copper *d-d* transitions, and this increases slightly upto the addition of 10 equivalents of $Cu(BF_4)_2.6H_2O$, **figure 3.19**. As a control experiment, $Cu(BF_4)_2.6H_2O$, was added to a solution of pyridine, which shows a band at 250 nm, **figure 3.20**. Upon addition of half an equivalent of $Cu(BF_4)_2.6H_2O$, there is a increase in the absorbance, followed by further smaller increases in absorbance upon addition of more $Cu(BF_4)_2.6H_2O$, until the addition of six equivalents, after which there is little change in the absorbance of this band. There is another broad band which appears upon addition of $Cu(BF_4)_2.6H_2O$, and appears to grow in absorbance until a maximum of 10 equivalents of $Cu(BF_4)_2.6H_2O$ is added. $Cu(BF_4)_2.6H_2O$ has been shown to interact with a variety of ligands, **2.2** – **2.6**, and pyridine. The observed changes in absorbance upon addition of $Cu(BF_4)_2.6H_2O$ with pyridine, suggests that the copper or anion is interacting with the pyridine, and thus it is suggested that in the case of ligands **2.2** – **2.6**, pyridyl group is involved with binding and complex formation. The complex nature of the spectra upon addition $Cu(BF_4)_2.6H_2O$ to **2.2** and **2.6**, suggest that the binding is more complicated than just a pyridine interaction, most likely including an amine interaction. The lack of evidence for binding of **2.5** and $Cu(BF_4)_2.6H_2O$, maybe explained by the electron-withdrawing nature

of nitro-group, pulling electron-density away from the aryl ring that is it is substituent on, and thus reducing the amount of charge transfer, thus reducing the electrostatic attraction with copper. The data suggests the formation of multiple complexes, where complexation occurs, but the exact nature of these species is unknown. Approximate binding constants were calculated for the addition of $Cu(BF_4)_2.6H_2O$ to solutions of all ligands, and it was observed that the strongest binding was observed with ligand **2.4** and **2.6**, and significant binding to pyridine was observed, suggesting that binding in a 1:1 stoichiometry involves binding to the pyridyl nitrogen in the other ligands also. Binding was measured to be less strong to ligands **2.2** and **2.5**, as is observed in **table 3.4**, and in all cases the best fit to the data was observed to be a 1:1 model. **Figure 3.20(a)** shows the change in absorbance of the bands assigned to the copper *d-d* transitions for ligands **2.2 – 2.6** and pyridine, upon addition of $Cu(BF_4)_2.6H_2O$. Upon addition of the first equivalent of $Cu(BF_4)_2.6H_2O$ to **2.6**, there is no absorbance at this wavelength, but the addition of 1.5 equivalents sees an increase in the absorbance. After the addition of 2.5 equivalents there is a sharper increase in the absorbance, until the addition of 5 equivalents, when this reaches a plateau, suggesting that there is no further ligand – metal interaction. The titration isotherm upon addition of $Cu(BF_4)_2.6H_2O$ to **2.2**, follows the same shape as for **2.6**, but it is after the addition of the first half equivalent, there is a slight increase in absorbance which continues until the addition of two equivalents, when there is a much sharper increase in the absorbance, which continues until a plateau is reached after the addition of six equivalents of $Cu(BF_4)_2.6H_2O$ to **2.2**. Upon addition of $Cu(BF_4)_2.6H_2O$ to **2.4**, there is an immediate increase in the absorbance at this point, suggesting immediate ligand – metal interaction, and there is a sharper increase in the absorbance after the addition of 1 equivalent. This increase continues until the addition of 2.5 equivalents when a plateau is reached, and no further change in the absorbance is observed. There is very little change in the absorbance for both **2.5** and pyridine upon addition of $Cu(BF_4)_2.6H_2O$. There is no initial change in the absorbance observed upon addition of $Cu(BF_4)_2.6H_2O$ to **2.5**, but after the addition of 1.5 equivalents, an increase in absorbance is observed as a smooth curve, which increases upto the addition of 10 equivalents, albeit with a very small gradient. Upon addition of $Cu(BF_4)_2.6H_2O$ to pyridine there is a liner increase in the absorbance upto the addition of ten equivalents.

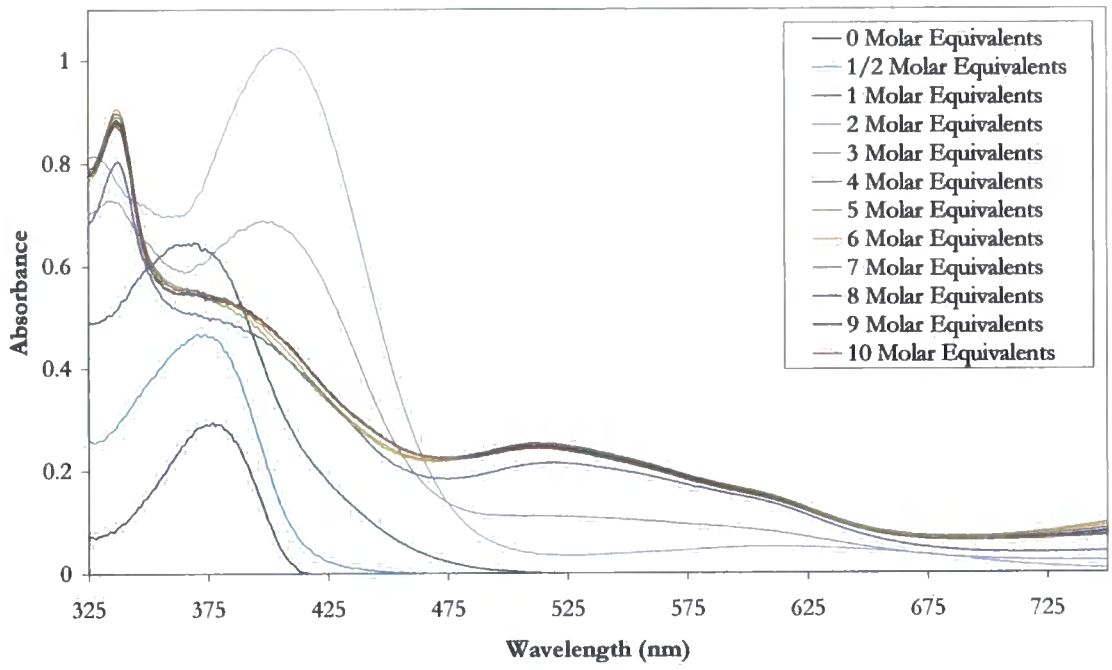

Figure 3.16: Absorption spectrum of **2.6** (1.03 x 10^{-4} M) in CH_3CN, and upon addition of increasing amounts of $Cu(BF_4)_2.6H_2O$ upto 10 equivalents.

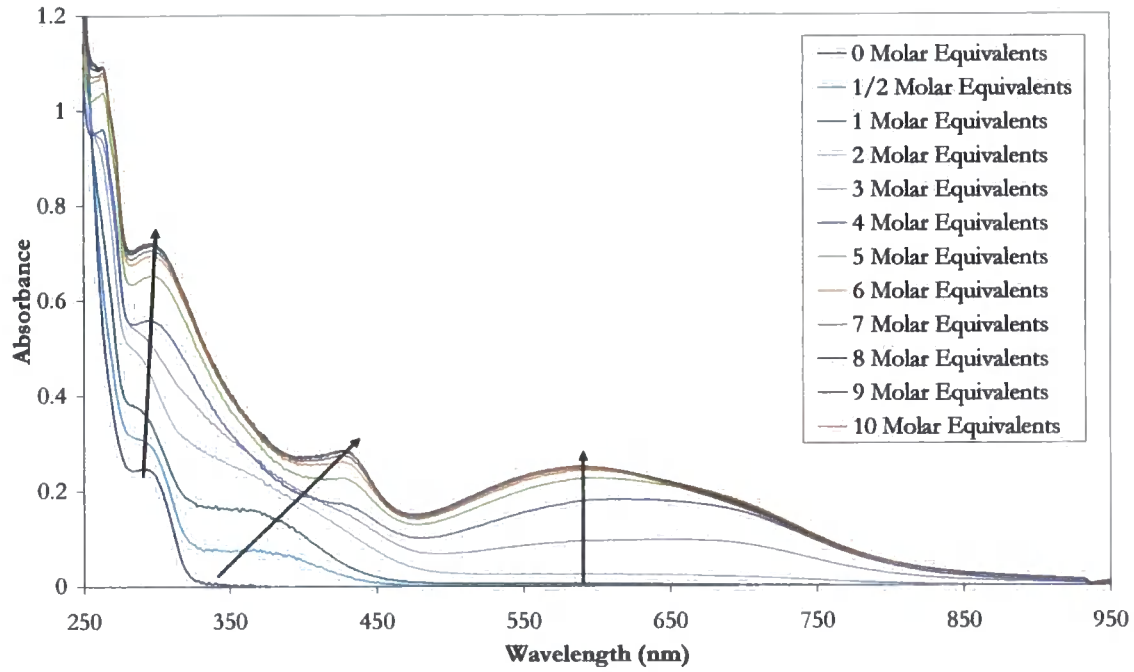

Figure 3.17: Absorption spectrum of **2.2** (1.03 x 10^{-4} M) in CH_3CN, and upon addition of increasing amounts of $Cu(BF_4)_2.6H_2O$ upto 10 equivalents.

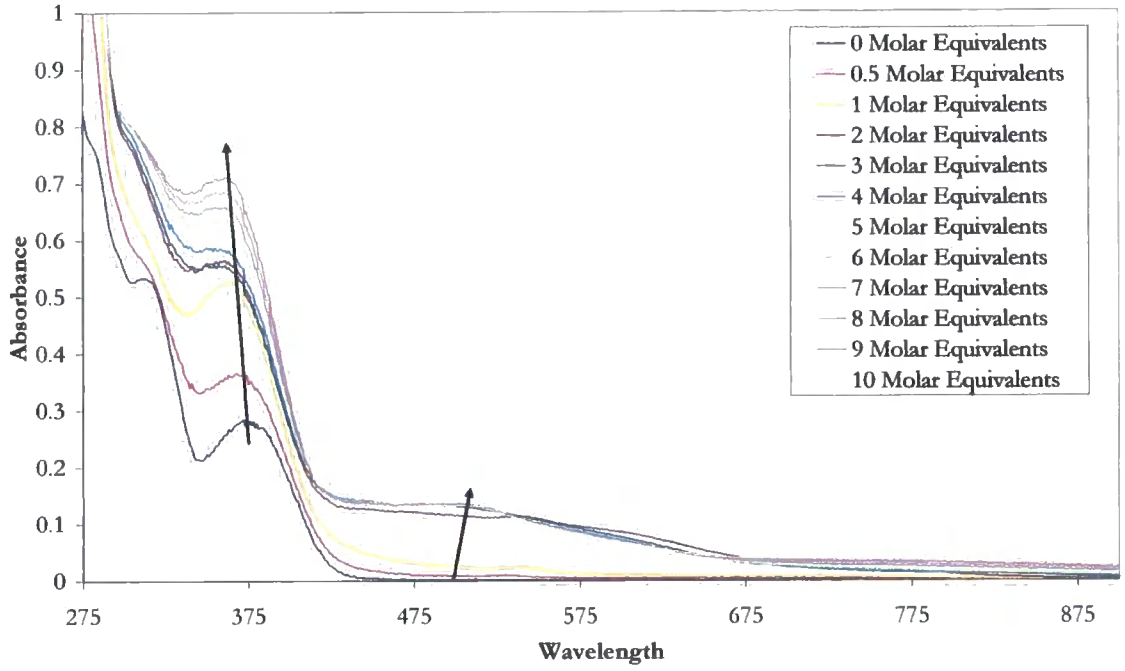

Figure 3.18: Absorption spectrum of **2.4** (1.03×10^{-4} M) in CH_3CN, and upon addition of increasing amounts of $Cu(BF_4)_2.6H_2O$ upto 10 equivalents.

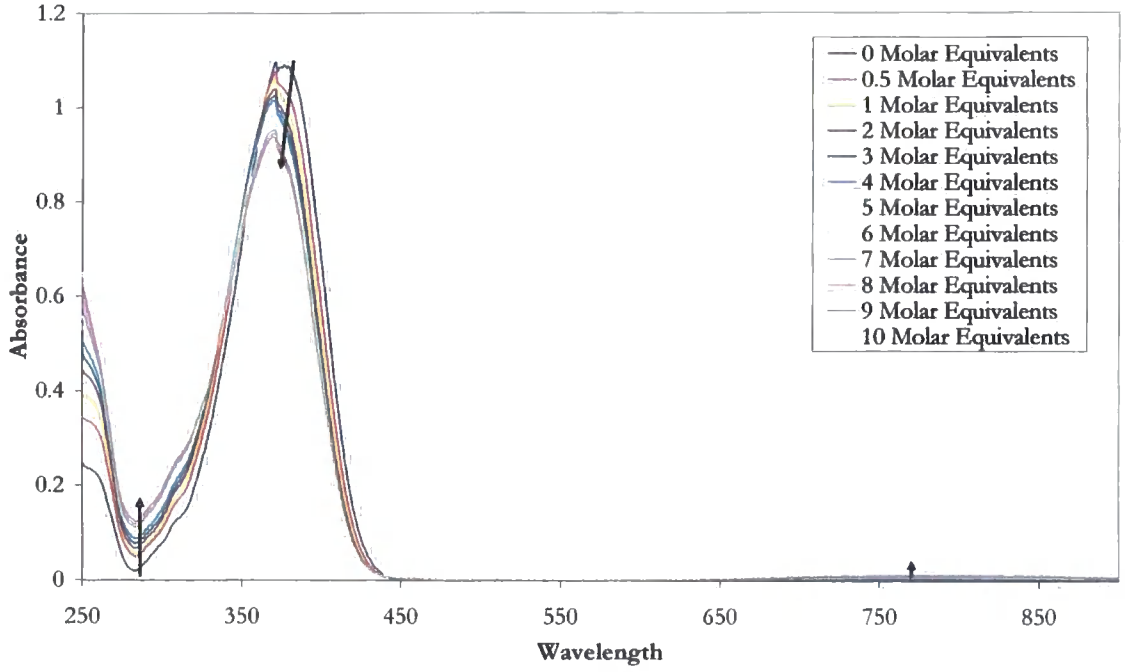

Figure 3.19: Absorption spectrum of **2.5** (1.03×10^{-4} M) in CH_3CN, and upon addition of increasing amounts of $Cu(BF_4)_2.6H_2O$ upto 10 equivalents.

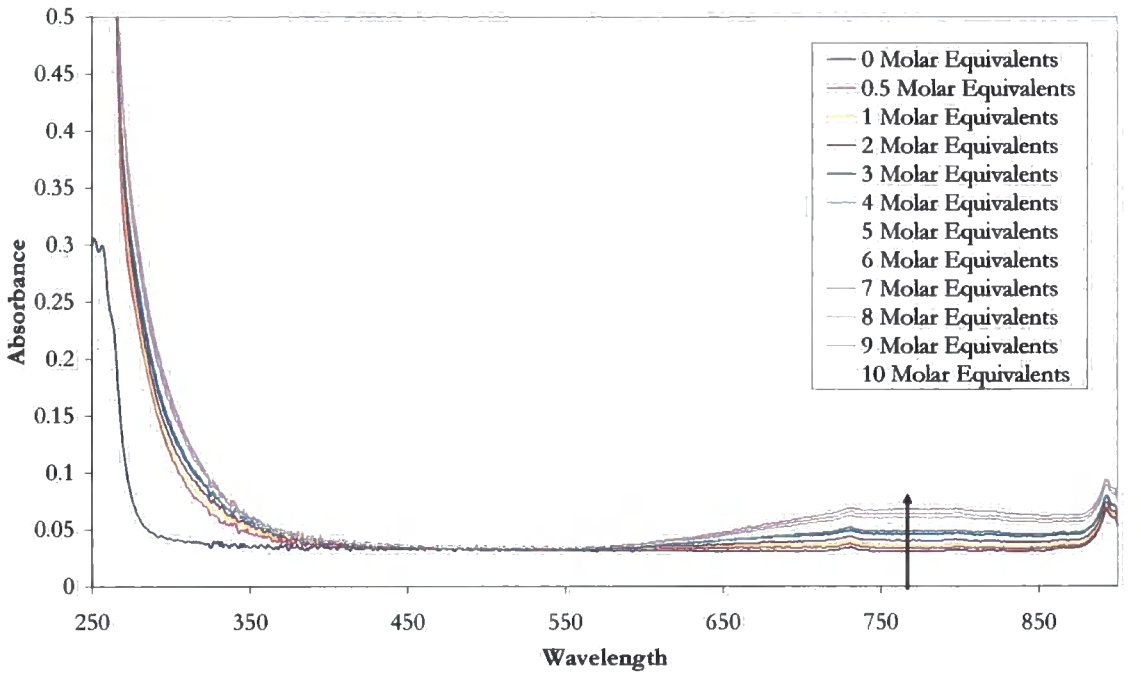

Figure 3.20: Absorption spectrum of Pyridine (1.03×10^{-4} M) in CH_3CN, and upon addition of increasing amounts of $Cu(BF_4)_2.6H_2O$ upto 10 equivalents.

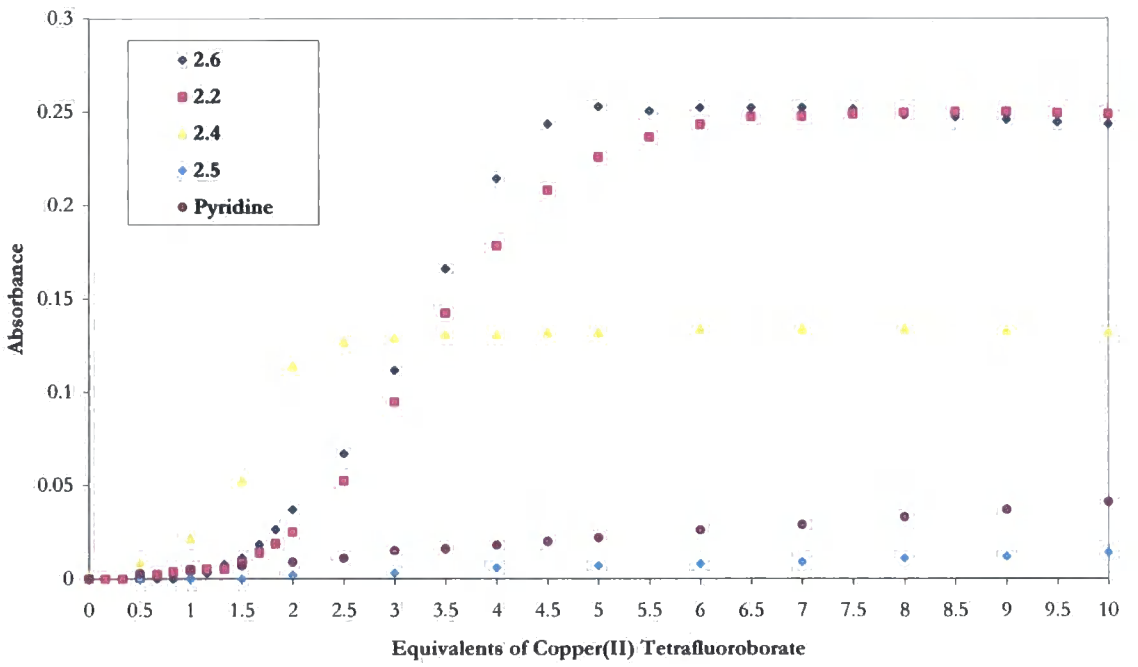

Figure 3.20(a): Change in absorbance of **2.6** (5.15×10^{-5} M) at 514 nm, **2.2** at 590 nm, **2.4** at 510 nm, **2.5** at 800 and **Pyridine** at 775 nm, in CH_3CN, and upon addition of increasing amounts of $Cu(NO_3)_2.2.5H_2O$ upto 10 equivalents.

Ligand	log K_{11} / M^{-1}
2.2	3.12(10)
2.4	4.54(13)
2.5	3.85(12)
2.6	4.44(18)
Pyridine	4.10(11)

Table 3.4: Binding constants (log *K*) for $Cu(BF_4)_2.6H_2O$(**L**) complexes in CH_3CN, determined using Specfit 32.[16] Errors are shown in brackets, ligand concentration 1.03 x 10^{-4} M.

3.2.3 Effect of Adding Metal Salts on the Emission of Ligand

As ligand **2.6** was shown to be fluorescent, fluorescence titrations were undertaken in which ligand solutions were titrated with those of metal salts. The samples were all excited at 375 nm, and the spectra measured from 385 to 700 nm. The emission spectrum of the ligand **2.6**, has a band at 440nm and is assigned to the charge transfer from carbazole to pyridine state, as was observed in the absorbance spectrum at 375 nm. In all titrations, this band at 440 nm was initially quenched, and with the exception of $Cu(CH_3COO)_2$, there is the appearance of a broad featureless band at 535 nm, which may be assigned to the formation of a carbazole excimer or exciplex and maybe the association of a two ligand to one metal, which from solid data we know does not occur with $Cu(CH_3COO)_2$.

Figure 3.21 shows the titration of **2.6** with $Co(NO_3)_2.6H_2O$. The quenching by $Co(NO_3)_2.6H_2O$ is gradual and reaches a minimum emission after about 7 equivalents. It is suggested that the emission is quenched by a charge transfer from the metal atom to the excited fluorophore. The results suggested that $Co(NO_3)_2.6H_2O$ is in fact interacting with the ligand, though the nature of the interaction is unclear. The emission is also gradually quenched upon addition of $Ni(NO_3)_2.6H_2O$, **figure 3.22**, as it is upon addition of $Zn(CF_3SO_3)_2$, **figure 3.23**, suggesting that the metals in both these hosts are interacting with the ligands, but as with $Co(NO_3)_2.6H_2O$, the nature of this interaction is not known.

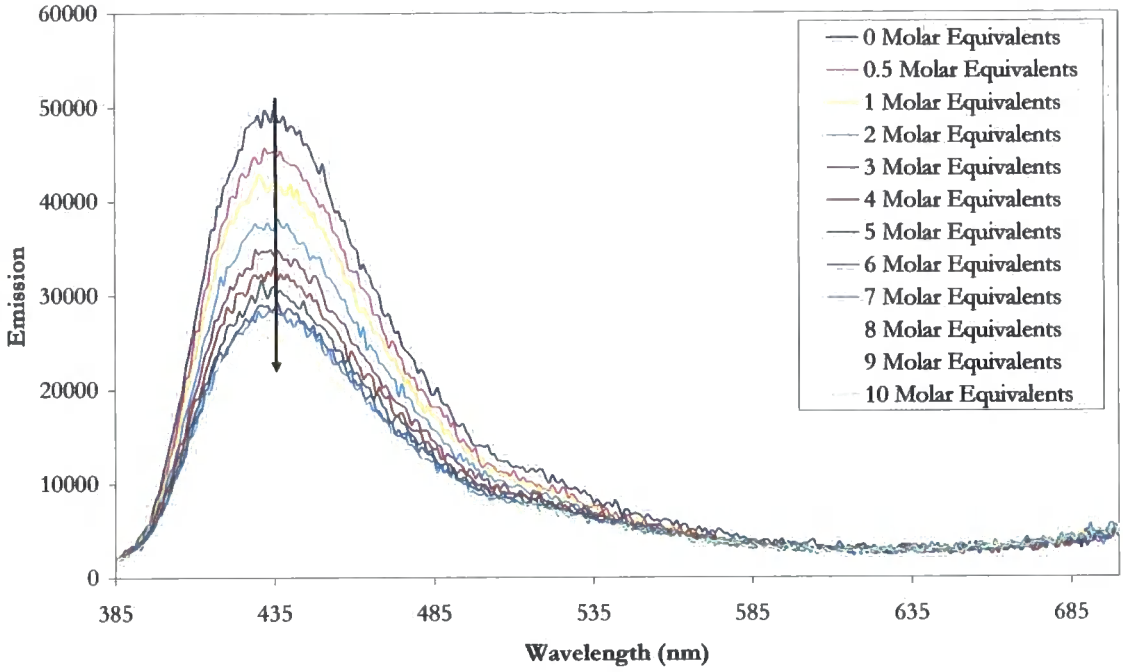

Figure 3.21: Emission spectrum of **2.6** (1.03 x 10^{-4} M) in CH_3CN, and upon addition of increasing amounts of $Co(NO_3)_2.6H_2O$ upto 10 equivalents.

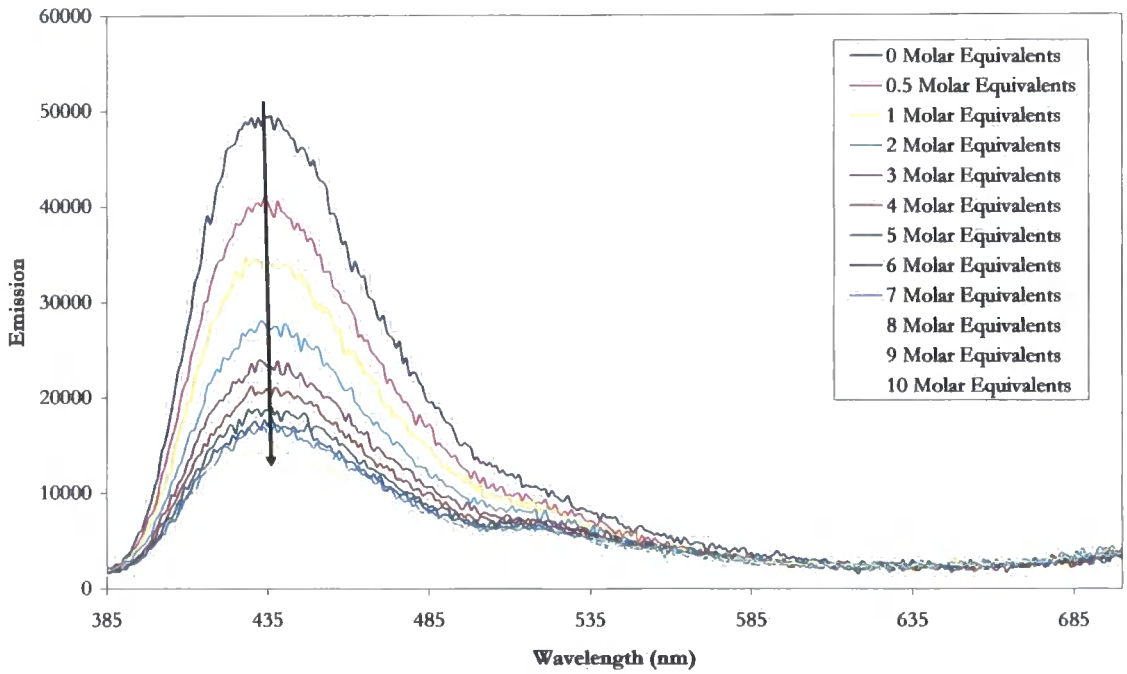

Figure 3.22: Emission spectrum of **2.6** (1.03 x 10^{-4} M) in CH_3CN, and upon addition of increasing amounts of $Ni(NO_3)_2.6H_2O$ upto 10 equivalents.

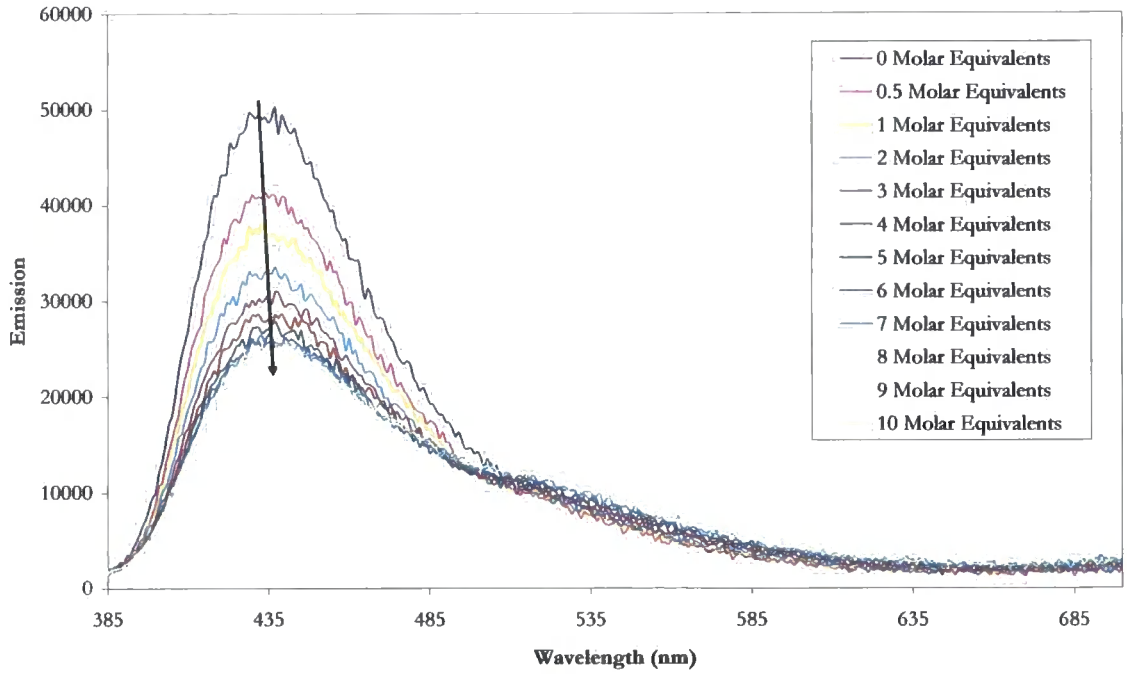

Figure 3.23: Emission spectrum of **2.6** (1.03×10^{-4} M) in CH_3CN, and upon addition of increasing amounts of $Zn(CF_3SO_3)_2$ upto 10 equivalents.

The quenching observed upon addition of $Cu(CH_3CO_2)_2.H_2O$, **figure 3.24**, is more interesting and informative than that observed upon addition of $Co(NO_3)_2.6H_2O$, $Ni(NO_3)_2.6H_2O$ $Zn(CF_3SO_3)_2$. The emission is overall quenched less than upon addition of the salts previously mentioned, but there is a relatively large quenching upon addition of the first half equivalent, and then the emission is quenched by a similar amount upon addition of a further half equivalent of $Cu(CH_3CO_2)_2.H_2O$. This suggested the formation of the 1:1 ligand:metal complex observed in the solid state. However upon addition of a further equivalent of $Cu(CH_3CO_2)_2.H_2O$, the emission is turned on again, to approximately the emission observed after the addition of half an equivalent of $Cu(CH_3CO_2)_2.H_2O$, and the addition of more equivalents of salt, sees a further increase in the emission to the initial emission observed for the unbound ligand, **2.6**. This could be explained by the formation of initially a 2:2 ligand:metal complex , and upon addition of excess metal, resulting in the formation of a 1:2 ligand:metal complex, as is shown in **scheme 3.1**.

$$L + M \longrightarrow L{-}M{-}M{-}L \xrightarrow{Xs\ M} L{-}M{-}M{-}H_2O$$

Scheme 3.1: Prosposed formation of ligand:metal complexes

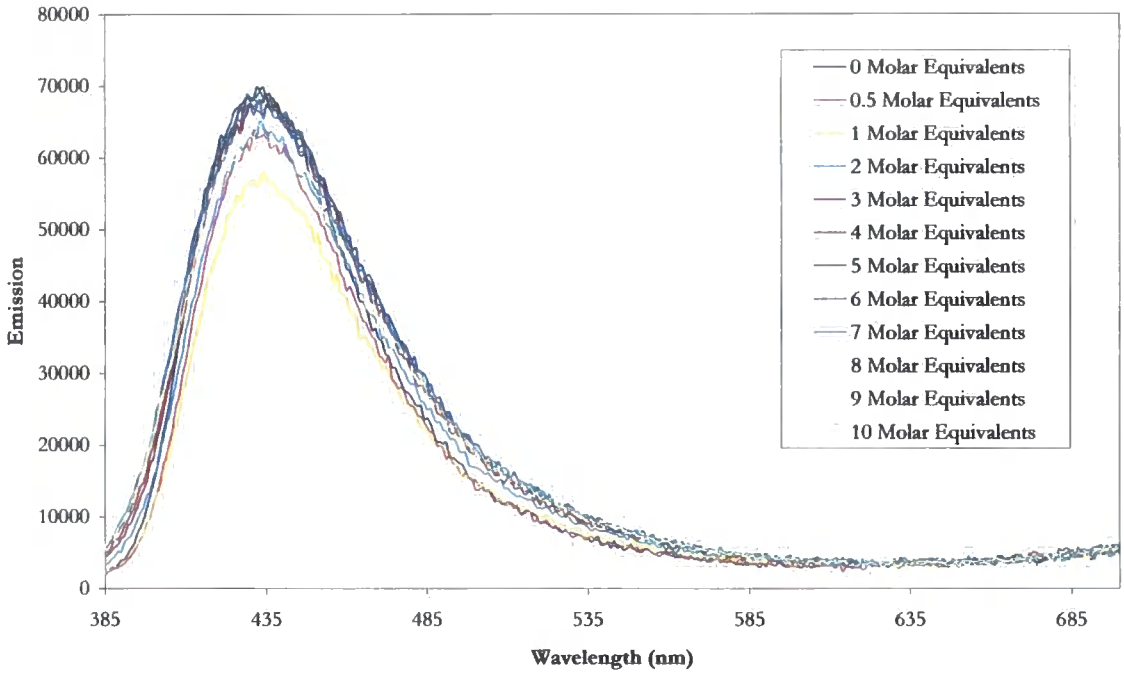

Figure 3.24: Emission spectrum of **2.6** (1.03 x 10^{-4} M) in CH_3CN, and upon addition of increasing amounts of $Cu(CH_3CO_2)_2.H_2O$ upto 10 equivalents.

Addition of $Cu(BF_4)_2.6H_2O$ to a solution of **2.6**, **figure 3.25**, sees a far greater decrease in the emission than has been previously observed in **figures 3.21 – 3.24**. The addition of the first half equivalent of $Cu(BF_4)_2.6H_2O$, sees a quenching of the emission, which is further quenched by the addition of another half equivalent salt. The addition of a second equivalent of $Cu(BF_4)_2.6H_2O$, sees the fluorescence almost completely quenching suggesting, the addition of two equivalents of copper is required to completely quench the ligand fluorescence. The same phenomenon is observed upon addition of $Cu(CF_3SO_3)_2.6H_2O$, **figure 3.25**, with the fluorescence completely quenched upon addition of two equivalents of $Cu(CF_3SO_3)_2.6H_2O$, suggesting that in the case of these two salts the anion is not involved in the quenching or some differences in the quenching would be expected. This suggesting that

the quenching is the result of an electronic energy transfer involving the metal atom and the excited fluorophore.

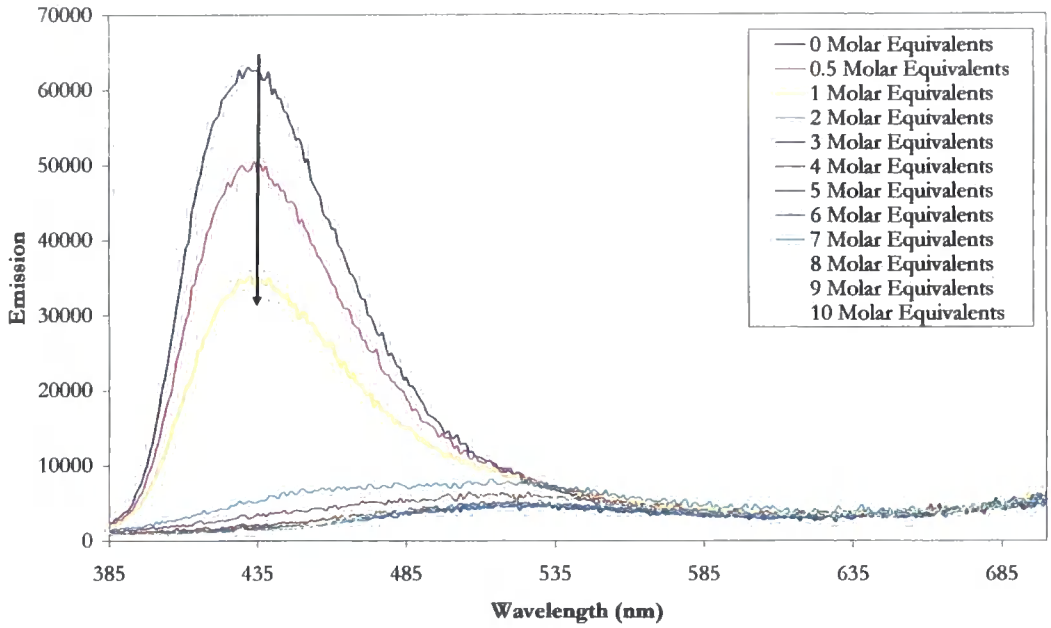

Figure 3.25: Emission spectrum of **2.6** (1.03 x 10^{-4} M) in CH_3CN, and upon addition of increasing amounts of $Cu(BF_4)_2.6H_2O$ upto 10 equivalents.

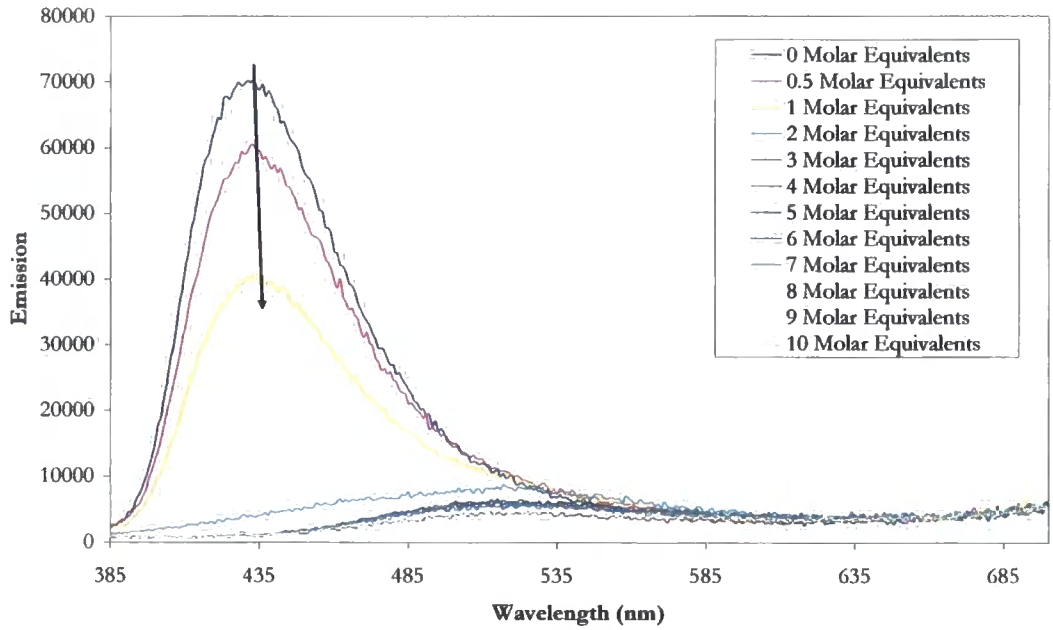

Figure 3.26: Emission spectrum of **2.6** (1.03 x 10^{-4} M) in CH_3CN, and upon addition of increasing amounts of $Cu(CF_3SO_3)_2$ upto 10 equivalents.

Upon addition of up to one equivalent $Cu(NO_3)_2.2.5H_2O$ to an acetonitrile solution of **2.6**, the fluorescence is quenched, **figure 3.27**, as was seen to a lesser extent in **figures 3.25** and **3.26** upon addition of $Cu(BF_4)_2.6H_2O$ and $Cu(CF_3SO_3)_2$ respectively. After the addition of a further equivalent of $Cu(NO_3)_2.2.5H_2O$, there is the appearance of a new band centred around 520 nm, which reaches a maximum emission upon addition of 3 equivalents. This band is red-shifted compared to that of the host molecule, suggesting the formation of a new complex which is itself fluorescent, as the peak is shifted compared to the unbound ligand **2.6**, **figure 3.24**. To investigate this further, the fluorescence of the ligand was firstly quenched by the addition of four equivalents of $Cu(CF_3SO_3)_2$, as this was seen in **figure 3.26** to completely quench the ligand fluorescence. Nitrate, as its tetrabutylammonium salt, was then titrated into the solution, **figure 3.28**, and an increase in the emission of the broad band centred on 520 nm, as was observed upon addition of greater than three equivalents of $Cu(NO_3)_2.2.5H_2O$, **figure 3.27**. After the addition of two equivalents of nitrate the band centred on 520 nm broadens, and reaches a maximum emission after the addition of four equivalents of nitrate. The broadening of this band includes a shoulder centred on 435 nm, which is the wavelength at which the free ligand emits, suggesting the formation of a new nitrate complex, which emits at 520 nm, and some free ligand, which emits around 435 nm. The addition of two equivalents of $Cu(CF_3SO_3)_2$, results in almost complete quenching of the fluorescence, and nitrate was added to the quenched solution, **figure 3.29**. The broad band centred on 520 nm, as has been seen previously in **figures 3.27** and **3.28**, and a maximum emission is observed at this wavelength after the addition of 6 equivalents of nitrate. After the addition of two equivalents of nitrate, there is also the re-appearance of the peak at 435 nm, which by the addition of six equivalents of nitrate emits more than after the quenching of the fluorescence observed in **figure 3.28**. To another solution of **2.6**, an equivalent of $Cu(CF_3SO_3)_2$ was added, before the partially quenched solution was titrated with nitrate, **figure 3.30**. The addition of nitrate saw a small increase in the emission centred on 420 nm, but a large increase in the emission at 435 nm, the wavelength at which the free ligand, **2.6**, emits. After the addition of 10 equivalents of nitrate the emission is close to that after the addition of half an equivalent of $Cu(BF_4)_2.6H_2O$, or $Cu(CF_3SO_3)_2$, suggesting that there is some interaction still occurring with copper at this point, but that there may also be some free ligand present in the solution. Approximate binding constants have been calculated from the emission data, and it is compared with those from the absorbance data,

table 3.5. The binding constants from both the absorption and the emission data are of similar values, and fit to the same models, suggesting that they are a reasonably accurate representation as to what is happening in solution.

	log K_{11} for **2.6**	
Metal Salt	Absorption	Emission
$Co(NO_3)_2.6H_2O$	3.98(11)	4.05(8)
$Ni(NO_3)_2.6H_2O$	4.47(11)	4.40(9)
$Zn(CF_3SO_3)_2$	4.50(9)	4.17(10)
$Cu(CH_3CO_2)_2.H_2O$	3.06(6) log β_{22} 10.69(7)	3.39(30) log β_{22} 10.92(33)
$CuCl_2.2H_2O$	log β_{11} 4.36(9) log β_{21} 7.21(15)	[b]
$Cu(CF_3SO_3)_2$	[b]	4.66(15)
$Cu(NO_3)_2.2.5H_2O$	[b]	[b]

Table 3.5: Binding constants (log *K*) for $Cu(BF_4)_2.6H_2O$(**L**) complexes in CH_3CN, determined using Specfit 32.[16]

b) binding constant not calculated due to complicated binding mode

These combined results suggest that we have designed a nitrate sensor, **scheme 3.2**, consisting of the formation of a copper ligand complex, which depending on the concentration of copper either forms a complex with nitrate which fluoresces with a band centered around 520 nm, or re-forms the free ligand, which fluoresces with a band centred around 435 nm.

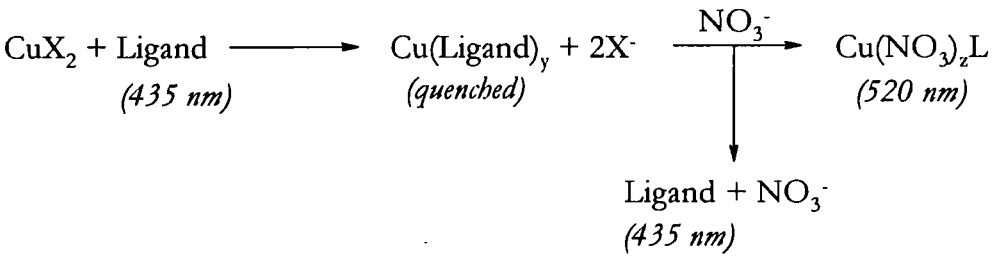

Scheme 3.2: Mechanism of Nitrate Sensor (wavelength of emission shown in italics)

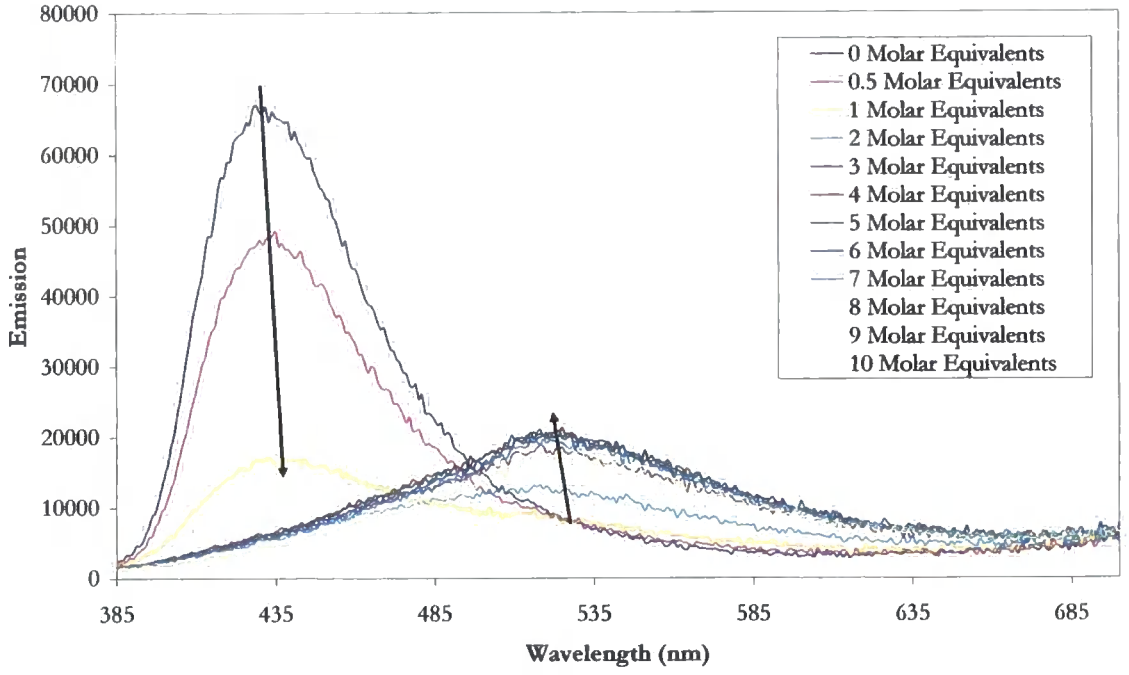

Figure 3.27: Emission spectrum of **2.6** (1.03 x 10^{-4} M) in CH_3CN, and upon addition of increasing amounts of $Cu(NO_3)_2.6H_2O$ upto 10 equivalents.

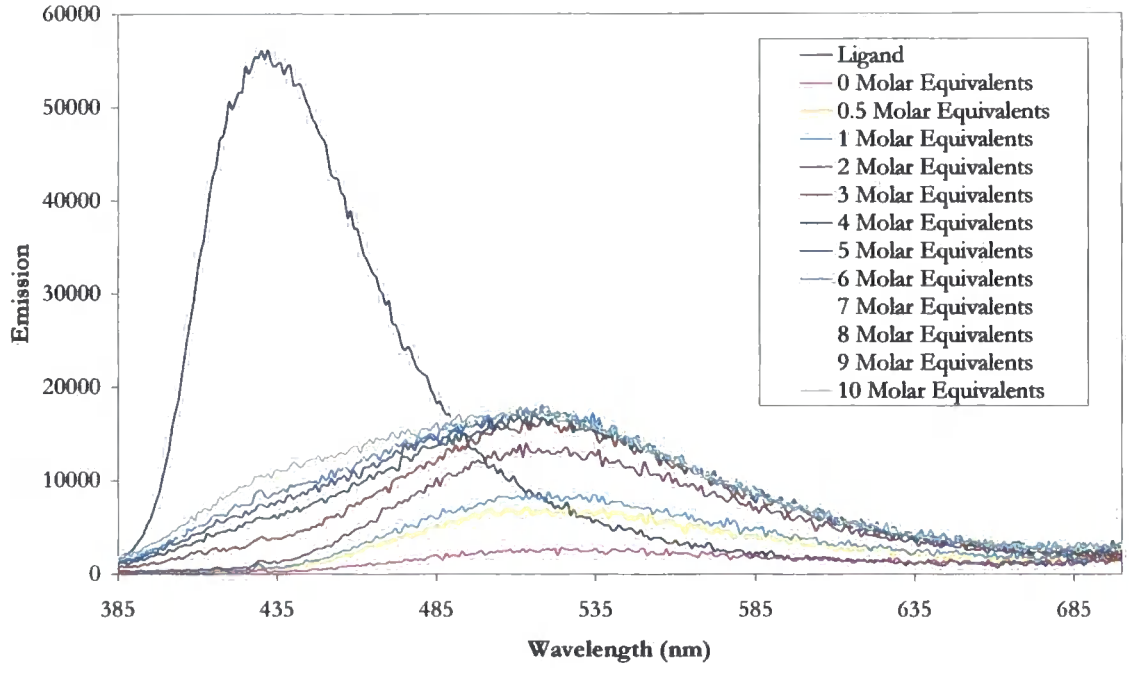

Figure 3.28: Emission spectrum of **2.6** (1.03 x 10^{-4} M) with four equivalents of $Cu(CF_3SO_3)_2$ in CH_3CN, and upon addition of increasing amounts of TBA-NO_3 upto 10 equivalents.

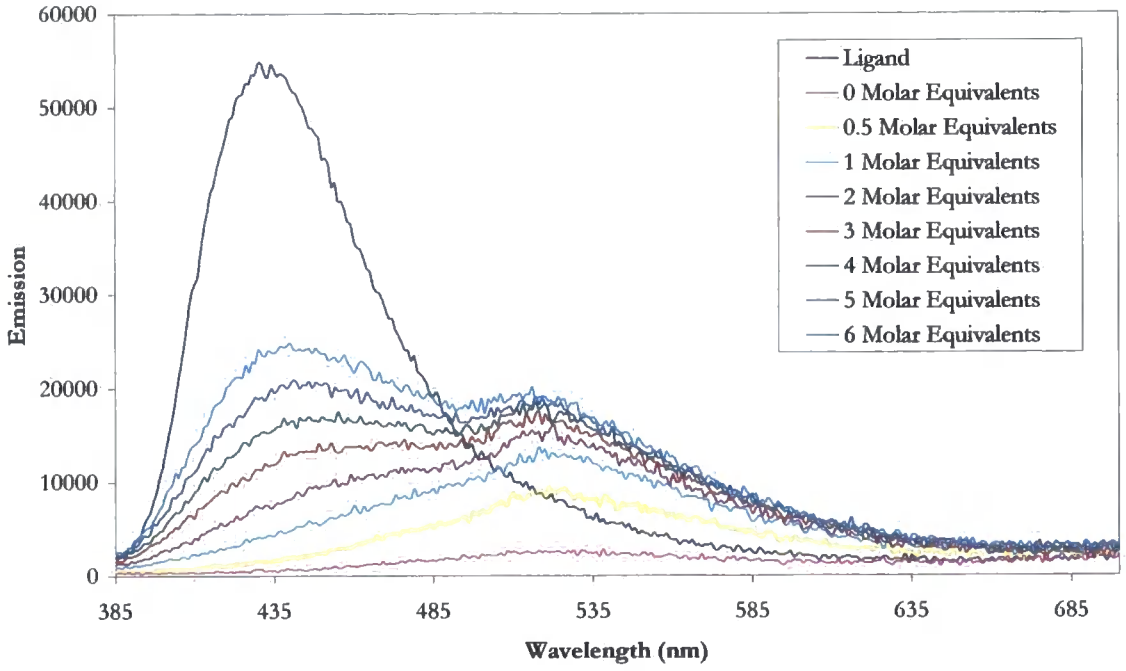

Figure 3.29: Emission spectrum of **2.6** (1.03×10^{-4} M) with two equivalents of $Cu(CF_3SO_3)_2$ in CH_3CN, and upon addition of increasing amounts of TBA-NO_3 upto 10 equivalents.

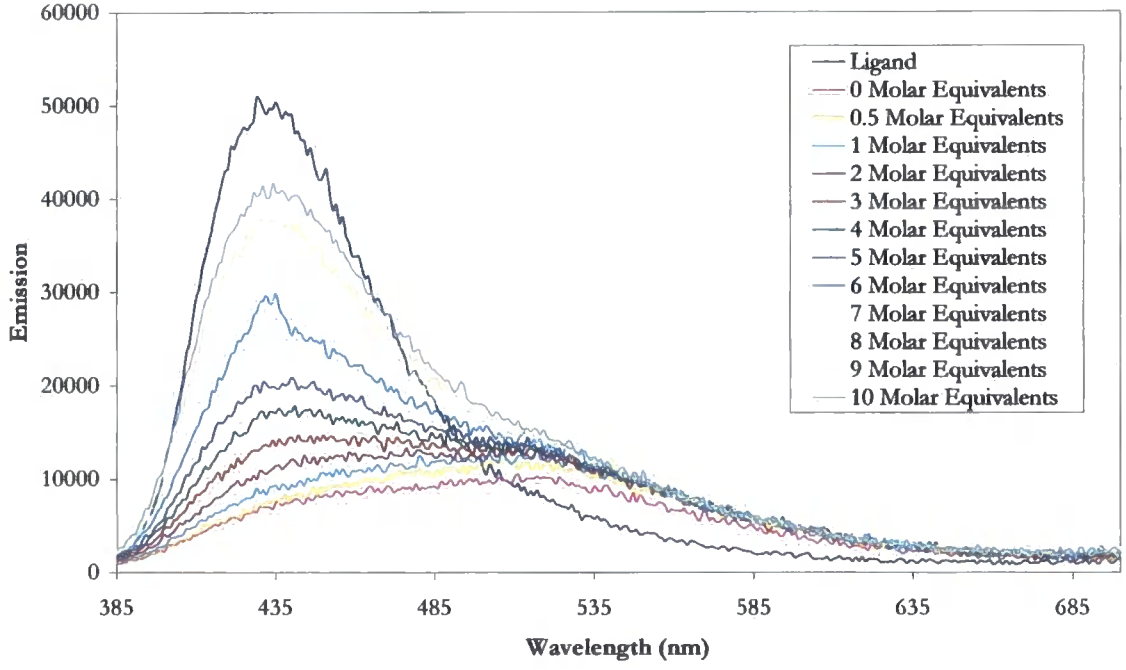

Figure 3.30: Emission spectrum of **2.6** (1.03×10^{-4} M) with one equivalent of $Cu(CF_3SO_3)_2$ in CH_3CN, and upon addition of increasing amounts of TBA-NO_3 upto 10 equivalents.

When comparing the quenching observed upon addition of copper(II) salts, it is interesting to note that the anion, affects the quenching as well as the copper, when small amounts of salt have been added. **Figure 3.31** shows the emission of ligand **2.6**, after the addition of one equivalent of the tested copper(II) salts, and it is observed that copper(II) acetate has had little effect on the emission, and copper(II) tetrafluoroborate and copper(II) triflate have quenched the emission by approximately half of the ligand emission. Copper(II) nitrate has quenched the emission to about two thirds of the ligand emission, and the emission is almost completely quenched by the addition of one equivalent of copper(II) chloride. Upon addition of ten equivalents of the copper(II) salts, **figure 3.32**, there effect of anion appears to be less significant, as the emission has been almost completely quenched upon addition of ten equivalents of copper(II) tetrafluoroborate, copper(II) triflate and copper(II) chloride. The emission remains fairly unchanged upon addition of copper(II) acetate, but upon addition of copper(II) nitrate, the ligand emission at 435 nm has been quenched, and a new broad band centred on 520 nm is observed.

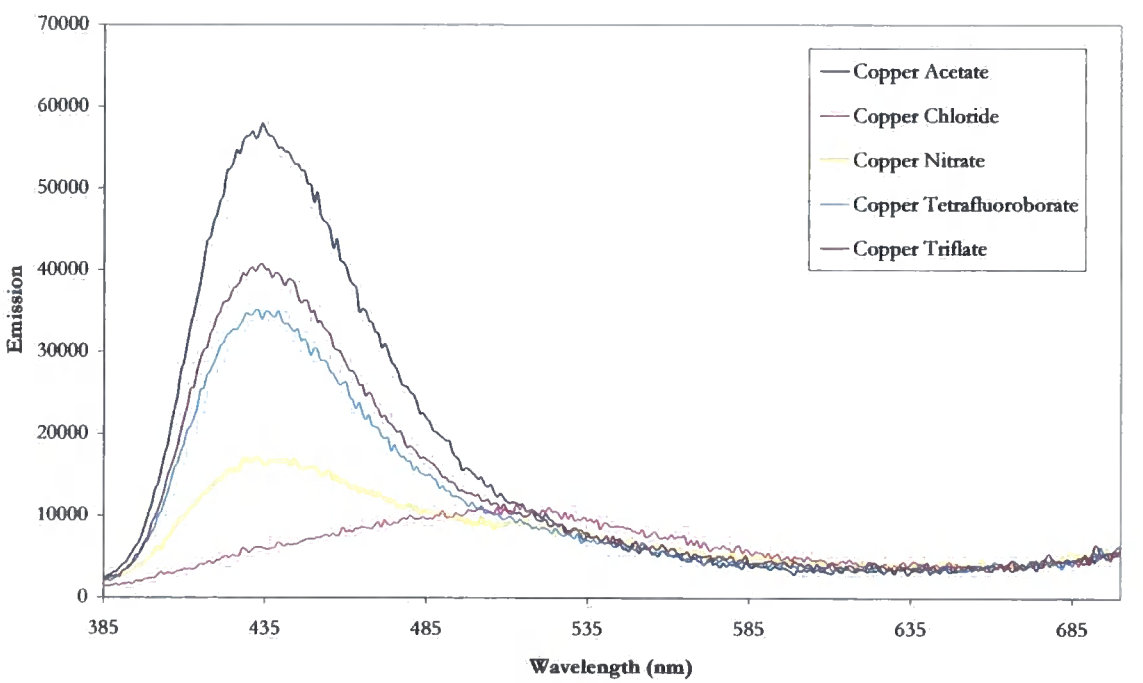

Figure 3.31: Emission spectrum of **2.6** (1.03×10^{-4} M) with one equivalent of CuX_2 in CH_3CN.

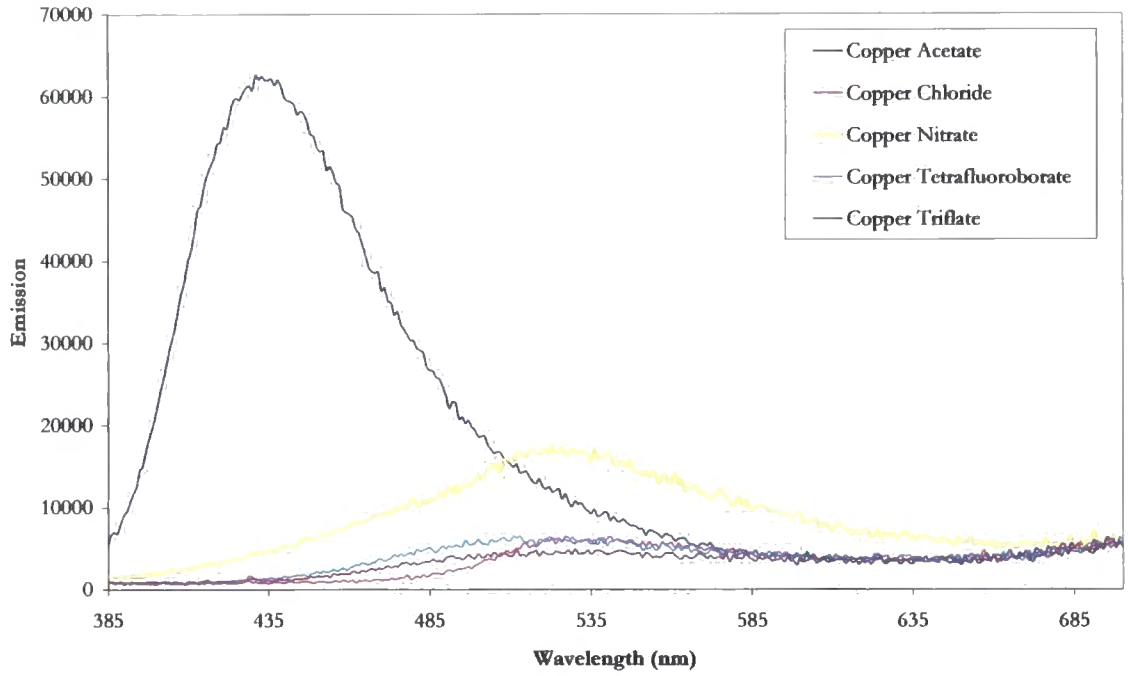

Figure 3.32: Emission spectrum of **2.6** (1.03 x 10^{-4} M) with ten equivalent of CuX_2 in CH_3CN.

3.3 Summary

By a combination of analysis from solution and solid complexes, some insight has been gained into the interaction of the aminomethyl-pyridyl ligands, **2.2** – **2.6**. The data suggests the formation of complexes upon addition of copper salts, which is dependant on the anion, as well as the copper, but without further studies, the exact nature and stoichiometry of these complexes can not be accurately obtained. It is also possible that the water content of the hydrated metal effects the species formed, possibly leading to the protonation of ligands, but without further studies, either in a more aqueous environment or by use of anhydrous metal(II) salts, without which it is not possible to determine the effect that water maybe having on the species formed. In several cases inspection of the spectra suggest that the metal is not immediately interacting with the ligand, as there is no appearance of a metal *d-d* transition until several equivalents have been added. This could be due to ligand – anion interactions forming a complex, which then forms a second metal complex, or a water – ligand interaction, from the water contained in the hydrated metal salts. The interactions between water and ligands could bring about protonation of the ligand, as has been observed

in the solid state. In the case of addition of copper(II) triflate and copper(II) tetrafluoroborate to **2.6**, very similar spectra are observed suggesting that the main interactions observed are between the ligand and metal cation. In comparison of the addition of copper(II) nitrate for example, a very different spectra is observed, suggesting that the anion is also very important in determining the species formed in solution. Initial calculations of binding constants from both absorbance and emission data, have suggested the formation of a 1:1 ligand:metal species for most of the studied examples, with the exception of copper(II) acetate, which forms a 2:2 ligand:metal species, as observed in the crystal structure, and copper(II) chloride with **2.6**, which appears to form both 1:1 and 1:2 ligand:metal species. However, it is suggested that upon addition of metals and their coordinated anions, several complexes are formed, and they are most likely to be either 2:1, 1:1 or 1:2 host:guest species, from the limited structural evidence obtained, and previous published examples. An *in situ*, fluorescent nitrate sensor has also been made, which is dependant on the concentration of copper in solution, so inadvertently, can also give an indication into the copper concentration in the solution.

3.4 Experimental

3.4.1 General Procedure for UV-Vis Experiments

UV-Vis titration experiments were carried out using a UNICAM UV-Vis spectrometer (UV2-100), which is PC-controlled using Vision software, at room temperature. A specific concentration (as indicated in figure captions) of host was made up in a single quartz cuvette in the acetonitrile (3.0 mL). The transition metal salts, were made up to 300 μL, 10 times the concentration of the host, in acetonitrile. 15 μL aliquots of the guest were added to the cuvette, with a path length of 1 cm and the spectra were recorded after each addition.

3.4.2 General Procedure for Fluorescence Experiments

Fluorescence titration experiments were carried out using Fluoromax-3, which is PC-controlled, at room temperature. A specific concentration of host (as indicated in figure captions) was made up in a single quartz cuvette, with a path length of 1 cm, in the acetonitrile (3.0 mL). The transition metal salts, were made up to 300 μL, 10 times the concentration of the host, in acetonitrile. 15 μL aliquots of the guest were added to the cuvette, the sample was excited at 375 nm, and spectra were recorded after each addition.

$[Cu(H_2O)_2(\mu.\mathbf{2.6})_2](CF_3SO_3)_2$

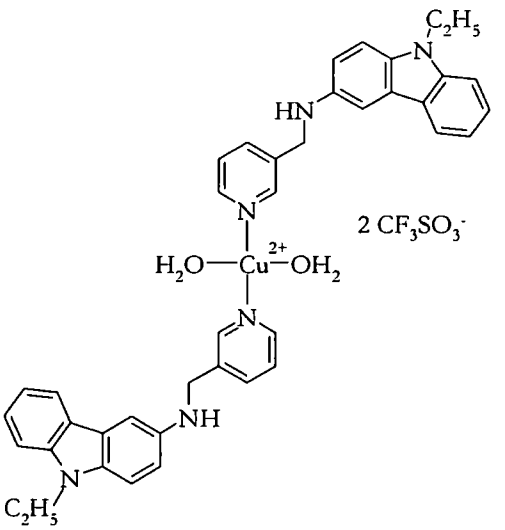

3.1

Compound **2.6**, (0.032 g, 0.11 mmol) and $Cu(CF_3SO_3)_2$ (0.020 g, 0.055 mmol) were dissolved in acetonitrile and stirred overnight, at room temperature. Some of the solvent was then removed under reduced pressure, and the solid product, **3.1**, was removed by filtration.

Anal: Calculated for $(C_{20}H_{19}N_3)_2Cu(CF_3SO_3)_2$ & $4H_2O$: C, 48.67; H, 4.47; N, 8.11 %
Found C, 48.59; H, 3.43; N, 7.92 %

$[Cu_2(H_2O)_4(\mu.\mathbf{2.6})_2](CF_3SO_3)_4$

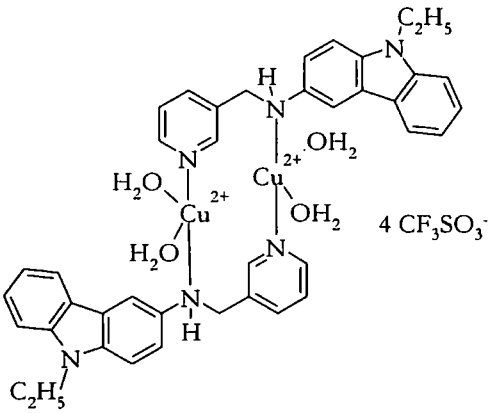

3.2

Compound **2.6**, (0.030 g, 0.10 mmol) and $Cu(CF_3SO_3)_2$ (0.037 g, 0.10 mmol) were dissolved in acetonitrile and stirred overnight, at room temperature. Some of the solvent was then removed under reduced pressure, and the solid product, **3.2** was removed by filtration.

Anal: Calculated for $C_{20}H_{19}N_3Cu(CF_3SO_3)_2$ & $2H_2O$: C, 37.80; H, 3.32; N, 6.01 %
Found C, 37.43; H, 3.54; N, 5.38 %

$[Cu_2(H_2O)_5(\mu.\mathbf{2.6})](CF_3SO_3)_4$ or $[Cu_2(H_2O)_6(\mu.\mathbf{2.6})](CF_3SO_3)_4$

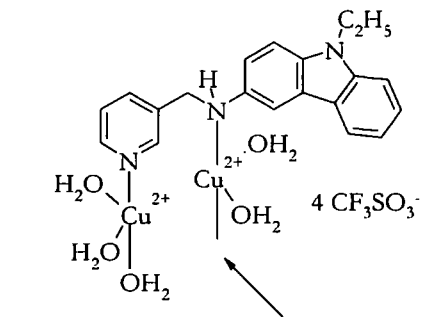

3.3

Compound **2.6**, (0.033 g, 0.11 mmol) and $Cu(CF_3SO_3)_2$ (0.079 g, 0.22 mmol) were dissolved in acetonitrile and stirred overnight, at room temperature. Some of the solvent was then removed under reduced pressure, and the solid product, **3.3**, was removed by filtration.

Anal:	Calculated for $C_{20}H_{19}N_3(Cu(CF_3SO_3)_2)_2$ & $5H_2O$:	C, 25.86; H, 2.62; N, 3.77 %
	Calculated for $C_{20}H_{19}N_3(Cu(CF_3SO_3)_2)_2$ & $6H_2O$:	C, 25.45; H, 2.76; N, 3.71 %
	Found	C, 25.53; H, 2.48; N, 3.73 %

3.5 Crystallographic Data

Crystal data for $[Cu_2(\mu\text{-}O_2CMe)_4(2.2)_2]$: $C_{32}H_{36}Cu_2N_4O_8$, M = 731.73, colourless block, 0.20 x 0.20 x 0.20 mm^3, triclinic, space group P-1 (No. 2), a = 8.2053(6), b = 10.2010(7), c = 10.4507(7) Å, α = 95.5990(10), β = 104.8310(10), γ = 106.3940(10)°, V = 797.51(10) Å^3, Z = 1, D_c = 1.524 g/cm^3, F_{000} = 378, MoKα radiation, λ = 0.71073 Å, T = 120(2)K, $2\theta_{max}$ = 60.1°, 7546 reflections collected, 4200 unique (R_{int} = 0.0765). Final *GooF* = 1.053, *R1* = 0.0484, *wR2* = 0.1159, R indices based on 3557 reflections with I >2sigma(I) (refinement on F^2), 212 parameters, 0 restraints. Lp and absorption corrections applied, μ = 1.390 mm^{-1}.

Crystal data for $[Cu_2(\mu\text{-}O_2CMe)_4(2.5)_2]$: $C_{32}H_{34}Cu_2N_6O_{12}$, M = 821.73, blue-green plate, 0.32 x 0.31 x 0.28 mm^3, monoclinic, space group $P2_1/c$ (No. 14), a = 15.1171(6), b = 13.9050(6), c = 8.4424(4) Å, β = 99.282(2)°, V = 1751.38(13) Å^3, Z = 2, D_c = 1.558 g/cm^3, F_{000} = 844, Smart 1K, MoKα radiation, λ = 0.71073 Å, T = 393(2)K, $2\theta_{max}$ = 60.0°, 15872 reflections collected, 5101 unique (R_{int} = 0.0306). Final *GooF* = 1.022, *R1* = 0.0355, *wR2* = 0.0897, R indices based on 4125 reflections with I >2sigma(I) (refinement on F^2), 235 parameters, 0 restraints. Lp and absorption corrections applied, μ = 1.285 mm^{-1}.

Crystal data for 2.2-H_2 + (NO_3): $C_{12}H_{13}N_3O_3$, M = 247.25, colourless block, 0.20 x 0.20 x 0.20 mm^3, orthorhombic, space group *Pbca* (No. 61), a = 9.5598(5), b = 7.8256(4), c = 31.3102(16) Å, V = 2342.4(2) Å^3, Z = 8, D_c = 1.402 g/cm^3, F_{000} = 1040, MoKα radiation, λ = 0.71073 Å, T = 120(2)K, $2\theta_{max}$ = 60.0°, 22738 reflections collected, 3356 unique (R_{int} = 0.0563). Final *GooF* = 1.042, *R1* = 0.0446, *wR2* = 0.1028, R indices based on 2650 reflections with I >2sigma(I) (refinement on F^2), 171 parameters, 0 restraints. Lp and absorption corrections applied, μ = 0.103 mm^{-1}.

Crystal data for 2.6-H_2 + $(NO_3)_2$: $C_{20}H_{21}N_5O_6$, M = 427.42, yellow block, 0.34 x 0.31 x 0.25 mm^3, triclinic, space group P-1 (No. 2), a = 8.6753(16), b = 14.833(3), c = 16.811(3) Å, α = 111.801(4), β = 95.164(4), γ = 90.250(4)°, V = 1998.6(7) $Å^3$, Z = 4, D_c = 1.420 g/cm^3, F_{000} = 896, SMART 1K, MoKα radiation, λ = 0.71073 Å, T = 120(2)K, $2\theta_{max}$ = 56.4°, 13386 reflections collected, 9603 unique (R_{int} = 0.0405). Final *GooF* = 1.029, *R1* = 0.0516, *wR2* = 0.1210, *R* indices based on 7279 reflections with I >2sigma(I) (refinement on F^2), 559 parameters, 0 restraints. Lp and absorption corrections applied, μ = 0.107 mm^{-1}.

Chapter Four

Arene ruthenium (II)-based hosts

There has recently been a large amount of work done in the use of transition metal ions as sensing and structural elements in the design of supramolecular hosts for anions.[117, 149-151] An early report by Hamilton concerning Ru(II) terpyridyl-thiourea derivatives[152] has been followed by recent results on monodentate pyridylurea complexes[1, 144, 153-156] and anion binding by coordinated, chelating biimidazole complexes.[157, 158] Anion templation has also been used to guide self assembly of coordination complexes, as in the elegant helicates reported by Rice and co-workers.[159] Steed and co-workers have previously reported anion binding and sensing by 3-aminopyridine ruthenium(II) derivatives, in which the semi-labile Ru(II) centre acts as a structural 'core', organising the two anion binding aminopyridine ligands.[160] This chapter, discusses the extension of this chemistry to ruthenium(II) complexes of 3-aminomethylpyridine derivatives,[160] based on ligands **2.1** – **2.6** (chapter two) and the consequences on the compounds anion binding behaviour and symmetry.

4.1 Synthesis and Characterization

Ligands **2.1** – **2.6** were prepared as discussed in chapter 2. The mono-adduct hosts, of type **A**, **scheme 4.1**, were synthesised by reaction of one of ligands, **2.2** – **2.6**, with the chloro-bridged dimer $[\{Ru(\eta^6\text{-}C_6H_4MeCHMe_2)Cl(\mu\text{-}Cl)\}_2]$,[161] for example, addition of ligand **2.2** to $[\{Ru(\eta^6\text{-}C_6H_4MeCHMe_2)Cl(\mu\text{-}Cl)\}_2]$, results in the formation of $[Ru(\eta^6\text{-}C_6H_4MeCHMe_2)Cl_2(\mathbf{2.2})]$, **4.3**. Further reaction of mono-adduct hosts with one equivalent of $AgBF_4$ and additional ligand in methanol/acetone (1:1 v/v) solution gives the monocationic Ru(II) complexes, type **B**, for example addition of an additional equivalent of **2.2** and an equivalent of $AgBF_4$, to **4.3**, results in the formation of $[Ru(\eta^6\text{-}C_6H_4MeCHMe_2)Cl(\mathbf{2.2})_2]BF_4$, **4.4**. An example of the synthetic procedure is shown in **scheme 4.1**.

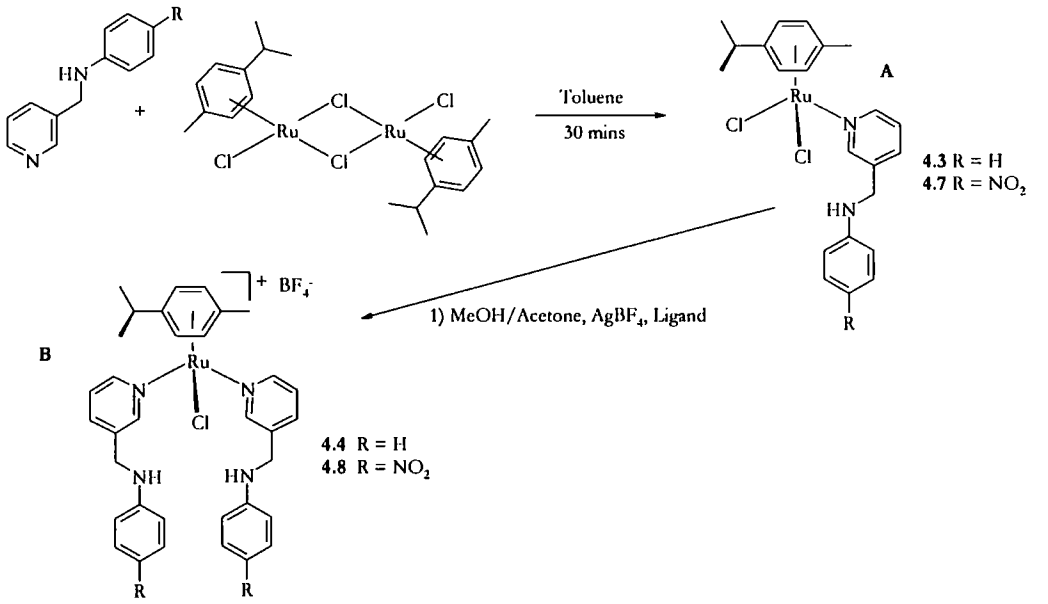

Scheme 4.1: Synthesis of Hosts **4.3** and **4.4** (other hosts are synthesised using the same scheme)

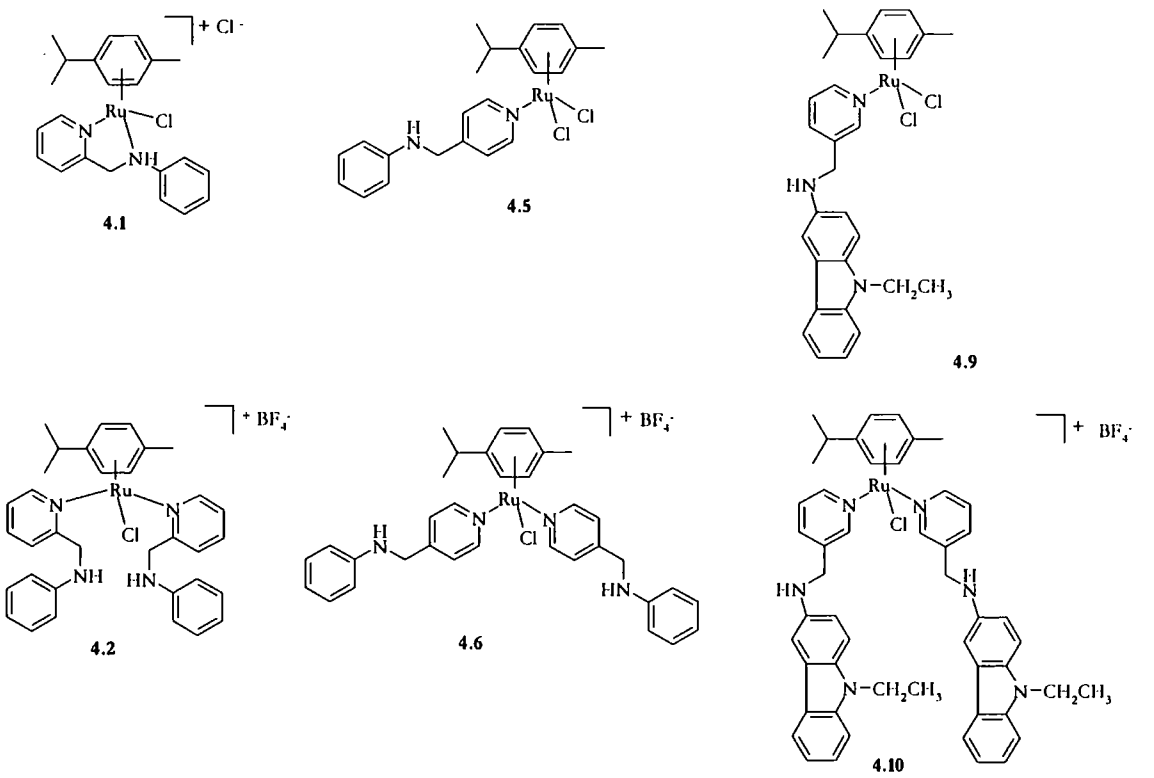

Figure 4.1: Compounds **4.1**, **4.2**, **4.5**, **4.6**, **4.9** and **4.10**, synthesised as described in **scheme 4.1**.

The new complexes were fully characterised by elemental analysis, ESI-MS, IR spectroscopy (nujol) and ^{1}H and $^{13}C\{^{1}H\}$-NMR spectroscopy, and experimental data confirmed the proposed structures. The ES+ mass spectrum of the mono-adduct hosts of type **A** shows a peak at m/z = 489 for **4.3**, 489 for **4.5**, 535 for **4.7** and 559 for **4.9**, all of which represent $[M^+]$. This is not the case for host **4.1**, which forms a ruthenium chelate complex, **figure 4.2**, upon addition of one equivalent of **2.1** to $[\{Ru(\eta^6\text{-}C_6H_4MeCHMe_2)Cl(\mu\text{-}Cl)\}_2]$, and the ES+ mass spectrum shows a peak at m/z = 455, and represents $[M^+\text{-}Cl]$. The ES+ mass spectrum of the monocationic hosts of type **B** shows a peak at m/z = 639 for **4.2**, **4.4** and **4.6**, and 873 for **4.10**, all of which represent $[M\text{-}BF_4]$, and 815 for **4.8**, which represents $[M^+]$, suggesting a stronger interaction of the counterion BF_4^- with the host molecule, **4.8**. There is a significant chemical shift change of the NH resonance in the ^{1}H-NMR spectrum, in the formation of the mono-adducts hosts from the ligands and the monocationic hosts from the mono-adduct hosts. For example, the NH resonance in the free ligand **2.5**, occurs at 4.92 ppm, in the mono-adduct host, **4.7** at 5.94 ppm and in the monocationic host, **4.8** at 6.67 ppm. The downfield chemical shift of this resonance suggests enhanced hydrogen bonding of **4.8** compared to the free ligand, **2.5**, and **4.7**, and presumably arises from hydrogen bonding to the BF_4^- anion. The degree of hydrogen bonding varies, depending on the pendant arm of the host, for example the more acidic NH of the nitro-substituted host, **4.8**, shows a greater degree of hydrogen bonding compared to the aryl host **4.4**. Host **4.1** shows the largest chemical shift change of the NH resonance compared to the free ligand, **2.1**, upon its formation, which supports the suggestion of the formation of a chelate complex, for example the chemical shift of the NH resonance in **2.1** is 4.66 ppm, and in **4.1** is 11.50 ppm, a shift of nearly 7 ppm, compared to the next largest shift which is in host **4.7**, which sees a shift of 1 ppm compared to the free ligand **2.5**. The NMR spectra of **4.1** and **4.3** are shown in **figure 4.3**, which shows the differences between the spectra. The main differences are the obvious shift in the NH proton, which is shifted significantly downfield in **4.1** compared to **4.3**, and in **4.1** there is splitting in the methylene protons next to the amine group, where this resonance appears as a singlet in **4.3**. There is also splitting of the aromatic resonances CH on the *p*-cymene group in **4.1** observed compared to **4.3** where they appear two doublets, which suggests that the compound has a chiral ruthenium centre, which is not observed in the other compounds, which do not contain a chiral ruthenium centre. To confirm the proposed chelate complex in **4.1**, an equivalent of $NaBPh_4$ in methanol was added to a

methanol solution of the complex, which immediately formed a yellow precipitate. A sample of this precipitate was analysed by NMR spectroscopy, and a 1:20 ratio of one of the protons of the aromatic ring coordinated to ruthenium, to the BPh_4 proton resonances, suggesting the formation of a BPh_4 salts of the complex, confirming its ionic nature. The NMR study was carried out in DMSO-d_6, which appears to replace the NH-Ru bond, and is acting as a ligand itself, suggesting that the NH-Ru bond is weak. Elemental analysis of the BPh_4-**4.1** complex, confirms the formation of this complex, and its purity, as did the elemental analysis of the ruthenium chelate complex, **4.1**.

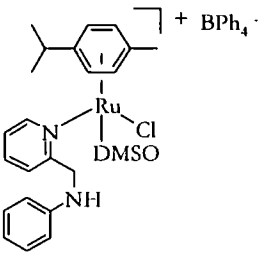

Figure 4.2: Proposed structure of ruthenium complex, **4.1**, upon addition of DMSO

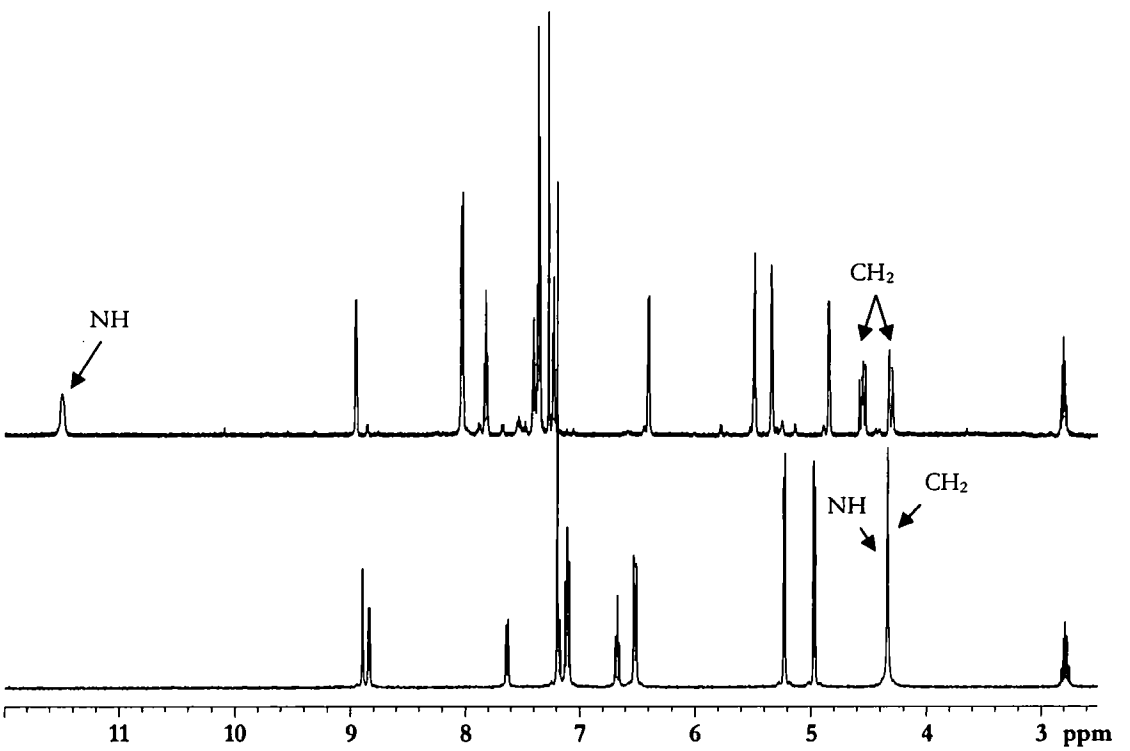

Figure 4.3: Comparison of NMR spectrum for **4.1** and **4.3**

By considering the ν(NH) stretch in the IR spectrum, the hydrogen bonding in the hosts can also be compared. **Figure 4.4** shows the IR spectrum recorded for the monocationic hosts, **4.2**, **4.4**, **4.8** and **4.10**, the amine NH stretch of **4.2** occurs at the lowest wavenumber, suggesting this host is the most strongly hydrogen bonded. The ν(NH) stretch in host **4.8** occurs at a slightly lower wavenumber than **4.10**, which in turn occurs at a slighly lower wavenumber than that of **4.4**. The hosts also show the appearance of a stretch at approximately 1050 cm^{-1} which is assigned to the BF_4^- stretch, which is evident in the monocationic hosts, **4.2**, **4.4**, **4.8** and **4.10**, confirming the ionic nature of these compounds, **figure 4.5**. A shift in the NH resonance is seen in the spectrum of **4.1** compared to that of **2.1** and **4.2**, **figure 4.5**, which is far greater than than the shifts seen in any of the other host molecules, for example the spectrum of **2.2**, **4.3** and **4.4**, **figure 4.6**.

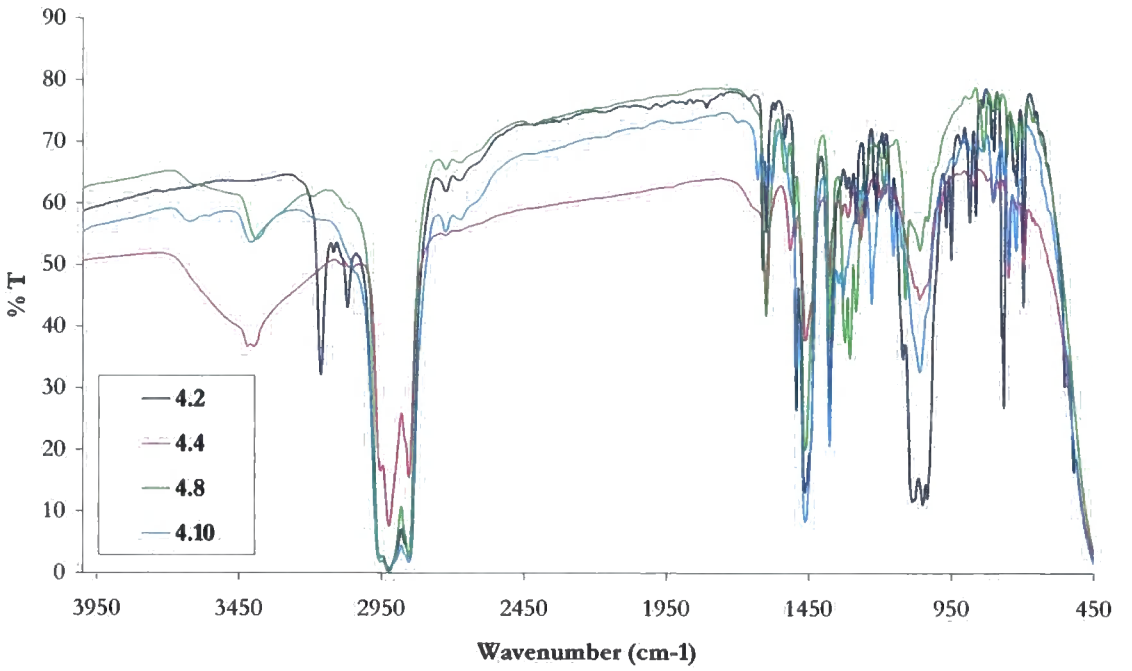

Figure 4.4: IR spectra of host **4.2**, **4.4**, **4.8** and **4.10**.

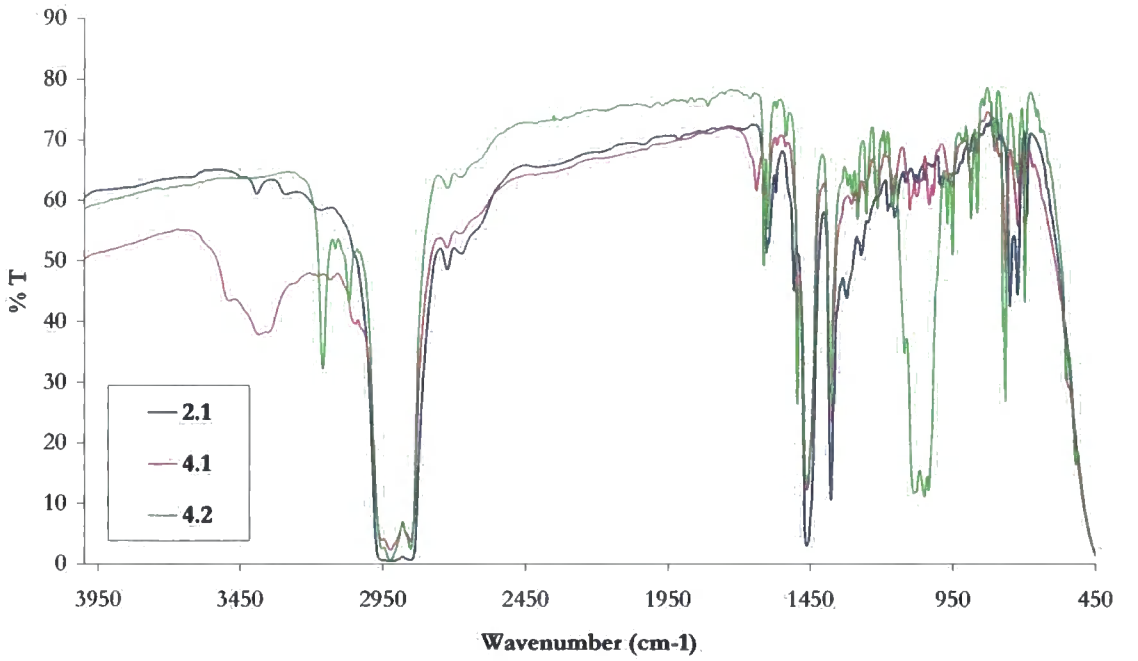

Figure 4.5: IR spectra of **2.1**, **4.1** and **4.2**.

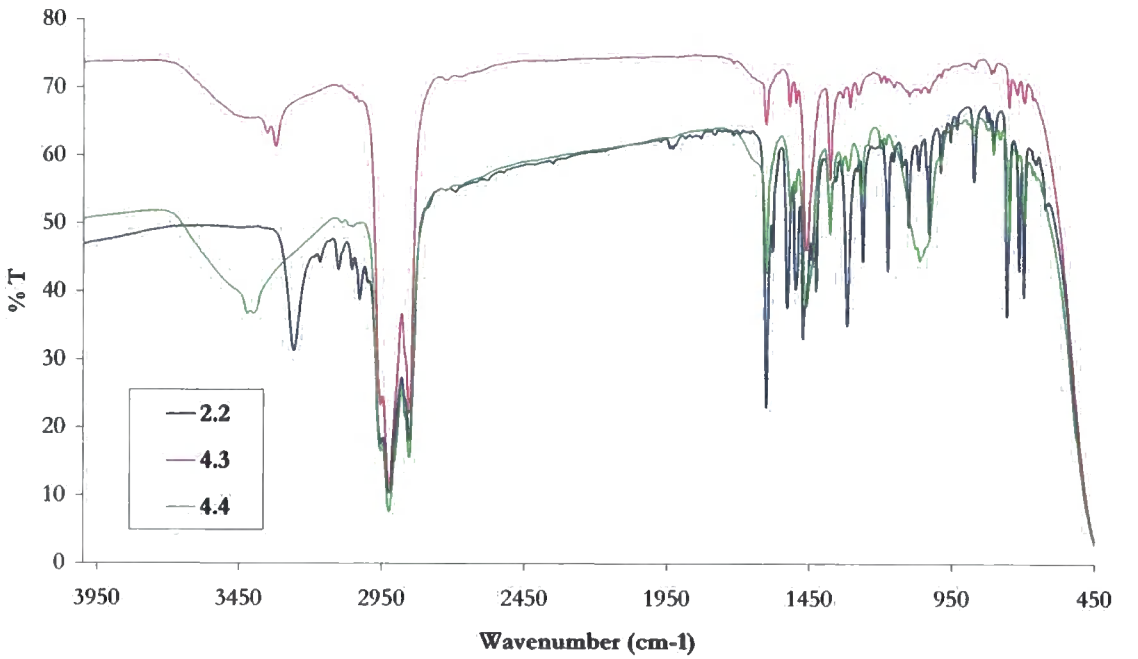

Figure 4.6: IR spectra of **2.2**, **4.3** and **4.4**.

The ^{1}H NMR spectrum of *meta* monocationic complex **4.4** shows a broad AB quartet resonance assigned to the methylene protons, $H^{a,a'}$ and $H^{b,b'}$ at 4.40 and 4.32 ppm, with ^{2}J

= 17.2 Hz, consistent with geminal coupling, **figure 4.7**. In contrast, in the ^{1}H NMR spectrum of the free ligand and in monoadduct **4.3** this resonance occurs as a singlet at 4.36 and 4.58 ppm, respectively. The inequivalence of protons H^a and H^b must arise from the fact that the molecule is point group C_s and H^a and H^b are not related by the mirror symmetry of the molecule. Instead the mirror plane relates H^a to $H^{a'}$ and H^b to $H^{b'}$. These protons remain diastereotopic even without invoking any restricted rotation or effects such as intramolecular hydrogen bonding of the amine protons to the coordinated chloride ligand.[155, 162, 163] The strongly hydrogen bonding nature of the protons, in **4.8**, is evident from the observation of the coupling to the methylene resonances, H^a and H^b, while this coupling is barely resolved for **4.4**. Compound **4.10** behaves similarily to both **4.4** and **4.8** with a AB pattern for the CH_2 resonance, but in the monocationic host the NH resonance is underneath this resonance. However complex **4.1** shows inequivalence of the CH_2 protons, which is not seen in any of the other hosts of type **A**. It is thought that this is due to the formation of a chelate complex in which the NH is interacting with the ruthenium, which has caused a large downfield shift from 4.66 ppm in the free ligand, **2.1**, to 11.50 ppm in the mono-substituted host, **4.1**, and one of the chloride ions forms a counterion to the complex. The monocationic host, **4.2**, shows the methylene protons as a doublet, and is shifted greatly upfield compared to the monoadduct host, **4.1**. The monocationic *para* host **4.6** shows a doublet for the CH_2, which is different from the other hosts of this type which show an AB quartet for these resonances, and could be explained by the *para* position of the secondary amine, increasing the distance from the adjacent ligand.

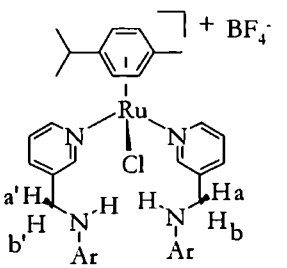

Figure 4.7: Monocationic host showing methylene protons

The hexamethylbenzene derivative of **4.3**, was synthesised by Charlotte Willans, a post-doc within the group, and a crystal of this compound, **4.11**, was grown from a methanol

solution, by slow evaporation, **figure 4.8**. The structure of the compound was analysed by x-ray crystallography, and as the data for the monosubstituted compounds discussed in this chapter, **4.3**, **4.5**, **4.7** and **4.9**, shows that there is not intramolecular hydrogen bonding between the amine proton, and the chloride ligands attached to the ruthenium.[164] Some intramolecular hydrogen bonding is observed between the two protons closest to the pyridyl nitrogen, and each of the coordinated chlorides. Intermolecular hydrogen bonding is observed between the amine proton(H2) and chloride(Cl2), on an adjacent molecule, the length of this hydrogen bond (3.436(3), N2-Cl2) is comparable to both the anthracenyl and ferrocenyl derivatives of **4.3**,[160] previously synthesised in the group, which have hydrogen bond lengths of 3.204(4) and 3.369(14), respectively. Intermolecular hydrogen bonding is also observed between coordinated chloride ligands, and the arene protons on adjacent molecules, H23A and Cl2, and H24B and Cl1.

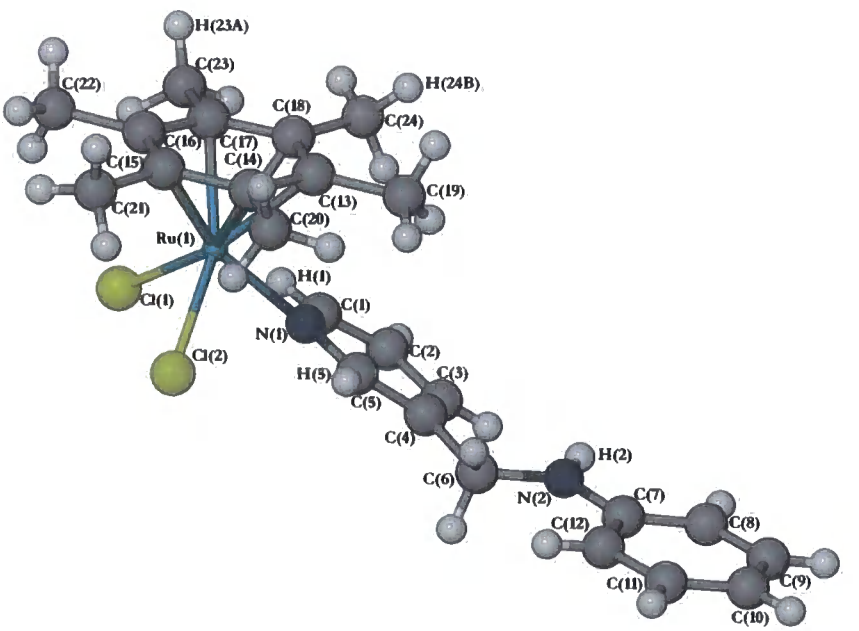

(a)

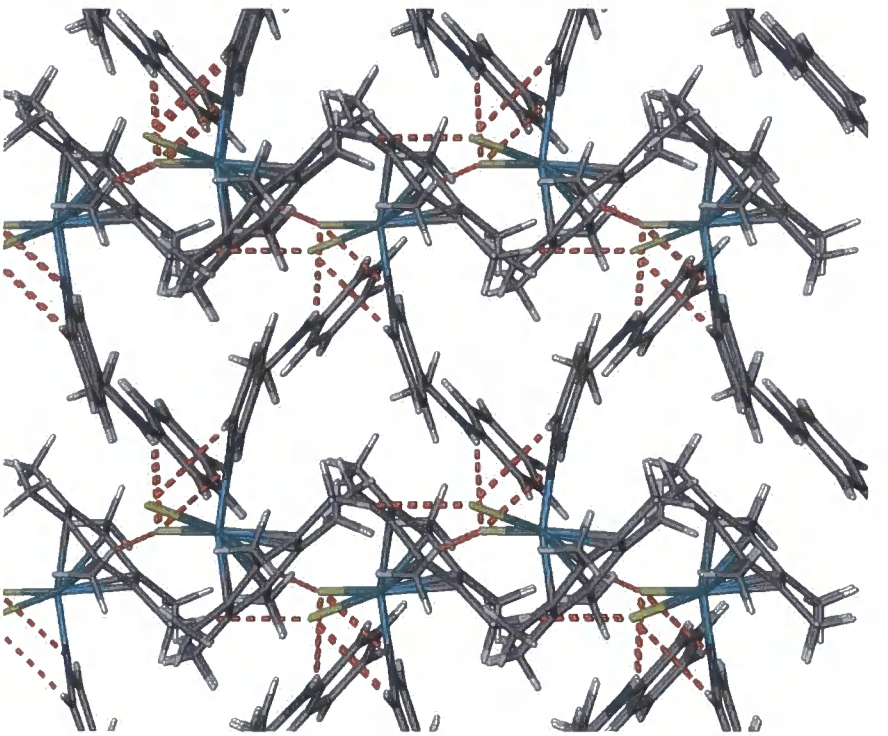

Figure 4.8: X-ray crystal structure of **4.11** (*hexamethylbenzene derivative of* **4.3**) (a)Molecular structure in ball and stick representation. (b) Packing diagram viewed along a-axis. Selected hydrogen bond lengths (Å): N2-Cl2 = 3.436(3); C1-Cl1 = 3.272(4); C3-Cl2 = 3.629(4); C5-Cl2 = 3.282(4); C23-Cl2 = 3.600(5); C24-Cl1 = 3.633(4).

The intrinsic asymmetry of **4.4** is supported by a dilution study. The chemical shift of the NH resonance remains essentially unchanged across the concentration range 1.9 – 31.0 mol dm^{-3}, **figure 4.9**. Any intermolecular association would be expected to exhibit concentration dependence.

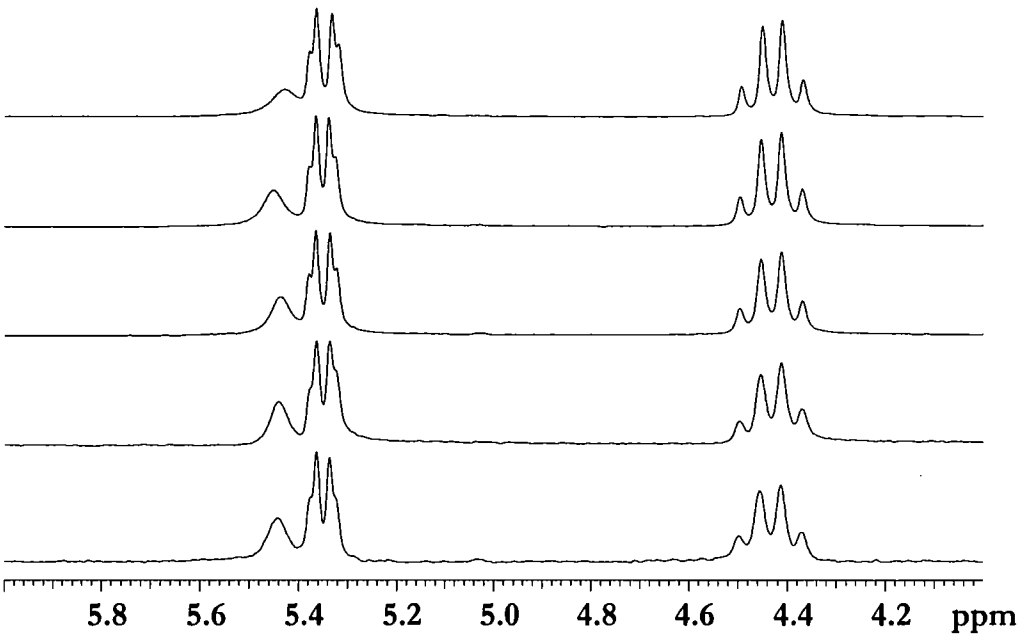

Figure 4.9: ^{1}H NMR spectra of the methylene region of host **4.4** as a function of concentration (bottom to top 31.0; 15.5; 7.6; 3.8; 1.9 mM^{-1}).

4.2 NMR Spectroscopic Binding Studies

Monocationic complexes **B** were designed as hosts for binding anions external to the complex. Their anion complexation ability was determined by ^{1}H NMR spectroscopic titration with a variety of anions as their tetrabutylammonium salts in $CDCl_3$ solution. Anion binding constants for the formation of 1:1 and 2:1 host:guest complexes are given in **Table 4.1**. The use of both 1:1 and 2:1 stoichiometry models for complexes **B** is consistent with previous work on 3-aminopyridine derivatives.[160] This suggests the formation of compounds in which a single anion is sandwiched between two hosts[160] and resulted in a much improved fit to the titration data than a 1:1 model alone.

	K_{11} and K_{21} / M^{-1}					
Anion	**4.3**	**4.7**	**4.9**	**4.4**	**4.8**	**4.10**[b]
Cl^-	~ 0	β_{11} 2.00(2)	-	β_{11} 3.64(3) β_{21} 6.01(9)	β_{11} 4.04(3) β_{21} 6.66(9)	β_{11} 3.95(3) β_{21} 7.03(9)
Br^-	-	-	-	β_{11} 3.28(2) β_{21} 5.32(9)	β_{11} 3.71(3) β_{21} 6.30(9)	β_{11} 3.38(3) β_{21} 5.69(9)
NO_3^-	~ 0	-	-	β_{11} 2.06(14) β_{21} 3.92(7)	β_{11} 3.44(4) β_{21} 6.11(9)	β_{11} 3.23(6)
$CF_3SO_3^-$	~ 0	-	-	β_{11} 1.94[a] β_{21} 2.19[a]	β_{11} 2.30(7) β_{21} 4.54(2)	~ 0
$MeCO_2^-$	-	-	-	β_{11} 3.53(10) β_{21} 2.06[a]	β_{11} 4.14(2) β_{21} 7.11(12)	β_{11} 3.41(2) β_{21} 6.20(2)

Table 4.1: Anion binding constants (M^{-1}) for complexes **4.3** – **4.10** in $CDCl_3$ at 20 °C. Errors are <10%, anions added as NBu_4^+ salts, host concentration 0.006 mol dm^{-3} (hyphen indicates not measured).

a) large error

b) not a true binding constant, as there is another species present in the compound, which appears to bind to the oxo-anions in preferance to the designed host, so the initial period has been removed in calculating binding constant (0-0.5 equivalents added).

* *Graphical representation of the fit of titration data is given in the Appendix*

It was not possible to synthesise a clean sample of **4.10**, but the synthesised sample was used to measure binding constants as the impurities were small compared to the product. The impurities appear to be a small amount of the mono-substituted host, **4.9**, and another species which has not been identified. Data suggests that halide anions bind directly to the desired host, **4.10**, but with the oxo-anions, it seems that one of the other products preferentially binds these anions, up to approximately 0.5 equivalents. The titration data for halide anions with this host, **4.10**, also fitted to 1:1 and 2:1 models as was seen in hosts **4.4** and **4.8**. The nitrate fitted to a 1:1 model better than to 1:1 and 2:1 models, **figure 4.10**. This is most obvious upon addition of acetate, where an upfield

shift is observed until the addition of 0.3 equivalents, before a downfield shift that mirrors those seen upon addition of halide anions. On addition of the first 0.2 equivalents of nitrate there is no chemical shift change of the pyridyl-H observed, and after this point a titration isotherm is observed which follows the same curvature as that for the halide anions, but with a much smaller overall chemical shift change. In calculation of binding constants, using HypNMR 2006[165] for the oxo-anions, the points which either don't shift or show an upfield chemical shift at the start of the titration are discounted, and the zero point is taken as being the where the resonance takes a downfield shift, so that approximate binding constants could be calculated. As halide anions appear to bind to **4.10**, rather than the impurities the binding constants are calculated from the addition of the first aliquot of anion. Binding in hosts **4.4** and **4.8** is strongest with chloride, followed by bromide, binding with both a 1:1 and 2:1 stoichiometric model, but **4.10** shows a greater affinity for bromide over chloride, both in a 1:1 and 2:1 stoichiometric models. This could be explained by the increased steric bulk of this molecule compared to **4.4** and **4.8**.

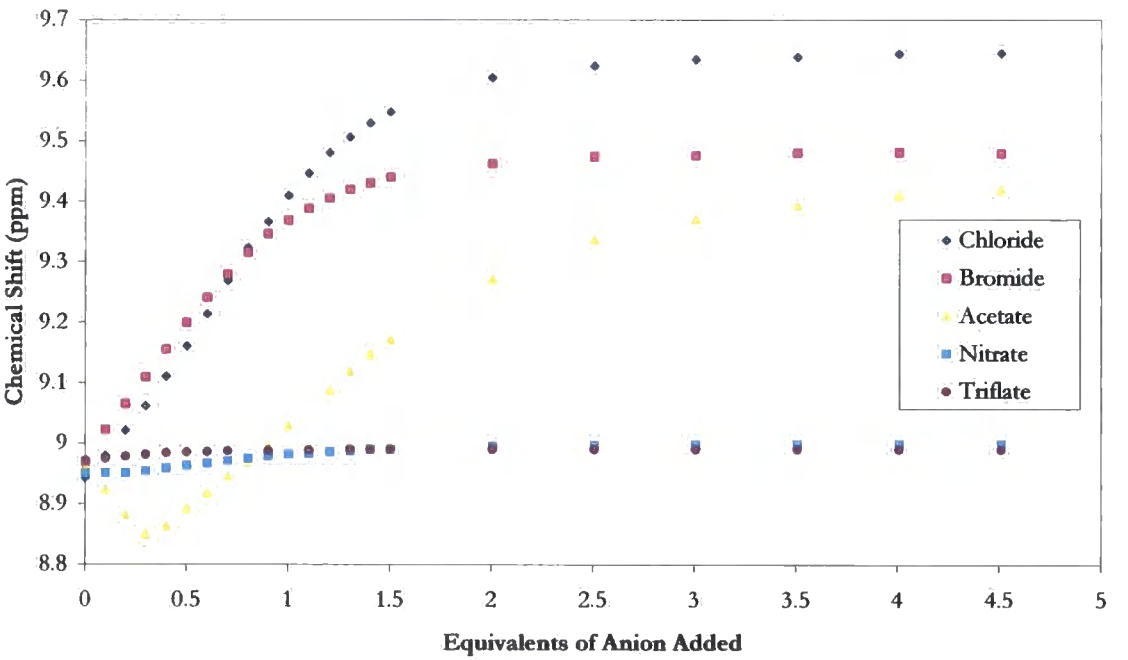

Figure 4.10: Titration data showing chemical shifts of the Pyridyl-H resonances for **4.10**

The proposed 2:1 host : guest stoichiometry was confirmed by Job's plot analysis for **4.4** binding Br^- which gave a maximum of 0.66, **figure 4.11** Furthermore an ESI mass spectrum of **4.4** in the presence of 0.5 equivalents of NBu_4Br gave a peak at m/z 1357, corresponding to $[(\mathbf{4.4})_2Br]^+$. Job plot analysis of the corresponding chloride complex suggests a strong preference for 1:1 binding, which is confirmed by the binding constants, as the second binding constant is presumably much smaller than the first. The single formal charge on the host presumably allows two hosts to fit around a single anion without severe electrostatic repulsion.

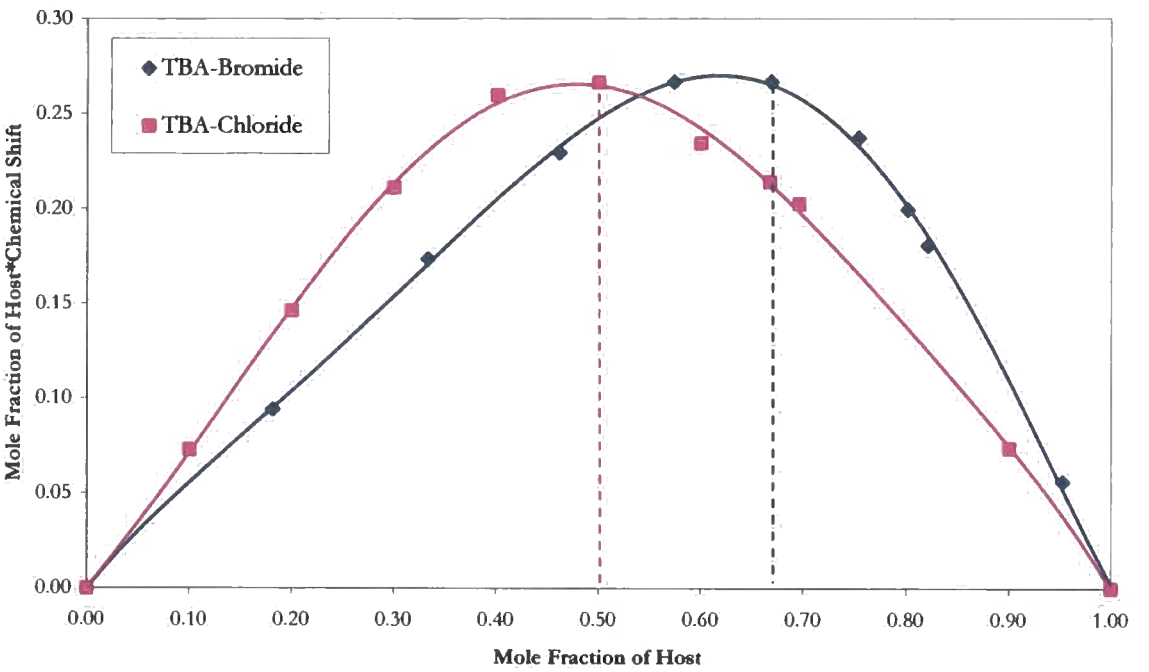

Figure 4.11: Job's Plot with Bromide and Chloride for **4.4**

Interestingly, virtually no displacement of the unidentate pyridyl ligands was observed during the titrations even in the presence of nucleophilic anions such as Cl^-, in contrast to previous work on 3-aminopyridine derivatives.[160] **Figure 4.12**, shows the conversion from the monocationic host, **4.4** to the monoadduct, **4.3** as a function of time after the addition of one equivalent of chloride, as the tetrabutylammonium salt. After one hour, a very small amount of **4.3** appears, this is slightly more obvious after 5 hours, when about 10 % has converted to **4.3**. After the solution has been left for a further 10 hours, about 30 % of the mixture is the monoadduct, **4.3**. After approximately 40 hours there is a

60:40 mixture of **4.4** : **4.3**, and after 64 hours there is more of the monoadduct, **4.3** than the moncationic, **4.4** host present in solution. The chemical shift of the peaks for **4.4**, after 64 hours, seems to be concentration dependent, as the amount of **4.4** decreases compared to the amount of **4.3** present, an upfield shift is seen in this resonance.

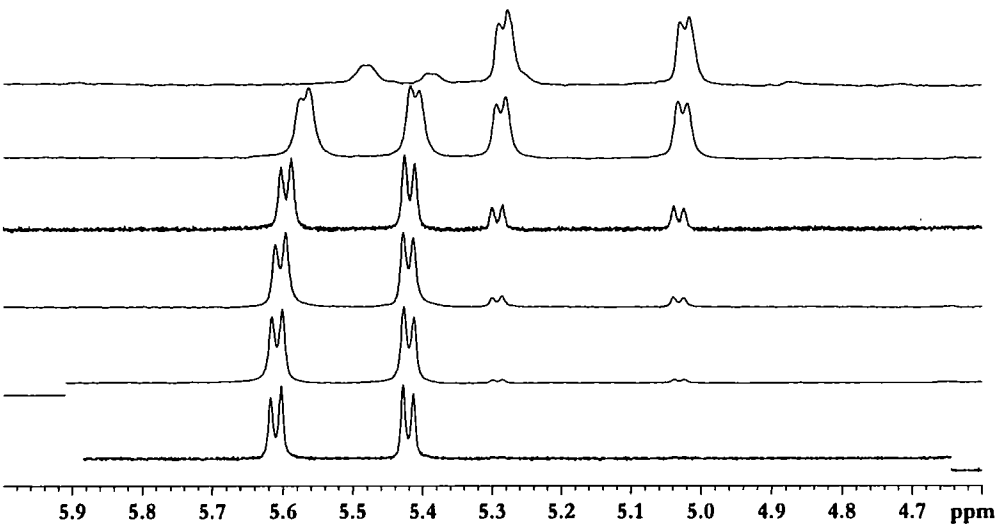

Figure 4.12: ^{1}H NMR spectra of the methylene region of host **4.4** as a function of time after addition of chloride (bottom to top 0, 1, 5, 15, 40, 64h after addition of 1 equivalent of chloride).

The titration results reveal that control compounds **4.3** and **4.9** do not bind anions, while a very small affinity is noted for the more acidic hydrogen bond donor **4.7**. Compounds **4.4** and **4.8** are both effective anion hosts, however, with the nitro-substituted **4.8** consistently binding more strongly than **4.4**. Titrations with HSO_4^- and $H_2PO_4^-$ resulted in precipitation in the case of **4.8** and small chemical shift changes for **4.4**. The hosts are moderately selective for chloride and acetate, consistent with anion basicity.

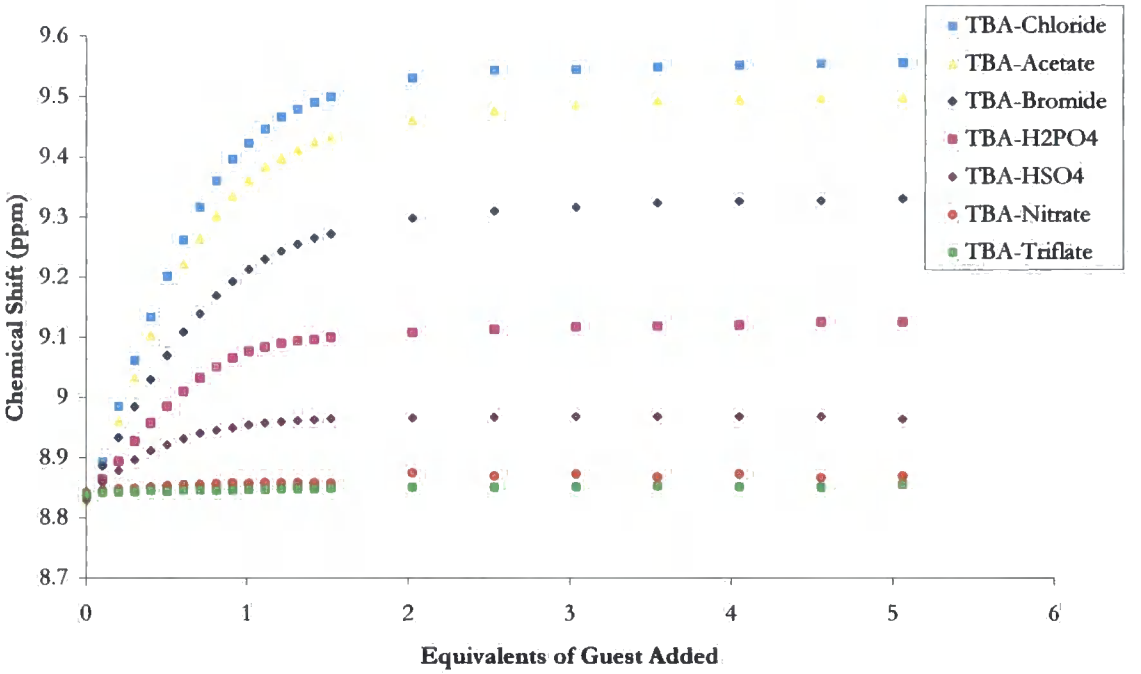

Figure 4.13: Titration data showing chemical shifts of the Pyridyl-H resonances for **4.4**

Surprisingly, monitoring the appearance of the ^{1}H NMR resonance assigned to the methylene protons H^a and H^b as a function of added anion showed that addition of strongly bound anions that are good hydrogen bond acceptors rapidly results in the collapse of this resonance to a singlet, for all the hosts tested, **4.4**, **4.8**, and **4.10**. In contrast, weakly interacting anions such as $CF_3SO_3^-$ do not affect the appearance of the resonance even after the addition of a fivefold excess, **Figure 4.14**. In the absence of added anion, the methylenic protons H^a and H^b are inequivalent and appear as a geminal AB quartet with added coupling to the NH proton just visible. Addition of strongly bound anions such as Br^- results in the collapse of the resonance to a singlet after *ca.* one equivalent. Analogous titration with weakly bound anions such as $CF_3SO_3^-$ results in the persistence of the AB quartet to at least 5 equivalents of added anion.

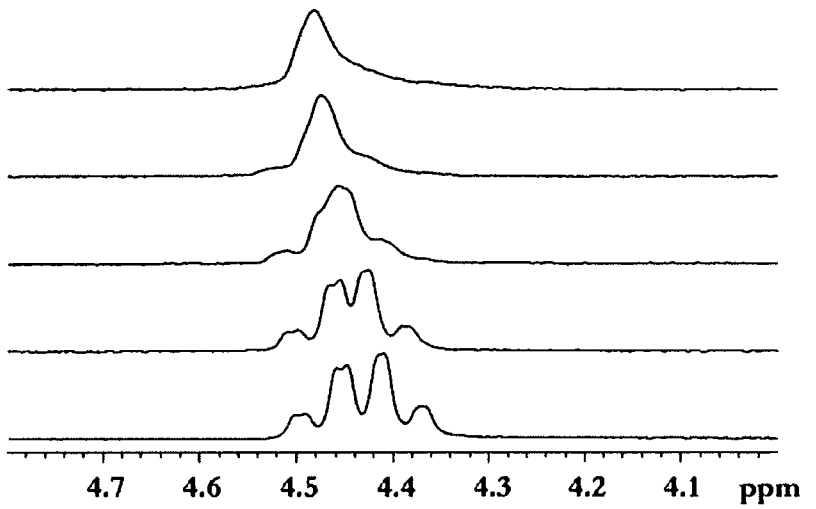

(a)

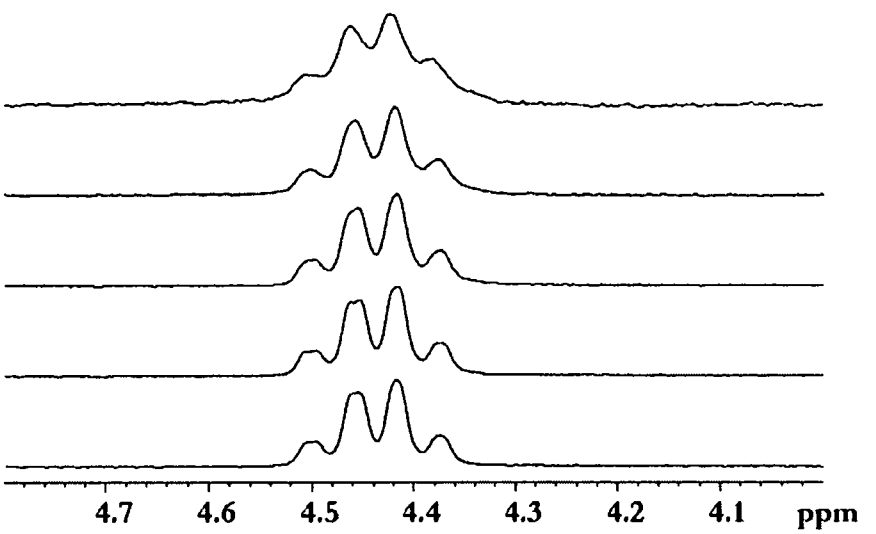

(b)

Figure 4.14: ^{1}H NMR spectra of the methylene region of host **4.4** as a function of (a) added $NBu_4^+Br^-$ and (b) added $NBu_4^+CF_3SO_3^-$ (bottom to top 0, 0.2, 0.5, 1.0 and 5.0 equivalents of anion).

In all cases more equivalents of anion are required to collapse the AB quartet to a singlet for **4.8** than for **4.4** and the number of equivalents required approximately inversely correlates with the anion binding affinity, thus a singlet methylene resonance is observed for **4.4** upon addition of only 0.4 equivalents of Cl^-, while 0.8 equivalents of acetate and two equivalents of nitrate are required. It took approximately twice as many equivalents

of anion to collapse the AB quartet to a singlet for **4.10** than for both **4.4** and **4.8**, **table 4.2.**

Anion	Number of Equivalents of Anion (Required to Collapse AB Quartet to Singlet)		
	4.4	**4.8**	**4.10**
Cl^-	0.4	0.6	2.0
Br^-	0.6	1.1	2.0
NO_3^-	2.0	>5	4.0
$CF_3SO_3^-$	>5	>5	>5
$MeCO_2^-$	0.8	1.3	1.5

Table 4.2: Number of equivalents of anion added to a solution of host **4.4**, **4.8** and **4.10** required for the AB quartet to collapse to a singlet.

The anion binding equilibria observed for complexes **B** are summarised in **Scheme 4.2.** In order to remove the inequivalence of protons H^a and H^b in complexes **B**, anion binding must induce a time-averaged plane of symmetry running along the N-Ru-N axis or involve temporary dissociation of the pyridyl ligand. The latter explanation seems relatively unlikely because we have shown that the displacement of ligand to form **4.4** in the presence of chloride takes hours to days (*vide supra*). The magnetic equivalence is also unlikely to occur by anion association to form a transient 20-electron complex since this would not result in increased symmetry in any case other than Cl^- binding. Chloride loss to form a transient 16-electron species is, however, possible and would result in the required symmetry. Thus we tentatively suggest that the evidence is consistent with strong anion association in hosts **B** leading to increased lability of the coordinated chloride ligand as a result of electrostatic repulsion, such that in the presence of tightly bound anions X^- the complex is rapidly interconverting between the 18-electron $[Ru(\eta^6\text{-}C_6H_4MeCHMe_2)Cl(\mathbf{2.1} - \mathbf{2.6})_2]^+\cdot X^-$ and the transient 16-electron $[Ru(\eta^6\text{-}C_6H_4MeCHMe_2)(\mathbf{2.1} - \mathbf{2.6})_2]^{2+}\cdot X^-\cdot Cl^-$. Sixteen electron Ru(II) compounds such as $[RuCl_2(PPh_3)_3]$ are well known in the literature.[166]

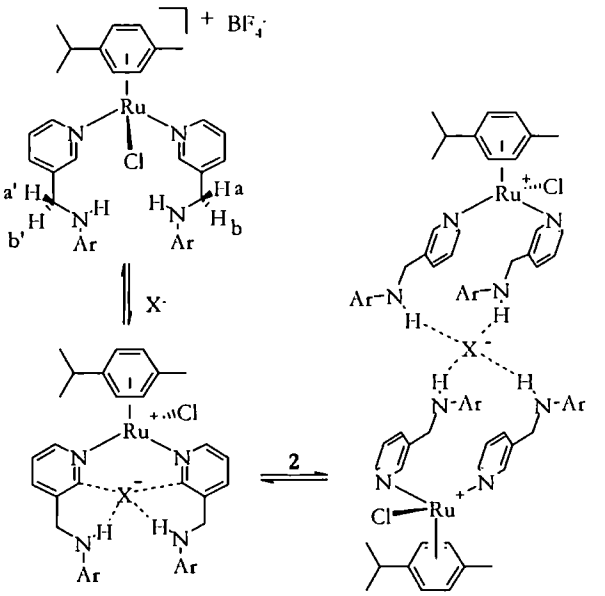

Scheme 4.2: Anion binding by complex **B** forms both 1:1 and 2:1 host:guest complexes.

4.3 Photophysical Binding Studies

Previous work discussed in chapter three, showed the fluorescent properties of ligand **2.6**, and this section now focuses on an extension of this work to measure the fluorescence of these compounds, **4.9** and **4.10**, in acetonitrile, and the effects adding anions to these compounds has on the emission. The fluorescence of the ligand, **2.6**, was compared with that of the monosubstituted host, **4.9**, and the monocationic host, **4.10**, **figure 4.15**. It is seen that the emission of the ligand has been almost completely quenched by the formation of the monosubstituted host. The formation of the monocationic host, **4.10**, also results in quenching of the fluorescence compared to the free ligand, but the host is still fluorescent. It is suggested that the quenching of the fluorescence in **4.9** is due to the complexation with the ruthenium, but in **4.10** the quenching is less than in **4.9,** which could be as there are two fluorescent molecules forming this ruthenium complex, it is not possible for the ruthenium to completely quench the fluorescence of both arms. The fluorescence maybe due to a ligand to metal charge transfer (LMCT), in which the carbazole moiety is transfering charge to the ruthenium, and the addition of a second ligand, means that the ruthenium cannot accept

charge from both ligands, hence the di-substituted complex, **4.10** is emissive and the monoadduct, **4.9** is not.[167] Alternatively, it is possible that the ruthenium is transfering charge to the ligand in a metal to ligand charge transfer (MLCT).[167] The origin of the fluorescence in the free ligand, is the emission from the fluorescent carbazole moiety. In the mono-adduct host, **4.9**, the quenching of the fluorescence observed in **2.6**, might be the result of an electronic energy transfer involving the ruthenium and the excited carbazole fluorophore.[168] It is suggested that the electronic energy transfer to the ruthenium is not enough to quench the emission of both excited carbazole fluorophores in **4.10**. The emission of **4.10** is red shifted compared to that of the free ligand, **2.6**, i.e. the energy of the emission of **4.10** is lower than that of the ligand **2.6**, which maybe caused by either the lowering of the LUMO or the raising of the HOMO, compared to the uncomplexed ligand.

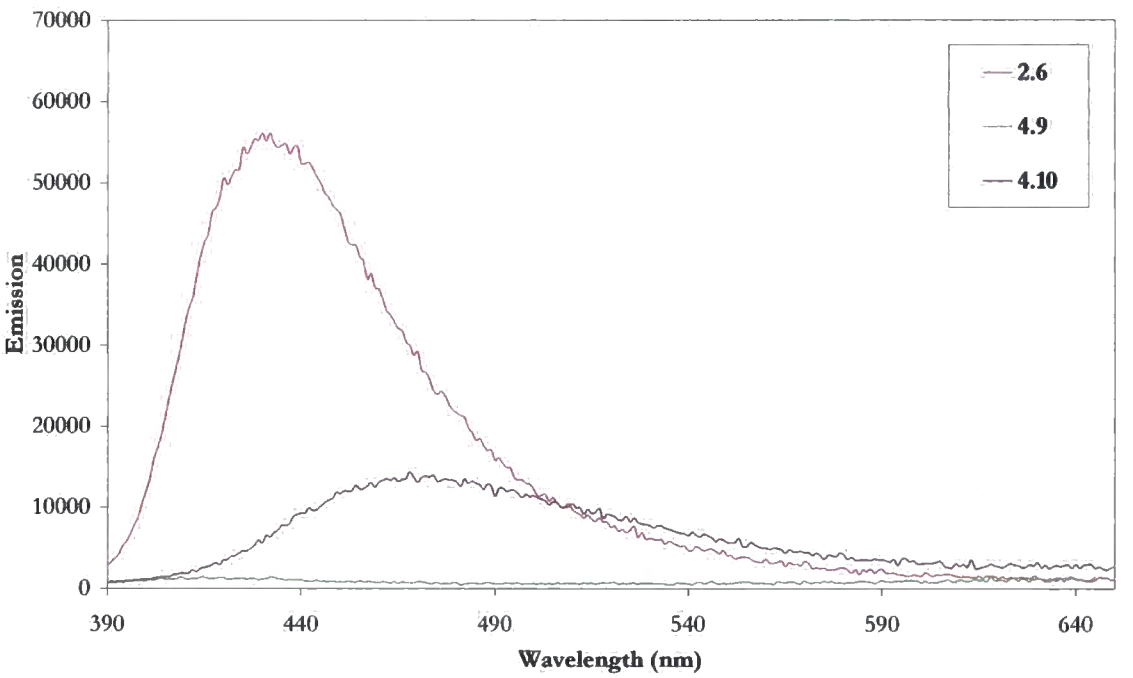

Figure 4.15: Comparison of the emission of hosts, **2.6**, **4.9** and **4.10** (1.03×10^{-4} M) in CH_3CN.

Fluorescence titration experiments were undertaken with host **4.9**, despite the host molecule not being fluorescent itself, to see if it was possible to switch on the fluorescent by the

addition of anion to a solution of the host molecule. As is seen in **figure 4.16**, upon addition of chloride, which is the anion which was measured to have the highest binding affinity by NMR spectroscopic titration experiments, the data showed that it was not possible to switch on the fluorescence of the host, **4.9**, and so no further experiments of this type were investigated with this compound.

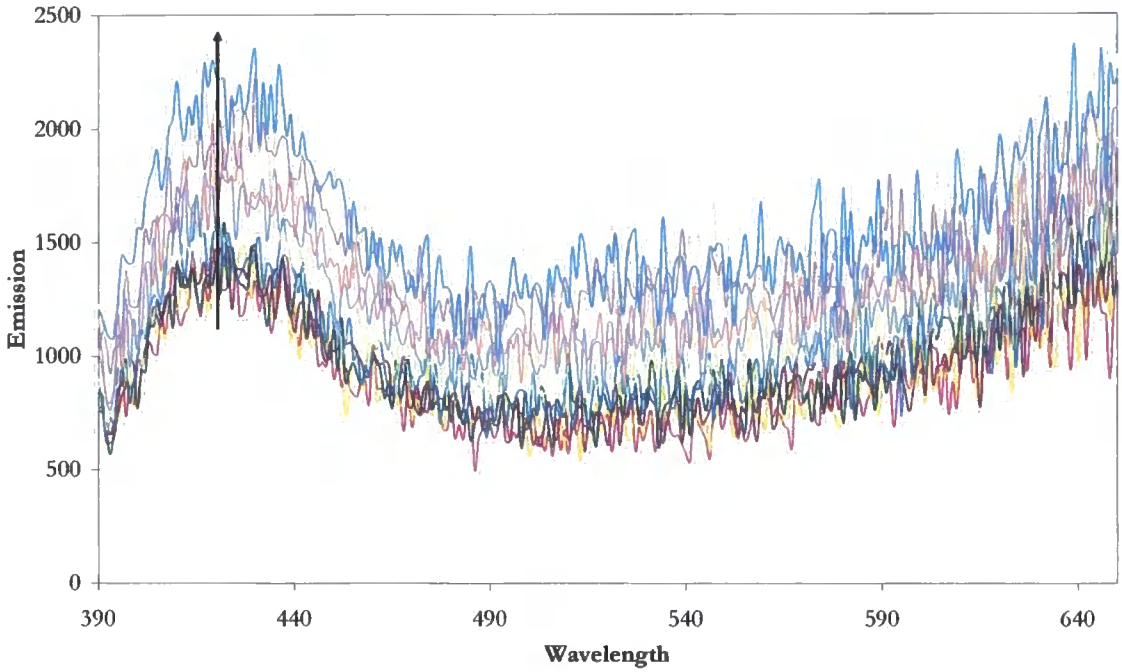

Figure 4.16: Emission spectrum of **4.9** (1.03×10^{-4} M) in CH_3CN, and upon addition of increasing amounts of chloride upto 10 equivalents.

Fluorescence titration experiments were undertaken with **4.10** and various anions as their tetrabutylammonium salts. Upon addition of chloride, as the tetrabutylammonium salt, to an acetonitrile solution of host, **4.10**, quenching of the emission of the host is seen, **figure 4.17(a)**. The addition of the first half equivalent of chloride results in the quenching of the emission of **4.10**, to about half that of the free host, **4.10**, which could be explained by the occurrence of an intra-complex electron transfer process from the electron rich chloride anion, to the photo-excited carbazole moiety. The quenching may also be a result of the formation of a complex which is less emissive than the free host, or the formation of some of the mono-adduct host, **4.9** and free ligand, **2.6**, which although was not seen during NMR spectroscopic titration experiment, has been seen for similar compounds.[160] The quenching

is accompanied by a blue shift in the emission, meaning the emission is at a higher energy, than the free host. The formation of the mono-adduct host and the free host, could be an explanation for the blue-shift observed, but an increase in the fluorescence may have been expected as the free ligand, **2.6**, is more emissive than either of the hosts, **4.9** or **4.10**. Upon addition of a further half equivalent of chloride, the emission is further quenched, and blue-shifted further, and the addition of further equivalents of chloride, results in no change in the emission. The addition of bromide, nitrate and acetate, under the same experimental conditions as for chloride also results in the quenching of the hosts fluorescence. As with the addition of the first half equivalent of chloride, the addition of the first equivalent of bromide to a solution of **4.10** results in a relatively large quenching of the fluorescence, **figure 4.17(b)**, which is further quenched by the addition of a second half equivalent of bromide. The addition of another equivalent of bromide results in a further much smaller amount of quenching, until the fluorescence no longer changes, after the addition of a total of two equivalents of bromide. The quenching of the fluorescence is also accompanied by a blue-shift in the emission, and it is proposed that the reasons for the quenching are common to both chloride and bromide. The addition of nitrate to a host **4.10** solution, results in the same three-step quenching as has been previously described for the addition of bromide, **figure 4.17(c)**. The addition of acetate to a host **4.10** solution, results in the same two-step quenching as has been explained for the addition of chloride, **figure 4.17(d)**. The addition of these four anions results in a blue-shift from 474 nm, in the free host, **4.10**, to 447 nm in the complex with chloride, bromide or acetate, but the blue shift upon addition of nitrate is less blue-shifted, shifting from 474 nm in **4.10** to 456 nm, in the nitrate complex. From this data, it is possible to propose the formation of 1:1 host : guest complex species for **4.10** and chloride or acetate, as a maximum quenching is reached after the addition of one equivalent of those anions. It is also suggested that bromide and nitrate form 1:1 host : guest complexes, as the quenching reaches a near maximum after the addition of one equivalent of anion, but that a small amount of 1:2 host : guest species may be formed. As in the cases of all the mentioned anions, chloride, bromide, nitrate and acetate, the host is quenched by a relatively large amount after the addition of half an equivalent of anion, there is some 2:1 host : guest species formed with **4.10** and the mentioned anions.

(a)

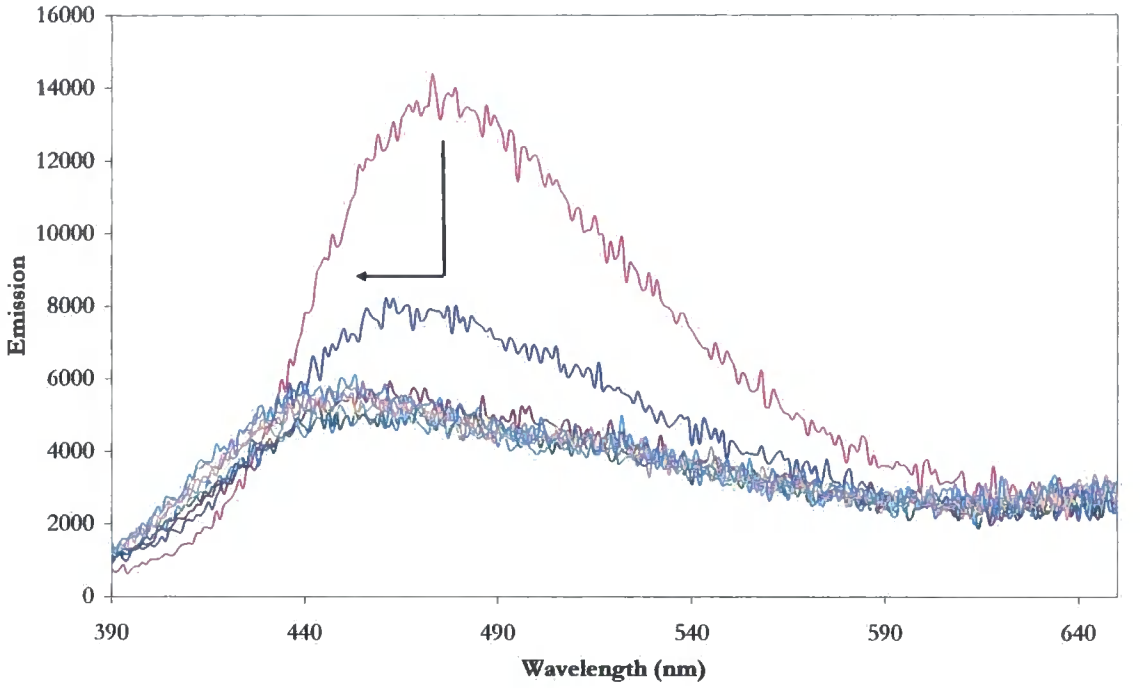
16000
14000
12000
10000
8000
6000
4000
2000
0
Emission
390
440
490
540
590
640
Wavelength (nm)

(b)

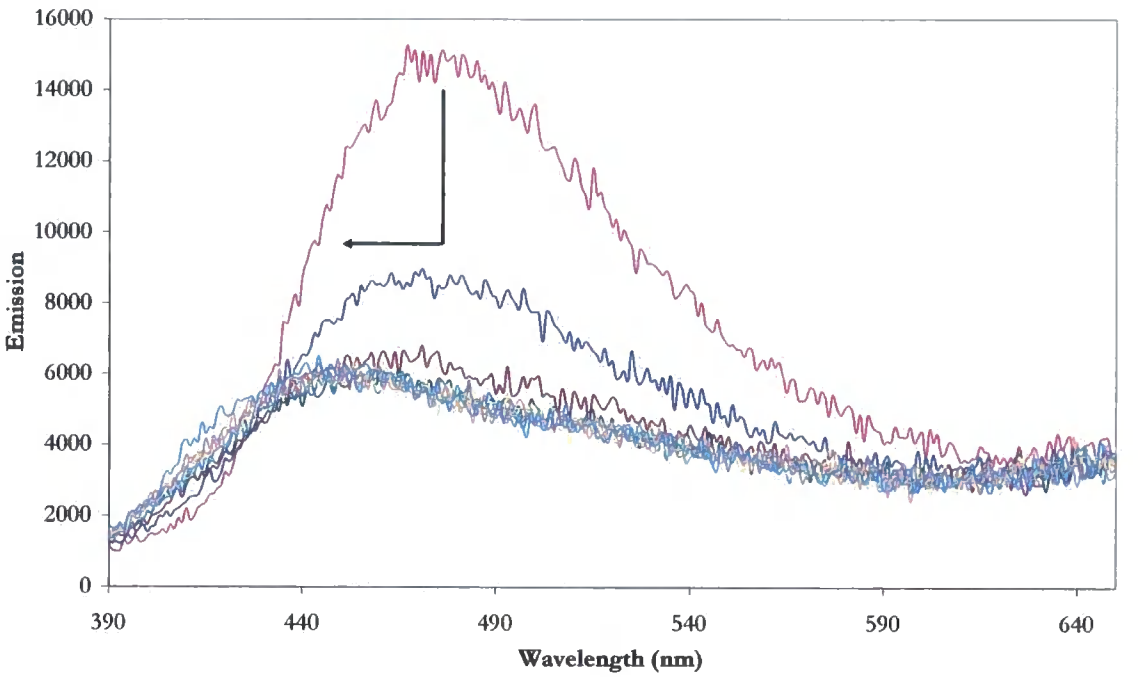
16000
14000
12000
10000
8000
6000
4000
2000
0
Emission
390
440
490
540
590
640
Wavelength (nm)

(c)

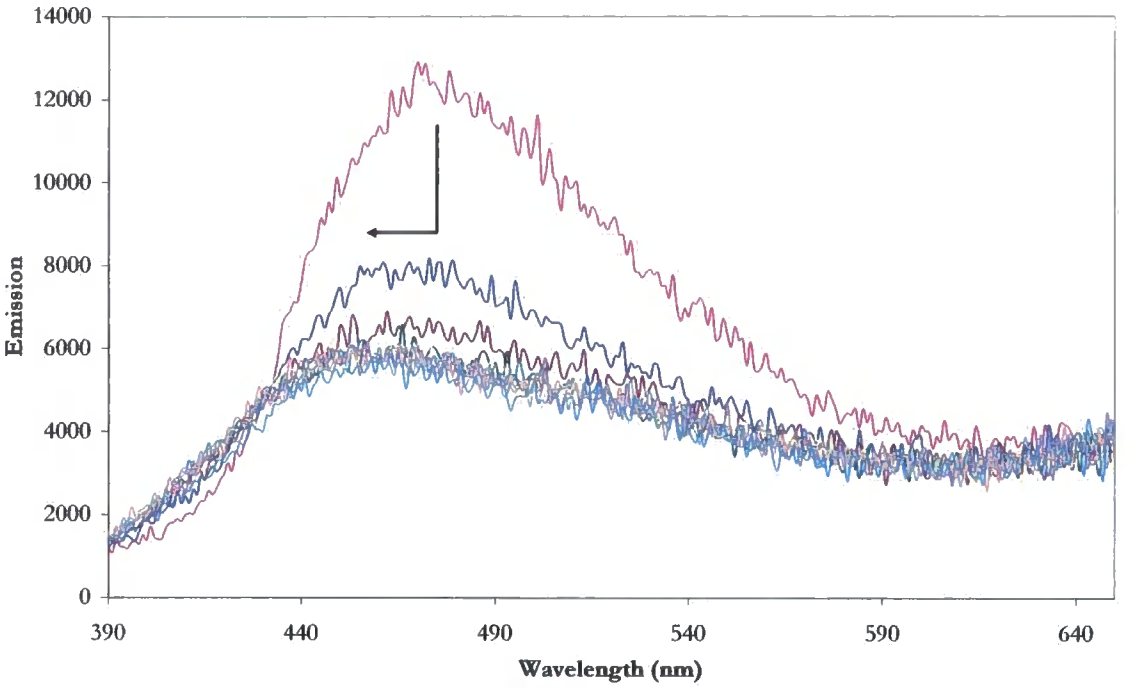

(d)

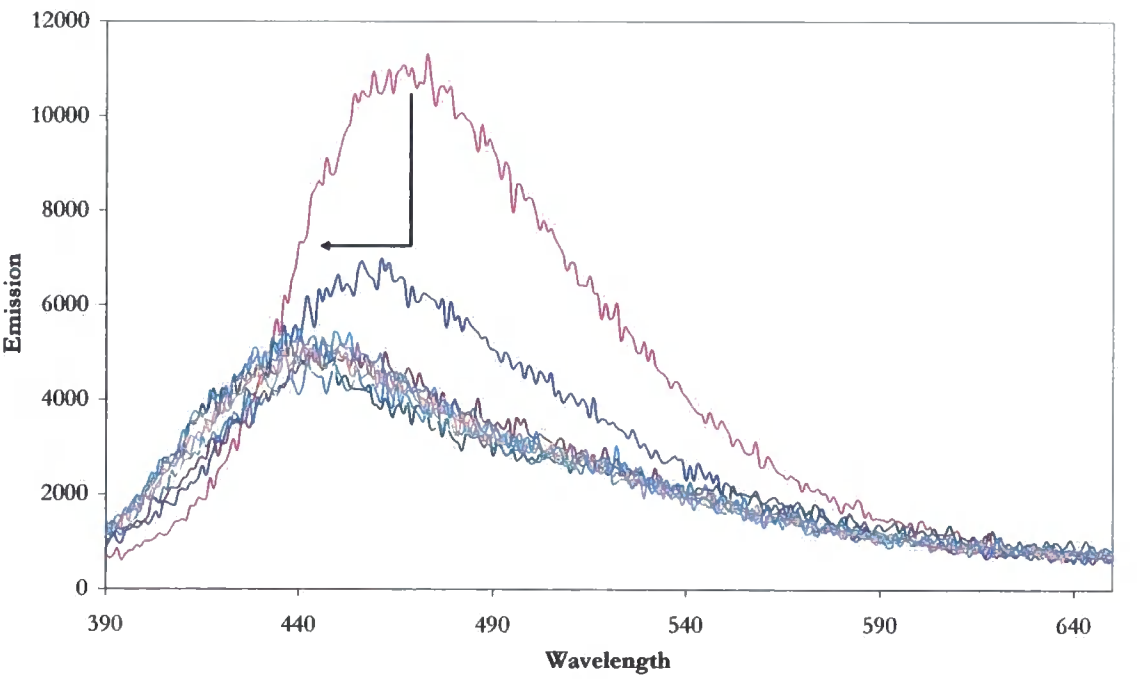

Figure 4.17: Emission spectrum of **4.10** (1.03 x 10^{-4} M) in CH_3CN and upon addition of increasing amounts of (a) chloride; (b) bromide; (c) nitrate; (d) acetate, upto 10 equivalents. Arrow indicates change in emission upon addition of increasing equivalents of anion.

Upon addition of triflate to a solution of host **4.10**, there is no quenching of the fluorescence, but a slight increase in the emission, **figure 4.18**. This could either be due to the formation of a complex, which is slightly more emissive than the host molecule, **4.10**, or that there is very little interaction between the host and guest. The maximum emission is reached after the addition of ten equivalents of triflate, but there is not rapid increase in the emission, it just gradually increases until the maximum is reached.

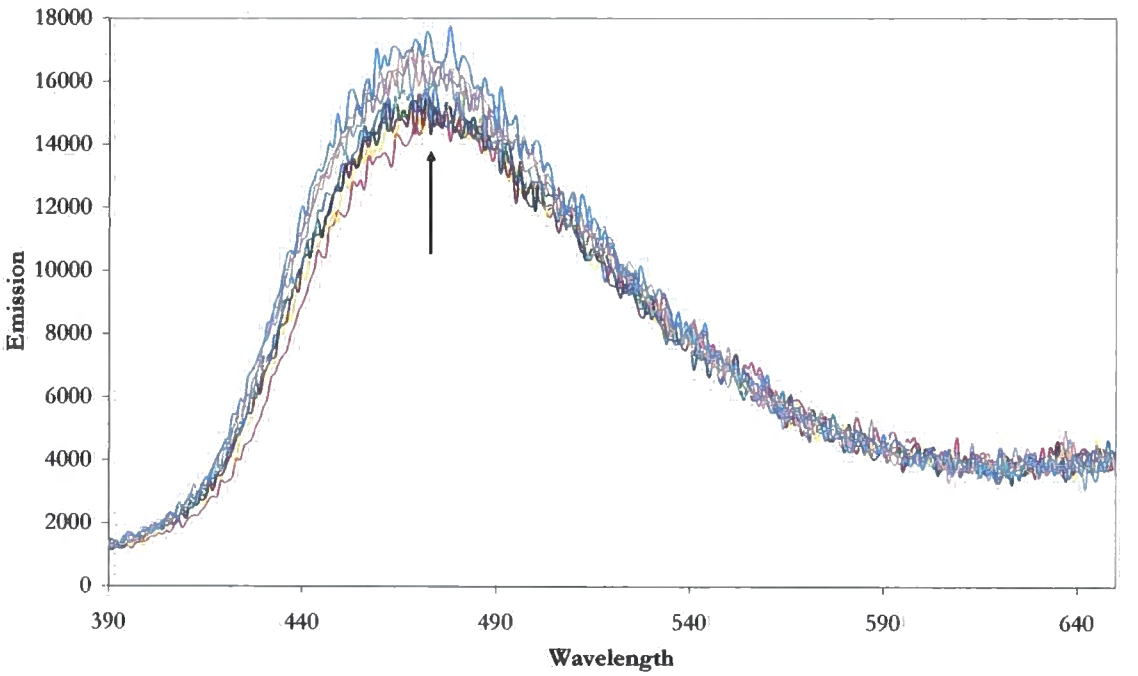

Figure 4.18: Emission spectrum of **4.10** (1.03 x 10^{-4} M) in CH_3CN and upon addition of increasing amounts of triflate upto 10 equivalents. Arrow indicates change in emission upon addition of increasing equivalents of anion. Arrow indicates change in emission upon addition of increasing equivalents of anion.

4.4 Summary

A new series of robust coordination compound hosts have been synthesised. These coordination compounds, **4.4**, **4.8** and **4.10** have shown the ability to bind a range of anions forming both 1:1 and 2:1 host:guest complexes. The host showed a particular affinity for halides and acetate, with weaker association observed for nitrate and triflate in all cases. These compounds, **4.4**, **4.8** and **4.10** exhibit a novel equilibrium in which anion binding promotes time-averaged equivalence of H^a and H^b. This time averaged equivalence of H^a and H^b is related to the strength of the anion interaction, with strongly bound anions resulting in a quicker equivalence of the protons being observed in all hosts. It is observed that host **4.10** is less emissive than the free ligand **2.6**, and the mono-substituted host **4.9**, is observed to be non-emissive. It is suggested that the reduced emission of these hosts compared to the uncomplexed ligand **2.6**, is due to a charge transfer between the ruthenium centre and the complexed ligand(s). The exact nature of this charge transfer is not clear, and it could be either due to a ligand to metal charge transfer (LMCT) or a metal to ligand charge transfer (MLCT), and the fact that the mono-substituted host **4.9** is non-emissive is due to the fact that the transfer of charge completely quenches the ligand fluorescence but the di-substituted host **4.10** is still emissive is due to the fact that either the ruthenium centre cannot accept or donate charge from both ligands. Host **4.10** has shown a quenching of the emission observed upon addition of anions, and a blue shift of this emission. The blue shift in emission maybe assigned to the co-ordination of anion resulting in a higher energy transfer. The exception of this is upon addition of triflate, which shows little change in the emission, which may be explained by considering the binding constant calculated from the NMR spectroscopic titration data, which showed little or no binding to triflate. There is no evidence of either excimer or exciplex formation upon addition of anions to this host, **4.10**. This synergic situation offers a new and, unrecognised and unutilised way to fine-tune and monitor anion binding and selectivity.

4.5 Experimental

4.5.1 General Procedure for ^{1}H NMR spectroscopic experiments

^{1}H-NMR spectroscopic titration experiments were carried out using Varian Mercury 400 spectrometer running at 400 MHz, at room temperature. All chemical shifts are report in ppm. A specific concentration of host was made up in a single NMR tube in the desired deuterated solvent (0.5 mL). The anions, as their tetrabutylammonium salts, were made up to 1 mL, 5 times the concentration of the host, with the desired deuterated solvent. 10 μL aliquots of the guest were added to the NMR tube and the spectra were recorded after each addition.

4.5.2 General Procedure for UV-Vis Experiments

UV-Vis titration experiments were carried out using a UNICAM UV-Vis spectrometer (UV2-100), which is PC-controlled using Vision software, at room temperature. A specific concentration (as indicated in figure captions) of host was made up in a single quartz cuvette in the acetonitrile (3.0 mL). The anions, as their tetrabutylammonium salts, were made up to 300 μL, 10 times the concentration of the host, in acetonitrile. 15 μL aliquots of the guest were added to the cuvette, with a path length of 1 cm and the spectra were recorded after each addition.

4.5.3 General Procedure for Fluorescence Experiments

Fluorescence titration experiments were carried out using a Fluoromax-3, which is PC-controlled, at room temperature. A specific concentration of host (as indicated in figure captions) was made up in a single quartz cuvette, with a path length of 1 cm, in the acetonitrile (3.0 mL). The anions, as their tetrabutylammonium salts, were made up to 300 μL, 10 times the concentration of the host, in acetonitrile. 15 μL aliquots of the guest were added to the cuvette, the sample was excited at 375 nm, and spectra were recorded after each addition.

[Ru(η^6-*p*-cymene)(*N*-((pyridin-2-yl)methyl)benzenamine)Cl_2]

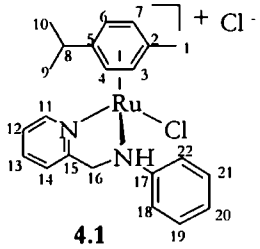

4.1

$[Ru(\eta^6\text{-}p\text{-cymene})Cl_2]_2$ (0.80 g, 1.3 mmol) and **2.1** (0.40 g, 2.2 mmol) were dissolved in toluene (100 mL), previously degassed for 1 h and left to stir at room temperature for 1 h. During this time an orange precipitate formed. The solid was collected by filtration, washed with toluene and dried in the air for 18 h (0.52 g, 1.1 mmol, 82%).

^{1}H-NMR ($CDCl_3$, 500 MHz, δ / ppm, J / Hz): 11.50 (1H, s, NH); 8.95 (1H, d, J=6.5, Pyridyl-H(H11)); 8.03 (2H, d, J=7.5, Ar-H(H18&22)); 7.82 (1H, t, J=6.5, Pyridyl-H(H13)); 7.40 (1H, t, J=6.5, Pyridyl-H(H12)); 7.39(1H, d, J=6.5, Pyridyl-H(H14); 7.38 (2H, t, J=7.5, Ar-H(H19&21)); 7.22 (1H, t, J=7.5, Ar-H(H20)); 6.40 (1H, d, J=5.5, Ar-H(H6)); 5.49 (1H, d, J=6.5, Ar-H(H4)); 5.34 (1H, d, J=6.5, Ar-H(H3)); 4.84 (1H, d, J=5.5, Ar-H(H7)); 4.55 (1H, dd, J=15.0, 5.0, CH_2(H16)); 4.30 (1H, dd, J=15.0, 10.0, CH_2(H16)) 2.80 (1H, q, J=7.0, CH(H8)); 2.25 (3H, s, CH_3(H1)); 1.15 (3H, d, J=7.0, CH_3(H9)); 0.65 (3H, d, J=7.0, CH_3(H10)).

^{13}C{^{1}H}-NMR ($CDCl_3$, 125 MHz, δ / ppm): 162.0(C17); 153.1(C11); 149.3(C15); 139.5(C13); 129.4(C18&22) 126.9(C20); 125.1(C12); 122.1(C14); 121.8(C19&21); 105.5(C5); 96.4(C2); 86.3(C6); 85.3(C4); 84.4(C7); 83.4(C3); 58.7(C16); 30.0(C8); 24.0(C9); 19.2(C10).

ES+ MS: m/z = 455 [M^+-Cl]

Anal: Calculated for $C_{22}H_{24}N_2Cl_2Ru$: C, 53.88; H, 5.34; N, 5.71; Cl, 14.46 %
Found: C, 53.52; H, 5.42; N, 5.69; Cl, 14.19 %

IR: 3382 ν(NH)

[Ru(η^6-*p*-cymene)(*N*-((pyridin-2-yl)methyl)benzenamine)Cl_2]BPh_4

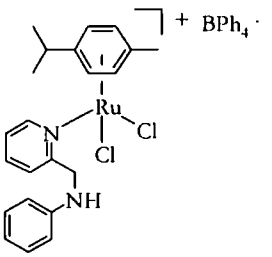

[Ru(η^6-*p*-cymene)(*N*-((pyridin-2-yl)methyl)benzenamine)Cl_2] (0.02 g, 0.041 mmol) was dissolved in methanol, and added to a methanol solution of $NaBPh_4$ (0.014 g, 0.041 mmol). A yellow precipitate was formed immediately, and collected by filtration (0.026 g, 0.032 mmol, 79 %).

Anal:	Calculated for $C_{22}H_{24}N_2Cl_2RuBPh_4$:	C, 71.36; H, 5.99; N, 3.62 %
Found:		C, 71.09; H, 6.00; N, 3.57 %

[Ru(η^6-*p*-cymene)(*N*-((pyridin-2-yl)methyl)benzenamine)Cl_2]BF_4

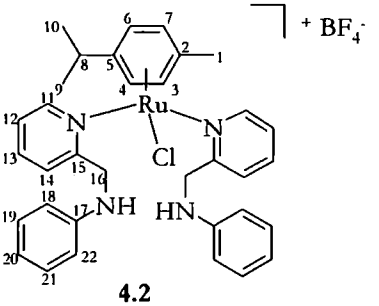

4.2

4.1 (0.4 g, 0.8 mmol), silver tetrafluoroborate (0.2 g, 0.9 mmol) and **2.1** (0.2 g, 0.8 mmol) were dissolved in 50:50 MeOH:Acetone (50 mL), previously degassed for 1 h and left to stir at room temperature for 20 min. The silver (I) chloride was removed through celite. The solvent volume was reduced under reduced pressure and the product was collected as an orange oil (0.3 g, 0.4 mmol, 44 %).

^{1}H-NMR ($CDCl_3$, 400 MHz, δ / ppm, J / Hz): 8.81 (2H, d, J=5.6, Pyridyl-H(H11); 7.85 (2H, dt, J=7.6, 1.2, Ar-H(H20)); 7.77 (2H, d, J=7.2, Pyridyl-H(H14); 7.60 (2H, d, J=7.6, Ar-H(H22)); 7.55(2H, d, J=7.6, Ar-H(H18)); 7.45 (4H, t, J=7.6, Ar-H(H19&21)); 7.28 (4H, t, J=7.2, Pyridyl-H(H12&13)); 5.65 (1H, d, J=5.6, Ar-H(H6)); 5.55 (1H, d, J=5.6, Ar-H(H4)); 5.04 (1H, d, J=5.6, Ar-H(H3)); 4.67 (1H, d, J=5.6, Ar-H(H7)); 4.35 (4H, dd, J=16, 2.8, CH_2(H16)); 2.34 (1H, q, J=6.8, CH, (H8)); 2.07 (3H, s, CH_3(H1)); 1.09 (3H, d, J=6.8, CH_3(H9)); 0.88 (3H, d, J=6.8, CH_3(H10)).

^{13}C{^{1}H}-NMR ($CDCl_3$, 125 MHz, δ / ppm): 158.3(C17); 154.4(C11); 147.6(C15); 139.8(C20); 139.7(C14); 129.8(H21); 127.5(C12&13); 126.2(C19); 123.1(C18); 119.4(C22); 105.9(C5); 97.5(C2); 85.5(C6); 84.9(C4); 84.1(C7); 83.5(C3); 59.8(C16); 30.7(C8); 22.4(C10); 21.9(C9); 17.3(C1).

ES+ MS: m/z = 639 [M^+-BF_4]

Anal: Calculated for $C_{34}H_{38}N_4ClRuBF_4$: C, 56.25; H, 5.28; N, 7.72 %
Found: C, 56.40; H, 5.56; N, 7.35 %

IR: 3161 ν(NH); 1050 ν(BF_4^-)

[Ru(η^6-*p*-cymene)(*N*-((pyridine-3-yl)methyl)benzenamine)Cl_2]

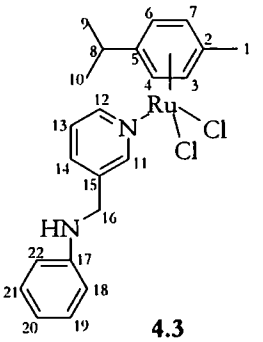

4.3

[Ru(η^6-*p*-cymene)Cl_2]$_2$ (0.4 g, 0.64 mmol) and **2.2** (0.24 g, 1.3 mmol) were dissolved in toluene (100 mL), previously degassed for 1 h and left to stir at room temperature for 1 h. During this time an orange precipitate formed. The solid was collected by filtration, washed with toluene and dried in the air for 18 h (0.57 g, 1.2 mmol, 89%)

^{1}H-NMR ($CDCl_3$, 400 MHz, δ / ppm, J / Hz): 8.95 (1H, s, Pyridyl-H(H11)); 8.89 (1H, d, J = 5.6, Pyridyl-H(H12)); 7.69 (1H, d, J = 8.0, Pyridyl-H(H14)); 7.10 (3H, m, Ar-H(H19-21)); 6.73 (1H, t, J = 8.0, Pyridyl-H(H13)); 6.57 (2H, d, J = 8.0, Ar-H(H18&22)); 5.29 (2H, d, J = 4.8, Ar-H(H4&6)); 5.03 (2H, d, J = 4.8, Ar-H(H3&7)); 4.40 (1H, bs, NH); 4.38 (2H, s, CH_2(H16)); 2.85 (1H, h, J = 6.8, CH(H8)); 1.94 (3H, s, CH_3(H1)); 1.22 (6H, dd, J = 6.8, 1.6, CH_3(H9&10)).

^{13}C{^{1}H}-NMR ($CDCl_3$, 125 MHz, δ / ppm): 154.1 (C17); 153.4(C15); 136.9(C11); 136.5(C12); 129.6(C19-21); 124.5(C14); 118.4(C13); 113.4(C18&22); 103.6(C5); 97.4(C2); 83.0(C4&6); 82.4(C3&7); 45.1(C16); 30.8(C8); 22.5(C9&10); 18.3(C1).

ES+ MS: m/z = 489 [M^+]

Anal: Calculated for $C_{22}H_{26}N_2Cl_2Ru$: C, 53.88; H, 5.34; N, 5.71 %
Found: C, 53.71; H, 5.34; N, 5.62 %

IR: 3352 ν(NH)

[Ru(η^6-*p*-cymene)(4-nitro-*N*-((pyridin-3-yl)methyl)benzenamine)$_2$Cl]BF$_4$

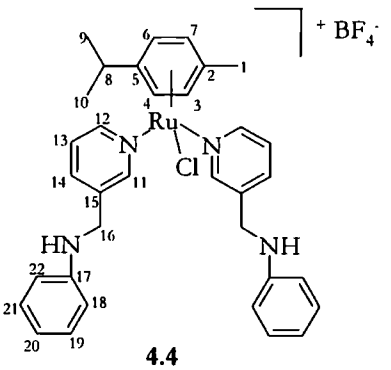

4.4

4.3 (0.4 g, 0.8 mmol) and silver tetrafluoroborate (0.16 g, 0.8 mmol) were dissolved in 50:50 MeOH:Acetone (50 mL), previously degassed for 1 h and left to stir at room temperature for 20 min. The silver (I) chloride was removed through celite and **2.2** (0.15 g, 0.8 mmol) was added to the MeOH:Acetone solution and stirred for a further 4 hours. The solvent was removed under reduced pressure to yield a crude orange solid, which was re-crystallised from CH_2Cl_2 and C_6H_{14}. The orange solid was filtered and washed with C_6H_{14}, and dried in air (0.3 g, 0.4 mmol, 56 %)

^{1}H-NMR ($CDCl_3$, 400 MHz, δ / ppm, J / Hz): 8.76 (2H, s, Pyridyl-H(H11)); 8.38 (2H, d, J = 5.8, Pyridyl-H(H12)); 7.54 (2H, d, J = 7.6, Pyridyl-H(H14)); 7.0 (6H, m, Ar-H(19 - 21)); 6.55 (2H, t, J = 7.6, Pyridyl-H(H13)); 6.42 (4H, d, J = 7.6, Ar-H(H18&22)); 5.37 (2H, bs, NH); 5.29 (4H, q, J = 18.7, 6.2, Ar-H(H3 - 7); 4.40 (2H, d, J =17.2, CH_2(H16)); 4.32 (2H, d, J =17.2, CH_2(H16)); 2.28 (1H, h, J = 6.8, CH(H8)); 1.59 (3H, s, CH_3(H1)); 0.83 (6H, d, J = 6.8, CH_3(H9&10)).

^{13}C{^{1}H}-NMR ($CDCl_3$, 125 MHz, δ / ppm): 154.1(C17); 151.2(C15); 139.0(C11); 138.1(C12); 129.5(C19-21); 125.1(C14); 117.3(C13); 112.9(C18&22); 102.6(C5); 102.4(C2); 90.5(C4&6); 81.2(C3&7); 44.5(C16); 30.9(C8); 22.6(C9&10); 17.6(C1).

ES+ MS: m/z = 639 [M-BF_4^-]

Anal: Calculated for $C_{34}H_{38}N_4ClRuBF_4$: C, 56.25; H, 5.28; N, 7.72 %
Found: C, 55.86; H, 5.22; N, 7.63 %

IR: 3421 ν(NH); 1062 ν(BF_4^-)

[Ru(η^6-*p*-cymene)(*N*-((pyridin-4-yl)methyl)benzenamine)Cl_2]

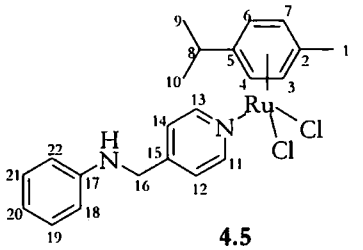

4.5

[Ru(η^6-*p*-cymene)Cl_2]$_2$ (0.8 g, 1.3 mmol) and **2.3** (0.5 g, 2.7 mmol) were dissolved in toluene (100 mL), previously degassed for 1 h and left to stir at room temperature for 1 h. During this time a yellow/orange precipitate formed. The solid was collected by filtration, washed with toluene and dried in the air for 18 h (0.69 g, 1.41 mmol, 52 %).

^{1}H-NMR ($CDCl_3$, 500 MHz, δ / ppm, J/ Hz): 8.87 (2H, d, J=6.5, Pyridyl-H(H11&13)); 7.3-7.1 (4H, m, Pyridyl-H (2H)(H12&14) & Ar-H (2H)(18&22)); 6.73 (1H, t, J=8.0, Ar-H(H20)); 6.51 (2H, d, J=8.0, Ar-H(H19&21)); 5.41 (2H, d, J=6.0, Ar-H(H4&6)); 5.21 (2H, d, J=6.0, Ar-H(H3&7)); 4.49 (1H, s, NH); 4.36 (2H, s, CH_2(H16)); 2.97 (1H, q, J=7.0, CH(H8)); 2.09 (3H, s, CH_3(H1)); 1.29 (6H, d, J=7.0, CH_3(H9&10)).

^{13}C{^{1}H}-NMR ($CDCl_3$, 125 MHz, δ / ppm): 154.7(C17); 147.3(C15); 129.6(C12&14); 129.3(C18&22); 123.0(C11&13); 118.3(C20); 113.1(C19&21); 103.8(C5); 97.2(C2); 82.9(C4&6); 82.5(C3&7); 46.7(C16); 30.9(C8); 22.5(C9&10); 18.4(C1).

ES+ MS: m/z = 490 [M^+]

Anal: Calculated for $C_{22}H_{26}N_2Cl_2Ru$: C, 53.88; H, 5,34; N, 5.71 %
Found: C, 54.43; H, 5.40; N, 4.99 %

IR: 3315 ν(NH)

[Ru(η^6-*p*-cymene)(4-nitro-*N*-((pyridin-4-yl)methyl)benzenamine)$_2$Cl]BF$_4$

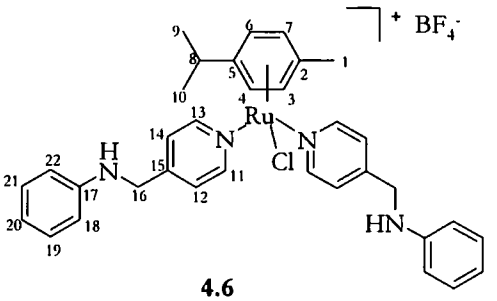

4.6

4.5 (0.4 g, 0.8 mmol), silver tetrafluoroborate (0.2 g, 0.9 mmol) and **2.3** (0.2 g, 0.8 mmol) were dissolved in 50:50 MeOH:Acetone (50 mL), previously degassed for 1 h and left to stir at room temperature for 20 min. The silver (I) chloride was removed through celite. The solvent volume was reduced under reduced pressure and the product was collected as an orange oil.

^{1}H-NMR (CDCl$_3$, 500 MHz, δ / ppm, J / Hz): 8.85 (4H, d, J=6.5, Pyridyl-H(H11&13)); 7.41 (4H, d, J=6.5, Pyridyl-H(H12&14)); 7.08 (4H, t, J=7.5, Ar-H(H19&21)); 6.67 (2H, t, J=7.5, Ar-H(H20)); 6.47 (4H, d, J=7.5, Ar-H(H18&22)); 5.84 (2H, d, J=6.0, Ar-H(H4&6)); 5.59 (2H, d, J=6.0, Ar-H(H3&7)); 4.57 (2H, s, NH); 4.36 (4H, d, J=2.0, CH_2(H16)); 2.55 (1H, q, J=7.0, CH(H8)); 1.68 (3H, s, CH_3(H1)); 1.11 (6H, d, J=7.0, CH_3(H9&10)).

^{13}C{^{1}H}-NMR (CDCl$_3$, 125 MHz, δ / ppm): 154.1(11&13); 154.0(C17); 147.3(C15); 129.6(C19&21); 124.7(C12&14); 118.3(C20); 113.1(C18&22); 103.5(C5); 102.0(C2); 88.4(C4&6); 82.3(C3&7); 46.7(C16); 31.0(C8); 22.5(C9&10); 17.9(C1).

ES+ MS: m/z = 638 [M^+-BF_4]

[Ru(η^6-*p*-cymene)(4-nitro-*N*-((pyridin-3-yl)methyl)benzenamine)$_2$Cl][BF_4]

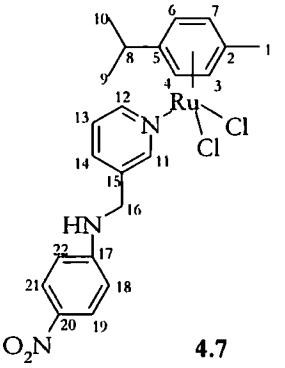

4.7

[Ru(η^6-*p*-cymene)Cl_2]$_2$ (1.0 g, 1.6 mmol) and **2.4** (0.8 g, 3.2 mmol) were dissolved in toluene (100 mL), previously degassed for 1 h and left to stir at room temperature for 1 h. During this time a yellow/orange precipitate formed. The solid was collected by filtration, washed with toluene and dried in the air for 18 h (1.2 g, 2.24 mmol, 68 %).

^{1}H-NMR ($CDCl_3$, 500 MHz, δ / ppm, J / Hz): 8.76 (1H, d, J=6.4, Pyridyl-H(H11)); 7.95 (2H, d, J=8.8, Ar-H(H19&21)); 7.45 (2H, d, J=6.4, Pyridyl-H(H12&14)); 7.07 (1H, t, J=6.4, Pyridyl-H(H13)); 6.44 (2H, d, J=8.8, Ar-H(H18&22)); 5.94 (1H, s, NH); 5.30 (2H, d, J=5.6, Ar-H(H4&6)); 5.09 (2H, d, J=5.6, Ar-H(H3&7)); 4.15 (2H, s, CH_2(H16)); 2.81 (1H, q, J=6.8, CH(H8)); 1.61 (3H, s, CH_3(1)); 1.18 (6H, d, J=6.8, CH_3(H9&10)).

^{13}C{^{1}H}-NMR ($CDCl_3$, 125 MHz, δ / ppm): 153.8(C20); 153.3(C17); 152.8(C15); 138.5(C12&14); 136.8(C11); 126.5(C19&21); 124.5(C13); 111.8(C18&22); 103.9(C5); 97.3(C2); 82.9(C4&6); 82.5(C3&7); 44.1(C16); 30.9(C8); 22.4(C9&10); 18.4(C1).

ES+ MS: m/χ = 535 [M^+]

Anal: Calculated for $C_{22}H_{25}N_3O_2Cl_2Ru$: C, 49.35; H, 4.71; N, 7.85 %
Found: C, 50.39; H, 4.70; N, 8.92 %

IR: 3238 ν(NH)

[Ru(η^6-*p*-cymene)(4-nitro-*N*-((pyridin-3-yl)methyl)benzenamine)$_2$Cl][BF$_4$]

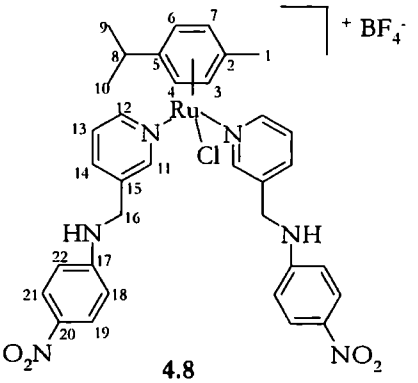

4.8

4.7 (0.3 g, 0.6 mmol), silver tetrafluoroborate (0.2 g, 0.9 mmol) and **2.4** (0.2 g, 0.8 mmol) were dissolved in 50:50 MeOH:Acetone (50 mL), previously degassed for 1 h and left to stir at room temperature for 20 min. The silver (I) chloride was removed through celite. The solvent volume was reduced under reduced pressure and the product recrystallised in the freezer from MeOH:Acetone:Diethyl Ether solution overnight. During this time an orange solid formed and was collected by filtration and washed with ether (0.1 g, 0.2 mmol, 33 %).

^{1}H-NMR (CDCl$_3$, 500 MHz, δ / ppm, J / Hz): 8.84 (2H, s, Pyridyl-H(H11)); 8.54 (2H, d, J=5.5, Pyridyl-H(H12)); 7.98 (4H, d, J=9.0, Ar-H(H19&20)); 7.63 (2H, d, J=5.5, Pyridyl-H(H14)); 7.12 (2H, t, J=5.5, Pyridyl-H(H13)); 6.67 (2H, s, NH); 6.49 (4H, d, J=9.0, Ar-H(H18&22)); 5.47 (2H, d, J=6.0, Ar-H(H4&6)); 5.44 (2H, d, J=6.5, Ar-H(H3&7)); 4.57 (2H, dd, J=7.0, 17.0, CH_2(H16)); 4.49 (2H, dd, J=7.0, 17.0, CH_2(H16)); 2.30 (1H, q, J=7.0, CH(H8)); 1.56 (3H, s, CH_3(H1)); 0.85 (6H, d, J=7.0, CH_3(H9&10)).

^{13}C{^{1}H}-NMR (CDCl$_3$, 125 MHz, δ / ppm): 153.7(C20); 152.6(C11); 151.9(C12); 138.4(C14); 138.1(C17); 137.4(C15); 126.4(C19&21); 125.2(C13); 111.6(C18&22); 102.8(C5); 102.3(C2); 90.2(C4&6); 44.2(C16); 30.8(C8); 22.4(C9&10); 17.7(C1).

ES+ MS: m/z = 815 [M$^+$]

Anal: Calculated for $C_{34}H_{36}N_6O_4ClRuBF_4$: C, 50.04; H, 4.45; N, 10.30 %
Found: C, 50.35; H, 4.86; N, 10.38 %

IR: 3390 ν(NH); 1061 ν(BF_4)

Ru(η^6-*p*-cymene)(9-ethyl-*N*-((pyridine-3-yl)methyl)-9*H*-carbazol-3-amine)Cl_2

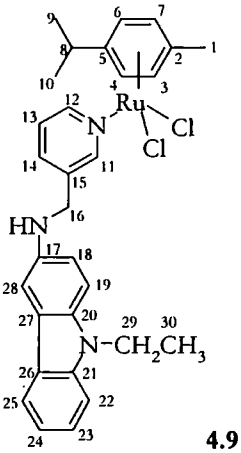

4.9

$[Ru(\eta^6\text{-}p\text{-cymene})Cl_2]_2$ (0.50 g, 0.8 mmol) and **2.6** (0.50 g, 1.7 mmol) were dissolved in toluene (100 mL), previously degassed for 1 h and left to stir at room temperature for 1 h. During this time an orange precipitate formed. The solid was collected by filtration, washed with toluene and dried in the air for 18 h (0.97 g, 1.3 mmol, 76%)

^{1}H-NMR ($CDCl_3$, 400 MHz, δ / ppm, J/ Hz): 8.94 (1H, s, Pyridyl-H(H11)); 8.80 (1H, d, J=7.6, Pyridyl-H(H12)); 7.87 (1H, d, J=8.0, Ar-H(H25)); 7.68 (1H, d, J=7.6, Pyridyl-H(H14)); 7.34 (1H, t, J=7.6, Pyridyl-H(H13)); 7.3-7.1 (5H, m, Ar-H(H18-24)) 6.80 (1H, d, J=8.0, Ar-H(H28)); 5.13 (2H, d, J=6.0, Ar-H(H3&7)); 4.86 (2H, d, J=6.0, Ar-H(H4&6)); 4.39 (2H, s, CH_2(H16)); 4.22 (2H, q, J=7.6, CH_2(H29)); 2.68 (1H, q, J=7.0, CH(H8)); 1.74 (3H, s, CH_3(H1)); 1.29 (3H, t, J=7.6, CH_3(H30)); 1.04 (6H, d, J=7.0, CH_3(H9&10)).

^{13}C{^{1}H}-NMR ($CDCl_3$, 125 MHz, δ / ppm): 154.5; 153.3; 140.5; 138.1; 137.1; 136.8; 129.3; 128.5; 125.9; 125.5; 124.5; 123.8; 122.5; 120.5; 118.4; 115.0; 109.7; 108.8(C11 – 15, C17 – 28); 103.3 (C5); 97.5(C2); 83.2(C4&6); 82.2(C3&7); 46.5(C16); 37.8(C29); 30.8(C8); 22.4(C9&10); 18.1(C1); 14.1(C30).

ES+ MS: m/z = 559 [M^+]

Anal: Calculated for $C_{30}H_{33}N_3Cl_2Ru$: C, 59.30; H, 5.47; N, 6.92
Found: C, 59.18; H, 5.61; N, 6.79

IR: 3379 ν(NH)

[Ru(η^6-*p*-cymene)(9-ethyl-*N*-((pyridine-3-yl)methyl)-9*H*-carbazol-3-amine)$_2$Cl]BF$_4$

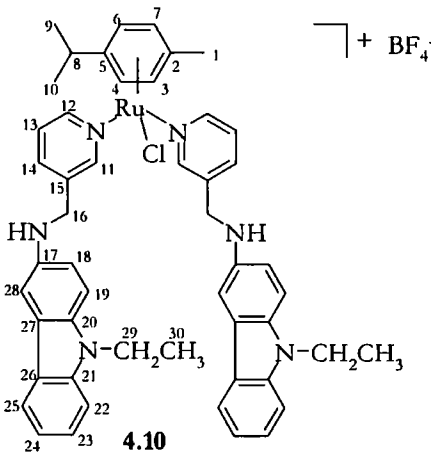

4.10

4.9 (0.5 g, 0.7 mmol) and silver tetrafluoroborate (0.15 g, 0.8 mmol) were dissolved in 50:50 MeOH:Acetone (50 mL), previously degassed for 1 h and left to stir at room temperature for 20 min. The silver (I) chloride was removed through celite and **2.6** (0.25 g, 0.8 mmol) was added to the MeOH:Acetone solution and stirred for a further 4 hours. The solvent was removed under reduced pressure to yield a crude orange oil. The oil was washed with ethanol and re-crystallised from CH_2Cl_2 and C_6H_{14}. The green solid was filtered and washed with C_6H_{14}, and dried in air. (0.13 g, 0.1 mmol, 19 %)

^{1}H-NMR ($CDCl_3$, 400 MHz, δ / ppm, J/ Hz): 8.96 (2H, s, Pyridyl-H(H11)); 8.48 (2H, d, J=5.5, Pyridyl-H(H14)); 7.88 (2H, d, J=7.5, Ar-H(H25)); 7.39 (2H, t, J=7.5, Ar-H(H24)); 7.11 (2H, t, J=7.5, Ar-H(H23)); 7.6-6.9 (12H, m, Pyridyl-H(4H)(H12&13) & Ar-H(8H)(H18, 19, 22, 28)); 5.31 (4H, s, Ar-H(H3 - 7)); 4.54 (2H, d, J=16.5, CH_2(H16)); 4.46 (2H, d, J=16.5, CH_2(H16)); 4.21 (4H, d, J=7.0, CH_2(H29)); 2.13(1H, q, J=6.5, CH(H8)); 1.46 (3H, s, CH_3(1)); 1.33 (6H, t, J=7.0, CH_3(H30)); 0.54 (6H, d, J=6.5, CH_3(H9&10)).

^{13}C{^{1}H}-NMR ($CDCl_3$, 125 MHz, δ / ppm): 153.9; 151.3; 140.4; 140.2; 139.0; 138.2; 133.9; 125.7; 125.7; 125.1; 123.7; 122.6; 120.6; 118.3; 114.6; 109.7; 109.0; 108.5; 103.0(C11-15, C17-28); 102.8(C5); 101.9(C2); 90.6(C4&6); 80.7(C3&7); 45.5(C16); 37.7(C29); 30.6(C8); 22.0(C9&10); 17.4(C1); 14.2(C30). *(Incomplete assignment due to solubility problems)*

ES+ MS: m/z = 873 [M-BF_4]

IR: 3409 ν(NH); 1060 ν(BF_4)

[Ru(η^6-hexamethylbenzene)(*N*-((pyridine-3-yl)methyl)benzenamine)Cl_2][164]

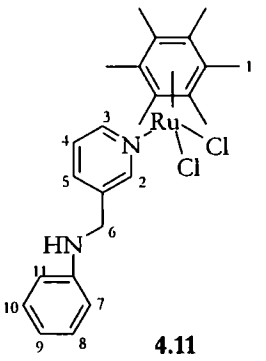

4.11

$[Ru(\eta^6\text{-}C_6Me_6)Cl_2]_2$ (0.1 g, 0.15 mmol) and **2.2** (0.049 g. 0.27 mmol) were stirred in dry toluene (20 mL) at room temperature overnight. Over this time a dark red solid precipitates from solution, and is collected by filtration. The crude product was then washed with toluene, and the pure red solid is collected by filtration (0.089 g, 0.096 mmol, 64%).

^{1}H-NMR ($CDCl_3$, 400 MHz, δ / ppm, J/ Hz): 8.71 (1H, s, Pyridyl-H(H2)); 8.62 (1H, d, J=6.0, Pyridyl-H(H3)); 7.60 (1H, d, J=6.0, Pyridyl-H(H5)); 7.17 (1H, dd, J=6.0, 1.8, Pyridyl-H(H4)); 7.09 (2H, t, J=7.5, Ar-H(H8&10); 6.65 (1H, t, J=7.5, Ar-H(H9)); 6.51 (2H, d, J=7.5, Ar-H(H7&11); 4.32 (3H, s, NH & CH_2(H6)).

4.6 Crystallographic Data

Crystal data for 4.11: $C_{24}H_{30}Cl_2N_2Ru$, M = 518.47, yellow block, 0.30 x 0.10 x 0.10 mm^3, monoclinic, space group Cc (No. 9), a = 15.291(4), b = 18.987(5), c = 8.376(2) Å, β = 94.100(7)°, V = 2425.6(11) $Å^3$, Z = 4, D_c = 1.420 g/cm^3, F_{000} = 1064, SMART 6k, MoKα radiation, λ = 0.71073 Å, T = 120(2)K, $2\theta_{max}$ = 58.4°, 19681 reflections collected, 6518 unique (R_{int} = 0.0599). Final *GooF* = 0.992, *R1* = 0.0380, *wR2* = 0.0755, R indices based on 5580 reflections with I >2sigma(I) (refinement on F^2), 268 parameters, 2 restraints. Lp and absorption corrections applied, μ = 0.879 mm^{-1}. Absolute structure parameter = 0.00(3).[169]

Chapter Five

Di and Tripodal Anion Hosts

The binding and sensing of simple anions such as chloride is particularly topical.[8, 99, 149, 150, 170-189] A typical molecular sensor involves an analyte binding moiety coupled to a signaling group such as a fluorophore or redox-active substituent *via* a spacer capable of signal transduction.[190] Alternatively a ternary indicator displacement mechanism may be employed.[191, 192] It is a double challenge to both produce selective receptors and transduce the selective binding into an observable signal. While rigidly preorganised receptors such as macrobicycles[178, 193] can give highly selective binding, effective sensing is often achieved in both natural and artificial systems by arrays of more flexible, differential receptors that respond to varying degrees to each analyte.[194-197] Flexible receptors offer the interesting possibility of *induced fit signal transduction* in which analyte binding results in a conformational change that brings about signal generation (*e.g.* Ca^{2+} binding by calmodulin[198, 199]). The interesting point about this mechanism is that it is only analytes that result in the appropriate conformational change that will result in signal generation, *even if they are not the strongest bound by the receptor.* Thus a relatively unselective receptor may still prove highly effective at sensing particular anions because of the differential conformational changes induced by different analytes. Steed *et al* have applied this concept in the redox sensing of anions[23, 101, 200] using the flexible triethylbenzene scaffold, a very versatile platform for constructing small, flexible tripodal anion and cation receptors.[55, 177, 191, 194, 196, 201-206] They have explored in detail the anion-induced conformational changes in these kinds of receptors,[2, 185] and Duan *et al.* have used conformational flexibility in these systems in both redox and fluorescent sensing.[176, 207] Steed *et al* have also examined flexible anion hosts based on inorganic cores[1, 144, 160] and recently described the extension of their work to much larger calix[4]arene scaffolds.[8] In this chapter, di- and tripodal-based fluorescent anion sensors are discussed, and compared with that of a flexible calixarene-based fluorescent anion sensor, **figure 5.1**, *synthesised by Maria Filby within the Steed group*, as well as the NMR spectroscopic binding studies of two tripodal systems based on ligands **2.2** and **2.5**, discussed in chapter two. All host have a secondary

amine linkage, enabling binding to anions via hydrogen bonding, and the addition of a fluorescent pyrene functionality to act as a sensing moiety.

5.1 Synthesis and Characterisation

Ligand **5.1** was synthesised by reacting 3-aminopyridine with 1-pyrene carboxaldehyde. The straight-forward synthetic procedure involves a condensation step followed the reduction of the imine, using $NaBH_4$ to produce a secondary amine. Reactions were carried out in dry 1,2-dichloroethane at reflux for 6 hours. The amine product, **5.1**, was recrystallised from dichloromethane and hexane, and the product was collected by filtration, as is shown in **scheme 5.1**.

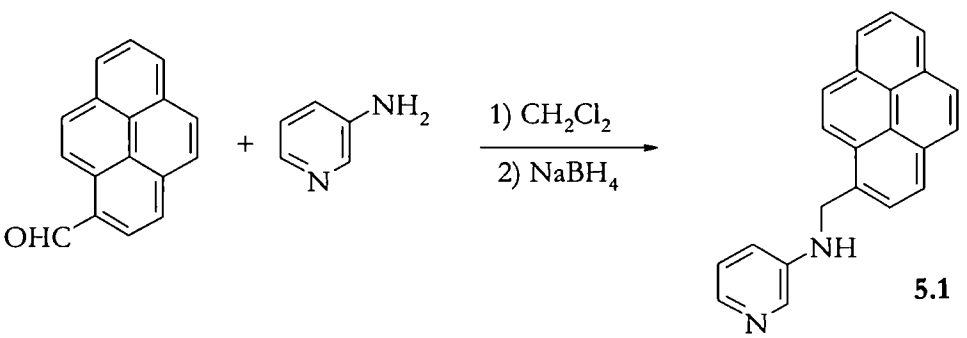

Scheme 5.1: Synthesis of Ligand **5.1**

Evidence that the reaction had gone to completion was the disappearance of the aldehyde peak from the ^{1}H-NMR spectrum, and the appearance of the broad singlet assigned to the NH resonance at 4.05 ppm. The mass spectra also agreed with the proposed structures, with a peak at m/z = 309 $[M+H]^+$ for the amine product, **5.1**. The experimental data obtained from mass spectroscopy, infra-red spectroscopy, and elemental analysis also confirm the proposed structures.

Hosts **5.2**, **5.3**, **5.4** and **5.5** were synthesised by reacting pyridyl-amine arms **5.1**, **2.2** and **2.5**, with a brominated core, either α, α'-dibromo-*p*-xylene, to give **5.2** or 1,3,5-tri(bromomethyl)-2,4,6-triethylbenzene, to give **5.3** – **5.5**.[202] Reactions were carried out in either dichloromethane, 1,2-dichloroethane or ethanol, and stirred at room temperature or reflux

for between 2 and 120 hours, **scheme 5.2**. Counter ion metathesis was undertaken to convert the bromide salts to hexafluorophosphate salts. Ammonium hexafluorophosphate was added to methanolic solutions of the bromide salts, and these were stirred for 2 hours, during which time the hexafluorophosphate salt precipitated from the solution, and was collected by filtration.

(a)

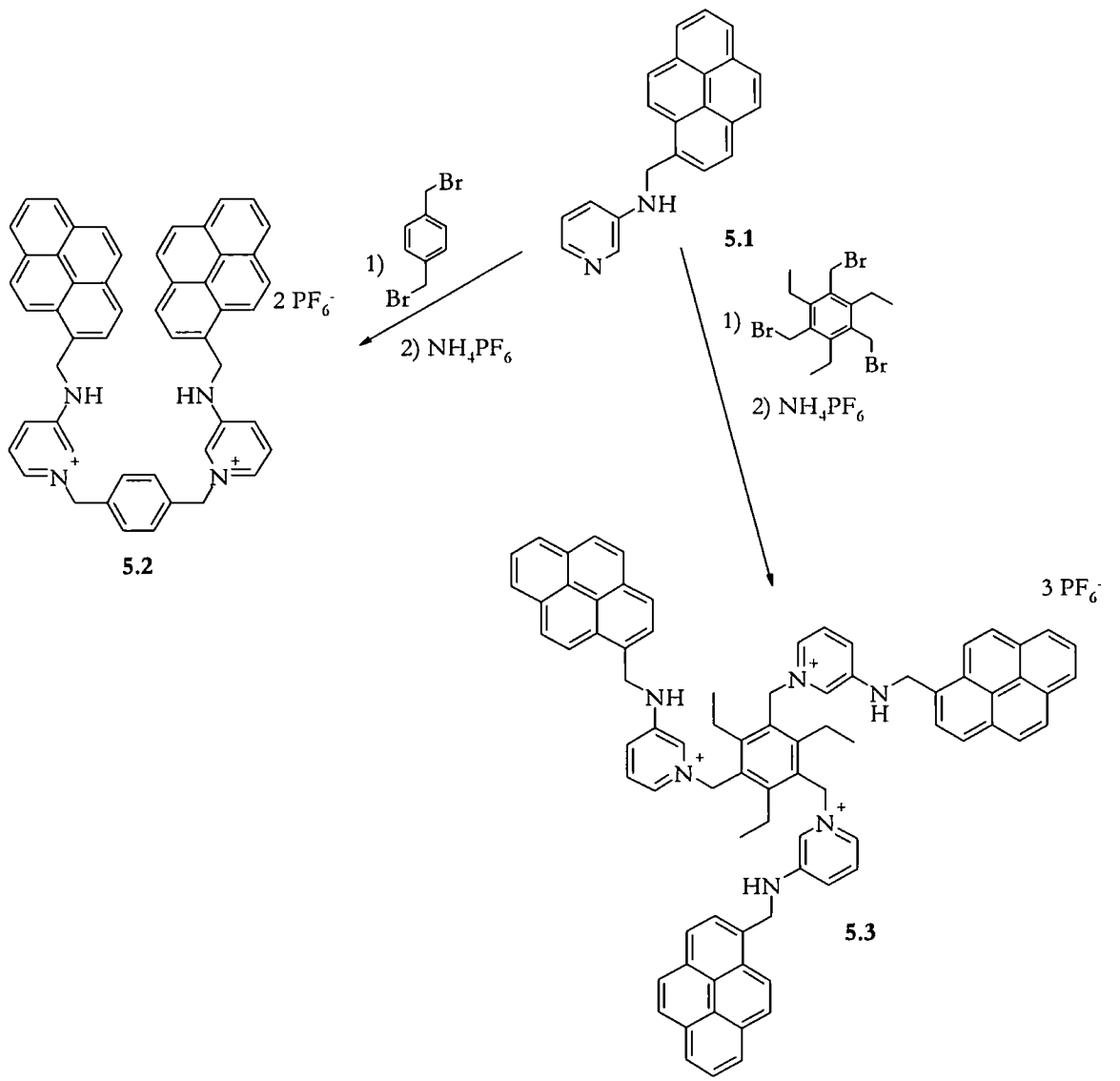

(b)

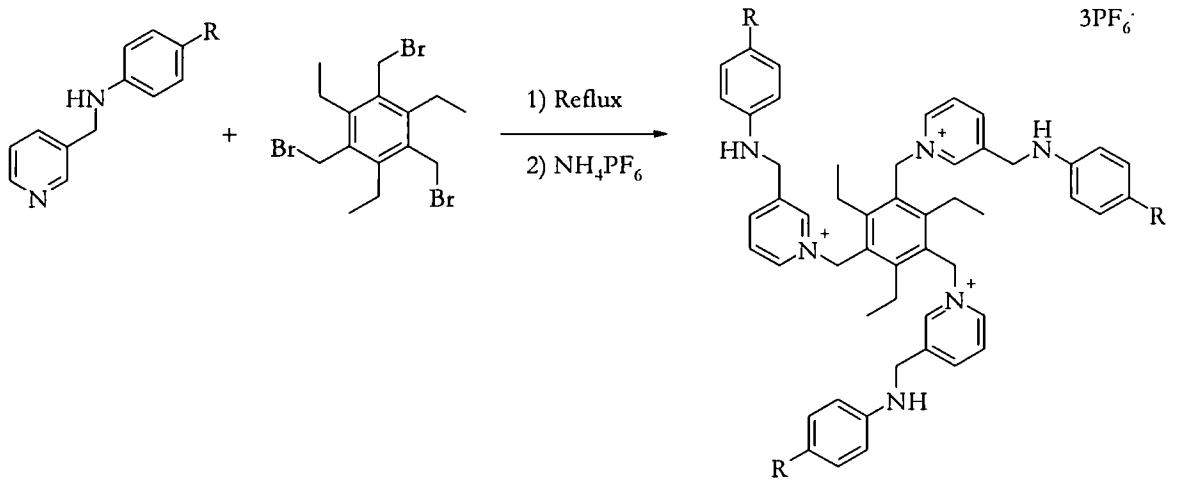

5.4 R = H
5.5 R = NO_2

Scheme 5.2: Synthesis of hosts (a) **5.2** and **5.3** (b) **5.4** and **5.5**.

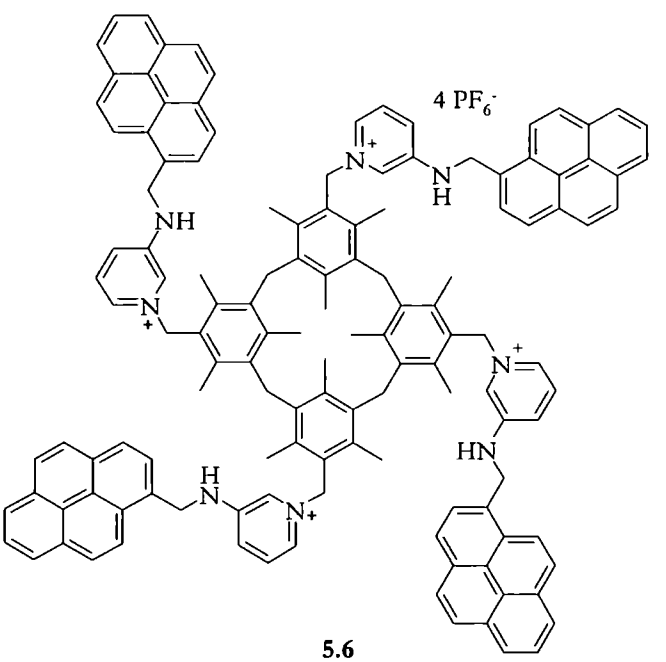

(a) **5.6**

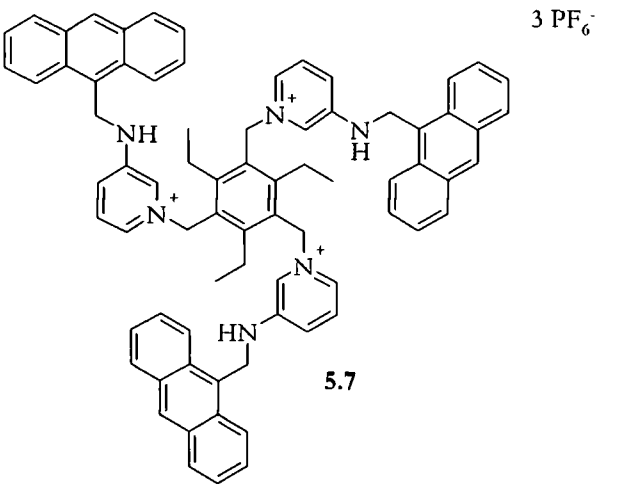

(b)

Figure 5.1: For comparison purposes (a) calix[4]arene analogous host, **5.6**[13] (b) tripodal anthracene host, **5.7**.[2]

The experimental data obtained agreed with the proposed structures, for example, the ES+ mass spectra shows a peak at m/z = 865 $[M\text{-}PF_6]^+$ and 360 $[M\text{-}2PF_6]^{2+}$ for **5.2**, 1415 $[M\text{-}PF_6]^+$, 635 $[M\text{-}2PF_6]^{2+}$ and 375 $[M\text{-}3PF_6]^{3+}$ for **5.3**, 1043 $[M\text{-}PF_6]^+$, 449 $[M\text{-}2PF_6]^{2+}$ and 251 $[M\text{-}3PF_6]^{3+}$ for **5.4**, and 1178 $[M\text{-}PF_6]^+$, 516 $[M\text{-}2PF_6]^{2+}$ and 296 $[M\text{-}3PF_6]^{3+}$ for **5.5**, confirming the fragmentation is consistent with the proposed structure in each case. The IR data also confirmed the proposed structures, with the absence of an NH stretch for the intermediate imine material of ligand **5.1**, and a characteristic NH stretch in the amine product **5.1**, at 3204 cm^{-1}. The addition of this ligand to an aromatic core, sees a significant shift in the NH stretch appearing at 3422 cm^{-1} for **5.2**, and 3419 cm^{-1} for **5.3**. The same is true upon the formation of the tripodal system substituted with **2.2**, which sees a shift in the NH from 3258 cm^{-1} in **2.2** to 3419 cm^{-1} in **5.4**, this is because in the ligands hydrogen bonding is observed between amine NH, and pyridyl N, but in the hosts this is replaced by weaker hydrogen bonding between amine NH and PF_6^-. For the nitro-substituted host **5.5**, there is no shift in the NH stretch from 3239 cm^{-1} in **2.5**, and 3239 cm^{-1} in **5.5**, which is in contrast to the other hosts. Thus it is suggested that the tripodal host is showing enhanced hydrogen bonding compared to that of the other tripodal ligands, which may be explained by hydrogen bonding between the amine NH, and the oxygen from the NO_2 group, but without more structural information, it is not possible to accurately assign the nature of this interaction.

The structure of ligand **5.1** was also confirmed by X-ray crystal analysis of crystals grown by slow evaporation from a ligand solution of dichloromethane and hexane. Hydrogen bonding is seen between the amine proton, H1N, and the pyridyl nitrogen, N1, on adjacent molecules to form 1D hydrogen bonded chains, as shown in **figure 5.2**. The hydrogen bond distances were measured, as they were in chapter two for ligands **2.2** – **2.6**. The D--H = 0.88(3) Å, H-----A = 2.22(3) Å, D------A = 3.092(4)Å and D--H-----A = 171(2)°, which when compared to the anthracene arm from the tripodal host **5.7**, H-----A = 2.23(3) Å, D------A = 3.135(3)Å are very similar, particularly the distance between the amine proton, and pyridyl nitrogen.[208] The hydrogen bond distances are also comparable to those observed for ligands **2.2** – **2.6**, **table 2.1** (Chapter Two).

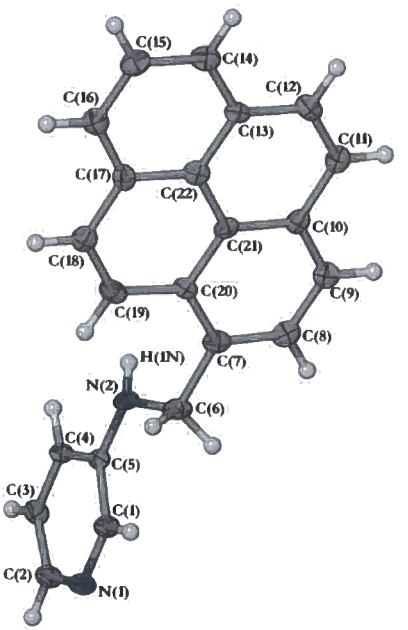

(a)

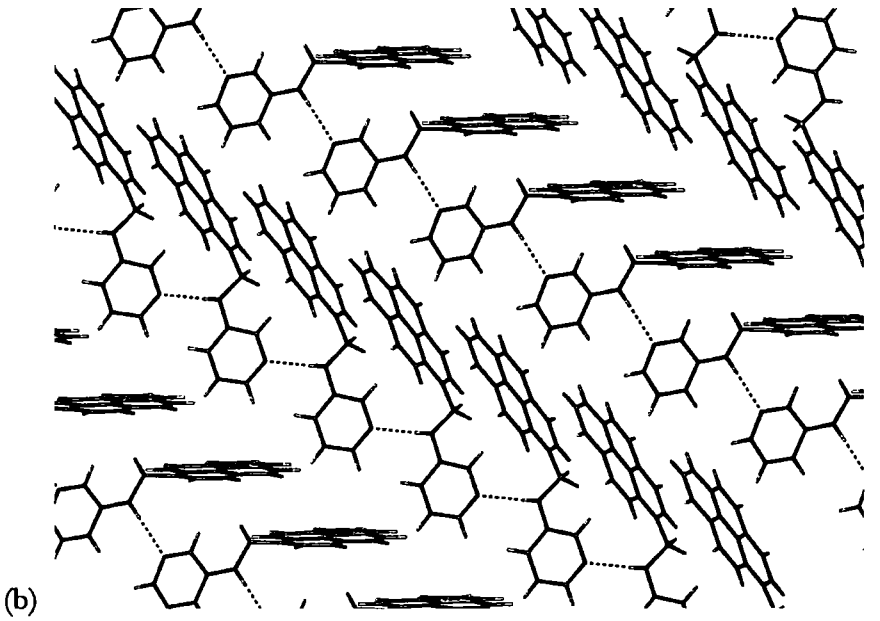

Figure 5.2: X-ray crystal structure of **5.1** (a) Asymmetric unit (ASU) of the crystal structure **5.1** Atoms shown in thermal ellipsoid representation at 50 % with labels. (b) 1D hydrogen bonded chains.

5.2 Photophysical studies

The group of Prof. Luca Prodi, University of Bologna, completed the photophysical studies of **5.2** and **5.3** as the hexafluorophosphate salts were studied in acetonitrile solution, and there anion binding abilities by photophysical methods. The results obtained are discussed here and later compared with my NMR binding studies, and those of related compounds.

The absorption spectra of **5.2**·$2PF_6^-$ and **5.3**·$3PF_6^-$ are almost superimposable, **figures 5.3** and **5.4** respectively, all showing two sets of bands in the 250-300 and in the 300-400 nm region, similar to the spectrum of pyrene itself in the same experimental conditions.[209] In these hosts, however, the absorption band in the 300-400 nm region is broader and less intense, with a small tail above 380 nm which is not present in the pyrene itself. This behaviour can be attributed to small intramolecular interactions among the different pyrene units at the ground state and/or to the occurrence of a charge transfer transition between the pyrene and the pyridinium groups.

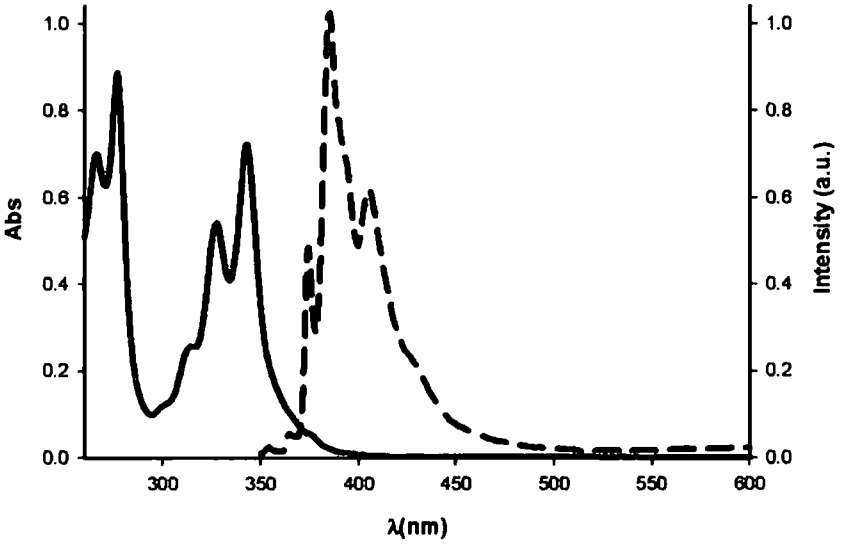

Figure 5.3: Absorbance and fluorescence spectra of **5.2** in acetonitrile solution.

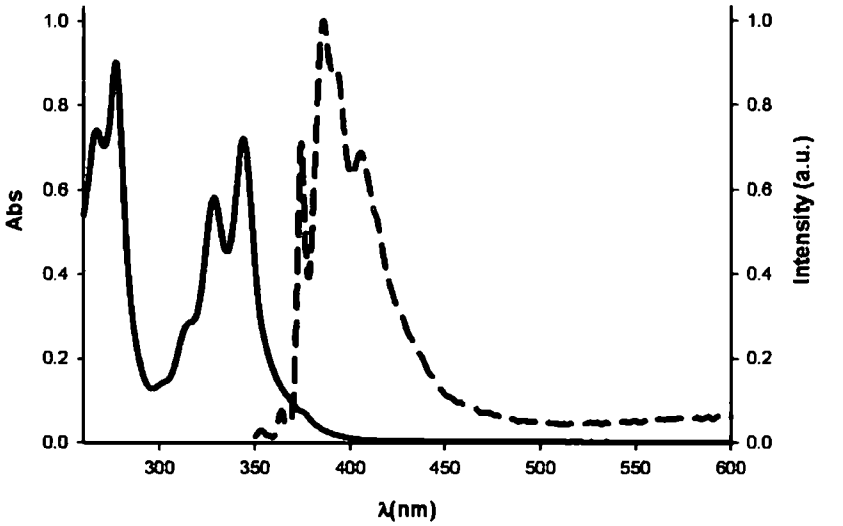

Figure 5.4: Absorbance and fluorescence spectra of **5.3** in acetonitrile solution.

In contrast, the fluorescence spectra of hosts, **5.2** and **5.3**, are very different from those typically presented by pyrene derivatives. In particular, the band at *ca.* 400 nm typical of the pyrene monomer is, in all cases, much less intense. The quantum yields for **5.2**·$2PF_6^-$ and **5.3**·$3PF_6^-$ are $\Phi = 2.0 \times 10^{-3}$, and 1.4×10^{-3}, respectively, while that for pyrene itself in aerated solution is 0.07.[210] The excited state lifetimes are also very short for **5.2**·$2PF_6^-$ and **5.3**·$3PF_6^-$ ($\tau < 0.3$ ns for both compounds, compared to 18 ns, for pyrene in aerated solution) ruling out the possibility of the formation of intermolecular excimers or exciplexes. However in

photophysical studies of host **5.7**, the formation of either excimer or exciplex species was observed, suggesting interactions between the anthracene arms, which was concluded by the appearance of an additional broad band, observed after a solution of **5.7** had been exposed to ambient light.[2] An excimer band was also observed for the calix[4]arene pyrene host **5.6**, which appeared as an unstructured band in the region of 520 – 600 nm, interestingly this band was red-shift about 80 nm, compared to the excimer of pyrene, which is consistent with the formation of intramolecular excimers.[13] With both hosts **5.6** and **5.7**, the excimers observed were intramolecular excimers, and in none of the hosts intermolecular excimers were observed, the latter being consistent with hosts **5.2** and **5.3**.

The strong quenching of the fluorescence in **5.2** and **5.3** is most probably due to a photoinduced electron transfer (PET) process from the excited state of the pyreneyl moiety to one of the electron deficient pyridinium ions. Together with the favourable redox potentials of the different units ($E_{red}(P^+/P)$ of pyrene = +1.16 V vs SCE;[211] $E_{red}(P^+/P)$ of pyridinium = -1.2 V *vs.* SCE[212]) and the energy of the singlet excited state of the chromophore (E^{oo} = 3.26 eV), this assignment is supported by the evidence of a band centered at 465 nm in the transient absorption spectrum of both compounds (*e.g.* **Figure 5.5** for **5.2**·$2PF_6$ and **Figure 5.6** for **5.3**·$3PF_6$), that can be attributed to the pyrene radical cation.[213]

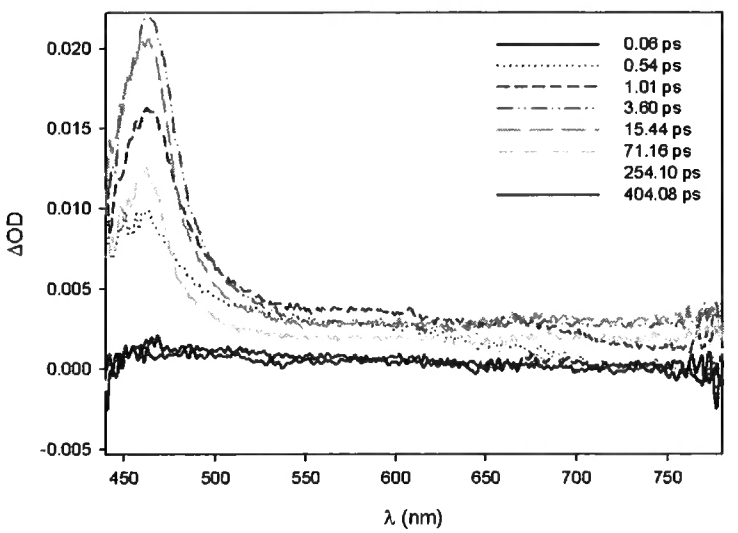

Figure 5.5: Transient absorption spectral changes of **5.2**·$2PF_6$ in acetonitrile solution, obtained with nanosecond laser photolysis upon excitation at 266 nm, at room temperature.

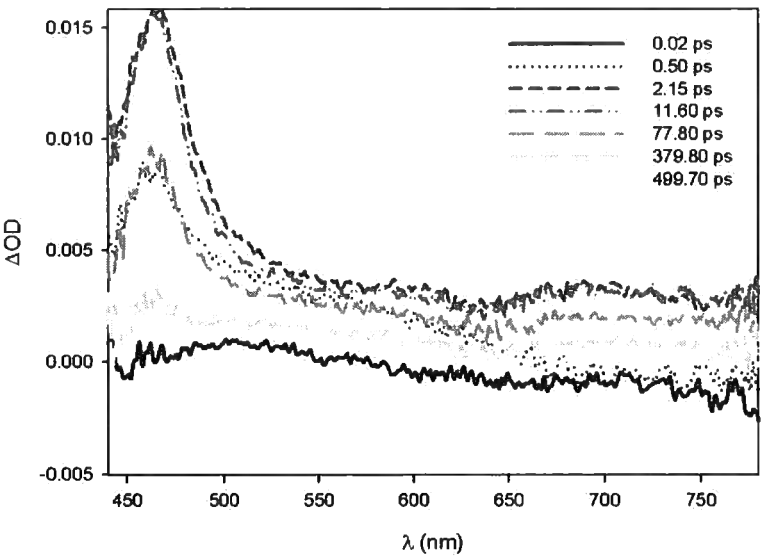

Figure 5.6: Transient absorption spectral changes of **5.3**·3PF_6 in acetonitrile solution, obtained with nanosecond laser photolysis upon excitation at 266 nm, at room temperature.

5.3 Anion Binding

5.3.1 Photophysical Anion Binding Studies

Anion binding of mono-anionic compounds chloride, bromide, nitrate, acetate, and di-anionic compounds malonate and succinate by **5.2**·2PF_6^- and **5.3**·3PF_6^- was studied by means of UV-Vis and fluorescence titrations in acetonitrile, again in collaboration with the Bologna group. The association constants derived from these experiments, fitted using the Specfit software[16] are shown in **Table 1**.

Anion/Receptor	Stoichiometry (Host : Guest)	**5.2**	**5.3**
Cl^-	2:1	9.2 ± 0.3	12.1 ± 0.4
	1:1	4.2 ± 0.1	5.7 ± 0.3
	1:2		
Br^-	2:1	< 4	11.7 ± 0.1
	1:1	3.2 ± 0.2	5.1 ± 0.4
	1:2		
NO_3^-	2:1	low	low
	1:1		
	1:2		
CH_3COO^-	2:1	12.7 ± 0.2	11.6 ± 0.3
	1:1	6.0 ± 0.3	5.5 ± 0.2
	1:2	10.5 ± 0.3	< 4
$CH_2CH_2(COO)_2^{2-}$	2:1		10.5 ± 0.6
	1:1	5.0 ± 0.2	5.3 ± 0.3
	1:2		< 4
$CH_2(COO)_2^{2-}$	2:1		10.0 ± 0.3
	1:1	5.4 ± 0.2	4.7 ± 0.3
	1:2		

Table 5.1: Binding constants (log β) of receptors **5.2** and **5.3** as the PF_6^- salts with various anions obtained from UV-Vis titration in acetonitrile with anions added as NBu_4^+ salts. Titrations were carried out at 25 °C. Binding constants were assessed using Specfit.[16]

For both hosts, addition of nitrate did not cause any appreciable change in the absorption or in the fluorescence spectra, indicating that the association constant is too small to observe any complexation process in our experimental conditions, or that the formation of the adduct does not cause any appreciable change in the structure of the hosts. Binding to halides for both hosts was seen, and the formation of both 2:1 host:guest species and 1:1 host:guest species was observed, with strongest binding being seen in the formation of 2:1 species for **5.3**, and with chloride for **5.2**, but very small binding constant is observed for the formation of a 2:1 complex with **5.2** and bromide. Binding to chloride was observed to be stronger than to bromide for both hosts, **5.2** and **5.3**. In the case of acetate both hosts showed binding in three different stoichiometries, 1:1, 2:1 and 1:2 host:guest, but the strongest binding is seen for the 2:1 complex in both hosts, and very weak binding is observed with the 1:2 complex of **5.3** and acetate. Host **5.3** shows a similar affinity for malonate and succinate when forming a 2:1 host:guest complex with both anions, as does host **5.2** when forming a 1:1 complex with these anions, and a similar affinity as host **5.3** has with these anions in the 1:1 stoichiometry.

Much smaller changes in the absorption spectra were observed for **5.2**·$2PF_6$ and in **5.3**·$3PF_6$, than for the analogous calix[4]arene compound, **5.6**.[13] (*e.g.* see **figure 5.8** for the example of the titration of **5.3**·$3PF_6$ with chloride), resulting in a less pronounced decrease of the typical bands of pyrene in all the monitored spectral region (and for this reason, no isosbestic points are observed) and in the lack of the increase of the absorbance above 380 nm.

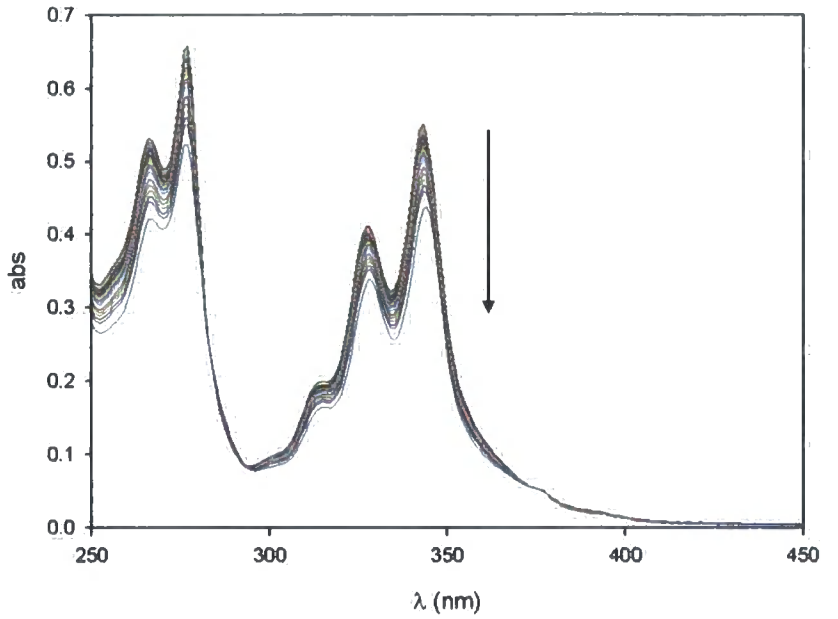

Figure 5.7: Absorption spectra of **5.2**·$2PF_6^-$ (9.2×10^{-6} M) in CH_3CN and upon addition of increasing amounts of Cl^- up to 50 equivalents.

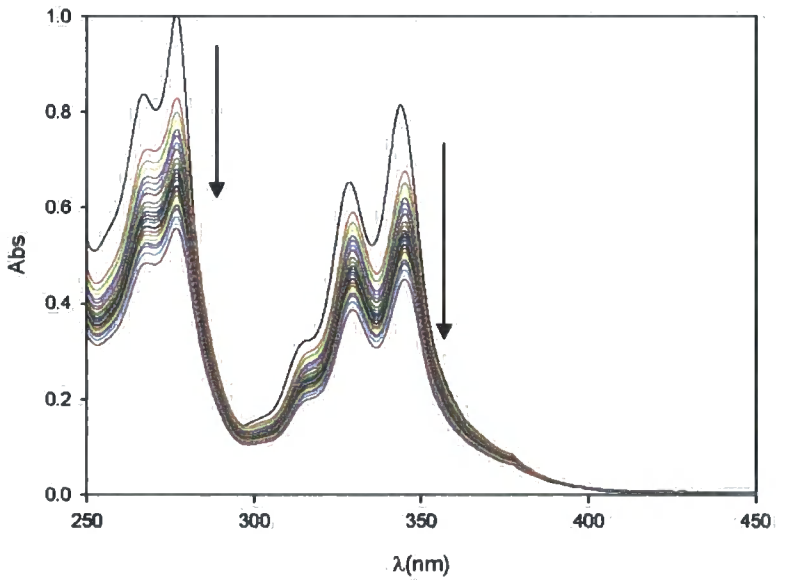

Figure 5.8: Absorption spectra of **5.3**·$3PF_6^-$ (8.2×10^{-6} M) in CH_3CN and upon addition of increasing amounts of Cl^- up to 50 equivalents.

In particular, the smaller changes in the absorption spectra indicates that anion complexation does not lead to the formation of strong ground state dimers of pyrene, in contrast to the results obtained for the analogous calix[4]arene, **5.6**.[13] For both **5.2** and **5.3** hosts the formation of 1:1 adducts was observed, in contrast to the ditopic calix[4]arene which readily forms 1:2 (host:guest) complexes.[13] However for **5.3** in particular there appears to be a strong tendency for two hosts to wrap around a single anionic guest to give a 2:1 complex as well.

As far as the fluorescence spectra are concerned, in general the addition of anions to solutions containing receptors **5.2** and **5.3** does not lead to significant changes. This finding contrasts to parallel work within our group on calix[4]arene, **5.6**, an increase of the emission intensity of *both* the monomer and excimer bands is observed upon addition of chloride, **figure 5.8**. This in contrast to related pyrene systems in which conformational changes result in an increase in the intensity of the excimer band and a corresponding *decrease* in the emission of the monomer emission.[172, 214] In contrast upon addition of bromide and acetate, to **5.6** it is only the monomeric band in the 380-400 nm that increases in intensity, and addition of malonate and succinate cause only negligible changes in the spectra and the fluorescence remains quenched despite the very strong binding of these anions, and addition of F^-, HPO_4^{2-} or triflic acid, results in no change in the fluorescence spectra. This suggests anion binding induces an increase in monomer emission, but conformational changes are observed upon addition of chloride.

5.3.2 Solution Behavior by ^{1}H NMR Spectroscopic Titration

The anion binding behavior of hosts **5.2**, **5.3**, **5.4** and **5.5** was also studied by ^{1}H NMR spectroscopic titration. The dipodal host **5.2** readily precipitates from acetonitrile and DMSO solution on addition of the tetrabutylammonium salts of a range of halide anions and hence no quantitative data could be obtained by this method. In the case of tetrabutylammonium acetate, however, the host remained soluble in acetonitrile solution up to *ca.* 2.5 mole equivalents giving a chemical shift change of 2.84 ppm for the methylene protons and K_{11} = 500 M^{-1}, which is in contrast to the photophysical data, where a K_{11} = 10^6 M^{-1}, is observed. This difference may be attributed to the more limited nature of the NMR data which did not allow the fitting of multiple equilibria.

The anion binding properties of tripodal host **5.3** proved remarkable and radically different to **5.2, 5.4** and **5.5** and those of the closely related anthracenyl analogue, **5.7**[2] and other similar systems.[2] On titration of **5.3** with tetrabutylammonium salts of Cl^-, Br^-, NO_3^-, $MeCO_2^-$, *p*-toluene sulfonate and succinate^{2-} no precipitation was observed. In all cases except succinate, a distinct change in gradient was observed in the ^1H NMR titration isotherms at a host : anion of 2:1 suggesting the surprising encapsulation of a single anion by two host molecules. The analogous anthracene compound showed no evidence of 2:1 host:guest binding, and in this host the predominate binding mode was a 1:1 host:guest species.[2] This 2:1 ratio was confirmed by Job plot analysis in the case of Cl^- and Br^-. A cumulative plot along with representative data for Br^- is shown in **Figure 5.9**. Analysis of the titration data for multiple nuclei proved very challenging, with titration isotherms suggesting the presence of multiple equilibria comprising the formation of 2:1, 1:1 and 1:2 host:guest complexes. The sharpness of the isotherm gradients suggests very strong binding in the case of all of the anions studied (tetrabutyl ammonium salts of Cl^-, Br^-, NO_3^-, $MeCO_2^-$, *p*-toluene sulfonate and succinate^{2-}). In the previously studied anthracene analogue, **5.7**, binding of acetate is observed to be far stronger than the other anions tested, where K_{11} = 49 000, compared to chloride, which sees the next strongest binding, where K_{11} = 5270, and the binding of the other anions to be in the order of magnitude of 10^2.[2] Although the binding complexity in host **5.3** has prevented the calculation of binding constants, it is suggested that the hosts bind halide anions with a similar affinity to that of acetate. As illustrated by **Figure 5.9(a)** the data for acetate is atypical and clearly indicative of more than one binding process involving different conformational characteristics in which the chemical shift of the methylene resonance at 5.52 ppm (plotted in **Figure 5.9(a)**) is not greatly affected by addition of the first equivalent of anion. Related behavior has been observed in similar systems.[2]

(a)

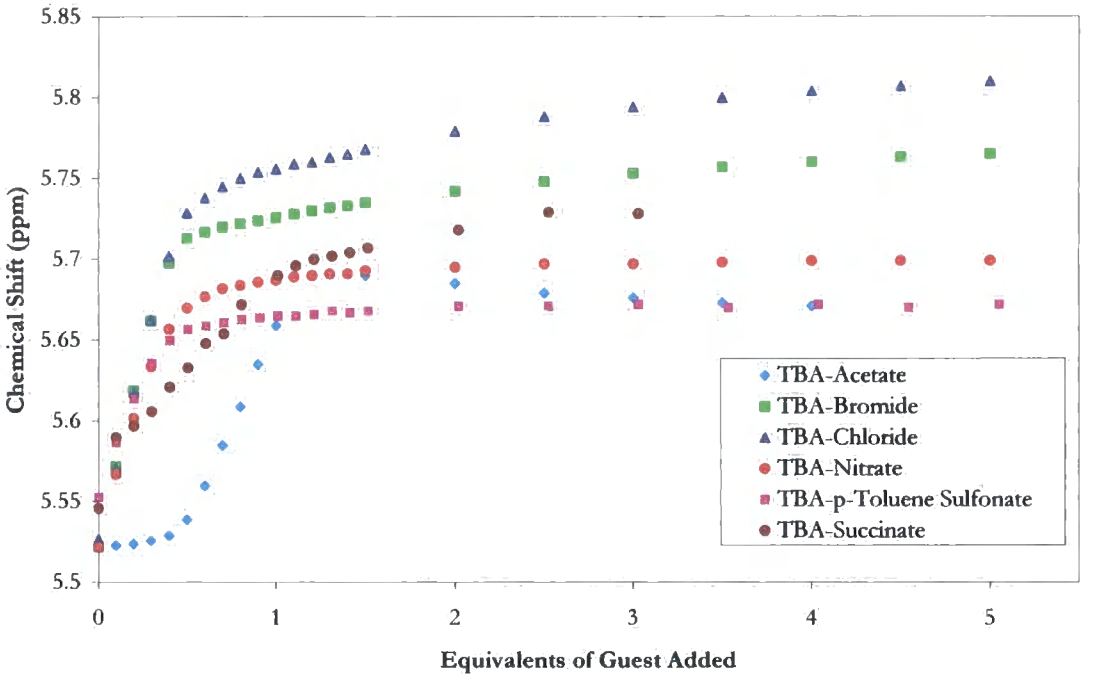
5.85
5.8
5.75
5.7
5.65
5.6
5.55
5.5
Chemical Shift (ppm)
0
1
2
3
4
5
Equivalents of Guest Added
TBA-Acetate
TBA-Bromide
TBA-Chloride
TBA-Nitrate
TBA-p-Toluene Sulfonate
TBA-Succinate

(b)

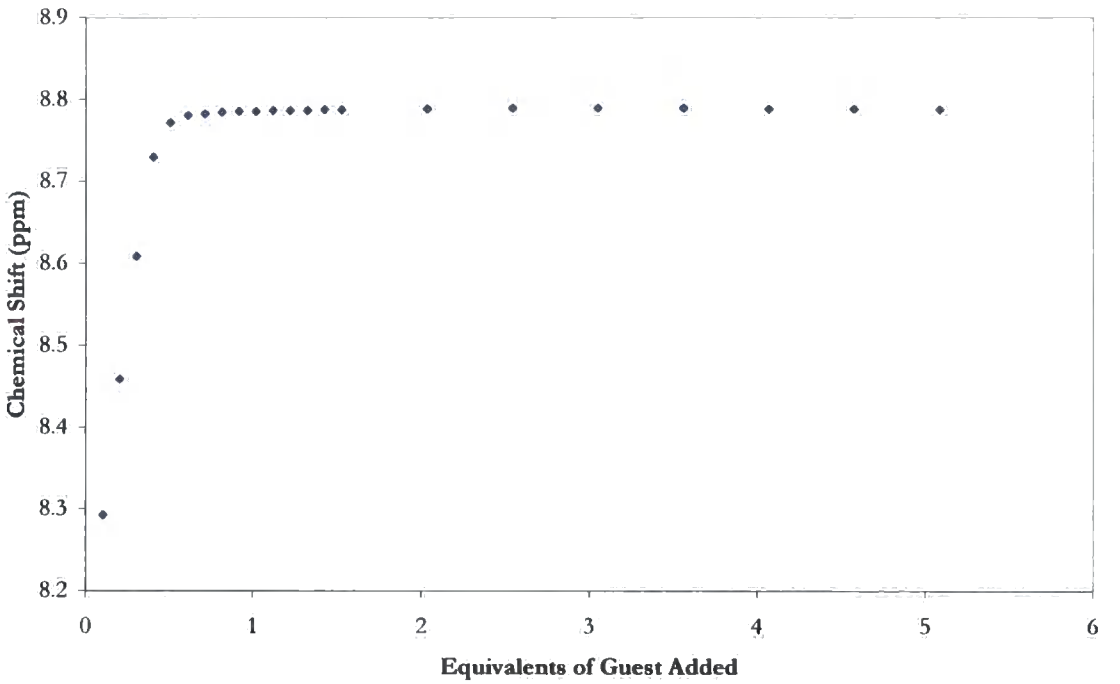
8.9
8.8
8.7
8.6
8.5
8.4
8.3
8.2
Chemical Shift (ppm)
0
1
2
3
4
5
6
Equivalents of Guest Added

(c)

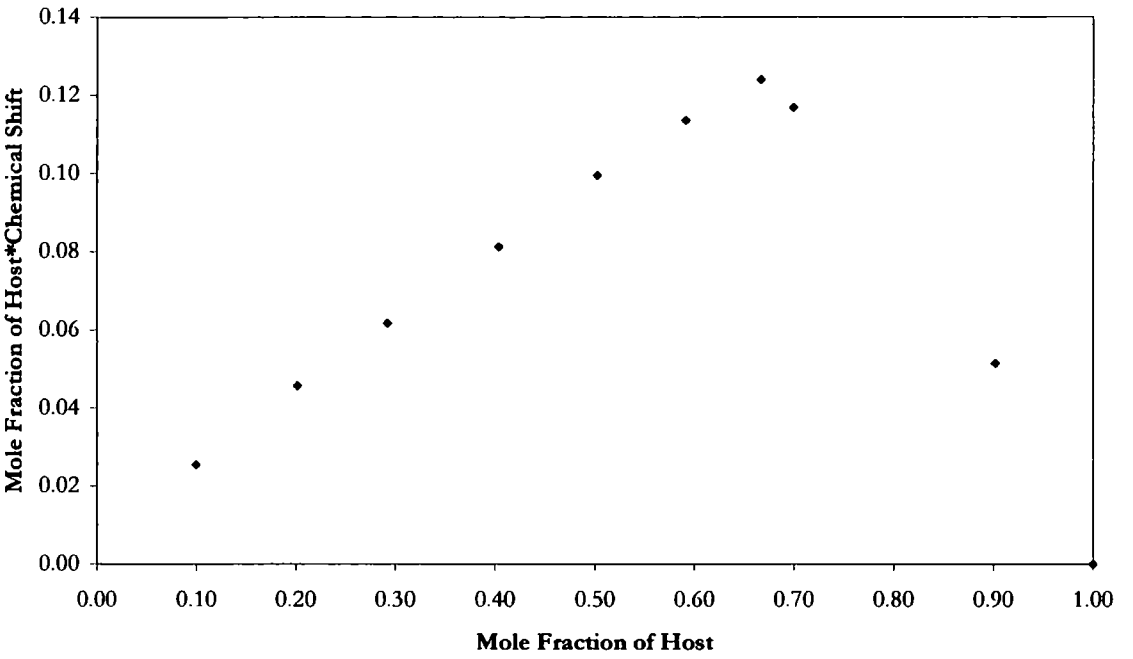

Figure 5.9: ^{1}H NMR titration data for anion binding by host **5.3** in acetonitrile-d_3 solution (a) titration isotherm following methylene resonance at 5.52 ppm for all anions, (b) CH_2NH resonance on addition of $NBu_4^+Br^-$, (c) Job plot for $NBu_4^+Br^-$ by showing 2:1 host:guest stoichiometry.

The possibility of self-association of the tripodal compound **5.3** was assessed by an ^{1}H NMR spectroscopic dilution study from 1.6 mM – 26 mM. Over this concentration range the resonance assigned to the NH proton shifted from 7.11 ppm to 6.94 ppm in a non-linear fashion suggesting some degree of dimerisation even in the absence of added anion, **figure 5.10**. The negative chemical shift change with increasing concentration and hence increasing dimer concentration implies decreased hydrogen bonding interaction with anions and solvent on dimerisation and/or increased shielding due to the orientation of the pyrenyl groups in the dimer.

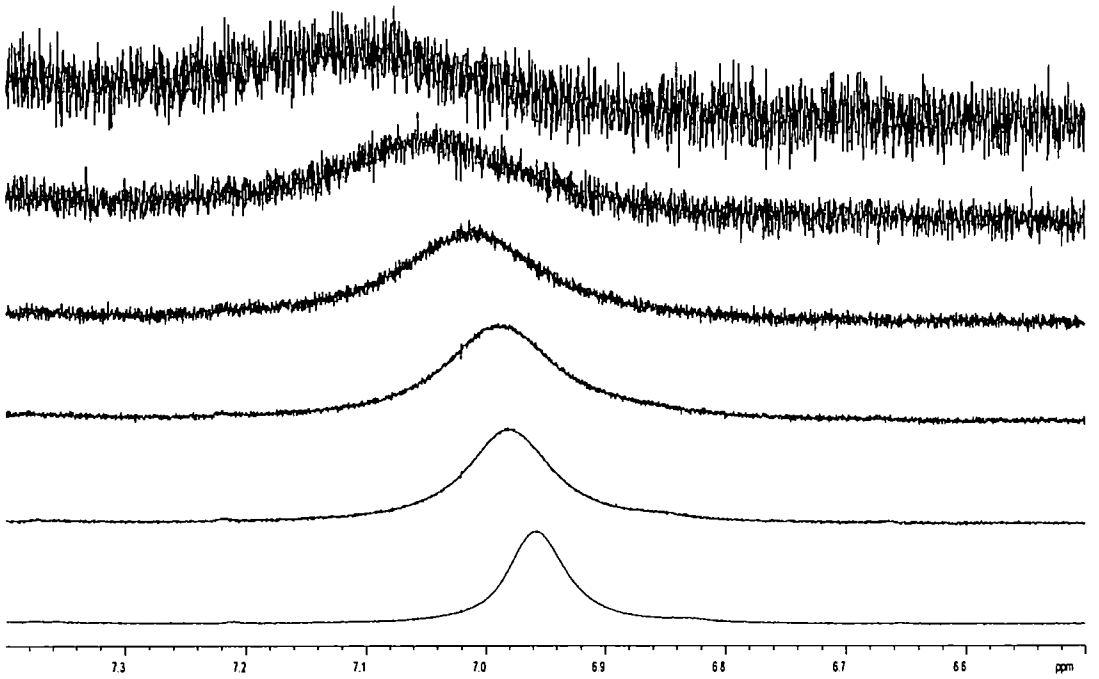

Figure 5.10: ^{1}H-NMR spectra of **5.3** as a function of concentration, NH resonance (bottom to top 26, 19.5, 13, 6.5, 3.25, 1.6 mM).

For hosts **5.4** and **5.5** it was possible to calculate their binding constants by NMR spectroscopic titration experiments. Binding for both **5.4** and **5.5** was calculated to be in a 1:1 host:guest stoichiometric complex, as was observed for the anthracene host, **5.7**.[2] The strongest binding was observed upon addition of acetate to **5.7**[2], but it was not possible to calculate a binding constant upon addition of acetate to host **5.5**, which shows the largest chemical shift change, but no curvature of the isotherm is observed, upto the point of precipitation, **figure 5.11**. The strongest binding was seen between both hosts and chloride, as was seen in the spectrophotometric experiments with **5.3**, and so it is suggested that chloride has the best fit into the cavity of the molecule. The binding affinity of **5.4** and chloride is similar to that observed with **5.7** and chloride, K_{11} = 4517, **5.4**, and 5270 M^{-1}, **5.7**,[2] but that observed with **5.5**, is much smaller, K_{11} = 1481 M^{-1}. Precipitation also occurred in the titration experiment with **5.4** and *p*-Toluene sulfonate and **5.4** and **5.5** after addition of 2.5 equivalents of chloride and with **5.4** after the addition of 3 equivalents. In some cases it

was not possible to calculate binding constants from the data obtained, which could be due to the equilibria being too complex to analyse by NMR methods, as was seen with **5.3**. The anion binding affinity of both hosts **5.4** and **5.5** is consistent with anion basicity, and the binding is consistently stronger for **5.4** than for **5.5**, with the hosts having a similar affinity for nitrate, **table 5.2**.

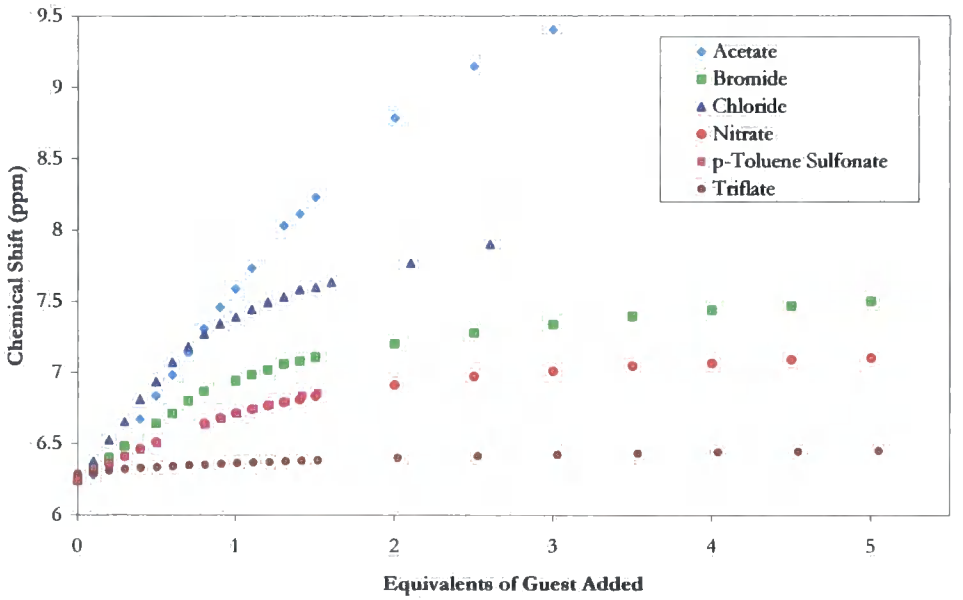

(a)

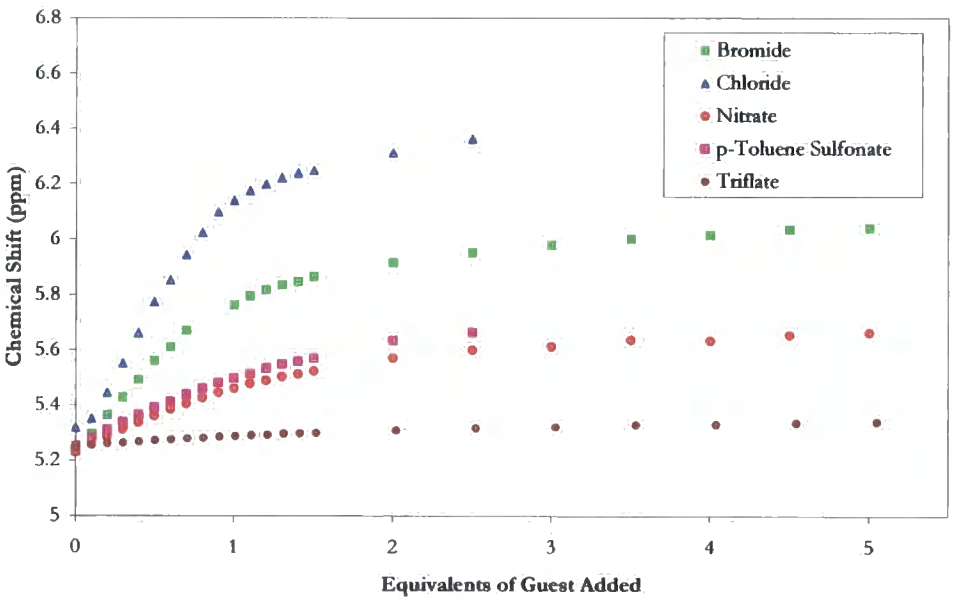

(b)

Figure 5.11: ^{1}H NMR titration data for anion binding by host (a) **5.5** in acetonitrile-d_3 solution titration isotherm following NH resonance at 6.25 ppm for all anions and (b) **5.4** in acetonitrile-d_3 solution titration isotherm following NH resonance at 5.25 ppm for all anions.

	log K_{11} / M^{-1}		log β
Anion	**5.4**	**5.5**	**5.3**[a]
Chloride	3.65(14)	3.17(8)	K_{21} 12.1 ± 0.4 K_{11} 5.7 ± 0.3
Bromide	3.17(5)	2.78(4)	K_{21} 11.7 ± 0.1 K_{11} 5.1 ± 0.4
Nitrate	2.73(5)	2.75(4)	low
Acetate	-	[b]	K_{21} 11.6 ± 0.3 K_{11} 5.5 ± 0.2 K_{12} < 4
***p*-Toluene Sulfonate**	[b]	[b]	-
Triflate	[b]	[b]	-

Table 5.2: Anion binding constants (M^{-1}) for Hosts **5.4** and **5.5** in CD_3CN at 20 °C. Errors are <10%, anions added as NBu_4^+ salts, host concentration 0.006 mol dm^{-3} (hyphen indicates not measured).

(a) Spectrophotometric data is included for **5.3** as binding constants could not be calculated from NMR data as a trend comparison.

(b) no refinement possible, maybe due to complex binding mode.

* *Graphical representation of the fit of titration data is given in the Appendix*

5.4 Summary

A new amino-pyridyl ligand containing both secondary amine and pyridyl functionalities, and a pyrene reporter group has been synthesised. The x-ray crystal structure was obtained and showed intermolecular hydrogen bonding between amine protons and pyridyl groups, as has been discussed in chapter two for ligands **2.2** – **2.6**. The absorbance was observed to be similar to that of pyrene itself, but the absorbance band in the 300-400 nm region is broader and less intense than pyrene itself, and contains a small tall above 380 nm, which is absent in pyrene, and attributed to a charge transfer from the pyrene to pyridinium groups, or interactions between pyrene units in the ground state. The fluorescence is similar to that of pyrene but less intense, and as the lifetimes are short, it is suggested that there is no excimer

or exciplex formation. The quenching of the fluorescence is probably due to a photo-electron transfer from the pyrenyl to the pyridinium moieties.

Four new potential anion receptors have been reported, two based on aminopyridinium di-tripodal hosts equipped with pyrenyl reporter groups, and two based on 3-aminomethylpyridinium tripodal hosts, with aryl groups, as discussed in chapter two. The conformational, associative and sensing properties of the hosts are highly dependent on the spacing and disposition of the binding and sensing components and hence on the size and shape of the core organizing scaffold. The pyrenyl-substituted aminopyridinium binding and sensing unit is fluorescence quenched as a result of pyrene-pyridinium charge transfer interactions in the excited state and hence hosts **5.2** and **5.3** do not exhibit a fluorescence response to anion binding. Host **5.3** exhibits atypical binding to anions different to hosts **5.4** and **5.5**, and previously reported anthracenyl derviatives[2], binding in a 2:1 stoichiometry, and showing very strong affinity for halide. While hosts **5.4** and **5.5** also exhibited strong halide binding but in a 1:1 host:guest stoichiometry, and both hosts showed a preference for chloride over bromide, suggesting chloride showed better size complementarity than bromide. However, host **5.3** showed a similar affinity for both halide anions.

5.5 Experimental

Pyren-4-yl-methylene-pyridin-3-ylamine

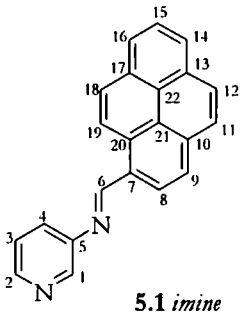

5.1 *imine*

Pyrene-1-carboxyldehyde (2.0g, 86.9 mmol) was weighed out (in a glove box) and then dissolved in a degassed dichloroethane (100 mL), 3-aminopyridine (0.81g, 86.85 mmol) and $MgSO_4$ were added. The reaction was stirred under reflux for 25 h under N_2. The solvent was removed under reduced pressure and the crude reaction mixture redissolved in diethyl ether. Undissolved material was filtered off. The crude imine was then purified by precipitating out the solid from reaction mixture by placing the flask in acetone and dry ice bath, and collected by filtration (2.2g, 71.89 mmol, 82%).

NMR spectroscopic data agrees with data reported by Maria Filby.[215]

ES+ MS: m/z = 307 $[M+H]^+$

Anal: Calculated for $C_{22}H_{14}N_2$: C, 86.25, H, 4.60, N, 9.14%.
Found: C, 86.04, H, 4.49, N, 8.60%.

IR: 1612 *s* (CH=N).

Pyren-4-yl-methyl-pyridin-3-ylamine

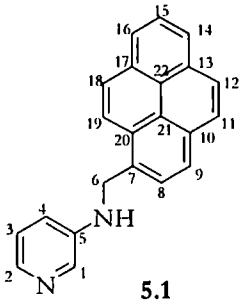

5.1

Pyren-1-ylmethyl-pyridin-3-yl-imine (2.0 g, 6.5 mmol) was dissolved in MeOH (700 mL) and 3 molar equivalents of $NaBH_4$ were added slowly. The reaction mixture was stirred for 2h. 2M HCl was added until the pH was 3 followed by a 2M NaOH until the pH was 9. The solvent was then removed under reduced pressure and during the process orange crystals of pure amine (1.32 g, 4.3 mmol, 66%) appeared which were separated. Further removal of MeOH followed by extraction into CH_2Cl_2 and washing with water resulted in crude amine which was washed with diethyl ether to remove any remaining unreacted aldehyde.

NMR spectroscopic data agrees with data reported by Maria Filby.[215]

ES+ MS: m/z = 309 $[M+H]^+$.

Anal: Calculated for $C_{22}H_{16}N_2$ 0.75 H_2O: C, 82.08, H, 5.47, N, 8.70%.
Found: C, 81.90, H, 4.99, N, 8.49%.

IR: 3419m ν (NH)

α,α'-bis(Pyren-4-yl-methyl-pyridin-3-ylamine)-*para*-xylene Bromide

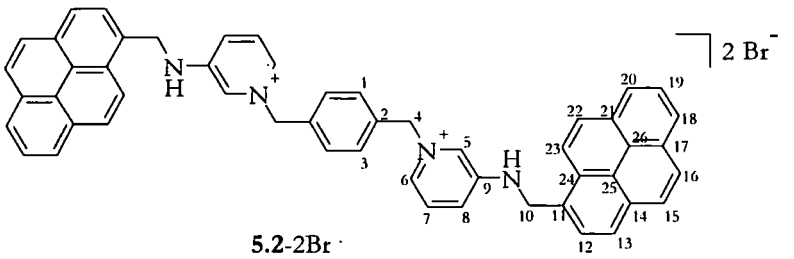

5.2-2Br

Pyren-4-yl-methyl-pyridinium-3-ylamine (0.48 g, 1.6 mmol) and α,α'-dibromo-*para*-xylene (0.20 g, 0.77 mmol) were dissolved in dichloromethane (100 mL). This solution was placed under reflux for 2 hours. After this time the solution was cooled and a solid was formed. This solid was collected by filtration and was found to be the desired product (0.53 g, 0.59 mmol, 77 %).

^{1}H-NMR (CD_3CN, 500 MHz, δ / ppm, J / Hz): 8.4-7.6 (30H, m, Ar & Py(H1, 3, 5-9, 11-26)); 6.47 (2H, bs, NH); 5.28 (4H, s, CH_2(H4)); 5.12 (4H, d, J = 5.4, CH_2(H10)).

^{13}C{^{1}H}-NMR: *No ^{13}C spectrum recorded due to poor solubility of host.*

ES+ MS: m/z = 800 $[M-Br]^+$, 360 $[M-2Br]^{2+}$

Anal: Calculated for $C_{52}H_{40}N_4Br_2$: C, 70.92; H, 4.58; N, 6.36
Found: C, 70.18; H, 4.99; H, 6.70

α,α'-bis(Pyren-4-yl-methyl-pyridin-3-ylamine)-*para*-xylene Hexafluorophosphate

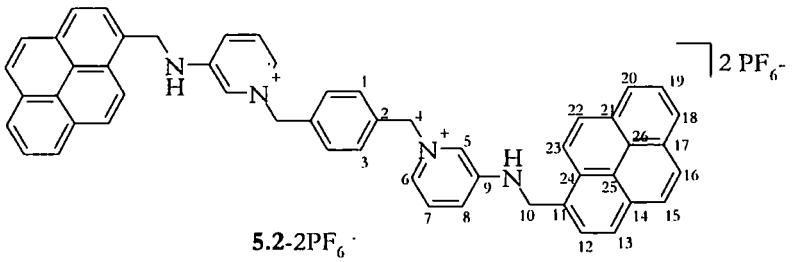

5.2-2PF$_6$

5.2-2Br (0.39 g, 0.45 mmol) was dissolved in methanol (50 mL) with an excess of NH_4PF_6 (1.45 g, 8.9 mmol). This solution was warmed to ~35°C, to aid the solubility of the bromide salt, and stirred for 2 hours. After this time the solution was cooled, and an off-white precipitate formed. The solid was collected by filtration, and washed with methanol, and was found to be the desired product. (0.26 g, 0.26 mmol, 58 %).

^{1}H-NMR (CD_3CN, 400 MHz, δ /ppm, J / Hz): 8.4-7.6 (30H, m, Ar & Py(H1, 3, 5-9, 11-26)); 6.48 (2H, bs, NH); 5.27 (4H, s, CH_2(H4)); 5.10 (4H, d, J = 4.0, CH_2(H10)).

^{13}C{^{1}H}-NMR: *No ^{13}C spectrum recorded due to poor solubility of host.*

ES+ MS: 865 [M-PF_6]$^+$, 360 [M-2PF_6]$^{2+}$

Anal: Calculated for $C_{52}H_{40}N_4(PF_6)_2$: C, 61.79; H, 3.99; N, 5.54
Found: C, 61.14; H, 3.69; N, 5.09

IR: 3423 ν (NH)

Tris(Pyren-4-yl-methyl-pyridin-3-ylamine) Bromide

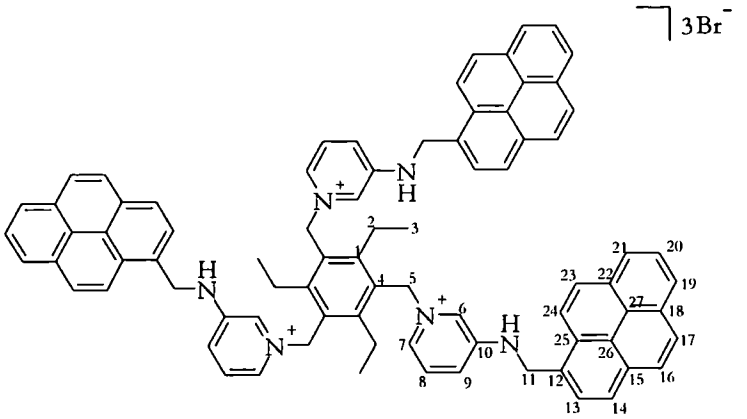

5.3-3Br⁻

Pyren-4-yl-methyl-pyridinium-3-ylamine (0.30 g, 0.98 mmol) and 1,3,5-tris(bromomethyl)-2,4,6-triethylbenzene (0.14 g, 0.32 mmol) were dissolved in dichloromethane (100 mL), and the resulting solution stirred at room temperature for 20 hours. After this time the solvent was removed under reduced pressure to yield the bromide salt as a yellow oil (0.40 g, 0.29 mmol, 90 %).

^{1}H-NMR ($CDCl_3$, 400 MHz, δ / ppm, J / Hz): 8.82 (3H, s, Pyridyl-H(H6)); 8.50 (3H, d, J=6.0, Pyridyl-H(H7)); 8.0-7.6 (27H, m, ArH(H1, 4, 12-27)); 7.46 (3H, dd, J = 6.0, 2.8, Pyridyl-H(H8)); 7.05 (3H, d, J=6.0, Pyridyl-H(H9)); 5.87 (6H, s, CH_2(H5)); 4.72 (6H, s, CH_2(H11)); 2.49 (6H, t, J=7.0, CH_2(H2)); 1.01 (9H, d, J=7.0, CH_3(H3)).

^{13}C{^{1}H}-NMR ($CDCl_3$, 125 MHz, δ / ppm): 150.7(C26); 148.3(C27); 131.3; 131.1; 130.6; 130.5; 128.8; 128.6; 128.5; 128.2; 127.8; 127.6; 127.4(C6, 7, 10, 12 – 25); 126.3(C8); 125.6; 125.5; 125.3; 125.0; 124.5; 124.6(C6, 7, 10, 12 – 25); 123.3(C9); 122.3(C6, 7, 10, 12 – 25); 58.0(C5); 44.9(C11); 24.8(C2); 15.5(C3).

ES+ MS: 1286 [M-Br]$^+$, 603 [M-2Br]$^{2+}$, 375 [M-3Br]$^{3+}$

Tris(Pyren-4-yl-methyl-pyridin-3-ylamine) Hexafluorophosphate

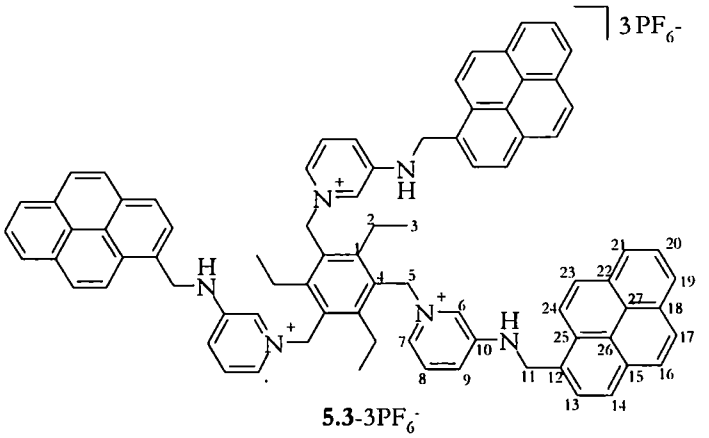

5.3-3PF$_6^-$

5.3-3Br$^-$ (0.40 g, 0.29 mmol) was dissolved in dichloromethane (100 mL), and excess NH_4PF_6 (0.53 g, 3.26 mmol) dissolved in methanol (25 mL) was added. The solution was stirred at room temperature for 2 hours. After this time, the solution was concentrated, and a yellow precipitated formed. The solid was collected by filtration, and washed with methanol, and was found to be the desired product (0.33 g, 0.21 mmol, 65 %).

^{1}H-NMR (CD_3CN, 500MHz, δ / ppm, J / Hz): 8.3-7.4 (39H, m, Ar/Py(H4)); 7.04 (3H, bs, NH); 5.51 (6H, s, CH_2(H5)); 4.79 (6H, s, CH_2(H11)); 2.41 (6H, s, CH_2(H2)); 1.98 (9H, q, J=2.45, CH_3(H3))

^{13}C{^{1}H}-NMR (CD_3CN, 125MHz, δ / ppm): 128.85(C26); 128.58(C27); 128.21, 127.78, 127.60, 127.39, 126.26, 125.62, 125.47, 125.29, 125.02, 124.85, 124.61(C6 – 10, C12 – 25); 58.05(C5); 44.90(C11); 24.81(C2); 15.52(C3).

ES+ MS: 1415 [M-PF_6]$^+$, 635 [M-2PF_6]$^{2+}$, 375 [M-3PF_6]$^{3+}$

Anal: Calculated for $C_{81}H_{69}N_6(PF_6)_3$: C, 62.31; H, 4.45; N, 5.38
Found: C, 62.45; H, 4.17; N, 5.67

IR: 3420 ν (NH)

Tris(*N*-((pyridin-3-yl)methyl)benzenamine) Hexafluorophosphate

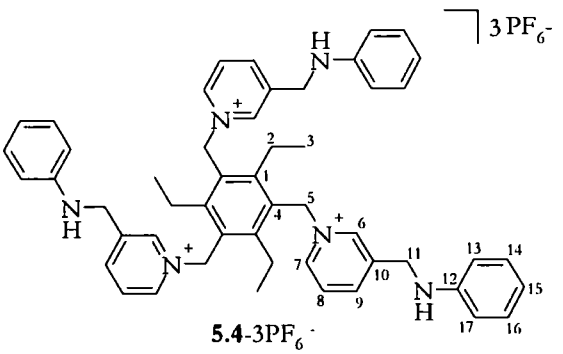

5.4-3PF_6^-

1,3,5-tribromomethy-2,4,6-triethylbenzene (0.62 g, 1.4 mmol) and *N*-((pyridine-3-yl)methyl)benzeneamine (1.5 g, 8.2 mmol) were dissolved in ethanol and refluxed for 120 hours. After this time the solvent was removed under reduced pressure, to yield the bromide salt as a yellow oil. Without purification the bromide salt (0.32 g, 0.32 mmol) was dissolved in methanol (100 mL), and excess NH_4PF_6 (0.53 g, 3.2 mmol) was added. The solution was stirred at room temperature for 6 hours. During this time and a yellow precipitated formed. The solid was collected by filtration, and washed with methanol, and was found to be the desired product (0.30 g, 0.25 mmol, 79 %).

^{1}H-NMR (CD_3CN, 500 MHz, δ / ppm, J/ Hz): 8.52 (3H, d, J=6.0, Pyridyl-H(H7)); 8.49 (3H, s, Pyridyl-H(H6)); 8.40 (3H, d, J=6.0, Pyridyl-H(H9)); 8.01 (3H, t, J=6.0, Pyridyl-H(H8)); 7.13 (6H, t, J=8.5, Ar-H(H14&16)); 6.73 (3H, t, J=8.5, Ar-H(H15)); 6.55 (6H, d, J=8.5, Ar-H(H13&17); 5.76 (6H, s, CH_2(H5)); 5.27 (3H, s, NH); 4.60 (6H, s, CH_2(H11)); 2.45 (6H, q, J=7.5, CH_2(H2)); 0.77 (9H, t, J=7.5, CH_3(H3)).

^{13}C{^{1}H}-NMR (CD_3CN, 125 MHz, δ / ppm): 150.8(C10); 147.2(C12); 145.3(C6); 143.3(C7); 142.2(C4); 129.6(C14); 128.6(C13); 128.0(C9); 118.2(C8); 117.6(C1); 113.0(C17); 58.1(C5); 44.1(C11); 24.1(C2); 14.4(C3).

ES+ MS: 1043 [M-PF_6]$^+$, 449 [M-2PF_6]$^{2+}$, 251 [M-3PF_6]$^{3+}$

Anal: Calculated for $C_{51}H_{57}N_6(PF_6)_3$: C, 51.52; H, 4.83; N, 7.07
Found: C, 51.51; H, 4.89; N, 6.86

IR: 3452 ν (NH)

Tris(4-nitro-*N*-((pyridin-3-yl)methyl)benzenamine) Hexafluorophosphate

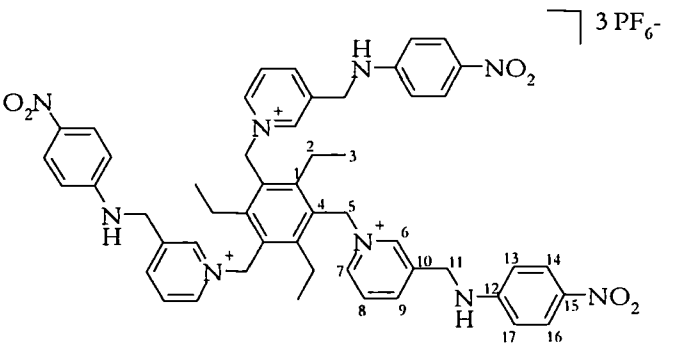

5.5-3PF_6^-

1,3,5-tribromomethy-2,4,6-triethylbenzene (0.64 g, 1.5 mmol) and 4-nitro-*N*-((pyridine-3-yl)methyl)benzeneamine (1.0 g, 4.4 mmol) were dissolved in 1,2-dichloroethane and refluxed for 120 hours. After this time the solvent was removed under reduced pressure, to yield the bromide salt as a yellow oil. Without purification the bromide salt (0.40 g, 0.29 mmol) was dissolved in methanol (100 mL), and excess NH_4PF_6 (2.3 g, 14.1 mmol) was added. The solution was stirred at room temperature for 6 hours. During this time and a yellow precipitated formed. The solid was collected by filtration, and washed with methanol, and was found to be the desired product (0.33 g, 0.21 mmol, 65 %).

^{1}H-NMR (CD_3CN, 400 MHz, δ / ppm, J/ Hz): 8.57 (3H, s, Pyridyl-H(H6)); 8.51 (3H, d, J=8.4, Pyridyl-H(H9)); 8.37 (3H, d, J=6.0, Pyridyl-H(H7)); 8.0 (9H, m, Ar-H(6H)(H14&16) & Pyridyl-H(3H)(H8)); 6.65 (6H, m, Ar-H(H13&17)); 6.28 (3H, t, J=6.4, NH); 5.80 (6H, s, CH_2(H5)); 4.71 (6H, d, J=6.4, CH_2(H11)); 2.50 (6H, q, J=7.2, CH_2(H2)); 0.80 (9H, t, J=7.2, CH_3(H3)).

^{13}C{^{1}H}-NMR (CD_3CN, 125 MHz, δ / ppm): 153.0(C15); 151.0(C14&16); 145.4(C12); 142.4(C10); 142.4(C6); 141.6(C7); 138.8(C4); 128.8(C9); 128.0(C13); 126.2(C13&17); 117.6(C1); 112.1(C8); 58.2(C2); 43.6(C5); 24.2(C11); 14.5(C3).

ES+ MS: 1178 [M-PF_6]$^+$, 516 [M-2PF_6]$^{2+}$, 296 [M-3PF_6]$^{3+}$

Anal: Calculated for $C_{51}H_{54}N_6O_9P_3F_{18}$: C, 46.26; H, 4.08; N, 9.52
Found: C, 45.73; H, 4.13; N, 9.30

IR: 3239 ν (NH)

Chapter Six

Tetrapodal Viologen-based Hosts

The low-lying reduction potential of 4,4'-bipyridinium derivatives ('viologens') has made them extremely useful as reporter groups in supramolecular systems and sensing ensembles,[216-219] with the binding of various electron donors giving rise to a purple colouration assigned to the radical cation arising from the single electron reduction of the viologen chromophore.[220] The redox potential of the viologens and their ability to form coloured charge-transfer complexes is very dependent on the nature of the substituents on the pyridyl nitrogen atoms and on the counter anion.[220] Commonly, in anion binding and sensing systems inter-anion selective binding and/or discrimination[192, 221] is achieved by including a number of binding sites able to interact simultaneously with a single anion, producing a well-defined anion binding cavity or cleft. A good example of such cooperative receptors are those based on the 2,4,6-trisubstituted-1,3-5-triethylbenzene core.[2, 23, 55, 150, 176, 177, 185, 191, 202, 205-207, 222, 223] This scaffold affords a degree of preorganisation arising from the steric preference for alternation about the central, hexasubstituted ring.[55] In previous work, Steed *et al* have shown that pyridinium derivatives of this core make effective anion-binding hosts, interacting with the anions *via* CH···X^- hydrogen bonds.[2, 9, 23, 150, 185] While it is possible to make a tripodal 4,4'-bipyridine derived receptor, functionalized at one end of the bipyridine units that is able to bind ATP in aqueous solution,[9] no viologen derivatives have been synthesized. In this chapter, the anion binding and sensing ability of a series of potentially di- or multitopic receptors based on a bis(triethylbenzyl)-viologen core is reported. The synthesis and binding studies discussed in this chapter were completed in collaboration with a masters student in the group, Emma Wallace.

6.1 Synthesis and Characterisation

The key starting material **6.1** as the bromide salt is readily prepared in excellent yield by reaction of 4,4'-bipyridyl with excess 1,3,5-tris(bromomethyl)-2,4,6-triethylbenzene.[202] The hosts were readily prepared by reacting together pyridine or 3-(3-*p*-tolylureido)pyridin-1-yl, with the starting material **6.1**, both of which are relatively cheap and readily available, or straight forward to synthesise. The simple synthetic procedure involves a substitution step followed the counter ion metathesis with NH_4PF_6, to produce a hexafluorophosphate salt, **scheme 6.1**. The bromide salts were sticky oils so not possible to fully characterize, but the hexafluorophosphate salts were obtained as powders and as such have been fully characterized. The experimental data obtained agreed with the proposed structures. For example, the ES+ mass spectrum shows a peak at m/z = 1024 for $[M\text{-}2PF_6^-]^{2+}$ and 634 for $[M\text{-}3PF_6^-]^{3+}$ for **6.3**, and a peak observed at m/z = 728 for $[M\text{-}2PF_6^-]^{2+}$ and 437 for $[M\text{-}3PF_6^-]^{3+}$ for **6.2**,. The fragmentation is also consistent with the proposed structure in each case. After substitution of bromine for either pyridine or the pyridyl urea ligand, there is a shift in the peak assigned to the methylene protons which are closest to the point of substitution. The chemical shift assigned to these protons is 4.78 ppm for **6.1**, 6.08 ppm for **6.2** and 5.92 ppm for **6.3**, with the greatest shift being between the starting material **6.1** and the two substituted hosts. In the IR spectrum, the peaks assigned to the C-Br stretch seen in the starting material **6.1**, ν(C-Br) = 699, 587 and 509 cm^{-1} disappear in those of the host molecules **6.2** and **6.3**, suggesting the reaction had gone to completion. There is also a shift of the stretches assigned to the CH_2 on the core common to both host molecules, **6.2** and **6.3** compared to the starting material **6.1**, shifting from 2967 for **6.1** to 2983 and 2978 for **6.2** and **6.3** respectively. For comparison purposes the tripodal host **6.4**, was synthesised according to the literature procedure[2] as is shown in **scheme 6.2**, and the data confirmed the structure and agreed with the reported data.

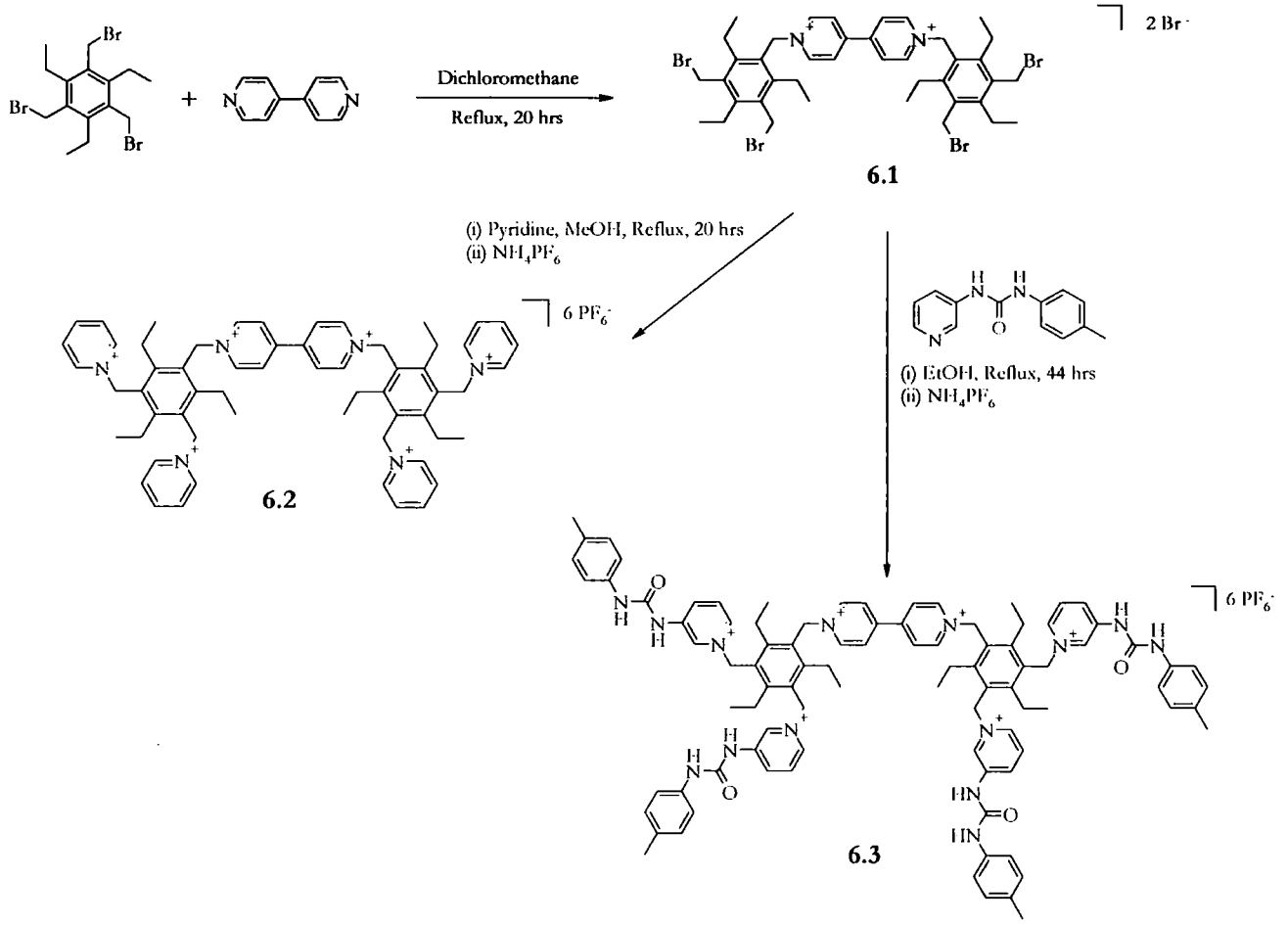

Scheme 6.1: Synthesis of Hosts **6.1** - **6.3**

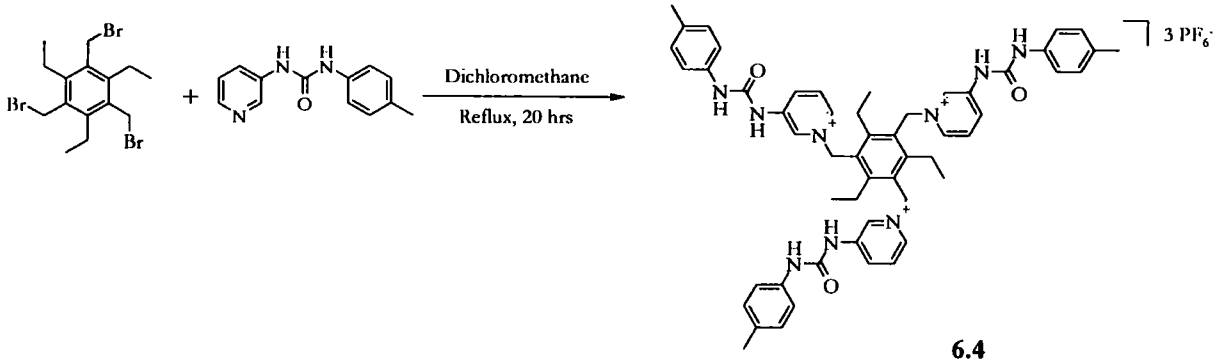

Scheme 6.2: Synthesis of Host **6.4**[2]

Since the completion of my research, a PhD student in the group, Adam Swinburne, has determined the crystal structure of host **6.2**, which confirms the proposed structure.

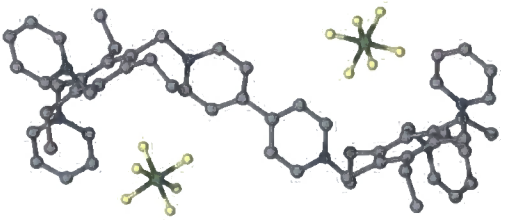

Figure 6.1: X-ray molecular structure of one of the independent cations in **6.2** showing two of the hexafluorophosphate anions located in close proximity to the viologen core.[224]

6.2 Binding studies

As hosts **6.2** and **6.3** were designed to bind anions, their anion binding ability was measured using NMR spectroscopic titration experiments. These experiments were undertaken with the two hosts, **6.2** and **6.3**, and a variety of anions as their tetrabutylammonium salts in acetonitrile-d_3. Anion binding constants for the formation of 1:1 and 1:2 host:guest complexes were calculated using HypNMR 2006,[165] and are given in **table 6.1**. The data showed strong binding to halide anions in the case of both hosts, with **6.3** showing a similar affinity for both chloride and bromide. The shift of the resonance assigned to the NH urea proton in host **6.3**, is shown in a stacked plot in **figure 6.3**, where the greatest shift is seen when the first equivalent of chloride is added to the host solution. It was not possible to determine a binding constant from the data obtained from the titration with nitrate, which could be due to complex binding. It is suggested that the binding of nitrate is less strong than with halide anions, due to the smaller chemical shift change upon addition of nitrate compared to that of addition of halide, as is seen in **figure 6.2**.

	K_{11} and K_{21} / M^{-1}	
Anion	**6.2**	**6.3**
Cl^-	log K_{11} 3.95(5) log K_{12} 3.21(6)	log K_{11} 3.55(6) log K_{12} 3.39(8)
Br^-	-	log K_{11} 3.75(7) log K_{12} 3.69(9)
NO_3^-	a	a
$MeCO_2^-$	b	b
$Succinate^{2-}$	b	b

Table 6.1: Anion binding constants (M^{-1}) for complexes **6.2** – **6.3** in CD_3CN at 20 °C. Errors are <10%, anions added as NBu_4^+ salts, host concentration 0.006 mol dm^{-3} (hyphen indicates not measured).

a) complex binding

b) decomposition of viologen

* *Graphical representation of the fit of titration data is given in the Appendix*

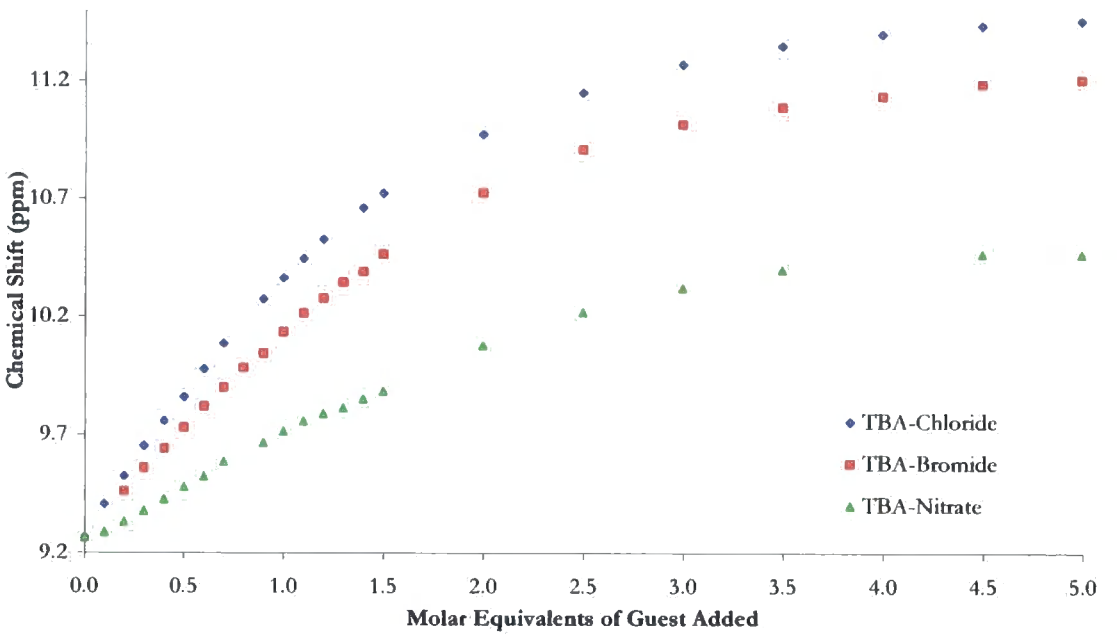

Figure 6.2: ^{1}H-NMR titration data of showing chemical shifts of NH resonances for **6.3** with tetrabutylammonium salts in CD_3CN at 20°C.

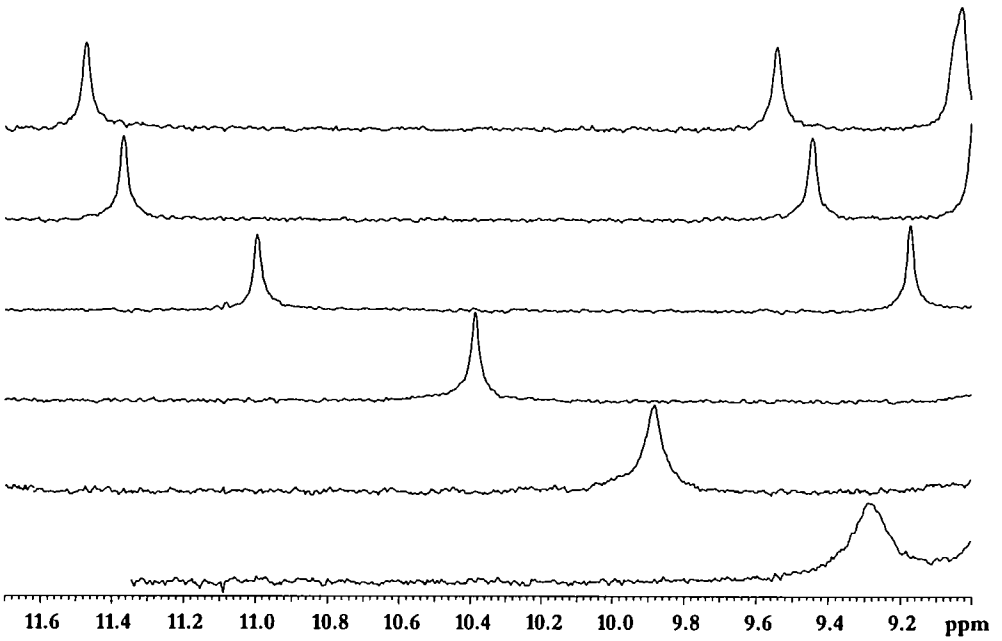

Figure 6.3: ^{1}H-NMR spectra of **6.3** as a function of added $NBu^{+}Cl^{-}$ (bottom to top 0.0, 0.5, 1.0, 2.0, 3.5, 5.0 equivalents of anion).

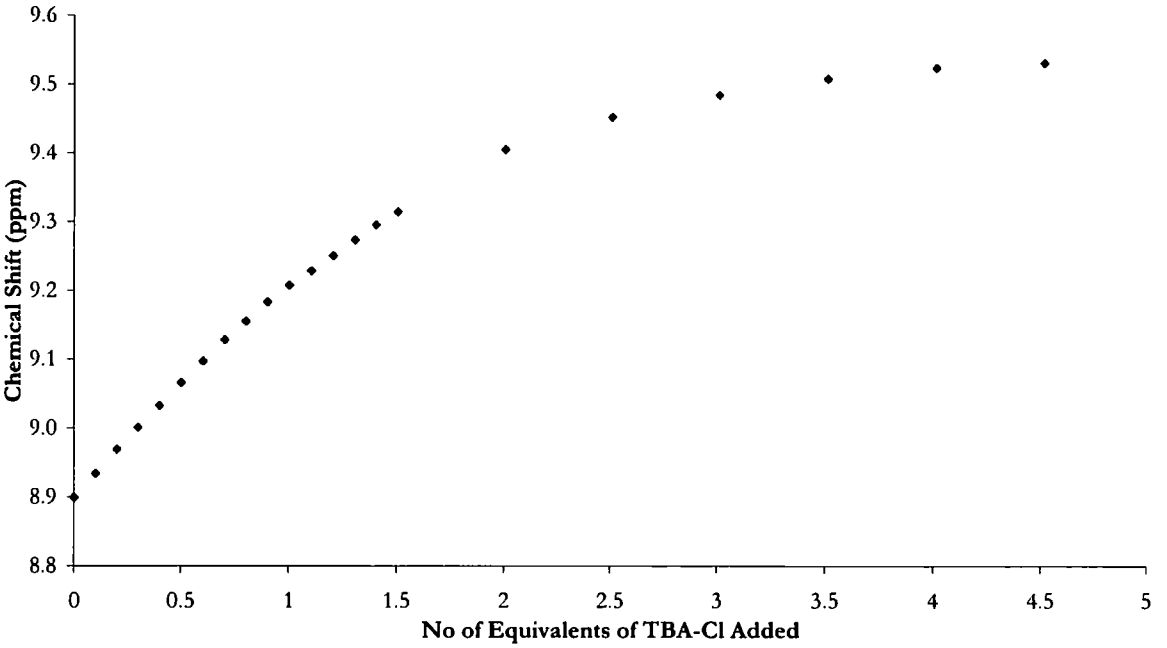

Figure 6.4: NMR titration data of showing chemical shifts of pyridyl resonances for **6.2** with tetrabutylammonium chloride in CD_3CN at 20°C.

In the urea host, **6.3**, the largest chemical shift is seen upon addition of chloride with a smaller shift upon addition of bromide and a significantly smaller shift upon addition of nitrate, **figure 6.2**, which is the same trend as was seen in calculated binding constants, **table 6.1**. This trend is consistent with both the urea, **6.3** and the pyridinium host, **6.2**, and also with the urea tripod, **6.4**.[185] The titration isotherms for the titrations with halides, show a smooth chemical shift in which the gradient decreases after the addition of one equivalent and further decreases after the addition of two equivalents of halide, in both hosts **6.2, figure 6.4,** and **6.2, figure 6.1**. The titration isotherm for the titration of **6.3** with nitrate, **figure 6.2**, is slightly sigmoidal in shape, suggesting the binding is more complex than that seen with halides, but the change in gradient is seen after addition of one equivalent of nitrate, suggesting that some 1:1 host:anion binding is seen. The ditopic nature of the hosts results in the strong binding of two chloride anions, with a similar affinity for bromide. The binding of nitrate and acetate was complex in nature and so binding constants could not be calculated from the data obtained. Upon addition of acetate the NMR spectrum became very complex, **figure 6.5**. Titrations were also undertaken with both malonate and succinate, as

their tetrabutylammonium salts, precipitation was seen after the addition of greater than 3.5 equivalents of dicarboxylates added, but the appearance of new peaks and increase in complexity of NMR spectra is seen, analogous to that which is shown in **figure 6.5**, upon addition of acetate to **6.3**. Viologen radical cations are known to react readily with molecular oxygen, to produce hydroxide, from the reduction of dioxygen, **scheme 6.3**, and the increase in complexity of the NMR spectra upon addition of carboxylates could be explained by considering the viologen host is undergoing chemical decomposition by the hydroxide present.

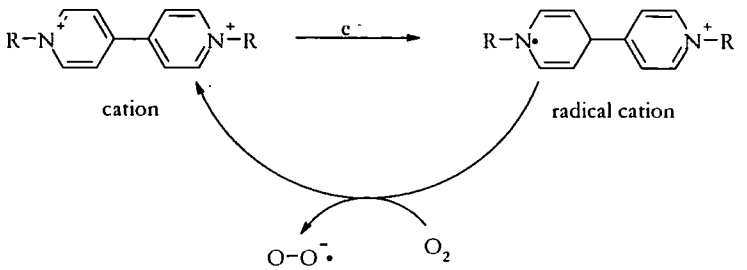

Scheme 6.3: Example of the dioxygen reduction by a viologen radical cation

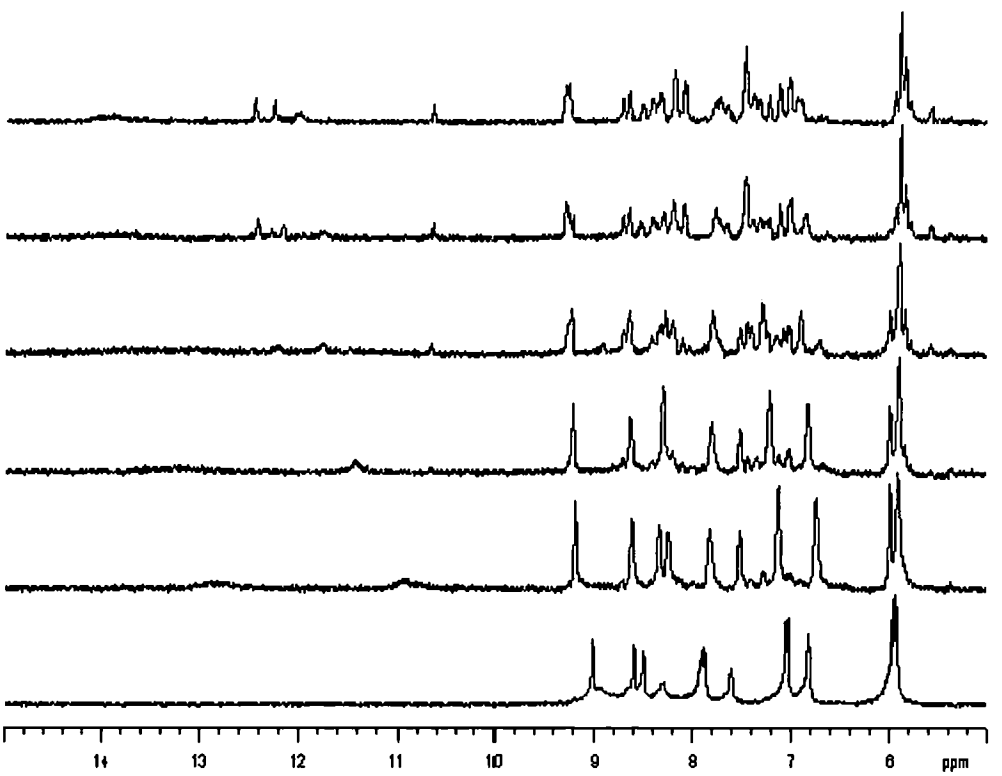

Figure 6.5: ^{1}H-NMR spectra of **6.3** as a function of added $NBu^+MeCO_2^-$. (bottom to top 0, 2.5, 3.0, 3.5, 4.5 and 5.0 equivalents of anion).

6.3 Colourimetric response to carboxylates

Addition of carboxylate anions (acetate, malonate and succinate) to both hosts, **6.2** and **6.3** resulted in the formation of an intense purple coloration. The solutions remain colourless in the presence of a wide variety of other anions (halides, nitrate and perrhenate). The colour change is strongly evident for the pyridinium host, **6.2**, upon addition of one equivalent of monocarboxylate (acetate) and 0.5 equivalents of dicarboxylates (malonate and succinate), but it does not become evident until addition of two equivalents of dicarboxylates (malonate and succinate) and three equivalents of the monocarboxylate (acetate) are added to the urea host, **6.3**, **figure 6.6**. The purple colour suggests the formation of a charge transfer complex of these anions with the viologen core. This phenomenon has been noted for viologens with biologically relevant phosphates.[225] As a control, starting material **6.1**, was reacted with carboxylates but this did not result in any colour change, which may be explained because **6.1** would be less readily reduced due to the lack of additional pyridinium functionalities.

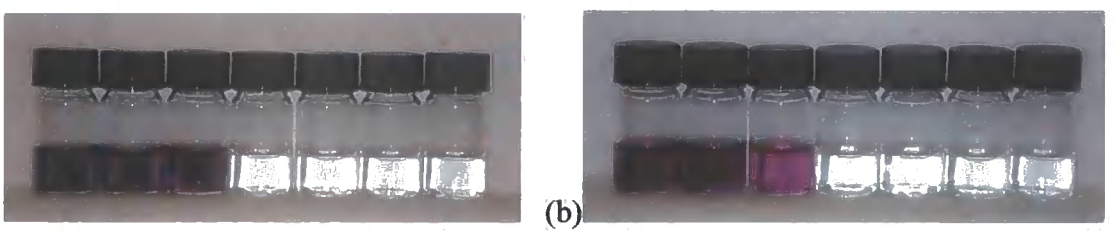

Figure 6.6: Degassed 1 x 10^{-4} M solutions of hosts **6.2** and **6.3** in the presence of NBu_4^+ salts of the following anions (from left to right): succinate; malonate: acetate; chloride; bromide; nitrate; perrhenate. (a) Host **6.2**, one equivalent of anion (0.5 equivalents of dicarboxylates); (b) Host **6.3** with four equivalents of anion (2 equivalents of dicarboxylates).

In the case of both hosts **6.2** and **6.3** the purple color gradually fades to red, after 2-3 hours and ultimately orange, after between 18 and 24 hours, on standing, after the solutions have been degassed, but in aerated solutions the colour changes occur on a much shorter timescale. In the aerated solutions the colour degrades from purple to pink, very rapidly, and so is barely visible, with an intense pink colour visible before rapidly fading to red after less than 5 minutes, and ultimately orange after 30 minutes for **6.2**, and for **6.3** the solution immediately forms a pink solution fading to red and then orange after several hours, **figure**

6.7. The intensity of the colour is also more intense in solutions which have been previously degassed, though this effect is more noticeable in the urea host **6.3**. Viologen radical cations are known to react readily with molecular oxygen and hence anion complexation was attempted in degassed solutions. This resulted in a persistent purple color that took much longer to fade.

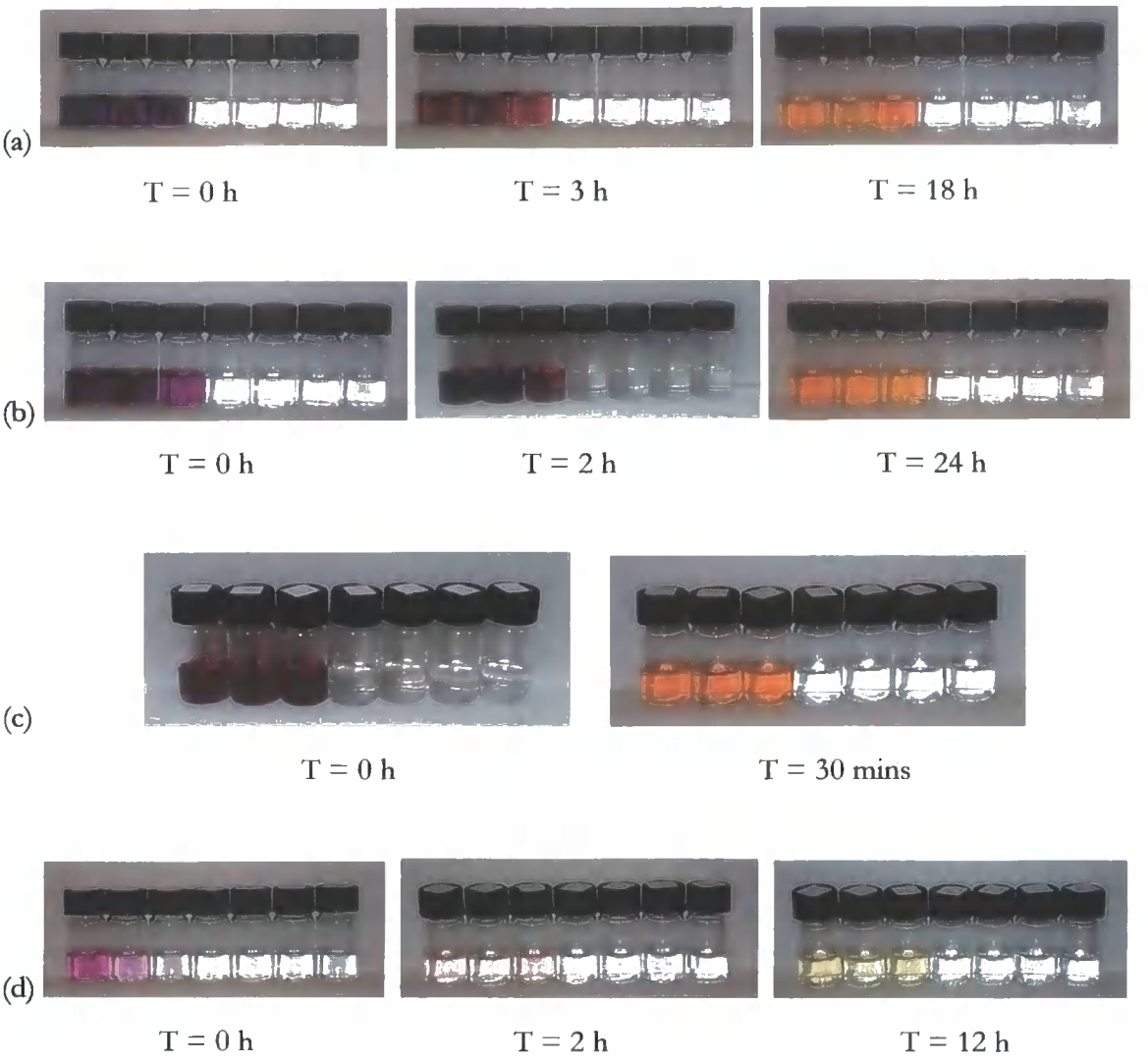

Figure 6.7: 1 x 10^{-4} M solutions of hosts **6.2** and **6.3** in the presence of NBu_4^+ salts of the following anions (from left to right): succinate; malonate: acetate; chloride; bromide; nitrate; perrhenate. (a) Degassed solution of host **6.2**, one equivalent of anion; (b) Degassed solution of host **6.3** with four equivalents of anion; (c) Aerated solution of host **6.2**, one equivalent of anion; (d) Aerated solution of host **6.3**, one equivalent of anion (in all cases 0.5 equivalents of dicarboxylates are added).

T = time elapsed since anions are added.

The anion-induced colour changes were studied by UV-Vis spectrophotometric titration both in the presence and absence of oxygen (method for anerobic measurements is shown in

experimental section **6.5**), **figures 6.8 - 6.12**. UV-Vis spectrophotometric titration with both ditopic hosts, **6.2** and **6.3**, and tripodal host **6.4** were undertaken in the presence of oxygen with chloride, which had previously showed no colour change. As is seen in the titration data there is a small change in the absorbance upon addition of chloride, for host **6.3**, **figure 6.8**, suggesting a host – anion interaction. An isosbestic point is observed at 320 nm, indication an equilibrium between two or more species. Upon addition of chloride to host **6.2**, **figure 6.9**, there is a small increase in the absorbance as is seen by the broad peak centred around 535 nm, which reaches a maximum after the addition of 1 equivalents, and remains unchanged after the addition of a further equivalents. After the addition of greater than 2 equivalents of chloride results in a reduction of the absorbance at this point. The absence of a visible colour change upon addition of chloride to the host solutions, **6.2** and **6.3**, maybe explained because the origin of the colour change is the formation of a charge transfer complex. The small increase in absorbance which occurs upon addition of chloride to host **6.2**, shown in **figure 6.9**, centred on 538 nm, which appears in the same region as the broad band seen in the degassed titration of **6.2** with acetate, so it is suggested that this is due to the formation of a small amount of the charge transfer complex.

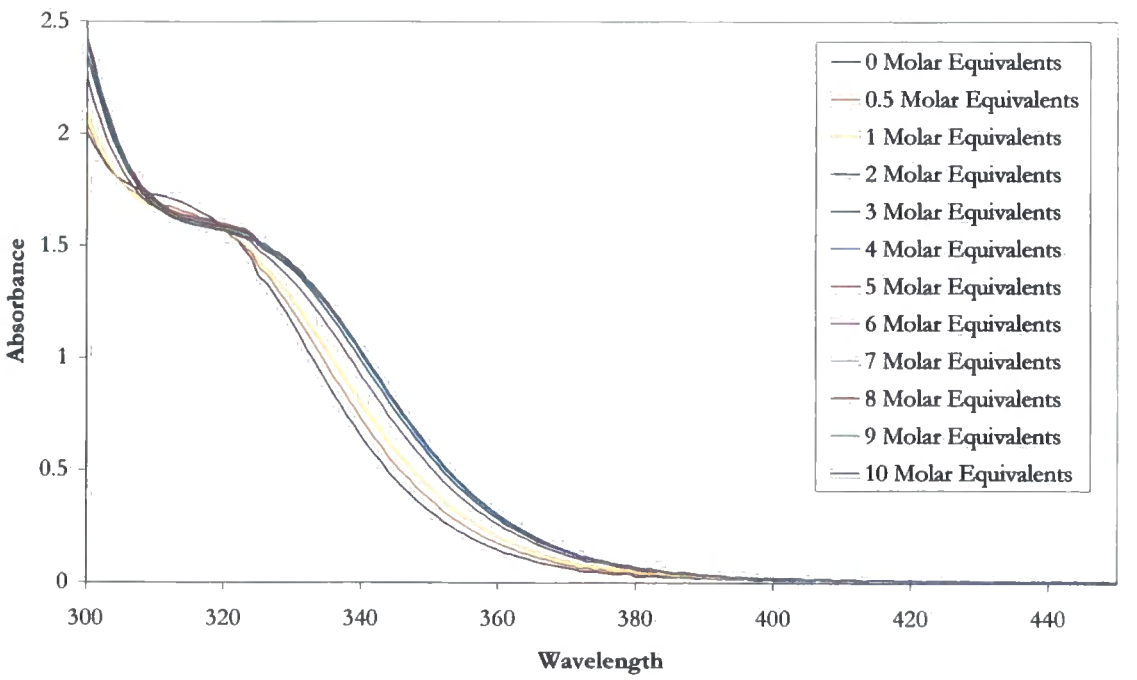

Figure 6.8: Absorption spectra of **6.3** (1.03×10^{-4} M) in CH_3CN and upon addition of increasing amounts of chloride up to 10 equivalents.

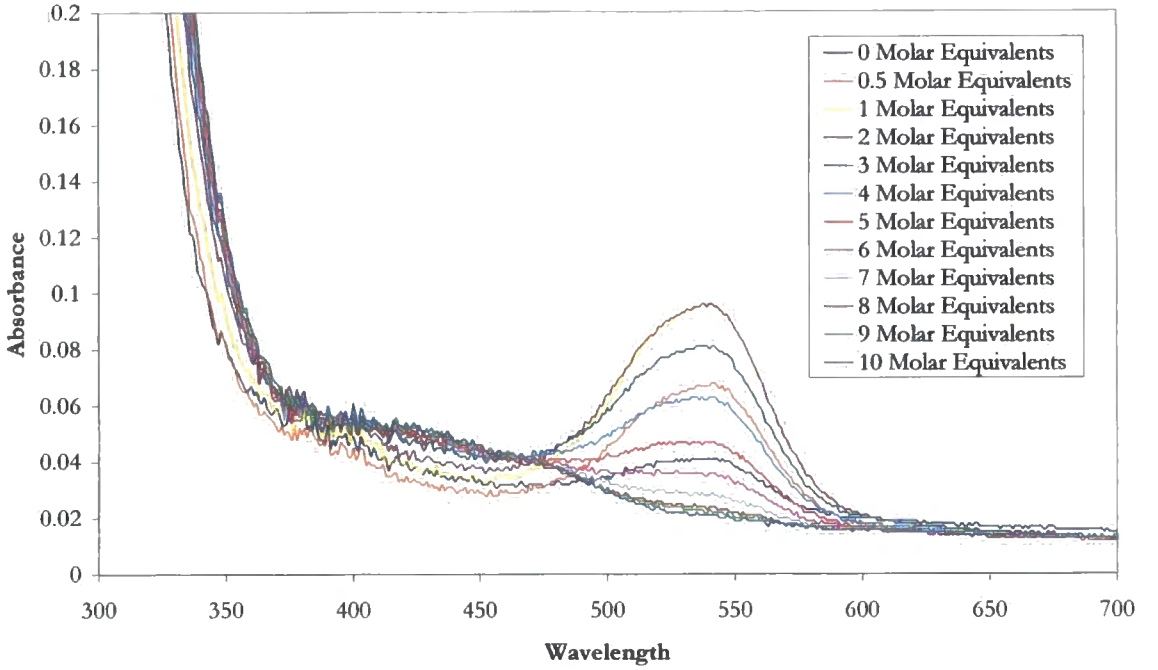

Figure 6.9: Absorption spectra of **6.2** (1.03×10^{-4} M) in CH_3CN and upon addition of increasing amounts of chloride up to 10 equivalents.

Upon addition of acetate, there is a significant change in the absorbance, which is affected by the presence and absence of oxygen. The aerated data shown in **figure 6.10(a)**, shows a broad band centred on 488 nm, which has been assigned to the compound resulting from the chemical decomposition, as was seen in the NMR spectra, which results in the solution forming an orange colour. The band centred on 543 nm, with a shoulder centred at a lower wavelength, is assigned to the charge transfer complex appearing in both the aerated and degassed data. In the aerated data the peak assigned to the charge transfer complex reaches a maximum after the addition of four equivalents of acetate, but a maxima is reached after the addition of 8 equivalents of acetate. In both data sets there is a large increase in the absorbance upon addition of the fourth equivalent of acetate. The appearance of the chemical decomposition band appears after the addition of 6 equivalents of acetate, but it is unclear as to whether the appearance of this band is time dependant or dependant on the concentration of carboxylate. The degassed data, **figure 6.10(b)** gives the smooth growth of a band at 543 nm with a shoulder at a lower wavelength. The intensity of this band increases suddenly on addition of over two equivalents of acetate. Both the aerated and degassed data

shows an isosbestic point at 320 nm, suggesting the formation of two or more species which are in equilibrium.

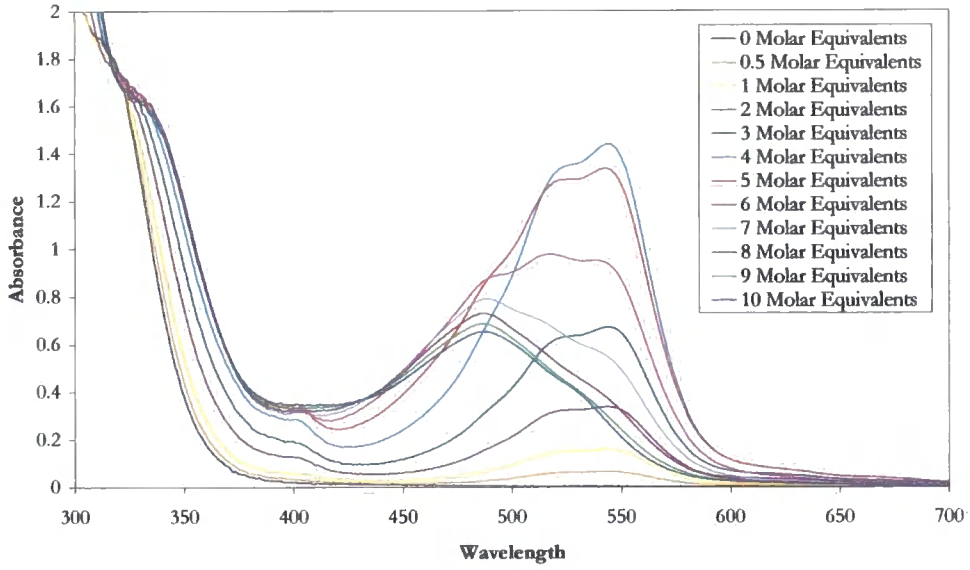

(a)

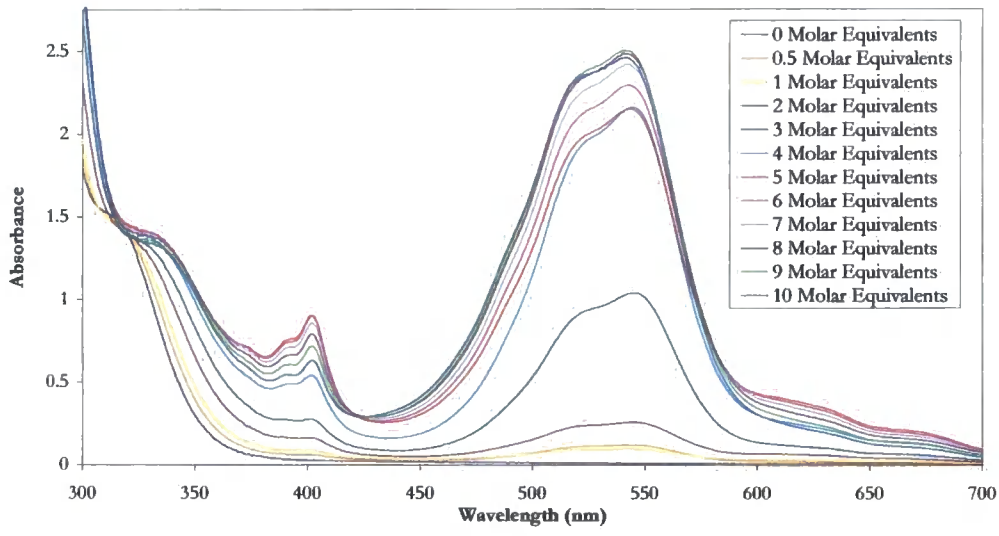

(b)

Figure 6.10: Absorption spectra of **6.3** (1.03×10^{-4} M) in CH_3CN and upon addition of increasing amounts of acetate up to 10 equivalents (a) in the presence of oxygen and (b) in degassed solution.

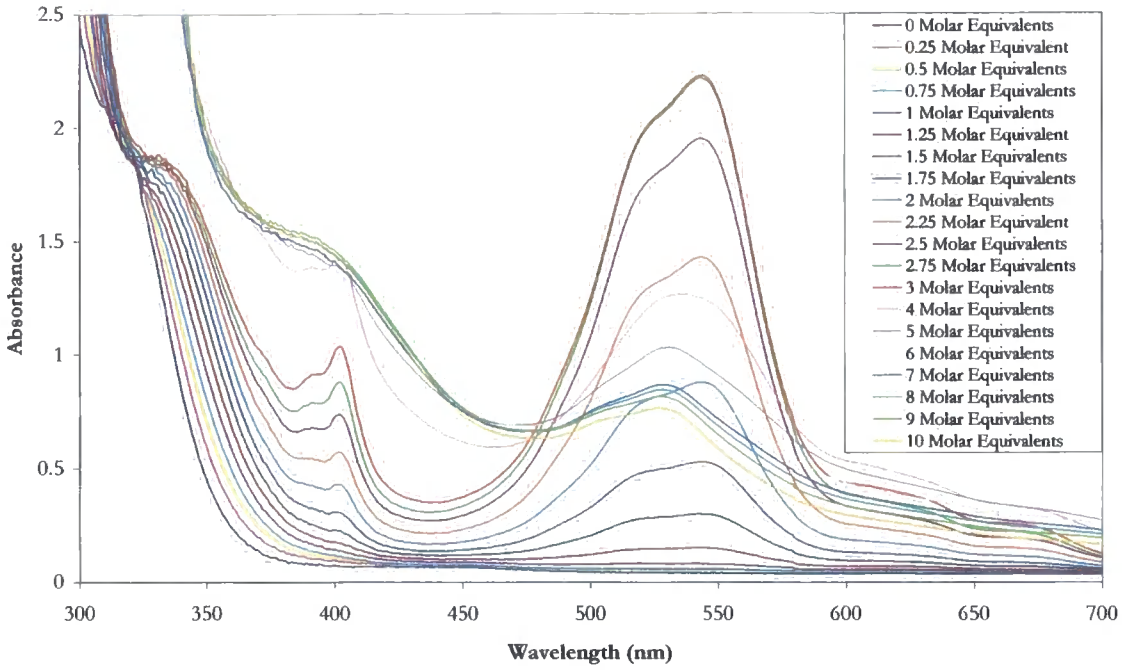

Figure 6.11: Absorption spectra of **6.3** (1.03×10^{-4} M) in degassed CH_3CN and upon addition of increasing amounts of succinate up to 10 equivalents.

Upon addition of the dicarboxylate, succinate, as its tetrabutylammonium salt, a significant change in the absorbance is observed in degassed solution, **figure 6.11**. The absorbance remains unchanged until after the addition of one equivalent of succinate, and it is not until the addition of two equivalents, that a visible change occurs. Upto the addition of three equivalents of succinate, there is a significant change in the absorbance, which reaches a maximum, upon addition of three equivalents. As with the addition of acetate, there is a band centred on 543 nm, with a shoulder at a lower wavelength, which is assigned to the charge transfer complex. The addition of a fourth equivalent of succinate sees a significant decrease in the absorbance of the charge transfer band, and a large increase in the band centred on 402 nm, which is also related to the charge transfer. As with the addition of acetate, in degassed solution, the band centred on 490 nm and assigned to the decomposition is not visible, but there is a broad band centred on 531 nm, which appears after the addition of four equivalents of succinate, which maybe due to some decomposition, as despite effort to ensure the sample is oxygen free, the opening of the cuvette to add aliquots of succinate, mean that is it possible for some oxygen to enter the cuvette. There is

also a loss of definition of the spectrum, after the addition of five equivalents, which is a reason for the suggested decomposition as well as the observation that the solution starts to turn orange, which was observed during the chemical decomposition.

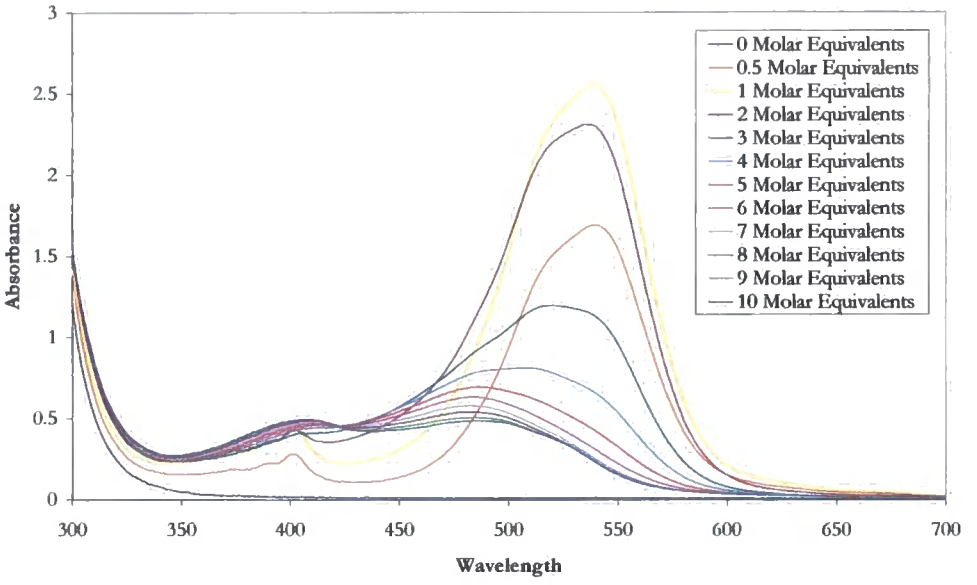

(a)

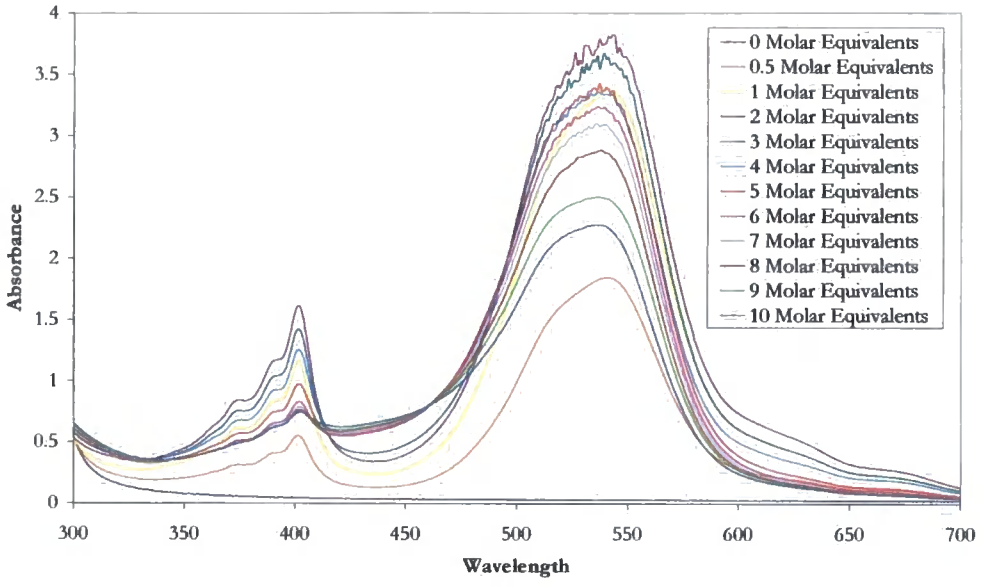

(b)

Figure 6.12: Absorption spectra of **6.2** (1.03×10^{-4} M) in CH_3CN and upon addition of increasing amounts of acetate up to 10 equivalents (a) in the presence of oxygen and (b) in degassed solution.

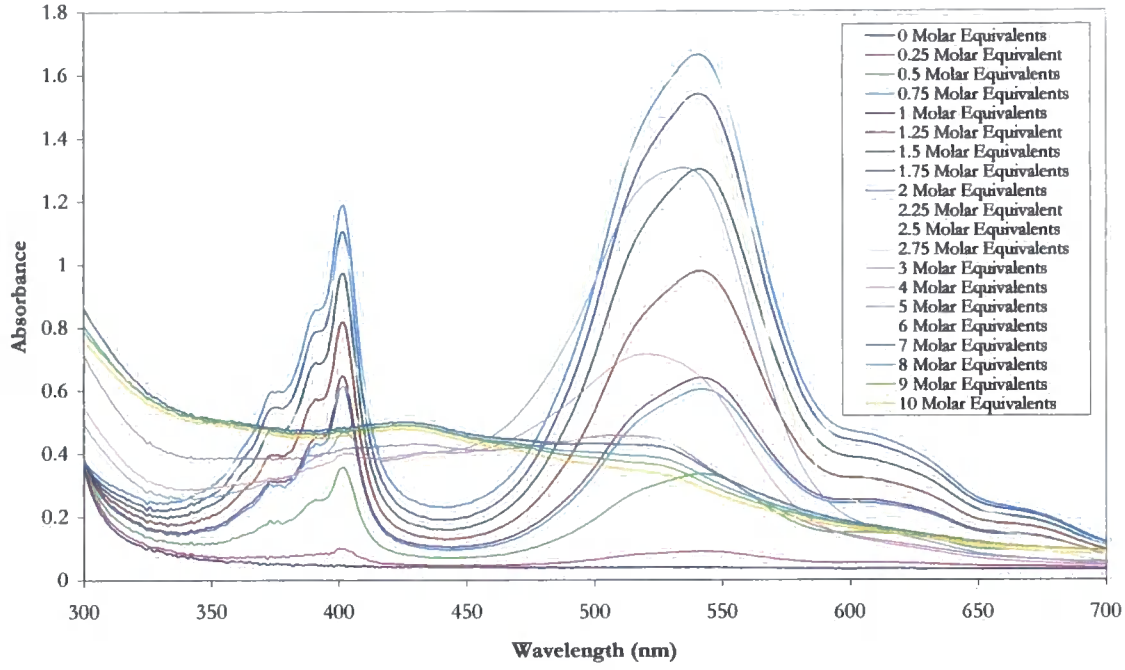

Figure 6.13: Absorption spectra of **6.2** (5.15×10^{-5} M) in degassed CH_3CN and upon addition of increasing amounts of succinate up to 10 equivalents.

The aerated data shown in **figure 6.12(a)**, shows a broad band centred on 488 nm, which has been assigned to the compound resulting from the chemical decomposition, as was seen in the NMR spectra for **6.2**, which results in the solution forming an orange colour. The band centred on 536 nm, with a shoulder centred at a lower wavelength, is assigned to the charge transfer complex appearing in both the aerated and degassed data. In the aerated data the peak assigned to the charge transfer complex reaches a maximum after the addition of one equivalents of acetate, but a maximum is reached after the addition of two equivalents of acetate, in degassed solution. In both data sets there is a large increase in the absorbance upon addition of the first equivalent of acetate, but in both data sets there is also a large increase in absorbance upon addition of 0.5 equivalents of acetate. The appearance of the chemical decomposition band appears after the addition of four equivalents of acetate, but it is unclear as to whether the appearance of this band is time dependant or dependant on the concentration of carboxylate. Upon addition of two equivalents of succinate, to a degassed solution of **6.2**, there is a significant increase in the absorption, and a maximum absorbance is reached. The addition of the first equivalent of succinate sees an increase in the

absorbance, which was not observed upon addition of one equivalent to **6.3**, and a visible colour change was obvious after the addition of one equivalent of anion. As with **6.3**, there is a loss of definition of the spectrum after the addition of five equivalents of succinate, and visible observations saw the intense purple colouration degrading to a red-orange colouration. As the experiments with both hosts **6.2** and **6.3** were undertaken under the same conditions, but the point at which the band assigned to the chemical decomposition of the hosts occurs after the addition of four equivalents of acetate for **6.2** and six equivalents for **6.3**, suggests that concentration of carboxylate, as well as time is a factor in the chemical composition The degassed data, **figure 6.12(b)** gives the smooth growth of a band at 536 nm with a shoulder at a lower wavelength. The intensity of this band increases suddenly on addition of over two equivalents of acetate.

Upon addition of acetate to the urea host **6.3**, the charge transfer band reaches near to its maximum intensity upon addition of one equivalent of acetate, in degassed solution, **figure 6.10(b)**. This behaviour can be explained by competitive anion binding by the urea host, **6.3**, between the urea and pyridium groups. In this host, **6.3**, the binding of the first two equivalents of acetate is by the urea protons remote from the viologen core, resulting in little charge transfer. When these sites have been saturated, the binding of the third equivalent occurs near to the viologen chromophore resulting in a visible charge transfer response. In contrast, upon addition of one equivalent of acetate to the pyridinium host, **6.2**, shows an immediate visible charge transfer, when the anion is bound near to the viologen chromophore as there is no competing binding sites in this host. There is a band with absorption centred around 488 nm in the presence of oxygen, in hosts **6.2** and **6.3**, **figures 6.12(a)** and **6.10(a)** respectively, which is the origin of the orange colour, but the cause of this band is unclear. It could be due to the chemical decomposition as suggested earlier, in **section 6.2**, for the NMR spectra becoming highly complex during the NMR spectroscopic titration experiment.

In order to gain further inights into the anion binding modes and origin of the colour changes we undertook DFT calculations,[26] in collaboration with Dr Martin Paterson, Herriot-Watt University, on the representative systems **6.2**·malonate and **6.3**·$(acetate)_2$, the former of which displays the purple colouration whereas the latter require further

acetate addition to change colour. Geometry optimization was performed using the hybrid B3LYP density functional, with the following basis: 4-31G on the viologen system, 6-31+G* on the anion (malonate or acetate), and a set of diffuse s and p functions augmenting the basis on the proximal hydrogen atoms to the anions. The calculated geometry of **6.2**·malonate is shown in **figure 6.14(a)** which reveals the ability of the host to enfold the anion, binding via charge assisted pyridinium CH···O interactions. The anion is situated close to the bipyridinium core in a suitable geometry to give a charge transfer interactions. The electronic absorption characteristics of **6.2**·malonate were investigated using time-dependent linear response density functional theory based on the B3LYP functional and the 6-31G* basis on all atoms. The calculations revealed a dominant single particle-hole configuration of a state at 2.25 eV (550 nm(calculated), and 543 nm(measured), in good agreement with the observed visible absorption), **figure 6.15**. The transition thus arises from promotion of an electron in a localised π orbital on the malonate anion to the π^* orbital on the bipyridinium moiety. The transition has a large oscillator strength (f=0.005) and so would be expected to give rise to an intense vibronic band, consistent with observation. The calculated structure of **6.3**·$(acetate)_2$ is shown in **figure 6.14(b)**. The acetate anions interact with the strongly hydrogen bonding urea groups as observed for analogous host **6.4**[185] and are remote from the viologen core. Calculations of the electronic absorption characteristics of this system indicate that there is no comparable transition in the 550 nm region of the electronic absorption spectrum.

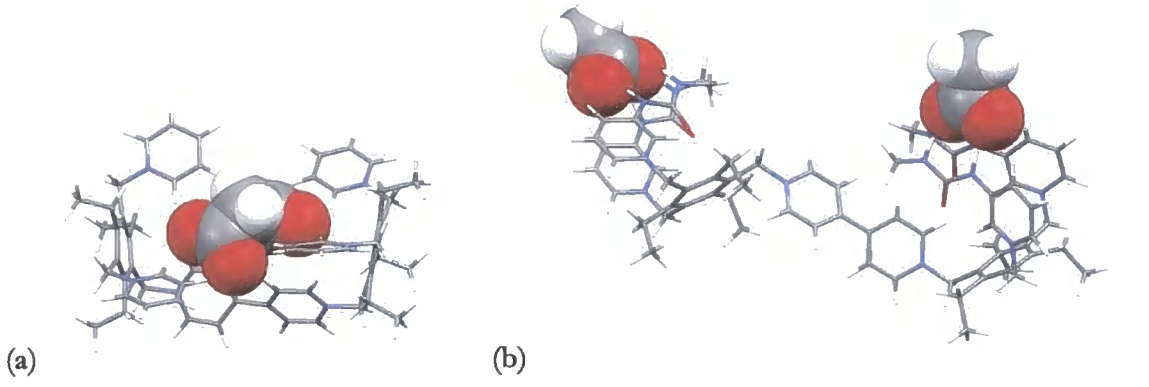

Figure 6.14: DFT calculated structures for (a) **6.2**·malonate and (b) **6.3**·$(acetate)_2$. Anions shown in space filling mode.

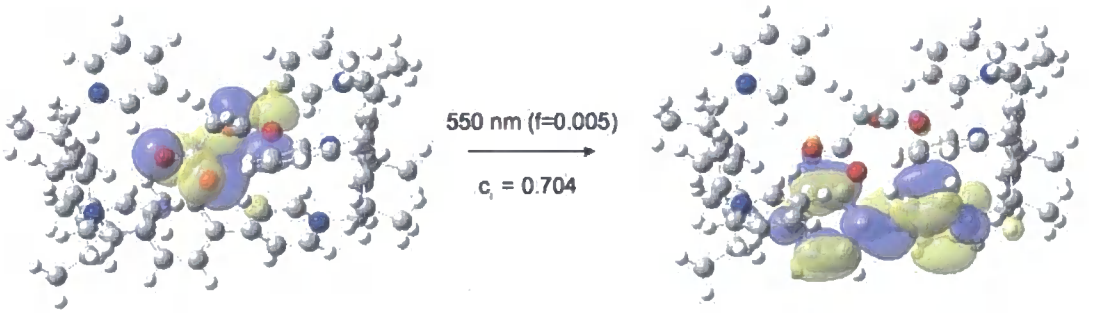

Figure 6.15: A representation of a transition at 550 nm from time-dependent DFT calculations of the malonate with **6.2**.

An analogous titration with the tripod, **6.4**,[185] which contains three ureidopyridine groups but no bipyridinium moiety, was undertaken. There was no colour change in the visible region, upon addition of chloride, **figure 6.16**, and acetate, **figure 6.17**, which suggested that processes such as deprotonation of the urea protons was not involved. There is a small increase upon addition of chloride, with a clear isosbestic point at 268 nm, and the peak shifts and reaches a maximum absorbance after the addition of 10 equivalents of chloride. The same trend is seen upon addition of acetate, **figure 6.17**, but upon addition of acetate there is a greater increase in the absorbance, but this increase is very small when compared

to that seen in the tetrapodal hosts, **6.2** and **6.3**. There is also a clear isosbestic point seen, as in the chloride titration.

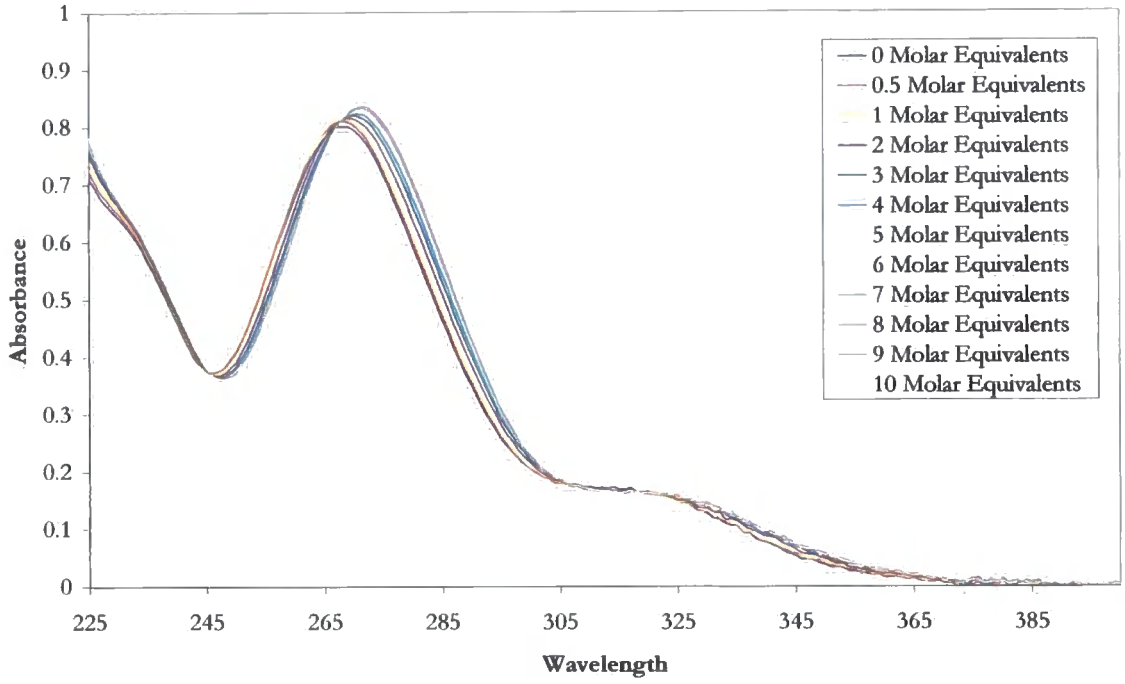

Figure 6.16: Absorption spectra of **6.4** (1.03×10^{-4} M) in CH_3CN and upon addition of increasing amounts of chloride up to 10 equivalents, in the presence of oxygen.

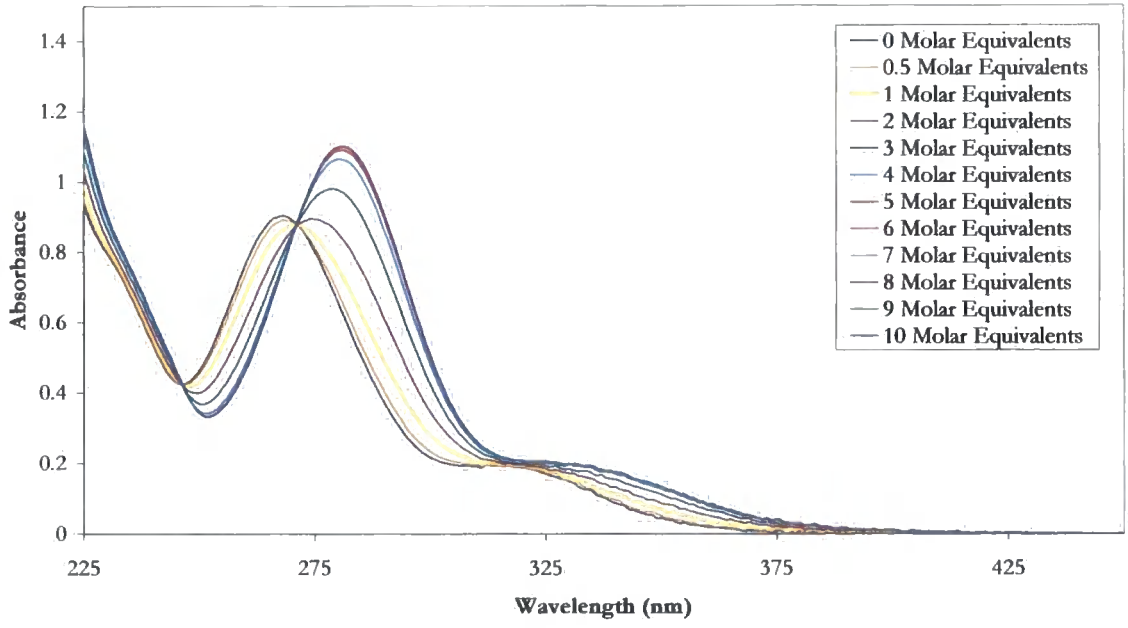

Figure 6.17: Absorption spectra of **6.4** (1.03×10^{-4} M) in CH_3CN and upon addition of increasing amounts of acetate up to 10 equivalents, in the presence of oxygen.

6.4 Summary

The two receptors showed strong halide binding, but due to complex binding to oxo-anions the binding affinity to these anions could not be calculated, but a smaller overall chemical shift was observed upon addition of nitrate compared to both chloride and bromide, so it is suggested that the binding to nitrate is less than to halides. Binding to carboxylates results in a complex NMR spectra, and it is suggested the appearance of new peaks is due to decomposition of the complex, by hydroxide attack, from the reduction of dioxygen, a phenomenon previously observed by viologen cations. Carboxylate binding brings about a visual color change at relatively low concentrations upon binding to the polytopic receptors. The amount of anion needed to trigger a colorimetric response can be controlled in a step-fashion by the identity of the peripheral binding groups. This ability to tune the amount of acetate needed to cause a response by internal binding site competition, coupled to the distinct carboxylate selectivity, could prove highly useful in anion sensing applications.

6.5 Experimental

6.5.1 Degassed UV-Vis spectroscopic titration experiments

3 mL of host solution in acetonitrile is added to the cuvette, this is degassed, by freeze-pump-thaw methods, several times, to ensure the solution is completely oxygen free. An absorbance measurement is then taken of the degassed solution. Nitrogen is blown over the solution and an aliquot of anion is added through the Youngs' tap, the solution is then thoroughly mixed, and another measurement is taken. This process is repeated until all measurements have been completed.

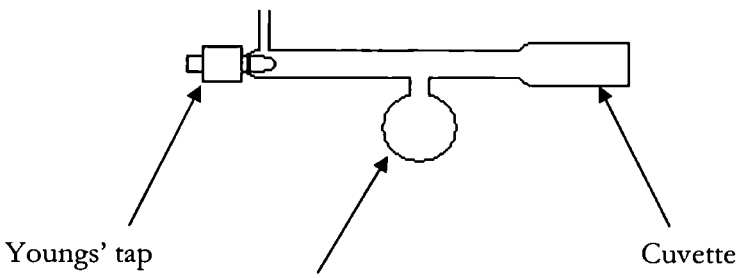

1,1'-bis(3,5-bis(bromomethyl)-2,4,6-triethylbenzyl)-4,4'bipyridine-1,1'-diium

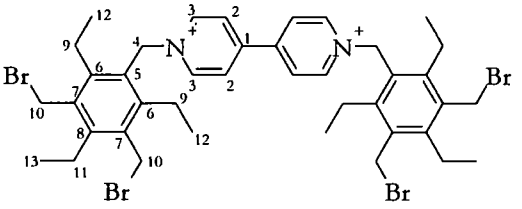

1,3,5-tri(bromomethyl)-2,4,6-triethylbenzene (6.00 g, 13.60 mmol) and 4,4'bipyridine (0.21 g, 1.36 mmol) were dissolved in dichloromethane (150 ml) and stirred at reflux for 20 hours. During this time, a pale yellow precipitate of 1,1'-bis(3,5-bis(bromomethyl)-2,4,6-triethylbenzyl-4,4'bipyridine-1,1'-diium bromide was formed. This was filtered and washed with dichloromethane (3 x 50 ml). This yielded the bromide salt as a pale yellow solid (1.32 g, 1.27 mmol, 93%).

^{1}H-NMR (DMSO-d_6, 500 MHz, δ/ppm, J/Hz): 9.01 (4H, d, J = 7.0, H(3)); 8.71 (4H, d, J = 7.0, H(2)); 6.05 (4H, s, CH2(4)); 4.78 (8H, s, CH_2(10)); 2.96 (4H, q, J = 7.3, -CH_2(11)); 2.76 (8H, q, J = 7.3, CH_2); 1.34 (6H, t, J = 7.3, CH_3(13)); 1.07 (12H, t, J = 7.3, CH_3(12)).

^{13}C{^{1}H}-NMR (DMSO-d_6, 100 MHz, δ/ppm): 149.8 (C1), 147.6 (C8), 147.1 (C6), 145.3(C3), 134.3 (C7), 127.8 (C2), 127.2 (C5), 58.3 (C4), 31.4 (C10), 23.6 (C9), 23.2 (C11), 16.0 (C12&13).

ES+ MS: *m/z* = 878 $[M-2Br]^{\bullet+}$, 517 $[M]^{2+}$, 494, 439 $[C_{20}H_{25}Br_2N]^+$, 361 $[C_{15}H_{19}Br_2]^+$, 261 $[M]^{4+}$, 179 $[M-4Br]^{4+}$.

Anal: Calculated for $C_{40}H_{50}N_2Br_6$: C, 44.72; H, 4.85; N, 2.70 %
Found: C, 44.43; H, 4.80: N, 2.51 %

IR (ν/cm^{-1}): 3120 (s, Ar C-H), 3044 (s, Ar C-H), 2967 (s, CH_2/CH_3), 2923 (s, CH_2/CH_3), 2879 (s, CH_3/CH_2), 1636 (s, Ar C=C), 1560 (s, Ar C=C), 1501 (m, Ar C=C), 1444 (s, CH_2/CH_3 def), 1381 (m, CH_3) 699 (m, C-Br), 587 (m, C-Br), 509 (m, C-Br)

1,1'-bis(2,4,6-triethyl-3,5-bis((pyridinium-1-ylmethyl)benzyl)-4,4'-bipyridine-1,1'-diium Hexafluorophosphate

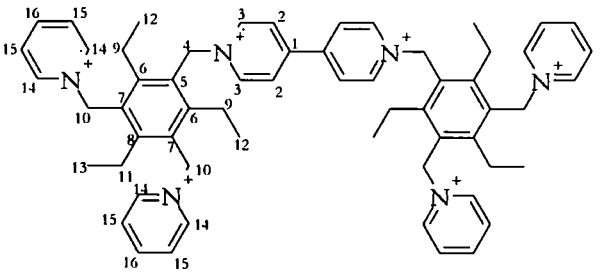

1,1'-bis(3,5-bis(bromomethyl)-2,4,6-triethylbenzyl)-4,4'bipyridine-1,1'-diium bromide (0.25 g, 0.24 mmol) and pyridine (2.85 g, 36 mmol) were dissolved in methanol (125 ml) and stirred at reflux for 6 h. The reaction mixture was then cooled and the solvent (105 ml) removed under reduced pressure. Diethyl ether (30 ml) was added to the solution and a yellow precipitate was observed. This was filtered and a ^{1}H NMR spectrum was taken of the bromide salt. The resultant precipitate was sticky and was not fully characterised. The solid was dissolved in methanol (30 ml) with 10 equiv of NH_4PF_6 (0.39 g, 2.41 mmol) and stirred at ambient temperature for 6 h. A very pale yellow precipitate of 1,1'-bis(2,4,6-triethyl-3,5-bis(pyridinium-1-ylmethyl)benzyl)-4,4'-bipyridine-1,1'-diium hexafluorophosphate was observed which was recovered by filtration and dried under ambient conditions. The solid was recrystallised in acetonitrile and diethyl ether, producing a sticky, pale yellow solid. This was filtered, re-dissolved in acetonitrile (10ml) and then the solvent was removed under reduced pressure to producing a pale yellow solid powder (0.23 g, 0.13 mmol, 55%).

^{1}H NMR (DMSO-*d*$_6$, 500 MHz, δ/ppm, J/Hz): 9.17 (4H, d, J = 6.7, bipy-H(3)); 8.93 (8H, d, J = 6.2, PyH(14)); 8.65 (8H, m, bipy-H(2) and PyH(16)); 8.18 (8H, t, J = 7.1, PyH(15)); 6.14 (4H, s, Py-CH_2(4)); 6.08 (8H, s, Py-CH_2(10)) 2.69 (12H, q, J = 7.5, CH_2(11)); 0.82 (18H, m, CH_3(12&13)).

^{13}C{^{1}H}-NMR (DMSO-d$_6$, 125 MHz, δ/ppm): 151.1(C4), 151.0, 150.0, 146.9(C15), 145.7, 144.7(C10), 129.2(C14), 129.0, 128.4, 127.6, 58.4, 58.1, 24.2(C12&13), 15.5(C11), 15.4. *(due to solubility of the host, complete assignment of this spectrum could not be completed)*

ES$^+$ MS: m/z = 805 $[C_{35}H_{39}N_4P_2F_{12}]^+$, 728 $[M\text{-}2(PF_6)]^{2+}$, 519, 437 $[M\text{-}6(PF_6)]^{\cdot 2+}$, 437 $[M\text{-}3(PF_6)]^{3+}$, 330, 291 $[M\text{-}4(PF_6)]^{4+}$, 204 $[M\text{-}5(PF_6)]^{5+}$.

Anal: Calculated for $C_{60}H_{70}N_6P_6F_{36}$: C, 41.30; H, 4.04; N, 4.82 %
Found: C, 41.77; H, 4.14; N, 4.75 %

IR (ν/cm^{-1}): 3143 (m, Ar C-H), 3104 (m, Ar C-H), 2978 (m, CH_2/CH_3), 2940 (m, CH_2/CH_3), 1637 (s, Ar C=C), 1567 (s, Ar C=C), 1503 (s, Ar C=C), 1448 (m, CH_2/CH_3), 1391 (m, CH_3)

1,1'-bis(2,4,6-triethyl-3,5-bis((3-(3-p-tolylureido)pyridinium-1-yl)benzyl)-4,4'-bipyridine-1,1'-diium Hexafluorphosphate

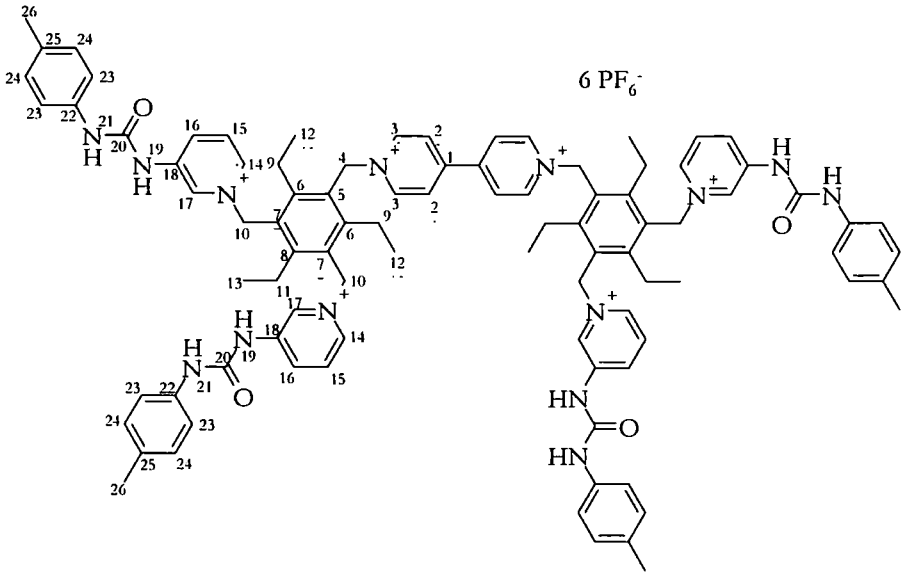

1,1'-bis(3,5-bis(bromomethyl)-2,4,6-triethylbenzyl)-4,4'bipyridine-1,1'-diium bromide (0.75 g, 0.72 mmol) and 1-pyridin-3-yl-3-*p*-tolyl-urea (1.31 g, 5.77 mmol) were dissolved in ethanol (340 ml) and stirred at reflux for 44 h. During this time, a brown precipitate was formed, stuck to the round-bottomed flask. The reaction mixture was filtered to remove any of the brown solid. The solution was concentrated by removing ethanol (290 ml) under reduced pressure. The observed precipitate was filtered and a ^{1}H NMR spectrum was taken of the bromide salt. The resultant precipitate was sticky and was not fully characterised. The precipitate was dissolved in methanol (50 ml) with 10 equiv of NH_4PF_6 (1.17 g, 7.22 mmol) and stirred at ambient temperature for 6 h. A pale orange precipitate of 1,1'-bis(2,4,6-triethyl-3,5-bis((3-(3-p-tolylureido)pyridinium-1-yl)benzyl)-4,4'-bipyridine-1,1'-diium hexafluorophosphate was observed which was recovered by filtration and dried under ambient conditions (0.44 g, 0.19 mmol, 31%).

^{1}H NMR (CD_3CN-d_3, 400 MHz, δ/ppm, J/Hz): 9.26 (4H, s, NH(19)); 8.97 (4H, s, PyH(17)); 8.95 (4H, br s, NH(21)); 8.62 (4H, d, J = 6.6, bipy-H(3)), 8.51 (4H, d, J = 6.8, PyH(14)); 7.97 (4H, d, J = 8.4, PyH(16)); 7.92 (4H, dd, J = 9.0, 5.9, PyH(15)); 7.65 (4H, d, J = 6.6, bipy-H(2)); 7.04 (8H, d, J = 8.1, ArH(23)), 6.79 (8H, d, J = 8.1, ArH(24)); 5.96 (4H, s, Py-CH_2(4)); 5.92 (8H, s, Py-CH_2(10)); 2.79 (4H, q, J = 7.4, CH_2(11)); 2.53 (8H, br s, CH_2(9)), 2.08 (12H, br s, CH_3(26)), 1.29 (6H, t, J = 7.4, CH_3(13)); 1.22 (12H, t, J = 7.5, CH_3(12)).

^{13}C{^{1}H}-NMR (CD_3CN-d_3, 100 MHz, δ/ppm): 206.5, 152.4, 152.0, 151.4, 149.6, 144.8. 141.4, 137.5, 135.6, 133.8, 133.4, 132.0, 129.6, 128.6, 128.4, 127.3, 120.0, 58.4, 58.1, 24.5, 24.3, 20.0, 15.1, 14.8. *(due to solubility of the host, complete assignment of this spectrum could not be completed)*

ES$^+$ MS: m/z = 1024 $[M - 2(PF_6)]^{2+}$, 634 $[M - 3(PF_6)]^{3+}$, 227 $[TUP]^+$, 183 $[C_{12}H_{11}N_2]^+$.

IR (ν/cm^{-1}): 3413 (s, N-H), 3120 (m, Ar C-H), 2983 (m, CH_2/CH_3), 1714, 1636 (s, Ar C=C), 1593 (s, urea C=O), 1551 (s, Ar C=C), 1503 (s, Ar C=C), 1460, 1443, 1408 (m, CH_2/CH_3), 1390 (w, CH_3).

Anal: Calculated for $C_{92}H_{102}N_{14}P_6F_{36}$: C, 47.27; H, 4.40; N, 8.39 %
Found: C, 47.36; H, 4.56: N, 8.23 %

Chapter Seven
Conclusions

The original aims of this project were to synthesise novel amine containing ligands, based upon a pyridyl ring, for use within anion binding systems with both organic and transition metal cores.

A series of amino-pyridyl ligands have been successfully synthesised. These were prepared in good yields from a pyridine-carboxaldehyde and either, aniline, 4-methoxyaniline, 4-nitroaniline or 3-amino-9-ethylcarbazole. These ligands were shown to form intramolecular hydrogen bonds, between pyridyl nitrogen atoms and amine protons on adjacent ligands. Ligand **2.2** was shown to have to two polymorphs, in the first Z' = 1 polymorph hydrogen bonding is seen between adjacent molecules in an A-A-A pattern, but in the Z' = 2 polymorph, hydrogen bonding is seen between symmetry related molecules so in an A-A-A pattern and a B-B-B pattern. Ligands **2.2** and **2.5**, was also observed to be a Z' = 2 structure in which hydrogen bonding is observed between adjacent molecules, in an A-B-A pattern. As ligands **2.4** and **2.6**, all occur as one polymorph, which are all Z' = 1 structures bonding is observed in a A-A-A pattern (Chapter 2).

The aminomethyl-pyridyl ligands were shown to interact with transition metals in solid and solution states. The addition of copper(II) acetate has shown the formation of a stable copper acetate dimer with ligands **2.2** and **2.5**. The addition of metal nitrates resulted in the formation of nitrates hydrogen bonded to protonated ligands, but in these cases no metal interactions were observed (Chapter 3). Proposed structures of ligands and $Cu(CF_3SO_3)_2$ were given, from elemental analysis results, and it was proposed that by addition of different molar equivalents of $Cu(CF_3SO_3)_2$ to a ligand solution, it was possible to form solid complexes, and from literature consultation propose possible structures of these complexes. Photophysical solution studies of the fluorophore containing ligand **2.6**, resulted in the suggestion of the formation of copper complexes, which were dependant on the anion, although little change was observed in the absorbance with addition other transition metals, cobalt, zinc and nickel. Fluorescence studies of this ligand and these salts, showed quenching

upon addition of all metals to greater or less extents, suggesting interactions with metals, and possible an energy transfer between the metal atom and the excited fluorophore. Binding constants calculated from both absorbance and emission data suggested the formation for 1:1 ligand:metal complexes for those tested with the exception of copper(II) chloride, which appears to form both 1:1 and 1:2 ligand:metal complexes and copper(II) acetate which showed a much better data fit for a 2:2 model as suggested by the crystal structure. In general the binding constants calculated were stronger between **2.6** and metals than **2.2** and metals. The binding constant of the methoxy-substituted ligand, **2.4** was stronger than that of the nitro-substituted ligand **2.5**. The addition of copper(II) nitrate to a solution of **2.6** resulted in first quenching of fluorescence, and the enhancement of the fluorescence upon further addition of copper(II) nitrate. It was shown that this enhancement in the fluorescence was due to the addition of nitrate rather than an interaction with the copper, as the effect was only observed upon addition of copper(II) nitrate, and the addition of nitrate, as its tetrabutylammonium salt, after the ligand fluorescence had been quenched by the addition of copper(II)triflate. As a result, it was concluded that an *in situ*, nitrate sensor was prepared.

A series of hosts based around a ruthenium core, which have been mono- and di-substituted with organic ligands, **2.1** – **2.6**. Due to the symmetry of the di-substituted molecule the methylene protons are inequivalent, but upon addition of anions, they exhibit a time average equivalence of these protons. The mono-substituted hosts have shown very little binding to anions, with a weak affinity for chloride observed. The di-substituted hosts have shown the ability to bind a variety of anions, forming both 1:1 and 2:1 host:guest complexes. The formation of the mono-substituted host resulted in complete quenching of the fluorescence compared to the ligand **2.6**, but the di-substituted host, **4.10**, was shown to fluoresce, but the emission was far lower than that of the free ligand, and at a slightly higher wavelength. The reason for this quenching is suggested to be from an electronic energy transfer involving the metal centre, and the excited fluorophore. The addition of chloride to the mono-substituted host, **4.9**, resulted in no change in the fluorescence. The addition of anions to **4.10**, resulted in the quenching of the fluorescence, in the case of all anions added.

A second fluorophore containing amino-pyridyl ligand, **5.1**, has been synthesised, and this showed hydrogen bonding between the pyridyl nitrogen and amine proton on adjacent molecule, in forming 1D hydrogen bonded chains. A series of organic host molecules, consisting of di- and trisubstituted aryl core, to which the fluorophore ligand, **5.1** and two tripodal host based around the same aryl core, elaborated by the addition of **2.2** or **2.5**. NMR titration experiments on the three tripodal compounds have shown a dominance for 2:1 host:guest binding with a variety of anions for **5.3**, and a dominance for 1:1 host:guest binding for **5.4** and **5.5**. The 2:1 host:guest binding was a surprising results, and is not consistent with previous work in the group on an anthracene analogue of the host, which showed 1:1 host:guest binding, and hosts **5.4** and **5.5**. Photophysical data upon addition of anions to **5.5**, showed the formation of 2:1 and 1:1 host:guest complexes with halide anions, and the highest binding constant was observed for the formation of a 2:1 host:guest complex with chloride, and a similar affinity for both bromide and acetate. The strong binding to halides was observed with all hosts, but due to the complex nature of the binding of **5.4** and **5.5** to acetate, it was not possible to calculate binding constants. Complex binding was also observed with **5.5** and acetate, in the formation of three different stoichiometric complexes, 2:1, 1:1 and 1:2 host:guest binding.

Two viologen hosts were synthesised, in which two tripodal aryl host molecules were added to 4,4'-bipyridine, to form a viologen core, which was then elaborated by a urea molecule, previously reported by the group, and as a control molecule pyridine. The binding of these two molecules was measured using NMR titration experiments and showed strong halide binding, as was observed with the tripodal urea host. In contrast, it was observed that addition of carboxylates to these polytopic receptors brings about a visual colour change at relatively low concentrations. The amount of anion needed to trigger the colourimetric response can be controlled in a step-wise fashion by the identity of the peripheral binding groups.

References

1 D. R. Turner, B. Smith, E. C. Spencer, A. E. Goeta, I. R. Evans, D. A. Tocher, J. A. K. Howard, and J. W. Steed, *New J. Chem.*, 2005, **29**, 90.

2 K. J. Wallace, W. J. Belcher, D. R. Turner, K. F. Syed, and J. W. Steed, *J. Am. Chem. Soc.*, 2003, **125**, 9699.

3 K. Niikura, A. P. Bisson, and E. V. Anslyn, *J. Chem. Soc. Perkin Trans. 2*, 1999, 1111.

4 P. A. Gale, *Coord. Chem. Rev.*, 2001, **213**, 79.

5 A. Metzger and E. V. Anslyn, *Angew. Chem. Int. Ed.*, 1998, **37**, 649.

6 R. Prohens, G. Martorell, P. Ballester, and A. Costa, *Chem. Commu.*, 2001, 1456.

7 D. Esteban-Gomez, L. Fabbrizzi, and M. Licchelli, *J. Org. Chem.*, 2005, **70**, 5717.

8 M. H. Filby and J. W. Steed, *Coord. Chem. Rev.*, 2006, **250**, 3200.

9 W. J. Belcher, M. Fabre, T. Farhan, and J. W. Steed, *Org. Biomol. Chem.*, 2006, **4**, 781.

10 S. Camiolo, P. A. Gale, M. I. Ogden, B. W. Skelton, and A. H. White, *J. Chem. Soc. Perkin Trans. 2*, 2001, **2**, 1294.

11 L. Applegarth, A. E. Goeta, and J. W. Steed, *Chem. Commun.*, 2005, 2405.

12 M.-C. Lagunas, R. Gossage, A. W. Smeets, J. J. A. Spek, G. van Koten, and L. van Koten, *Eur. J. Inorg. Chem.*, 1998, 163.

13 M. H. Filby, S. Dickson, N. Zaccheroni, L. Prodi, S. Bonacchi, M. Montalti, M. J. Paterson, T. D. Humphries, and J. W. Steed, *J. Am. Chem. Soc*, 2008, **in press**.

14 L. Nie, Z. Li, J. Han, X. Zhang, R. Yang, W.-X. Liu, F. Y. Wu, J. W. Xie, Y. F. Zhao, and Y. B. Jiang, *J. Org. Chem.*, 2004, **69**, 6499.

15 P. A. Gale and R. Quesada, *Coord. Chem. Rev.*, 2006, **250**, 3219.

16 R. A. Binstead, in 'SPECFIT', Chapel Hill, NC, 1996.

17 J. M. Lehn, *Science*, 2002, **295**, 2400.

18 P. A. Gale, *Coord. Chem. Rev.*, 2003, **240**, 191.

19 P. A. Gale, *Coord. Chem. Rev.*, 2000, **199**, 181.

20 C. R. Bondy and S. J. Loeb, *Coord. Chem. Rev.*, 2003, **240**, 77.

21 P. A. Gale, S. Camoilo, C. P. Chapman, M. E. Light, and M. B. Hursthouse, *Tetrahedron Lett.*, 2001, **42**, 5095.

22 P. D. Beer and P. Schmitt, *Curr. Opin. Chem. Biol*, 1997, **1**, 475.

23 J. Zhang, A. M. Bond, J. Belcher, K. J. Wallace, and J. W. Steed, *J. Phys. Chem. B*, 2003, **107**, 5777.

24 M. W. Hosseini, J. Blacker, and J.-M. Lehn, *J. Am. Chem. Soc.*, 1990, **112**, 3896.

25 H. Furuta, M. J. Cyr, and J. L. Sessler, *J. Am. Chem. Soc.*, 1991, **113**, 6677.

26 P. D. Beer, M. Drew, and D. Smith, *J. Organomet. Chem.*, 1997, **543**, 259.

27 J. L. Sessler, E. Katayev, D. G. Pantos, and Y. A. Ustynyuk, *Chem. Commun*, 2004, 1276.

28 C. F. Mason, 'Biology of Freshwater Pollution', Longman, 1996.

29 P. D. Beer, P. A. Gale, and D. K. Smith, 'Supramolecular Chemistry', ed. R. G. Compton, S. G. Davies, J. Evans, and L. F. Gladden, Oxford University Press, 1999.

30 F. Vogtle, 'Supramolecular Chemistry', John Wiley & Sons, Ltd., 1991.

31 J. W. Steed and J. L. Attwood, 'Supramolecular Chemistry', John Wiley & Sons, Ltd., 2000.

32 M. M. G. Antonisse and D. N. Reinhoudt, *Chem.Commun.*, 1998, 443.

33 V. Amendola, M. Boiocchi, L. Fabbrizzi, and A. Palchetti, *J. Am. Chem. Soc.*, 2005, submitted (Nov 04).

34 P. J. Garratt, Y. F. Ng, and J. W. Steed, *Tetrahedron*, 2000, **56**, 4501.

35 H. S. Simmons and C. H. Park, *J. Am. Chem. Soc.*, 1968, **90**, 2428.

36 B. J. Rosenstein and P. L. Zeitlein, *Lancet*, 1998, **351**, 277.

37 M. J. Carson, M. C. Winter, S. M. Travis, and M. J. Welsh, *J. Biol. Chem.*, 1995, **270**, 20466.

38 P. A. Gale, M. E. Light, B. McNally, K. Navakhun, K. E. Sliwinski, and B. D. Smith, *Chem. Commun*, 2005, 3773.

39 P. D. Beer, J. J. Davis, D. A. Drillsma-Milgrom, and F. Szemes, *Chem. Commun*, 2002, 1716.

40 A. P. de Silva, D. B. Fox, A. J. M. Huxley, and T. S. Moody, *Coord. Chem. Rev.*, 2000, **205**, 41.

41 M. E. Hutson, E. U. Akkaya, and A. W. Czarnik, *J. Am. Chem. Soc*, 1989, **23**, 8735.

42 J. M. Llinares, D. Powell, and K. Bowman-James, *Coord. Chem. Rev.*, 2003, **240**, 57.

43 M. T. Albelda, M. A. Bernardo, E. Garcia-Espana, M. L. Godino-Salido, S. V. Luis, M. J. Melo, F. Pina, and C. Soriano, *J. Chem. Soc. Perkin Trans. 2*, 1999, **2**, 2545.

44 M. A. Bernardo, J. A. Guerrero, E. Garcia-Espana, S. V. Luis, J. M. Llinares, F. Pina, J. A. Ramirez, and C. Soriano, *J. Chem. Soc. Perkin Trans. 2*, 1996, **2**, 2335.

45 M. A. S. Hossain and H. J. Schneider, *Chem. Eur. J.*, 1999, **5**, 1284.

46 A. Domenech, E. Garcia-Espana, J. A. Ramirez, B. Celda, M. C. Martinez, D. Monleon, R. Tejero, A. Bencini, and A. Bianchi, *J. Chem. Soc. Perkin Trans. 2*, 1999, 23.

47 M. Gonsalves, A. L. Barker, J. V. Macpherson, P. R. Unwin, D. O'Hare, and C. P. Winlove, *Biophys. J.*, 2000, **78**, 1578.

48 S. D. Kean, B. L. May, P. Clements, S. F. Lincoln, and C. J. Easton, *J. Chem. Soc. Perkin Trans. 2*, 1999, 1257.

49 M. Arca, A. Bencini, E. Berni, C. Caltagirone, F. A. Devillanova, F. Isaia, A. Garau, C. Giorgi, V. Lippolis, A. Perra, L. Tei, and B. Valtancoli, *Inorg. Chem.*, 2003, **42**, 6929.

50 C. Bazzicalupi, A. Bencini, E. Faggi, A. Garau, C. Giorgi, V. Lippolis, A. Perra, and B. Valtancoli, *Dalton Trans.*, 2006, 1409.

51 P. A. Gale, S. E. Garcia-Garrido, and J. Garric, *Chem. Soc. Rev.*, 2008, **37**, 151.

52 A. M. Hossain, J. A. Liljegren, D. Powell, and K. Bowman-James, *Inorg. Chem.*, 2004, **43**, 3751.

53 A. Metzger and E. V. Anslyn, *Angew. Chem. Int. Ed.*, 1998, **37**, 649.

54 L. A. Cabell, M. D. Best, J. J. Lavigne, S. E. Schneider, D. M. Perreault, M.-K. Katherine, and E. V. Anslyn, *J. Chem. Soc., Perkin Trans. 2*, 2001, 315.

55 A. Metzger, V. M. Lynch, and E. V. Anslyn, *Angew. Chem., Int. Ed. Engl.*, 1997, **36**, 862.

56 S. L. Wiskur and E. V. Anslyn, *J. Am. Chem. Soc.*, 2001, **123**, 10109.

57 V. D. Jadhav and F. P. Schmidtchen, *Org. Lett.*, 2005, **7**, 3311.

58 P. A. Gale, *Coord. Chem. Rev.*, 2001, **213**, 79.

59 S. Nishizawa, Y. Kato, and N. Teramae, *J. Am. Chem. Soc.*, 1999, **121**, 9463.

60 K. Kavallieratos, S. R. deGala, D. J. Austin, and R. H. Crabtree, *J. Am. Chem. Soc.*, 1997, **119**, 2325.

61 S. Valiyaveetti, J. F. J. Engbersen, W. Verboom, and D. N. Reinhoudt, *Angew. Chem. Int. Ed., Engl.*, 1993, **32**, 900.

62 P. D. Beer, D. Hesek, J. Hodacova, and S. E. Stokes, *J. Chem. Soc. Chem. Commun.*, 1992, 270.

63 M. A. Hossain, J. M. Llinares, D. Powell, and K. Bowman-James, *Inorg. Chem.*, 2001, **40**, 2936.

64 K. H. Choi and A. D. Hamilton, *J. Am. Chem. Soc.*, 2001, **123**, 2456.

65 A. Szumna and J. Jurczak, *Eur. J. Org. Chem.*, 2001, 4031.

66 A. P. Bisson, V. M. Lynch, M. K. C. Monahan, and E. V. Anslyn, *Angew. Chem. Int. Ed., Engl.*, 1997, **36**, 2340.

67 J. L. Sessler, S. Camiolo, and P. A. Gale, *Coord. Chem. Rev.*, 2003, **240**, 17.

68 J. L. Attwood and J. W. Steed, 'Encyclopedia of Supramolecular Chemistry', Marcel Dekker, Inc., 2004.

69 M. Scherer, J. L. Sessler, A. Gebauer, and V. Lynch, *Chem. Commun.*, 1998, 85.

70 J. L. Sessler, R. S. Zimmerman, G. J. Kirkovits, A. Gebauer, and M. Scherer, *J. Organometal. Chem.*, 2001, **637**, 343.

71 P. A. Gale, S. Camiolo, G. J. Tizzard, C. P. Chapman, M. E. Light, S. J. Coles, and M. B. Hursthouse, *J. Org. Chem.*, 2001, **66**, 7849.

72 J. L. Sessler, S. Camiolo, and P. A. Gale, *Coord. Chem. Rev.*, 2003, **240**, 17.

73 F. Hettche, P. Reiss, and R. W. Hoffmann, *Chem.-Eur. J.*, 2002, **8**, 4946.

74 J. Y. Kwon, Y. J. Yang, S. K. Kim, K.-H. Lee, J. S. Kim, and J. Yoon, *J. Org. Chem.*, 2004, **69**, 5155.

75 D. A. Jose, D. K. Kumar, B. Ganguly, and A. Das, *Tetrahedron Lett.*, 2005, **46**, 5343.

76 V. Amendola, M. Boiocchi, D. Esteban-Gomez, L. Fabbrizzi, and E. Monzani, *Org. Biomol. Chem.*, 2005, **3**, 2632.

77 R. Gu, S. Depraetere, J. Kotek, J. Budka, E. Wagner-Wysiecka, J. F. Biernat, and W. Dehaen, *Org. Biomol. Chem.*, 2005, **3**, 2921.

78 V. Amendola, D. Esteban-Gomez, L. Fabbrizzi, and M. Licchelli, *Acc. Chem. Res.*, 2006, **39**, 343.

79 T. Gunnlaugsson, P. E. Kruger, P. Jensen, F. M. Pfeffer, and G. M. Hussey, *Tetrahedron Lett.*, 2003, **44**, 8909.

80 D. E. Gomez, L. Fabbrizzi, M. Licchelli, and E. Monzani, *Org. Biomol. Chem.*, 2005, **3**, 1495.

81 S. Camiolo, P. A. Gale, M. B. Hursthouse, and M. E. Light, *Org. Biomol. Chem.*, 2003, **1**, 741.

82 X. He, S. Hu, K. Liu, Y. Guo, J. Xu, and S. Shao, *Org. Lett.*, 2006, **8**, 333.

83 D. Esteban-Gomez, L. Fabbrizzi, M. Licchelli, and D. Sacchi, *J. Mater. Chem.*, 2005, **15**, 2670.

84 A. Knoepfler-Muhlecker, B. Scheffter, H. Kopacka, K. Wurst, and P. Peringer, *J. Chem. Soc. Dalton Trans.*, 1999, 2525.

85 P. D. Beer and D. K. Smith, *Prog. Inorg. Chem.*, 1997, **46**, 1.

86 V. B. Arion, P. D. Beer, M. G. B. Drew, and P. Hopkins, *Polyhedron*, 1999, **18**, 451.

87 P. D. Beer, J. Cadman, J. M. Lloris, R. Martinez-Manez, M. E. Padilla, T. Pardo, D. K. Smith, and J. Soto, *J.Chem. Soc. Dalton Trans.*, 1999, 127.

88 T. J. Wedge and M. F. Hawthorne, *Coord. Chem. Rev.*, 2003, **240**, 111.

89 M. F. Hawthorne, *Angew. Chem. Int. Ed.*, 1991, **30**, 1507.

90 Z. P. Zheng, C. B. Knobler, and M. F. Hawthorne, *J. Am. Chem. Soc.*, 1995, **117**, 5105.

91 M. F. Hawthorne and Z. P. Zheng, *Acc. Chem. Res.*, 1997, **30**, 267.

92 X. G. Yang, C. B. Knobler, Z. P. Zheng, and M. F. Hawthorne, *J. Am. Chem. Soc.*, 1994, **116**, 7142.

93 Z. P. Zheng, C. B. Knobler, M. D. Mortimer, G. G. Kong, and M. F. Hawthorne, *Inorg. Chem.*, 1996, **35**, 1235.

94 Z. P. Zheng, X. G. Yang, C. B. Knobler, and M. F. Hawthorne, *J. Am. Chem. Soc.*, 1993, **115**, 5320.

95 H. Lee, C. B. Knobler, and M. F. Hawthorne, *Angew. Chem. Int. Ed.*, 2001, **40**, 2124.

96 X. G. Yang, C. B. Knobler, and M. F. Hawthorne, *J. Am. Chem. Soc.*, 1992, **114**, 380.

97 M. F. Hawthorne, X. G. Yang, and Z. P. Zheng, *Pure Appl. Chem.*, 1994, **66**, 245.

98 P. M. Monk and N. N. Hodgkinson, *Electrochim. Acta*, 1998, **43**, 245.

99 P. A. Gale, *Coord. Chem. Rev.*, 2003, **240**, 191.

100 S. Camiolo, P. A. Gale, M. E. Light, and M. B. Hursthouse, *Supramol. Chem.*, 2001, **13**, 613.

101 L. O. Abouderbala, W. J. Belcher, M. G. Boutelle, P. J. Cragg, M. Fabre, J. Dhaliwal, J. W. Steed, D. R. Turner, and K. J. Wallace, *Chem. Commun.*, 2002, 358.

102 C. Bazzicalupi, A. Bencini, A. Bianchi, L. Borsari, C. Giorgi, B. Valtancoli, C. Anda, and A. Llobet, *J. Org. Chem.*, 2005, **70**, 4257.

103 Z. Yin, Y. Zhang, J. He, and J.-P. Cheng, *Tetrahedron*, 2006, **62**, 765.

104 D. A. Amabilino, P. R. Ashton, V. Balzani, C. L. Brown, A. Credi, J. M. Frechet, J. W. Leon, F. M. Raymo, N. Spencer, J. F. Stoddart, and M. Venturi, *J. Am. Chem. Soc.*, 1996, **118**, 12012.

105 R. Toba, J. M. Quintela, C. Peinador, E. Roman, and A. E. Kaifer, *Chem. Commun*, 2001, 857.

106 P. J. Dandliker, F. Diederich, A. Zingg, J.-P. Gisselbrecht, M. Gross, A. Louati, and E. Sanford, *Helv. Chim. Acta*, 1997, **80**, 1773.

107 G. R. Newkome, A. K. Patri, and L. A. Godinez, *Chem. Eur. J.*, 1999, **5**, 1445.

108 K. W. Pollak, J. W. Leon, J. M. Frechet, M. Maskus, and H. D. Abruna, *Chem. Mater.*, 1998, **10**, 30.

109 Y. Wang, C. M. Cardona, and A. E. Kaifer, *J. Am. Chem. Soc.*, 1999, **121**, 9765.

110 C. M. Cardona, T. D. McCarley, and A. E. Kaifer, *J. Org. Chem.*, 2000, **65**, 1857.

111 G. R. Newkome, R. Guther, C. N. Moorefield, F. Cardullo, L. Echegoyen, E. Perez-Cordero, and H. Luftmann, *Angew. Chem. Int. Ed.*, 1995, **34**, 2023.

112 C. B. Gorman, B. L. Parkhust, W. Y. Su, and K. Y. Chen, *J. Am. Chem. Soc.*, 1997, **119**, 1141.

113 V. Balzani, S. Campagna, G. Denti, A. Juris, S. Serroni, and M. Venturi, *Acc. Chem. Res.*, 1998, **31**, 26.

114 F. Vogtle, M. Plevoets, M. Nieger, G. C. Azzellini, A. Credi, L. De Cola, V. De Marchis, M. Venturi, and V. Balzani, *J. Am. Chem. Soc.*, 1999, **121**, 6290.

115 V. Balzanni, F. Barigeletti, and L. D. Cola, *Top. Curr. Chem.*, 1990, **158**, 31.

116 A. Juris, V. Balzanni, F. Barigeletti, S. Campagna, P. Belser, and A. V. Zelewsky, *Coord. Chem. Rev.*, 1988, **84**, 85.

117 P. D. Beer and E. J. Hayes, *Coord. Chem. Rev.*, 2003, **240**, 167.

118 F. Szemes, D. Hesek, B. Chen, S. W. Dent, M. G. B. Drew, and A. J. Goulden, *Inorg. Chem.*, 1996, **35**, 5868.

119 P. D. Beer, *Acc. Chem. Res.*, 1998, **31**, 71.

120 P. D. Beer, S. W. Dent, and T. J. Wear, *J. Chem. Soc., Dalton Trans.*, 1996, 2341.

121 S. Camiolo, S. J. Coles, P. A. Gale, M. B. Hursthouse, T. A. Mayer, and M. A. Paver, *Chem. Commun.*, 2000, 275.

122 A. J. Blake, N. R. Brooks, N. R. Champness, M. Crew, L. R. Hanton, P. Hubberstey, P. C. Simon, and M. Schroder, *J. Chem. Soc. Dalton Trans.*, 1999, 2813.

123 C. Kaes, M. W. Hosseini, C. E. F. Rickard, B. W. Skelton, and A. H. White, *Angew. Chem. Int. Ed.*, 1998, **37**, 920.

124 C. P. Casey, A. J. Shusterman, N. W. Vollendorf, and K. J. Haller, *J. Am. Chem. Soc.*, 1982, **104**, 2417.

125 S. E. Kabir, E. Rosenberg, M. Day, K. Hardcastle, E. Wolf, and T. McPhillips, *Organometallics*, 1995, **14**, 721.

126 P. L. Boulas, M. Gomez-Kaifer, and L. Echegoyen, *Angew. Chem. Int. Ed.*, 1998, **37**, 216.

127 A. P. de Silva, H. Q. N. Gunaratne, T. Gunnlaugsson, A. J. M. Huxley, C. P. McCoy, and J. T. Rademacher, *Chem. Rev.*, 1997, **97**.

128 A. W. Czarnik, *Acc. Chem. Res.*, 1994, **27**, 302.

129 A. P. de Silva, H. Q. N. Gunaratne, C. McVeigh, M. G. E. Maguire, P. R. S. Maxwell, and E. O'Hanlon, *Chem. Commun*, 1996, 2191.

130 L. Fabbrizzi, G. Francese, M. Licchelli, A. Perotti, and A. Taglietti, *Chem. Commun*, 1997, 581.

131 H. Miyaji, P. Anzenbacher, J. L. Sessler, E. R. Bleasdale, and P. A. Gale, *Chem. Commun*, 1999, 1723.

132 G. De Santis, L. Fabbrizzi, M. Licchelli, A. Poggi, and A. Taglietti, *Angew. Chem. Int. Ed.*, 1996, **35**, 202.

133 L. Fabbrizzi, M. Licchelli, L. Parodi, A. Poggi, and A. Taglietti, *Eur. J. Inorg. Chem.*, 1999, 35.

134 J. H. Liao, C. T. Chen, and J. M. Fang, *Org. Lett.*, 2002, **4**, 561.

135 J. W. Steed and K. M. Anderson, *Cryst. Eng. Comm.*, 2007, **9**, 328.

136 K. J. Wallace and J. W. Steed, *unpublished results*, 2002.

137 M. J. Frisch, G. W. Trucks, H. B. Schlegel, G. E. Scuseria, M. A. Robb, J. R. Cheeseman, J. Montgomery, J. A. , T. Vreven, K. N. Kudin, J. C. Burant, J. M. Millam, S. S. Iyengar, J. Tomasi, V. Barone, B. Mennucci, M. Cossi, G. Scalmani, N. Rega, G. A. Petersson, H. Nakatsuji, M. Hada, M. Ehara, K. Toyota, R. Fukuda, J. Hasegawa, M. Ishida, T. Nakajima, Y. Honda, O. Kitao, H. Nakai, M. Klene, X. Li, J. E. Knox, H. P. Hratchian, J. B. Cross, V. Bakken, C. Adamo, J. Jaramillo, R.

Gomperts, R. E. Stratmann, O. Yazyev, A. J. Austin, R. Cammi, C. Pomelli, J. W. Ochterski, P. Y. Ayala, K. Morokuma, G. A. Voth, P. Salvador, J. J. Dannenberg, V. G. Zakrzewski, S. Dapprich, A. D. Daniels, M. C. Strain, O. Farkas, D. K. Malick, A. D. Rabuck, K. Raghavachari, J. B. Foresman, J. V. Ortiz, Q. Cui, A. G. Baboul, S. Clifford, J. Cioslowski, B. B. Stefanov, G. Liu, A. Liashenko, P. Piskorz, I. Komaromi, R. L. Martin, D. J. Fox, T. Keith, M. A. Al-Laham, C. Y. Peng, A. Nanayakkara, M. Challacombe, P. M. W. Gill, B. Johnson, W. Chen, M. W. Wong, C. Gonzalez, and J. A. Pople, in 'Gaussian 03', Wallingford, 2004.

138 R. Dennington II, T. Keith, J. Millam, K. Eppinnett, W. L. Hovell, and R. Gilliland, Shawnee Mission, 2003.

139 G. M. Sheldrick, in 'SHELXS-97', University of Göttingen, 1997.

140 L. J. Barbour, *J. Supramol. Chem.*, 2001, **1**, 189.

141 X.-M. Ouyang, D.-J. Liu, T.-A. Okamura, H.-W. Bu, W.-Y. Sun, W.-X. Tang, and N. Ueyama, *Dalton Trans*, 2003, 1836.

142 P. D. Beer and J. Cadman, *Coord. Chem. Rev.*, 2000, **205**, 131.

143 C. Stroh, E. Belorizky, P. Turek, H. Bolvin, and R. Ziessel, *Inorg. Chem.*, 2003, **42**, 2938.

144 D. R. Turner, E. C. Spencer, J. A. K. Howard, D. A. Tocher, and J. W. Steed, *Chem. Commun*, 2004, 1352.

145 P. A. Gale, J. Garric, M. E. Light, B. McNally, and B. D. Smith, *Chem. Commun.*, 2007, 1736.

146 M. Barquin, M. J. Gonzalez Garmendia, S. Pacheco, E. Pinilla, S. Quintela, J. M. Seco, and M. R. Torres, *Inorg. Chim. Acta*, 2004, **357**, 3230.

147 S. R. Batten, B. F. Hoskins, B. Moubaraki, K. S. Murray, and R. Robson, *Chem. Commun.*, 2000, 1095.

148 J. W. Steed and J. L. Atwood, 'Supramolecular Chemistry', J. Wiley & Sons, 2000.

149 P. D. Beer and S. R. Bayly, *Top. Curr. Chem.*, 2005, **255**, 125.

150 J. W. Steed, *Chem. Commun*, 2006, 2637.

151 C. R. Rice, *Coord. Chem. Rev.*, 2006, **250**, 3190.

152 M. S. Goodman, V. Jubian, and A. D. Hamilton, *Tetrahedron Lett.*, 1995, **36**, 2551.

153 C. R. Bondy, P. A. Gale, and S. J. Loeb, *Chem. Commun.*, 2001, 729.

154 C. R. Bondy, P. A. Gale, and S. J. Loeb, *J. Am. Chem. Soc.*, 2004, **126**, 5030.

155 D. R. Turner, B. Smith, A. E. Goeta, I. R. Evans, D. A. Tocher, J. A. K. Howard, and J. W. Steed, *Cryst. Eng. Comm.*, 2004, **6**, 633.

156 D. R. Turner, M. Henry, C. Wilkinson, G. J. McIntyre, S. A. Mason, A. E. Goeta, and J. W. Steed, *J. Am. Chem. Soc*, 2005, **127**, 11063.

157 L. Ion, D. Morales, J. Perez, L. Riera, V. Riera, A. Kowenicki, and M. McPartlin, *Chem. Commun*, 2006, 91.

158 S. Nieto, J. Perez, L. Riera, V. Riera, and D. Miguel, *New J. Chem*, 2006, **30**, 838.

159 L. P. Harding, J. C. Jeffery, T. Riis-Johannessen, C. R. Rice, and Z. T. Zeng, *Dalton Trans.*, 2004, 2396.

160 K. J. Wallace, R. Daari, W. J. Belcher, L. O. Abouderbala, M. G. Boutelle, and J. W. Steed, *J. Organomet. Chem.*, 2003, **666**, 63.

161 M. A. Bennett and A. K. Smith, *J. Chem. Soc., Dalton Trans.*, 1974, 233.

162 G. Aullon, D. Bellamy, L. Brammer, E. A. Bruton, and A. G. Orpen, *Chem. Commun.*, 1998, 653.

163 L. Brammer, E. A. Bruton, and P. Sherwood, *Cryst. Growth Des.*, 2001, **1**, 277.

164 J. W. Steed and C. E. Willans, *unpublished results.*

165 P. Gans, in 'HypNMR 2006', Leeds, 2006.

166 B. Chaudret, D. J. Cole-Hamilton, R. S. Nohr, and G. Wilkinson, *J. Chem. Soc. Dalton Trans.*, 1977, 1546.

167 A.-C. Ribou, T. Wada, and H. Sasabe, *Inorg. Chim. Acta*, 1999, **288**, 134.

168 L. Fabbrizzi, A. Leone, and A. Taglietti, *Angew. Chem. Int. Ed.*, 2001, **40**, 3066.

169 H. D. Flack, *Acta Crystallogr., Sect. A*, 1983, **39**, 876.

170 P. A. Gale, *Chem. Commun*, 2005, 3761.

171 J. L. Seganish and J. T. Davis, *Chem. Commun*, 2005, 5781.

172 B. Schazmann, N. Alhashimy, and D. Diamond, *J. Am. Chem. Soc*, 2006, **128**, 8607.

173 S. Nieto, J. Perez, L. Riera, V. Riera, and D. Miguel, *Chem. Eur. J.*, 2006, **12**, 2244.

174 A. Chaumont and G. Wipff, *New J. Chem.*, 2006, **30**, 537.

175 C. A. Ilioudis and J. W. Steed, *Org. Biomol. Chem.*, 2005, **3**, 2935.

176 Y. Bai, B.-G. Zhang, J. Xu, C. Y. Duan, D.-B. Dang, D. J. Liu, and Q.-J. Meng, *New J. Chem.*, 2005, **29**, 777.

177 V. Amendola, M. Boiocchi, L. Fabbrizzi, and A. Palchetti, *Chem. Eur. J*, 2005, **11**, 5648.

178 C. A. Ilioudis, D. A. Tocher, and J. W. Steed, *J. Am. Chem. Soc.*, 2004, **126**, 12395.

179 B. D. Smith and T. N. Lambert, *Chem. Commun,*, 2003, 2261.

180 F. Hettche and R. W. Hoffmann, *New J. Chem.*, 2003, **27**, 172.

181 V. McKee, J. Nelson, and R. M. Town, *Chem. Soc. Rev.*, 2003, **32**, 309.

182 P. Lhotak, *Top. Curr. Chem.*, 2005, **255**, 65.

183 P. A. Gale, *Coord. Chem. Rev.*, 2003, **240**, 1.

184 P. D. Beer and P. A. Gale, *Angew. Chem., Int. Ed.*, 2001, **40**, 487.

185 D. R. Turner, M. J. Paterson, and J. W. Steed, *J. Org. Chem.*, 2006, 1598.

186 L. Prodi, M. Montalti, N. Zaccheroni, G. Pickaert, L. Charbonniere, and R. Ziessel, *New J. Chem.*, 2003, **27**, 134.

187 L. Charbonniere, R. Ziessel, M. Montalti, L. Prodi, N. Zaccheroni, C. Boehme, and G. Wipff, *J. Am. Chem. Soc.*, 2002, **124**, 7779.

188 M. Montalti, L. Prodi, N. Zaccheroni, L. Charbonniere, L. Douce, and R. Ziessel, *J. Am. Chem. Soc.*, 2001, **123**, 12694.

189 L. Prodi, *New J. Chem.*, 2005, **29**, 20.

190 L. Fabbrizzi and A. Poggi, *Chem. Soc. Rev.*, 1995, 197.

191 G. Hennrich and E. V. Anslyn, *Chem.-Eur. J.*, 2002, **8**, 2219.

192 B. T. Nguyen and E. V. Anslyn, *Coord. Chem. Rev.*, 2006, **250**, 3118.

193 S. Arimori, M. G. Davidson, T. M. Fyles, T. G. Hibbert, T. D. James, and G. I. Kociok-Kohn, *Chem. Commun*, 2004, 1640.

194 A. T. Wright and E. V. Anslyn, *Chem. Soc. Rev.*, 2006, **35**, 14.

195 Y. S. Sohn, A. Goodey, E. V. Anslyn, J. T. McDevitt, J. B. Shear, and D. P. Neikirk, *Biosens.Bioelectron.*, 2005, **21**, 303.

196 S. L. Wiskur, P. N. Floriano, E. V. Anslyn, and J. T. McDevitt, *Angew. Chem.-Int. Ed.*, 2003, **42**, 2070.

197 S. C. McCleskey, M. J. Griffin, S. E. Schneider, J. T. McDevitt, and E. V. Anslyn, *J. Am. Chem. Soc.*, 2003, **125**, 1114.

198 Z. G. Xia and D. R. Storm, *Nat. Rev. Neurosci.*, 2005, **6**, 267.

199 W. A. Snedden and H. Fromm, *New Phytol.*, 2001, **151**, 35.

200 L. O. Abouderbala, W. J. Belcher, M. G. Boutelle, P. J. Cragg, J. W. Steed, D. R. Turner, and K. J. Wallace, *Proc. Nat. Acad. Sci. USA*, 2002, **99**, 5001.

201 S. L. Tobey, B. D. Jones, and E. V. Anslyn, *J. Am. Chem. Soc.*, 2003, **125**, 4026.

202 K. J. Wallace, R. Hanes, E. V. Anslyn, J. Morey, K. V. Kilway, and J. Siegel, *Synthesis-Stuttgart*, 2005, 2080.

203 P. J. Garratt, A. J. Ibbett, J. E. Ledbury, R. O'Brien, M. B. Hursthouse, and K. M. A. Malik, *Tetrahedron*, 1998, **54**, 949.

204 A. M. Christofi, P. J. Garratt, and G. Hogarth, *Tetrahedron*, 2001, **57**, 751.

205 C. Schmuck and M. Schwegmann, *J. Am. Chem. Soc.*, 2005, **127**, 3373.

206 S. Sasaki, D. Citterio, S. Ozawa, and K. Suzuki, *J. Chem. Soc., Perkin Trans. 2*, 2001, 2309.

207 Y. Bai, B.-G. Zhang, C. Y. Duan, D.-B. Dang, and Q.-J. Meng, *New J. Chem.*, 2006, **30**, 266.

208 J. W. Steed and K. J. Wallace, *unpublished results.*

209 F. M. Winnik, *Coord. Chem. Rev.*, 1993, **93**, 587.

210 L. Prodi, R. Ballardini, M. T. Gandolfi, and R. Roversi, *J. Photochem. Photo. A*, 2000, **2000**, 49.

211 M. Montalti, A. Credi, L. Prodi, and M. T. Gandolfi, 'Handbook of Photochemistry', CRC Taylor & Francis, 2006.

212 F. Bolletta, M. Montalti, L. Prodi, S. Romano, N. Zaccheroni, L. Canovese, G. Chessa, C. Santo, and F. Visentin, *Inorg. Chim. Acta*, 2004, **357**, 4078.

213 R. D. Fossum and M. Fox, *J. Phys. Chem. B*, 1997, **101**, 6384.

214 B. Schazmann and D. Diamond, *New J. Chem.*, 2007, **31**, 587.

215 M. H. Filby, 'Anion binding host systems based on calix[4]arenes and nanoparticles', PhD Thesis, Durham, University, Durham, 2007.

216 G. Rogez, B. F. Ribera, A. Credi, R. Ballardini, M. T. Gandolfi, V. Balzani, Y. Liu, B. H. Northrop, and J. F. Stoddart, *J. Am. Chem. Soc.*, 2007, **129**, 4633.

217 W. Silwa, B. Bachowska, and T. Girek, *Curr. Org. Chem.*, 2007, **11**, 497.

218 M. Ezoe, S. Yagi, H. Nakazumi, N. Itou, Y. Araki, and O. Ito, *Tetrahedron*, 2006, **62**, 2501.

219 S. P. Gromov, A. I. Vedernikov, E. N. Ushakov, N. A. Lobova, A. A. Botsmanova, L. G. Kuz'mina, A. V. Churakov, Y. A. Strelenko, M. V. Alfimov, J. A. K. Howard, D. Johnels, and U. G. Edlund, *New J. Chem.*, 2005, **29**, 881.

220 C. L. Bird and A. T. Kuhn, *Chem. Soc. Rev.*, 1981, 49.

221 J. F. Folmer-Andersen, M. Kitamura, and E. V. Anslyn, *J. Am. Chem. Soc.*, 2006, **128**, 5652.

222 H. J. Choi, Y. S. Park, S. H. Yun, H. S. Kim, C. S. Cho, K. Ko, and K. H. Ahn, *Org. Lett.*, 2002, **4**, 795.

223 G. Hennrich, V. M. Lynch, and E. V. Anslyn, *Chem.-Eur. J.*, 2002, **8**, 2274.

224 A. N. Swinburne and J. W. Steed, *unpublished results.*

225 H. Kunkely and A. Vogler, *Chem. Phys. Lett.*, 2001, **345**, 309.

List of Publications From This Work

'Anion binding in (arene)ruthenium(II)-based hosts'. *Chem. Commun.*, 2007, 4955-4957.

'Induced Fit Inter-Anion Discrimination by Binding-Induced Excimer Formation'. *J. Am. Chem. Soc.*, 2008, **130**, 4105-4113.

'Intramolecular binding site competition as a means of tuning the response of a colourimetric anion sensor'. *New J. Chem.*, accepted

Appendix

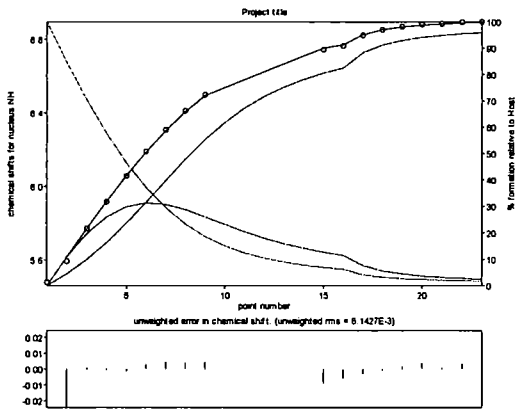

Figure 8.1: Plots showing the data fit of titration data for **4.4** upon addition of TBA-Cl in calculation of binding constants.

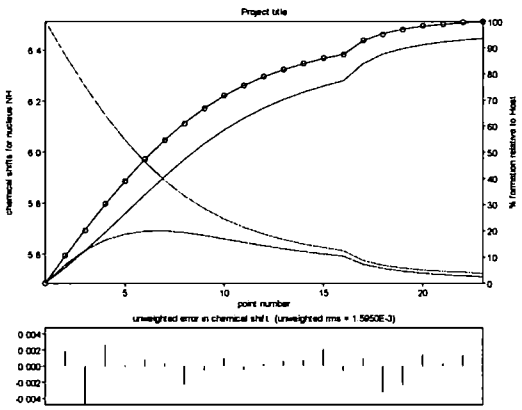

Figure 8.2: Plots showing the data fit of titration data for **4.4** upon addition of TBA-Br in calculation of binding constants.

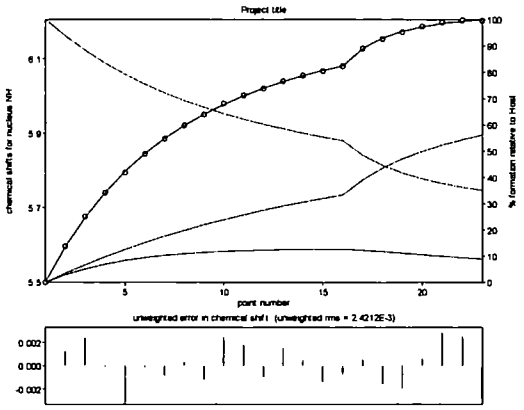

Figure 8.3: Plots showing the data fit of titration data for **4.4** upon addition of TBA- NO_3 in calculation of binding constants.

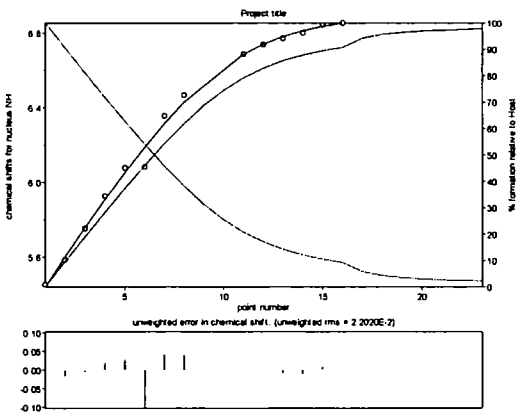

Figure 8.4: Plots showing the data fit of titration data for **4.4** upon addition of TBA-$MeCO_2$ in calculation of binding constants.

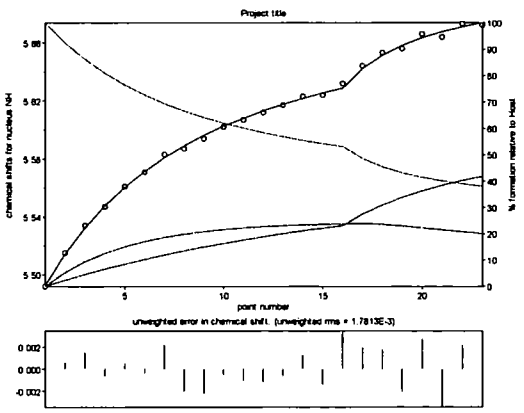

Figure 8.5: Plots showing the data fit of titration data for **4.4** upon addition of TBA-CF_3SO_3 in calculation of binding constants.

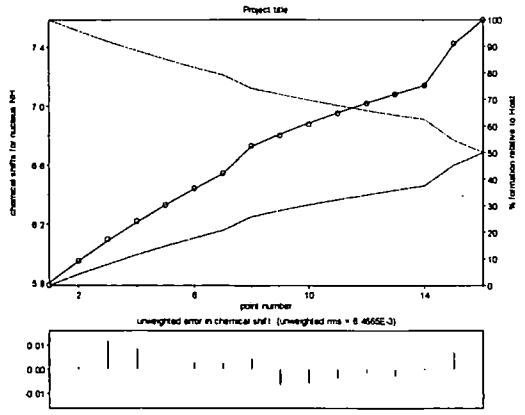

Figure 8.6: Plots showing the data fit of titration data for **4.7** upon addition of TBA-Cl in calculation of binding constants.

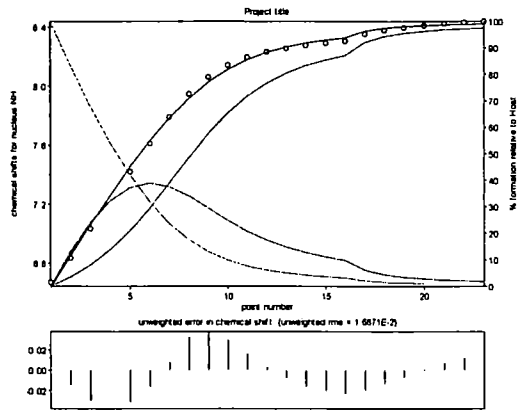

Figure 8.7: Plots showing the data fit of titration data for **4.8** upon addition of TBA-Cl in calculation of binding constants.

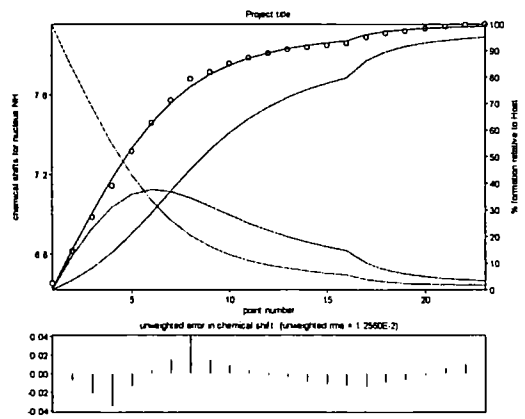

Figure 8.8: Plots showing the data fit of titration data for **4.8** upon addition of TBA-Br in calculation of binding constants.

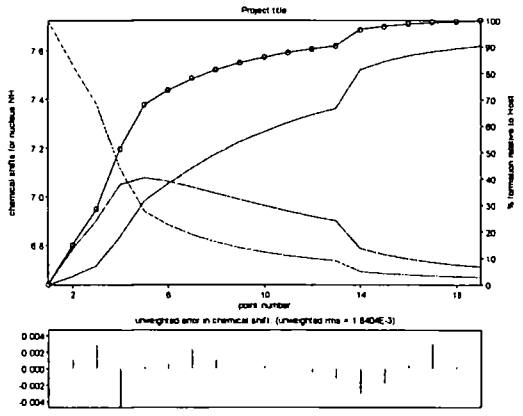

Figure 8.9: Plots showing the data fit of titration data for **4.8** upon addition of TBA-NO_3 in calculation of binding constants.

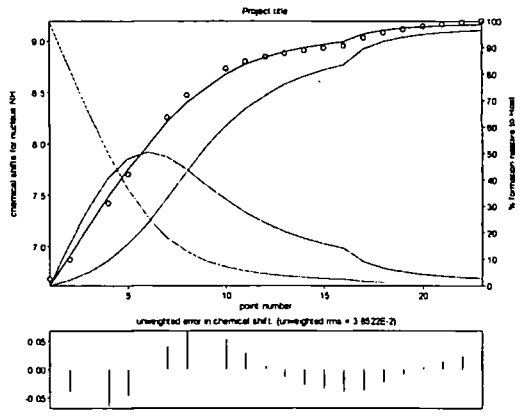

Figure 8.10: Plots showing the data fit of titration data for **4.8** upon addition of TBA-$MeCO_2$ in calculation of binding constants.

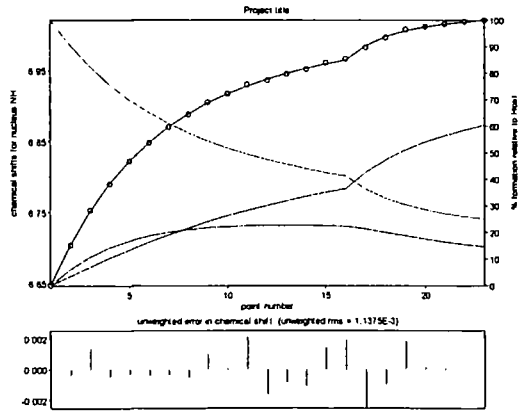

Figure 8.11: Plots showing the data fit of titration data for **4.8** upon addition of TBA-CF_3SO_3 in calculation of binding constants.

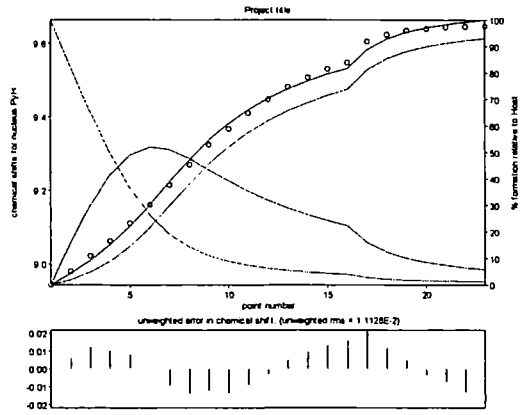

Figure 8.12: Plots showing the data fit of titration data for **4.10** upon addition of TBA-Cl in calculation of binding constants.

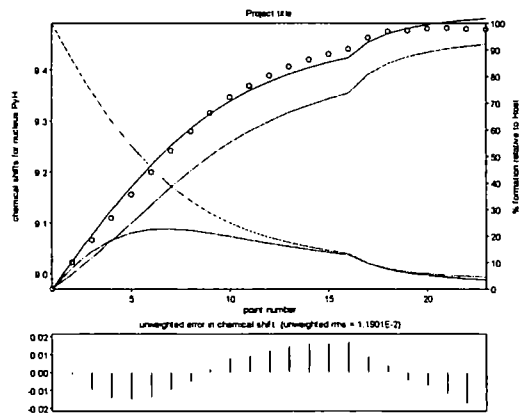

Figure 8.13: Plots showing the data fit of titration data for **4.10** upon addition of TBA-Br in calculation of binding constants.

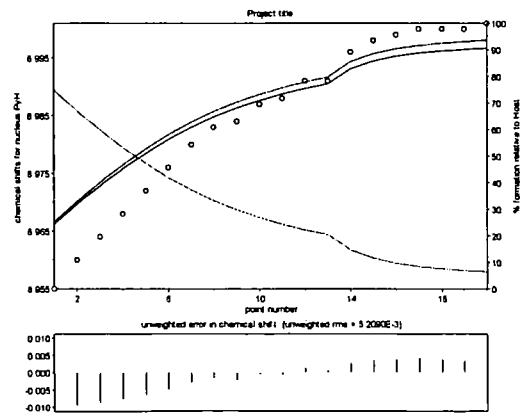

Figure 8.14: Plots showing the data fit of titration data for **4.10** upon addition of TBA- NO_3 in calculation of binding constants.

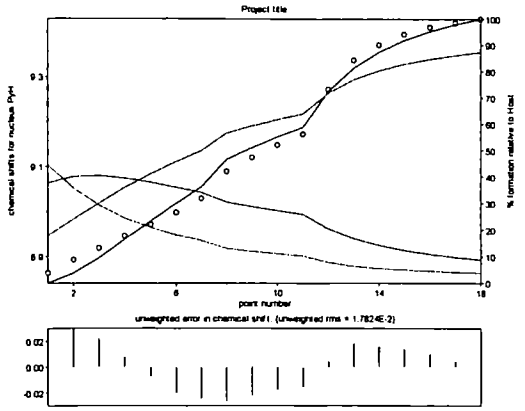

Figure 8.15: Plots showing the data fit of titration data for **4.4** upon addition of TBA-$MeCO_2$ in calculation of binding constants.

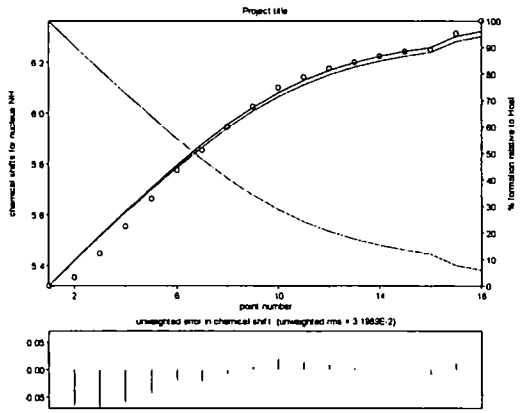

Figure 8.16: Plots showing the data fit of titration data for **5.4** upon addition of TBA-Cl in calculation of binding constants.

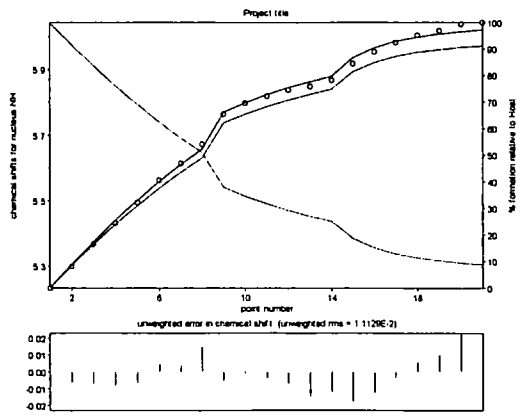

Figure 8.17: Plots showing the data fit of titration data for **5.4** upon addition of TBA-Br in calculation of binding constants.

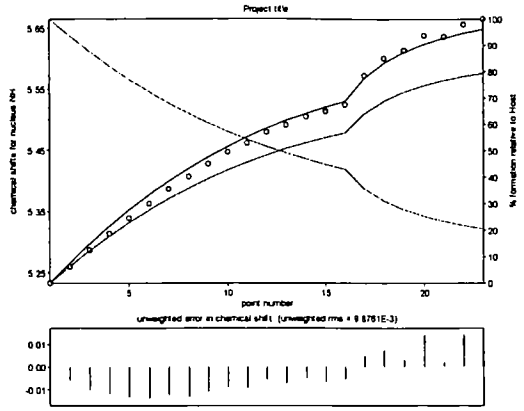

Figure 8.18: Plots showing the data fit of titration data for **5.4** upon addition of TBA- NO_3 in calculation of binding constants.

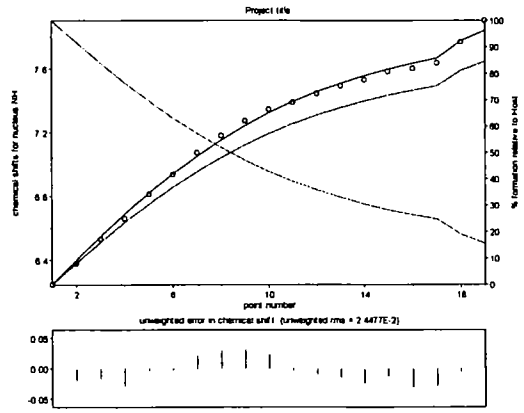

Figure 8.19: Plots showing the data fit of titration data for **5.5** upon addition of TBA-Cl in calculation of binding constants.

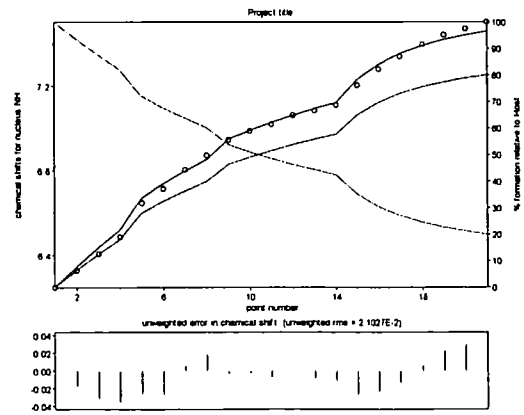

Figure 8.20: Plots showing the data fit of titration data for **5.5** upon addition of TBA- Br in calculation of binding constants.

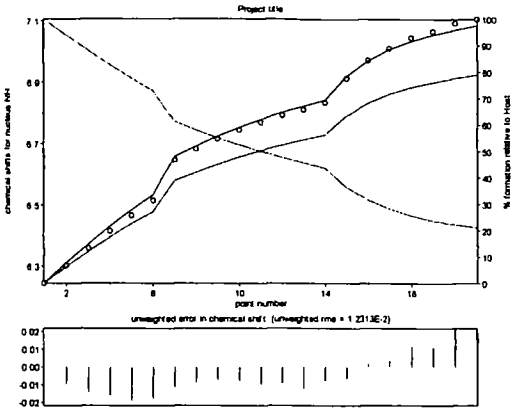

Figure 8.21: Plots showing the data fit of titration data for **5.5** upon addition of TBA- NO_3 in calculation of binding constants.

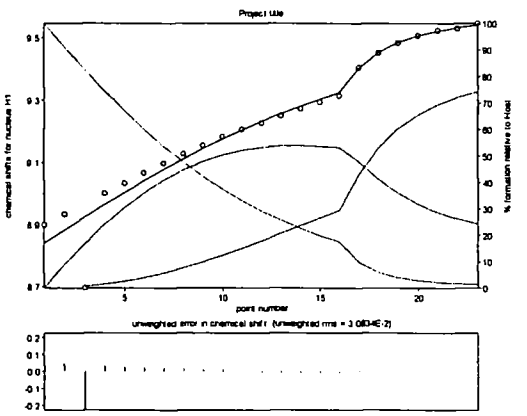

Figure 8.22: Plots showing the data fit of titration data for **6.2** upon addition of TBA- Cl in calculation of binding constants.

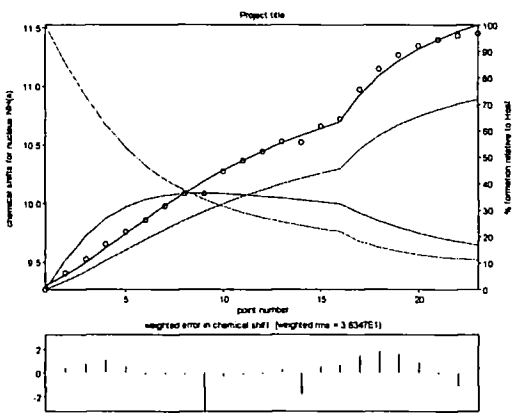

Figure 8.23: Plots showing the data fit of titration data for **6.3** upon addition of TBA- Cl in calculation of binding constants.

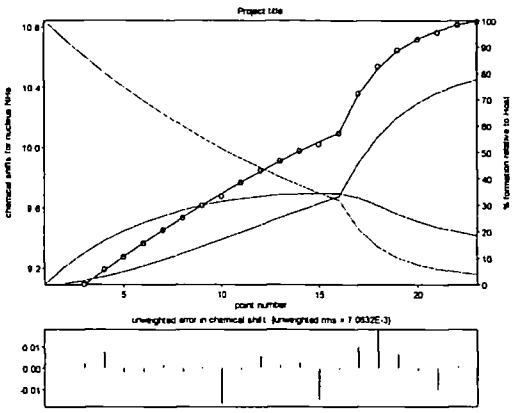

Figure 8.24: Plots showing the data fit of titration data for **6.3** upon addition of TBA-Br in calculation of binding constants.

This thesis is accompanied with a CD containing crystallographic data and titration data for all the binding studies carried out by the author.